Grainex Mar-M 247 Turbine Disk Life Study for NASA's High Temperature High Speed Turbine Seal Test Facility

Irebert R. Delgado
U.S. Army Research Laboratory, Glenn Research Center, Cleveland, Ohio

# NASA STI Program . . . in Profile

Since its founding, NASA has been dedicated to the advancement of aeronautics and space science. The NASA Scientific and Technical Information (STI) Program plays a key part in helping NASA maintain this important role.

The NASA STI Program operates under the auspices of the Agency Chief Information Officer. It collects, organizes, provides for archiving, and disseminates NASA's STI. The NASA STI Program provides access to the NASA Technical Report Server—Registered (NTRS Reg) and NASA Technical Report Server— Public (NTRS) thus providing one of the largest collections of aeronautical and space science STI in the world. Results are published in both non-NASA channels and by NASA in the NASA STI Report Series, which includes the following report types:

- TECHNICAL PUBLICATION. Reports of completed research or a major significant phase of research that present the results of NASA programs and include extensive data or theoretical analysis. Includes compilations of significant scientific and technical data and information deemed to be of continuing reference value. NASA counter-part of peer-reviewed formal professional papers, but has less stringent limitations on manuscript length and extent of graphic presentations.

- TECHNICAL MEMORANDUM. Scientific and technical findings that are preliminary or of specialized interest, e.g., "quick-release" reports, working papers, and bibliographies that contain minimal annotation. Does not contain extensive analysis.

- CONTRACTOR REPORT. Scientific and technical findings by NASA-sponsored contractors and grantees.

- CONFERENCE PUBLICATION. Collected papers from scientific and technical conferences, symposia, seminars, or other meetings sponsored or co-sponsored by NASA.

- SPECIAL PUBLICATION. Scientific, technical, or historical information from NASA programs, projects, and missions, often concerned with subjects having substantial public interest.

- TECHNICAL TRANSLATION. English-language translations of foreign scientific and technical material pertinent to NASA's mission.

For more information about the NASA STI program, see the following:

- Access the NASA STI program home page at http://www.sti.nasa.gov

- E-mail your question to help@sti.nasa.gov

- Fax your question to the NASA STI Information Desk at 757-864-6500

- Telephone the NASA STI Information Desk at 757-864-9658

- Write to:
  NASA STI Program
  Mail Stop 148
  NASA Langley Research Center
  Hampton, VA 23681-2199

Grainex Mar-M 247 Turbine Disk Life Study for NASA's High Temperature High Speed Turbine Seal Test Facility

Irebert R. Delgado
U.S. Army Research Laboratory, Glenn Research Center, Cleveland, Ohio

National Aeronautics and
Space Administration

Glenn Research Center
Cleveland, Ohio 44135

April 2015

Acknowledgments

The author wishes to acknowledge the invaluable help of the following individuals:

Revised Copy

This Revised Copy, numbered as NASA/TM—2005-213873/REV1, April 2015, supersedes the previous version, NASA/TM—2005-213873, October 2005, in its entirety.

Appendixes A to D have been inserted into the Contents and report. Citations to the appendixes have been inserted on pages 24, 39, 57, and 85.

Contents

List of Abbreviations

Symbol	Description	Units
$2L_{pctr}$	center potential probe spacing	[mm]
$2L_{pmax}$	maximum potential probe spacing	[mm]
$2L_{pmin}$	minimum potential probe spacing	[mm]
$2N_f$	reversals to failure	
$2r_{0\varepsilon}$	plastic zone size diameter under plane strain conditions	[mm]
$2r_{0\sigma}$	plastic zone size diameter under plane stress conditions	[mm]
$A_{649°C}$	gage section area at 649°C	[m²]
A_f	final gage section area	[m²]
A_i	initial gage section area	[m²]
a	desired percentile level	
a_c	crack depth	[mm]
a_{crit}	critical crack depth	[mm]
a_i	lowest detectable crack depth	[mm]
a_n	initial EDM crack depth	[mm]
b	fatigue strength exponent	
b_c	crack half-height	[mm]
b_n	initial crack half-height	[mm]
C	constant coefficient for Paris model	$\left[\dfrac{mm/cycle}{\left(MPa\sqrt{m}\right)^m}\right]$
$C1$	constant coefficient for elastic term of Method of Universal Slopes model	
$C2$	constant coefficient for plastic term of Method of Universal Slopes model	
c	fatigue ductility exponent	
c_c	crack surface half-width	[mm]
c_n	initial crack surface half-width	[mm]
$D_{21°C}$	gage section diameter at 21°C	[mm]
$D_{649°C}$	gage section diameter at 649°C	[mm]
E	Young's Modulus	[GPa]
F	F-table value	
F_s	boundary correction factor	
F^*	test statistic	
$\hat{F}$	dimensionless geometry factor	
h	half-height of K_b specimen gage section from EDM notch	[mm]
K	stress-intensity factor	[MPa$\sqrt{m}$]
k	transfer function	
K_I	stress-intensity factor (Mode I)	[MPa$\sqrt{m}$]
K_b	surface flawed fatigue crack growth specimen	
K_c	critical fracture toughness	[MPa$\sqrt{m}$]
K_{IC}	critical fracture toughness (Mode I)	[MPa$\sqrt{m}$]

K_{max}	maximum stress-intensity factor	$[\text{MPa}\sqrt{m}]$
L_f	final gage section length	[mm]
L_i	initial gage section length	[mm]
L_p	potential probe spacing half-width	[mm]
m	constant exponent for Paris model	
N	cycle	
N_f	cycles to failure	[cycles]
N_{fm}	cycles to failure in presence of mean stress	[cycles]
N_{f0}	cycles to failure under zero mean stress	[cycles]
N_i	cycles to crack initiation	[cycles]
N_t	transition life	
n_1	number of data points for data set 1	
n_2	number of data points for data set 2	
P	load	[N]
P_{max}	maximum load	[N]
$P_{\varepsilon=0.2\ percent}$	load at 0.2 percent strain	[N]
Q	shape factor	
R	load ratio	
R_ε	strain ratio = $(\varepsilon_{min}/\varepsilon_{max})$	
R_σ	stress ratio = $(\sigma_{min}/\sigma_{max})$	
R^2	coefficient of determination	
SSE(F)	sum of the squares of the errors of the full model	
SSE(R)	sum of the squares of the errors of the reduced model	
s	remote uniform tensile stress	[MPa]
t	through thickness of fatigue crack growth specimen	[mm]
V	crack length voltage	[volts]
V_{eff}	effective ratio of mean stress to stress amplitude	
V_N	reference voltage for fatigue crack growth tests	[volts]
V_σ	ratio of mean stress to stress amplitude	
w	width of fatigue crack growth specimen gage section	[mm]
X_{ij}	independent variable of the reduced statistical model	
Y_{ij}	predicted value of the reduced statistical model	
Z	constant coefficient	
$\dfrac{da_c}{dN}$	fatigue crack growth rate	[mm/cycle]
Δa	incremental striation spacing	[mm]
ΔK	stress intensity range	$[\text{MPa}\sqrt{m}]$
ΔK_c	critical fracture toughness range	$[\text{MPa}\sqrt{m}]$
ΔK_{th}	fatigue threshold stress intensity range	$[\text{MPa}\sqrt{m}]$
ΔT	temperature differential from 21°C to 649°C	[°C]
$\Delta\varepsilon$	total strain range	
$\dfrac{\Delta\varepsilon}{2}$	strain amplitude	

$\Delta \varepsilon_{el}$	elastic strain range	
$\dfrac{\Delta \varepsilon_{el}}{2}$	elastic strain amplitude	
$\Delta \varepsilon_{in}$	inelastic strain range	
$\dfrac{\Delta \varepsilon_{in}}{2}$	inelastic strain amplitude	
$\Delta \sigma$	stress range	[MPa]
$\alpha_{649\,°C}$	thermal expansion coefficient at 649°C	[m/m/°C]
$\beta 0$	intercept of the reduced statistical model	
$\beta 1$	slope of the reduced statistical model	
δ	crack tip opening displacement	[mm]
ε	strain	[m/m]
ε_{ij}	error term of the reduced statistical model	
ε_{min}	minimum strain	
ε_{max}	maximum strain	
ε_a	strain amplitude	
ε_f	true fracture ductility	
ε_f'	fatigue ductility coefficient	
$\tilde{\varepsilon}_f$	true fracture strain	
ϕ	ellipse parametric angle	[radians]
π	pi	
σ	stress	[MPa]
σ_a	stress amplitude	[MPa]
σ_f	engineering fracture stress	[MPa]
σ_f'	fatigue strength coefficient	[MPa]
$\tilde{\sigma}_f$	true fracture strength	[MPa]
σ_m	mean stress	[MPa]
σ_{max}	maximum stress during cycling	[MPa]
σ_{min}	minimum stress during cycling	[MPa]
σ_{UTS}	ultimate tensile strength	[MPa]
$\sigma_{y(0.2\ percent)}$	0.2 percent offset yield strength	[MPa]
ζ	constant exponent	
%EL	percent elongation	
%RA	percent reduction in area	
%$\Delta \varepsilon$	percent total strain	

Grainex Mar-M 247 Turbine Disk Life Study for NASA's High Temperature High Speed Turbine Seal Test Facility

Irebert R. Delgado
U.S. Army Research Laboratory
Glenn Research Center
Cleveland, Ohio 44135

Abstract

An experimental and analytical fatigue life study was performed on the Grainex Mar-M 247 disk used in NASA's Turbine Seal test facility. To preclude fatigue cracks from growing to critical size in the NASA disk bolt holes due to cyclic loading at severe test conditions, a retirement-for-cause methodology was adopted to detect and monitor cracks within the bolt holes using eddy-current inspection.

For the NASA disk material that was tested, the fatigue strain-life to crack initiation at a total strain of 0.5%, a minimum to maximum strain ratio of 0, and a bolt hole temperature of 649°C was calculated to be 665 cycles using -99.95% prediction intervals. The fatigue crack propagation life was calculated to be 367 cycles after implementing a safety factor of 2 on life. Thus, the NASA disk bolt hole total life or retirement life was determined to be 1032 cycles at a crack depth of 0.501 mm. An initial NASA disk bolt hole inspection at 665 cycles is suggested with 50 cycle inspection intervals thereafter to monitor fatigue crack growth.

1. Introduction, Background, Objective

1.1   Introduction

The High Temperature High Speed Turbine Seal test facility, located at NASA Glenn Research Center (NASA GRC) in Cleveland, Ohio provides a critical research capability in testing gas path air seals, such as labyrinth, brush, or finger seals, for next generation aircraft engines. Engine seals are located in the compressor and turbine engine sections as well as in the secondary flow areas and serve to minimize unwanted air leakage across blades tips and rims as well as main shafts. By maintaining a close clearance, they help to reduce specific fuel consumption and thereby aid in reducing direct operating costs.[1] The turbine seal test stand (Figure 1.1) can test candidate seal designs at high temperatures, high seal pressures, and surface speeds greater than 300 m/s.

Figure 1.1 NASA's turbine seal test facility.

The test facility uses a disk made of Grainex Mar-M 247 (hereafter called the NASA disk). It is a cast nickel based superalloy whose outer diameter is in contact with or is within close proximity of the test seal inner diameter. The Grainex Mar-M 247 material's high strength and creep resistance at temperatures between 150 to 1500°C make it an excellent material for turbine blades, vanes, and disks.[2]

Because the NASA disk experiences a severe test combination of high temperature, high pressure, and high speed, the possibility exists that fatigue cracks will develop with cycling at the 6 bolt hole locations, which fasten it to the main shaft of the turbine seal test stand. If allowed to grow to a critical size, the cracks could cause the NASA disk to catastrophically burst during use.

Preliminary analyses by Tong and Steinetz[3] have placed a strain-life limit, L_{sys}, of 6000 cycles based upon an equivalent -3σ reduction factor and a probabilistic approach[4] accounting for n = 6 bolt holes:

$$L_{sys} = \frac{L}{n^{\frac{1}{e}}}$$
                                                                    Eqn. 1.1   (Ref. 4)

where L_{sys} = overall system life
                       L   = calculated NASA disk life   = 10,000 cycles
                       n   =   number of bolt holes   = 6
                       e   = Weibull slope parameter = 3.57 (Gaussian Distribution)

Eqn. 1.1 is based on the Lundberg-Palmgren[4] analysis for rolling element bearing system lives. L is the predicted life for a disk with a single bolt hole. The predicted life, L, and Weibull slope parameter, e, are assumed to be identical for

all six disk bolt holes. However, the preliminary analysis does not address the existence of a crack at the bolt hole surface which, if allowed to grow to a critical size, would lead to a catastrophic NASA disk failure in the turbine seal test rig.

The 1996 engine failure of an MD-88 during take-off was a specific example of an uncontained disk failure resulting from a pre-existent crack.[5] During take-off the hub section of the Pratt & Whitney JT8D-219 engine separated from its low-pressure compressor section. The hub failure released high energy blade and engine fragments (Figure 1.2) which broke through the engine structure and penetrated the plane's main cabin killing 2 of the passengers. Metallurgical examination of the origin of the hub failure revealed a 25 mm crack found within one of the twenty-four 12.7 mm diameter tierod bolt holes which secure the hub to the low-pressure compressor (Figure 1.2). The crack was described by a National Transportation and Safety Board senior metallurgist as a "progressive crack that increased with time".[5] Inspection records indicated that the hub had accumulated approximately 13,000 cycles of an expected 20,000 cycles to replacement, a cycle being defined as a takeoff and touchdown. The hub had been visually inspected six months before using a dye penetrant procedure that should have indicated the presence of any cracks.[5]

The crack may have been missed during inspection or may have developed in the following months of engine operation. The consequences of such fatigue failures strongly emphasize the need to accurately detect the presence, location, and size of a crack within a structure and then to assess the integrity of that structure for further operation. Similarly, cracks within the bolt holes of the NASA disk of the turbine seal test facility may develop and grow over time with increasing number of cycles. NASA disk cycles are defined as a ramp up and down in speed at constant test air temperature and pressure.
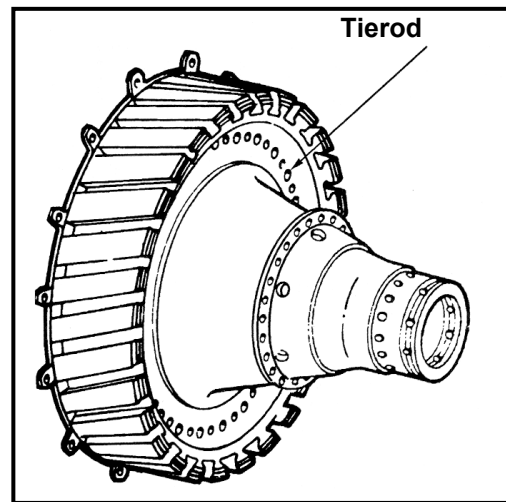
Figure 1.2 Uncontained failure of an engine hub with the crack location at the tierod holes of a Pratt & Whitney JT8D-219 engine.[5]

The process of regularly inspecting a critical component to detect the presence, location, and size of a crack is usually accomplished through non-destructive inspection methods, such as eddy-current inspection. Using strain-life and fatigue crack growth data, the cycles to crack initiation and failure can be determined. From this data, the inspection frequency and an appropriate NASA disk retirement criteria (i.e. crack length) can be determined.

Eddy-current inspection is based on electromagnetic induction principles, and is used to detect microscopic cracks at or near a material's surface. A wire coiled probe (Figure 1.3), containing an alternating current, is normally inserted into the disk bolt holes. Any surface or subsurface cracks can be sensed by the coil. A reference sample of the same material with a mechanically produced crack is used for comparison.[6]
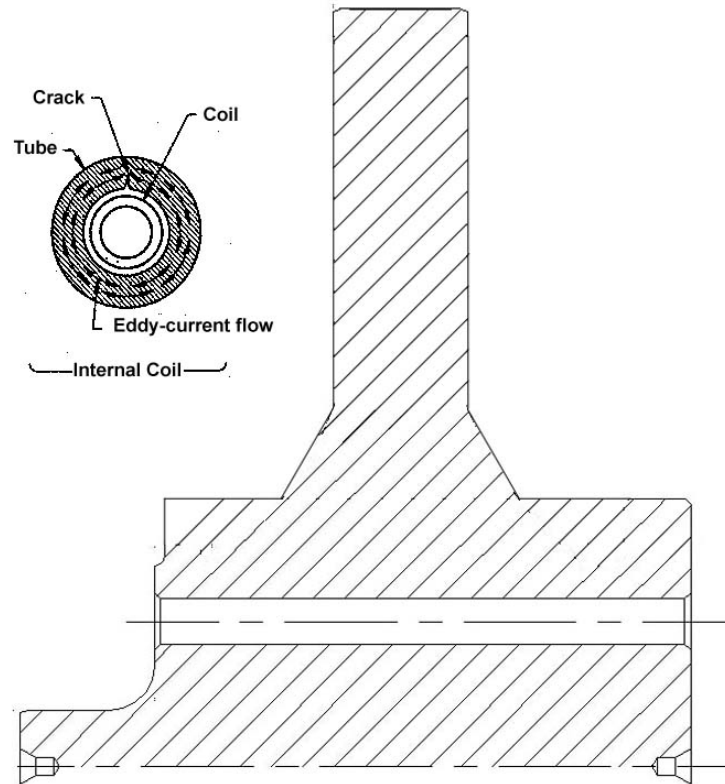
Figure 1.3 Eddy-Current inspection of disk bolt holes using a Bobbin-Type coil.[6]

The detection of cracks on aircraft engine components through eddy-current inspection is part of a fracture control philosophy in which critical engine parts are designed based upon a damage tolerance approach. This requires that a fracture critical part is still functional even though microscopic cracks, introduced during manufacture or service, are present. The Air Force's Engine Structural Integrity Program is an example of one program that has adopted this damage tolerance philosophy.[7] Damage tolerant approaches fit under fail-safe design methodologies which hold the view that a crack will not be allowed to grow to critical size within a component before it can be inspected and either replaced or repaired.[7]

1.2 Objectives

The Grainex Mar-M 247 NASA disk in the turbine seal test rig can be considered as the fracture critical component that may contain a defect that could grow to critical size during service. A damage tolerant approach for the NASA disk would require an inspection interval to monitor the growth of cracks within the bolt holes and would also require a critical crack length criterion from which to retire the NASA disk from service.

This study proposes a damage tolerant approach to monitoring the presence and growth of cracks within the bolt holes of the NASA disk. Fatigue crack-initiation and fatigue crack growth lives would be experimentally determined to obtain a total fatigue life for the NASA disk and an appropriate inspection interval.

Little has been published on the strain-life and fatigue crack growth of Grainex Mar-M 247, particularly at the 649°C operating temperature of interest.[8,9,10,11,12,13] The goals of the study were two-fold.

1. Determine the crack initiation life of the NASA disk, at various strain ratios, using experimentally determined strain-life fatigue behavior at its maximum operational test temperature. Conduct a statistical analysis of the test data to bound the fatigue life within known prediction limits.
2. Experimentally determine the critical crack size of the NASA disk and use the results to determine an eddy-current inspection interval. Perform a statistical analysis of the crack-growth data to determine the fit of the data to the Paris[14] relation.

1.3 Benefits of Study

The study will primarily benefit the safe operation of the turbine seal test facility. Specifically:

1. The study will result in a damage tolerant approach to monitoring the growth of cracks in the NASA disk bolt holes through scheduled eddy-current inspection.
2. The total life of the NASA disk, crack initiation and crack growth, will be statistically calculated to support the inspection interval placed on the bolt holes.

Chapter 1 Works Cited

1. Ludwig, Lawrence P., and Robert C. Bill. "Gas Path Sealing in Turbine Engines." ASLE Transactions 23.1 (1978):1-5.
2. Davis, Joseph R., ed. Heat Resistant Materials. Materials Park: ASM International, 1997.
3. Tong, Mike and Bruce Steinetz. "Mar-M 247 Disk Finite Element Thermal and Stress Analysis", NASA Glenn Research Center, Cleveland. 30 January 1997.
4. Melis, M.E., E.V. Zaretsky, and R. August. "Probabilistic Analysis of Aircraft Gas Turbine Disk Life and Reliability." Journal of Propulsion and Power, 15.5 (1999) 658-666.
5. Ott, James. "JT8D Hub Failure Sparks Intense Inquiry." Aviation Week & Space Technology, 15 July 1996: 29+.
6. ASM International Handbook Committee. "Eddy-Current Inspection." Metals Handbook 9th Edition Volume 17: Nondestructive Evaluation and Quality Control. Metals Park: ASM International, 1989. 164+.
7. Cowie, William D. "Fracture Control Philosophy." Metals Handbook 9th Edition Volume 17: Non-Destructive Evaluation and Quality Control. Metals Park: ASM International, 1989. 666+.
8. Howmet Turbine Components Corporation. TB 3000: Grainex Cast Mar-M 247 Alloy. Greenwich: Howmet Turbine Components Corporation.
9. Macha, D.E., G.R. Cole, and J.A. Butzer. "Fine Grain, Investment-Cast Integral Turbine Wheels." Grain Refinement in Castings and Welds. Ed. G.J. Abbaschian and S.A. David. New York: The Metallurgical Society of AIME, 1983. 197-219.
10. Kaufman, M. "Properties of Cast Mar-M-247 for Turbine Blisk Applications." Superalloys 1984. Ed. Maurice Gell et al. Warrendale: Metallurgical Society of AIME, 1984. 43-52.
11. "Microcast-X Mar-M 247." Alloy Digest May 1995.
12. Helmink, R.C. et. al. "Advanced Superalloys and Tailored Microstructures for Integrally Cast Turbine Wheels." Superalloys 2000. Ed. T.M Pollock et al. Warrendale: TMS, 2000. 171-179.
13. MacIntyre, Cal A. and P. Neil Agarwal. "Development of Fine Grain Cast Mar-M 247 Axial and Radial Turbine Wheels." Advanced Aerospace Materials Technology: SP-597. Warrendale: Society of Automotive Engineers, Inc., 1984. 35-45.
14. Dowling, Norman E. Mechanical Behavior of Materials : engineering methods for deformation, fracture, and fatigue. Upper Saddle River: Prentice-Hall, Inc., 1999.

2. Background on Grainex Mar-M 247

2.1 Grainex Mar-M 247 Material

Grainex Mar-M 247 is a class of cast nickel-based superalloys (Figure 2.1) and is primarily used in gas turbine engine components such as turbine blades, turbine disks, burner cans, and vanes.[1] In general 90 percent of superalloys produced are used for gas turbine engines and approximately half of the engine weight is composed of nickel-based superalloys.[1] Superalloys are well suited for jet engine applications where they generally operate from 540°C to over 80% of their melting temperature.[1] Additionally they retain their strength at these temperatures while providing creep and corrosion resistance.[1]
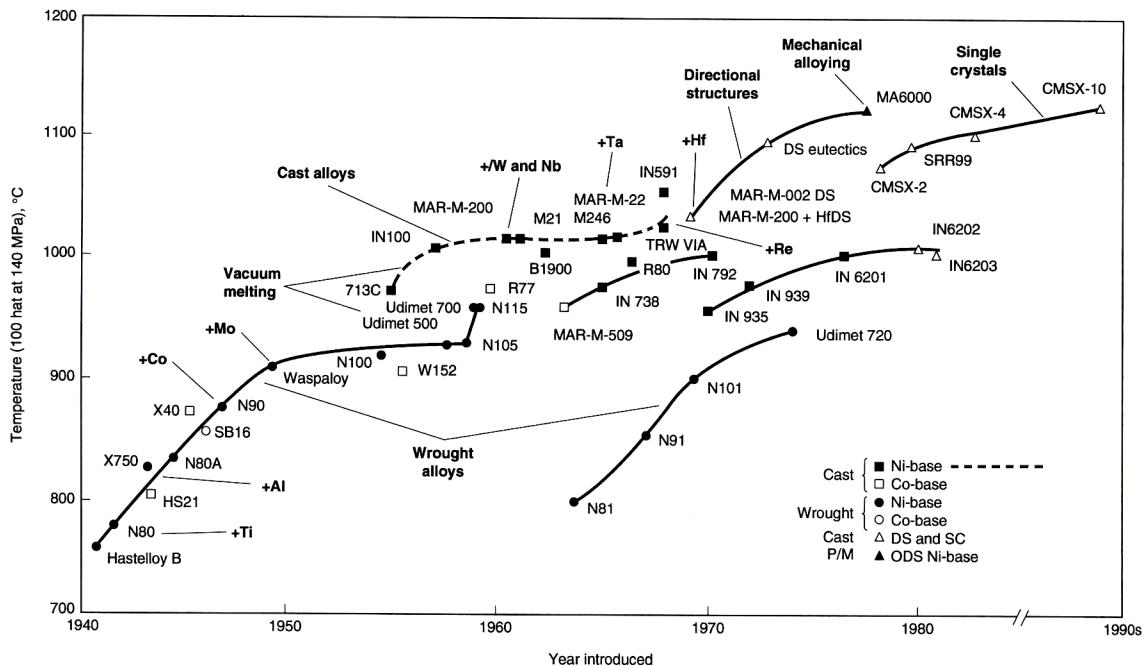
Figure 2.1 Grainex Mar-M 247 is part of the family of superalloys represented by the dashed line.[1]

2.2 Material Processing and Microstructure

The Mar-M 247 alloy (Table 2.1) was developed in the 1970s by Danesi and Thieleman.[2] It is manufactured by melting and investment casting under vacuum In contrast to wrought superalloys, cast superalloys exhibit improved creep and rupture characteristics due to coarser grain sizes and alloy segregation. However, the larger grain sizes reduce ductility and lower cyclic fatigue life.[3] Also, columnar grains are found in thin sections such as turbine disks (Figure 2.2) and blades resulting in material properties inconsistent with those found in the disk hub.

Table 2.1 Nominal chemical composition of Mar-M 247 alloy [4]

Element	Wt%	Element	Wt%	Element	Wt%
Co	10	Ta	3	C	0.16
W	10	Hf	1.5	Zr	0.05
Cr	8.2	Ti	1	B	0.015
Al	5.5	Mo	0.6	Ni	Balance
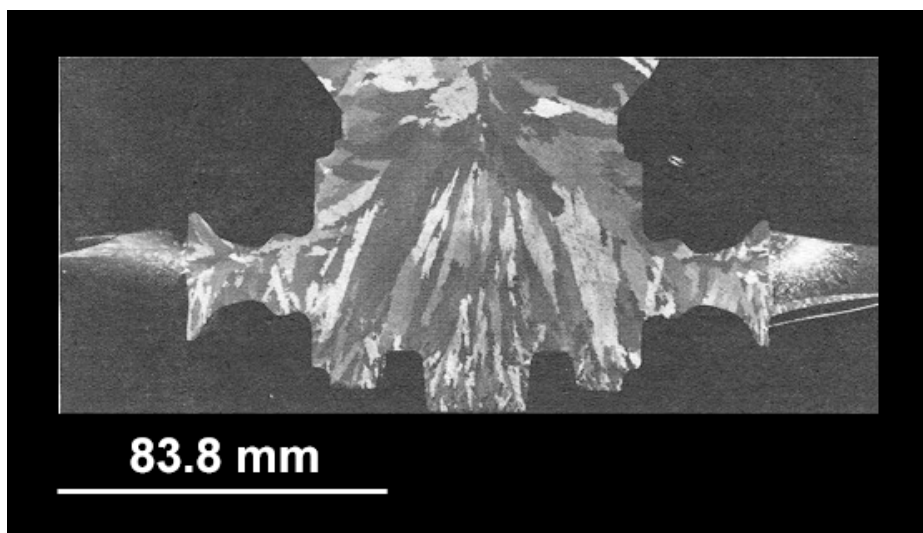
Figure 2.2 Conventionally cast Mar-M 247 macrostructure showing coarse, columnar oriented grains.[4]

The NASA Mar-M 247 test rotor was made through the Grainex investment casting process.[5] The Grainex process was developed by Howmet Turbine Components Corporation in the early 1980s and uses traditional investment casting processes in combination with mold-agitation during solidification to produce an equiaxed grain structure that results in more consistent material properties throughout the casting (Figure 2.3).[4]
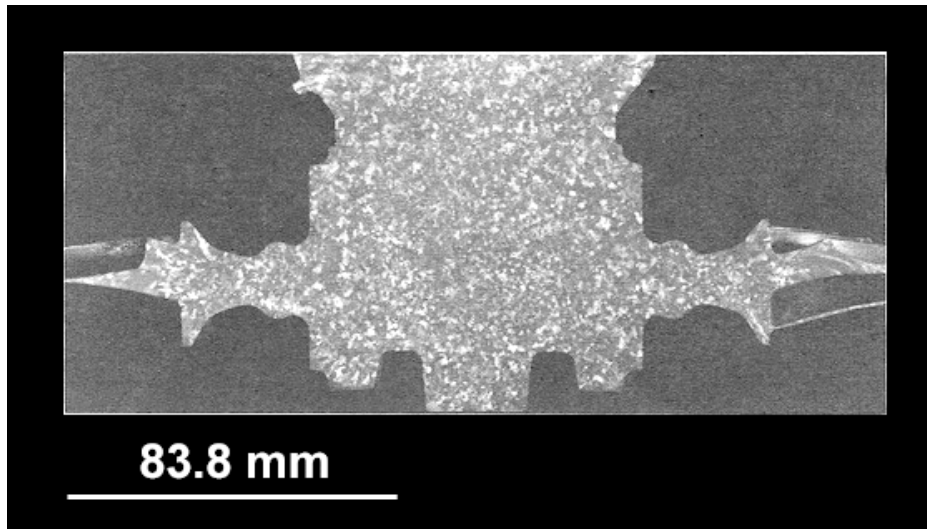
Figure 2.3 Grainex cast Mar-M 247 macrostructure showing fine, equiaxed grains.[4]

Investment casting is preferred over wrought processing for complex turbine engine components in that it produces near net shape structures. Following solidification, the casting is mechanically separated from its ceramic mold and then radiographically or ultrasonically inspected for cracks, pores or tears which would negatively affect material properties. Prior to final machining, the casting is hot-isostatic pressed (HIP) at 1185°C and 172 MPa for 4 hours, solution treated at 1185°C for 2 hours, and aged at 871°C for 20 hours. The HIP process reduces the porosity inherent in the investment casting process. Minimizing porosity reduces possible crack initiation sites and improves material fatigue life. Solution treating the casting homogenizes the microstructure to an austenitic FCC γ-phase matrix. Strengthening of the alloy is derived from solid solution strengthening constituents including Co, Cr, Mo, W, and Ta.[1] The aging process precipitates a coherent γ' phase [Ni$_3$,(Al,Ti)] which gives primary strengthening and improves tensile and creep-rupture properties.[1]

A number of sub-structures within the Grainex Mar-M 247 material serve major roles in strengthening or weakening the material. Metal carbides (M$_x$C$_y$) serve to strengthen grain boundaries, strengthen the γ matrix through precipitation of fine carbides, and combine with elements to promote phase stability.[1] For example, discontinuous M$_{23}$C$_6$ (M = Cr, Ni-Co, Mo, W) provides grain boundary strengthening by inhibiting the movement of grains thereby improving rupture strength. Borides serve as grain boundary strengtheners particularly under creep rupture loading.[6] Surface oxidation resistance is provided by scale build-up of Cr$_2$O$_3$ and Al$_2$O$_3$. However, metal carbide failure may occur by fracture of the M$_{23}$C$_6$ particle or by decohesion.[1] Topologically

closed-pack phases are harmful structures that deplete refractory elements which ultimately reduces creep rupture strength. Found primarily as grain boundary carbides they appear as long plates or needles and contribute to premature cracking due to their hard, brittle nature.[6]

2.3   Material Properties

2.3.1   Literature Review

   While much has been written on Mar-M 247, only a small number of references have been found on Grainex Mar-M 247 that report tensile, strain-life, and fatigue crack growth data.

2.3.2   Tensile Behavior

   Tensile properties determined from specimens taken from the rim of turbine disks show that Grainex Mar-M 247 is equal to if not better than the conventionally cast Mar-M 247 through 760°C (Figure 2.4).[4] The ultimate tensile strength for Grainex Mar-M 247 is 1034 MPa at room temperature and increases slightly through 760°C while that for conventionally cast Mar-M 247 is no higher than 1000 MPa. Also, the 0.2% offset yield strength for Grainex Mar-M 247 is 828 MPa from room temperature through 760°C while that for conventionally cast Mar-M 247 begins to fall off after 500°C. Finally, reduction in area and elongation for both Grainex and conventionally cast Mar-M 247 decrease above 482°C. Other sources cite comparable tensile properties for Grainex Mar-M 247.[7,8,9] Macha et. al. and Kaufman report Young's Modulus decreasing with increasing temperature (Table 2.2).
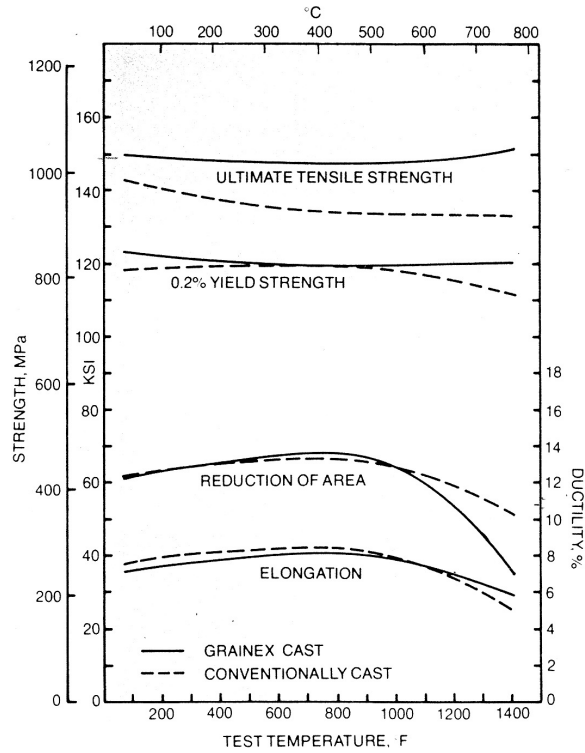
Figure 2.4 Comparison of tensile properties of Grainex Mar-M 247 and conventionally cast Mar-M 247.[4]

Table 2.2 Comparison of Young's modulus for Grainex Mar-M 247 at various temperatures

	Source	
	Macha et al. [7]	Kaufman[8]
Temp [°C]	E [MPa]	E [MPa]
21	226	n/a
204	n/a	210
427	205	203
760	n/a	175

2.3.3 Strain-Life Behavior

Strain-life data reported by Macha et al. at 427°C and R_ε = -1 (Figure 2.5)[7] for Grainex cast Mar-M 247 show a slight increase in cyclic fatigue life at the -3σ property line at higher strain ranges when compared to conventionally cast Mar-M 247. Kaufman reports Grainex Mar-M 247 data for R_ε = 0 at 204°C, 427°C, and 760°C (Figure 2.6).[8] As expected, lower cyclic lives result from increasing temperature for a constant strain range. Finally strain-life data reported by Helmink et al. for Grainex Mar-M 247 at 538°C (Figure 2.7)[10] is slightly better in comparison with directionally-solidified Mar-M 247.
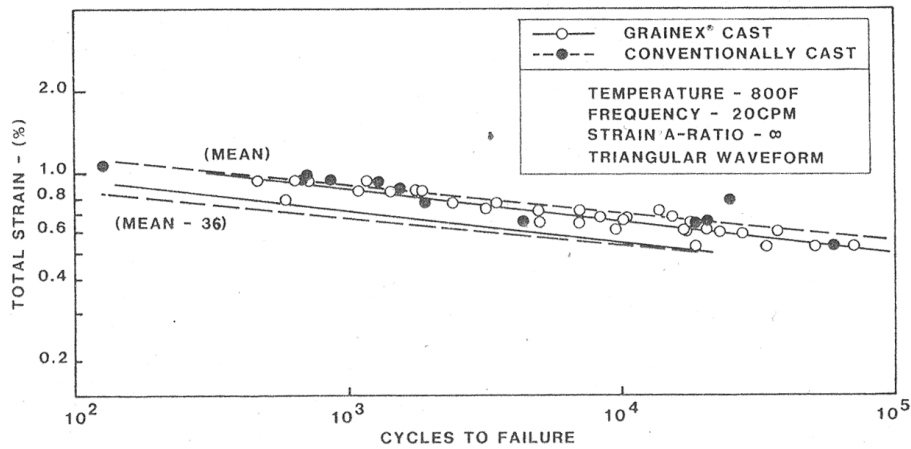
Figure 2.5   Grainex Mar-M 247 strain-life data at 427°C per Macha et al., R_ε = -1.[7]
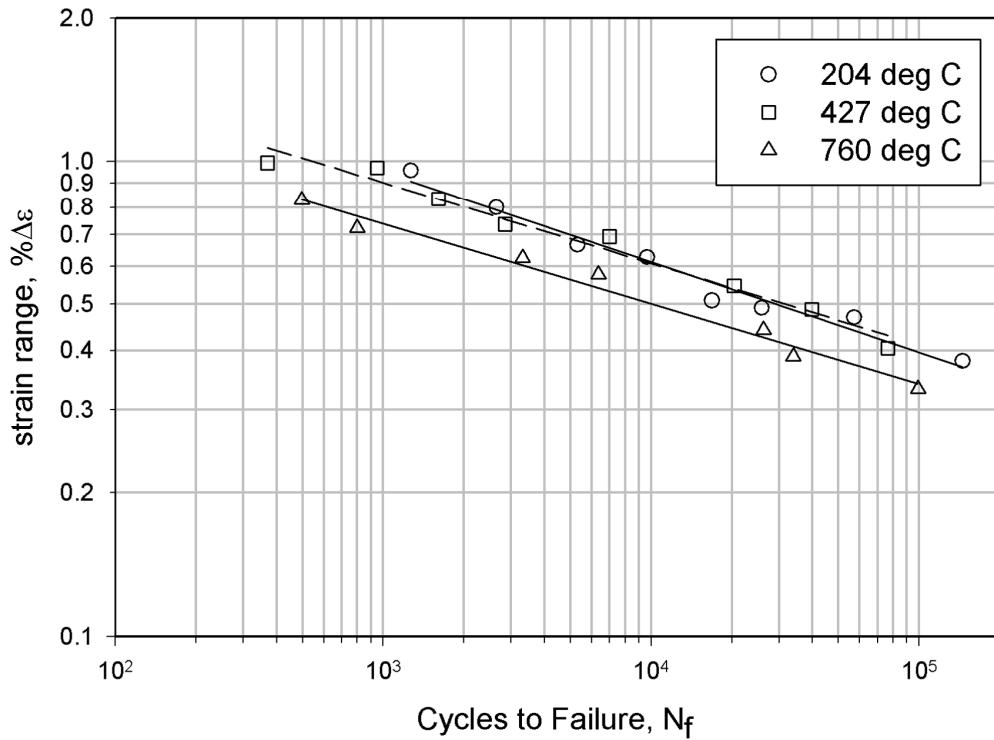
Figure 2.6 Grainex Mar-M 247 strain-life data per Kaufman at $R_\varepsilon = 1$.[8]
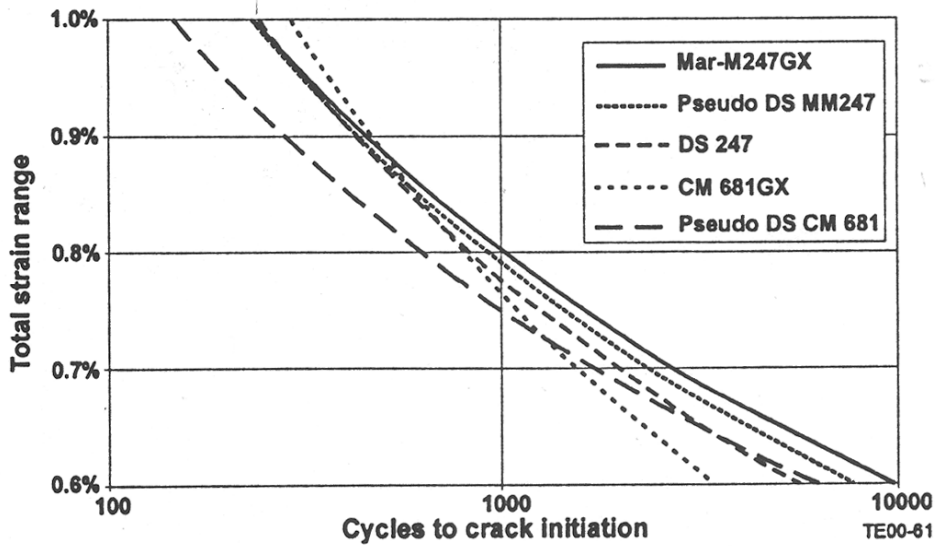
Figure 2.7 Strain-Life data per Helmink et al. at 538°C.[10]

2.3.4 Fatigue crack-growth data

Grainex Mar-M 247 shows a lower fatigue crack-growth rate for a constant stress intensity range than both conventionally cast Mar-M 247 at 427°C (Figure 2.8), as reported by Macha et al.[7] and for Inco 713LC at 538°C (Figure 2.9) as reported by MacIntyre et al.[11] Finally, the Grainex Mar-M 247 fatigue crack growth rate compares similarly with those of materials CM 681 and CM 681A at 538°C (Figure 2.10), as reported by Helmink et al.[10] However no fatigue crack-growth data were available at 649°C and greater than 300 m/s operating condition which is needed to determine a critical crack length for the NASA Grainex Mar-M 247 disk.
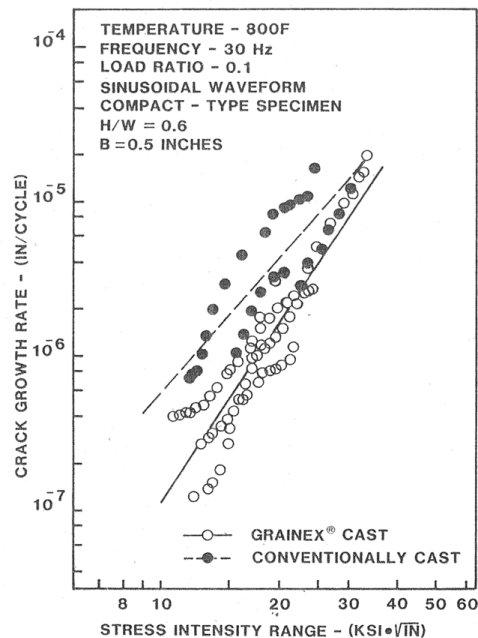
Figure 2.8 Comparison of Grainex Mar-M 247 and conventionally cast Mar-M 247 fatigue crack growth data per Macha et al. at 427°C.[7]
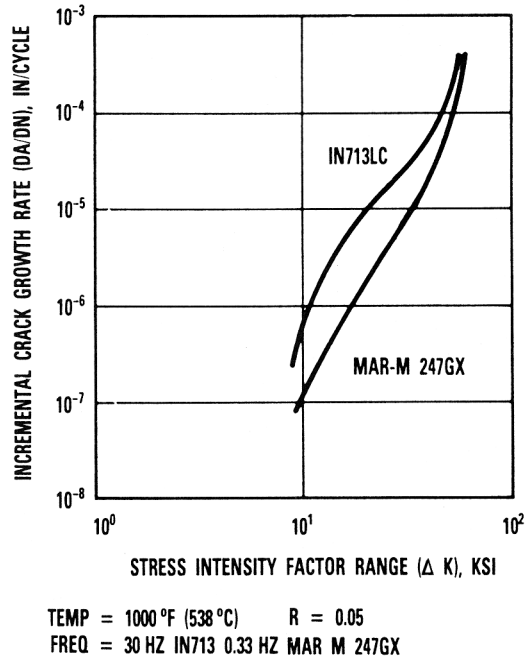
Figure 2.9 Comparison of Grainex Mar-M 247 and IN713LC fatigue crack-growth data at 538°C per MacIntyre et al.[11]
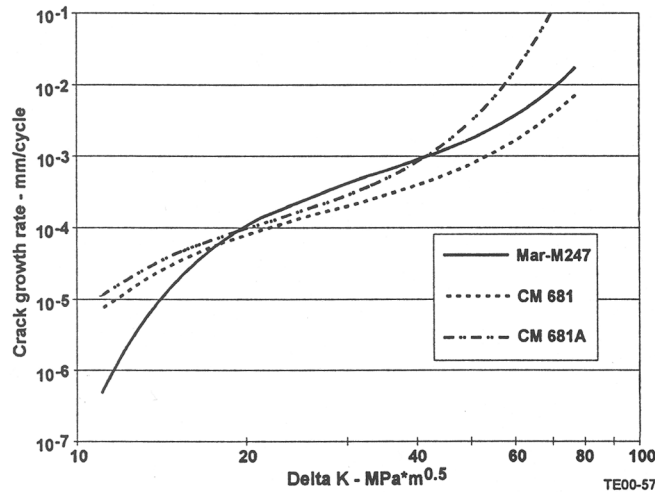
Figure 2.10 Comparison of Grainex Mar-M 247 data with CM681 and CM681A fatigue crack-growth data at 538°C per Helmink et al.[10]

Chapter 2 Works Cited

1. Davis, Joseph R., ed. <u>Heat Resistant Materials</u>. Materials Park: ASM International, 1997.
2. United States Patent and Trademark Office. <u>U.S. Patent 3720509: Nickel Base Alloy</u>. By Danesi, Wilbert P. and Rudolph H. Thielemann. 1973.
3. Freeman, William R., Jr. "Investment Casting." <u>Superalloys II</u>. Ed. Chester T. Sims et al. New York: John Wiley & Sons, Inc., 1987. 411-439.
4. Howmet Turbine Components Corporation. <u>TB 3000: Grainex Cast Mar-M 247 Alloy</u>. Greenwich: Howmet Turbine Components Corporation.
5. United States Patent and Trademark Office. <u>Trademark: Grainex, Registration No. 121275</u>. By Howmet Turbine Components Corporation. 1982.
6. Ross, Earl W., Chester T. Sims. "Nickel-Base Alloys." <u>Superalloys II</u>. Ed. Chester T. Sims et al. New York: John Wiley & Sons, Inc., 1987. 97-133.
7. Macha, D.E., G.R. Cole, and J.A. Butzer. "Fine Grain, Investment-Cast Integral Turbine Wheels." <u>Grain Refinement in Castings and Welds</u>. Ed. G.J. Abbaschian and S.A. David. New York: The Metallurgical Society of AIME, 1983. 197-219.
8. Kaufman, M. "Properties of Cast Mar-M-247 for Turbine Blisk Applications." <u>Superalloys 1984</u>. Ed. Maurice Gell et al. Warrendale: Metallurgical Society of AIME, 1984. 43-52.
9. "Microcast-X Mar-M 247." <u>Alloy Digest</u> May 1995.
10. Helmink, R.C. et. al. "Advanced Superalloys and Tailored Microstructures for Integrally Cast Turbine Wheels." <u>Superalloys 2000</u>. Ed. T.M Pollock et al. Warrendale: TMS, 2000. 171-179.
11. MacIntyre, Cal A. and P. Neil Agarwal. "Development of Fine Grain Cast Mar-M 247 Axial and Radial Turbine Wheels." <u>Advanced Aerospace Materials Technology: SP-597</u>. Warrendale: Society of Automotive Engineers, Inc., 1984. 35-45.

3. Material Sectioning Plan and Material Characterization

3.1 Sectioning Plan for the NASA Disk

A sacrificial Grainex Mar-M 247 NASA disk was cut-up for tensile, strain-life, and fatigue crack growth specimens following general guidelines:

1. A cross-section of the NASA disk from rim to centerline was used for metallurgical examination.
2. Tensile and strain-life specimens were taken in a randomized fashion throughout the hub and web sections (Figure 3.1a and Figure 3.1b).
3. Fatigue crack-growth specimens were taken as close to the bolt holes as possible since crack-initiation and growth were a concern within the bolt hole surfaces (Figure 3.1a) over repeated cycling at maximum operating conditions.
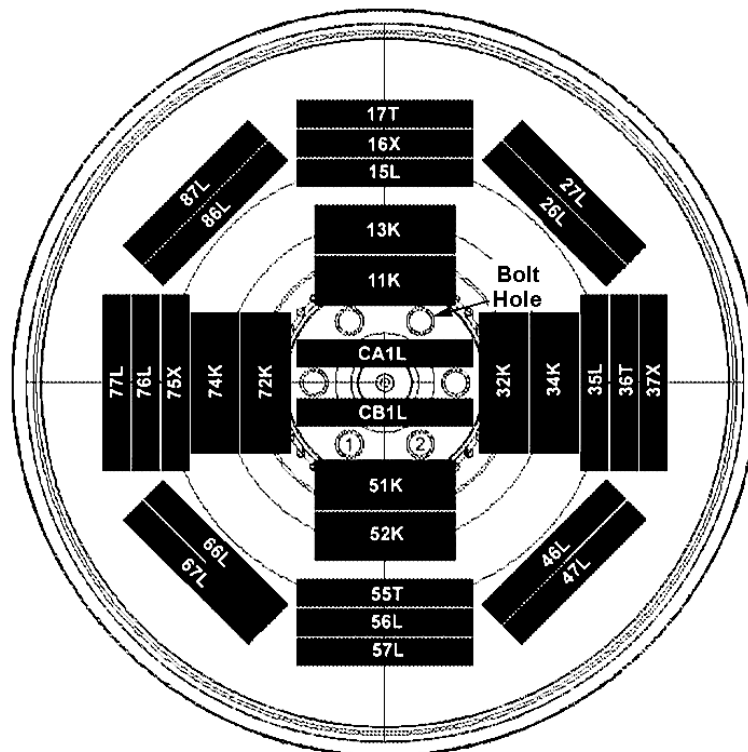
Figure 3.1a NASA disk specimen identification. Nomenclature: ##T = Tensile, ##K = fatigue crack-growth, ##X = extra, ##L = strain-life.
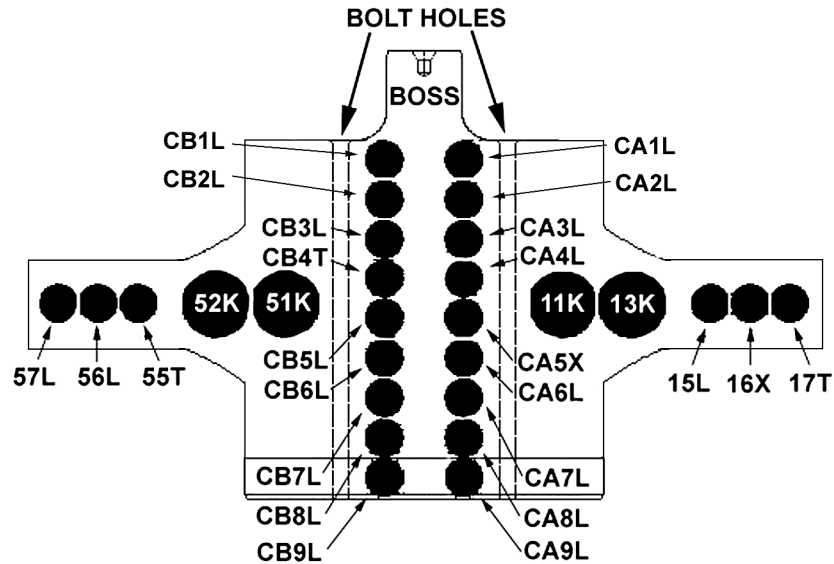
Figure 3.1b NASA disk specimen identification. Nomenclature: ##T = Tensile, ##K = fatigue crack-growth, ##X = extra, ##L = strain-life.

A total of four tensile specimens were also taken from the hub and web sections of the NASA disk. From statistical experimental design, 15 specimens were made for each strain-ratio ($R_\varepsilon = 0$ and $R_\varepsilon = -1$) with 3 repeats at each of 5 strain-ranges[1]. This complied with ASTM E606 suggested use of a minimum of 10 specimens to generate strain-life curves[2]. Minimum suggested strain-life specimens and percent replication were also followed per ASTM E739 and ASTM STP 588. Specifically, the 'design allowables' suggest a minimum of 12 to 24 strain-life specimens and a 50 to 75% replication. Thus, fifteen specimens with 3 repeats at 5 strain levels give a percent replication of 67% (ASTM STP 588):[3,4]

% replication = 100 [1 – (number of strain levels /total number of specimens)]

Eqn. 3.1

Finally, 8 fatigue crack growth (FCG) specimens were electro-discharged machined (EDM) near the bolt holes of the NASA disk.

3.2 Material Characterization

3.2.1 Objectives

   The metallurgical examination addressed the microstructure uniformity from the hub center to the rim of the NASA disk. Although the Grainex process gives a uniform, equiaxed grain structure resulting in uniform material properties, the relative difference in thickness between the hub and rim sections may cause the grain structure to vary. This is due to the relative cooling rates, during disk processing, from the thickest portion of the disk at the hub (slowest cooling) to its thinnest portion at the rim (fastest cooling). This may result in varying material properties. In a conventionally cast disk, differences in microstructure have resulted in varying tensile, strain-life, and fatigue crack-growth properties. [5] This was shown previously in Figure 2.4. Also, Figure 3.2 shows the variability in dynamic modulus for test specimens taken from different orientations from a conventionally cast disk of Mar-M 247. The data is compared to Grainex Mar-M 247 which shows minimal orientation effects on dynamic modulus. The effect of microstructural differences between Grainex and conventionally cast Mar-M 247 on fatigue strain life and fatigue crack growth was shown previously in Chapter 2 (Figure 2.5 and Figure 2.8).
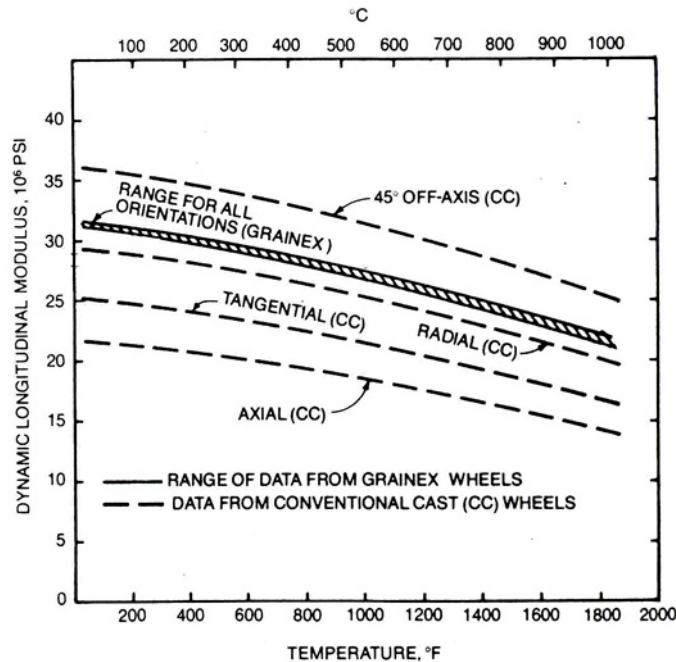
Figure 3.2 Comparison of the dynamic modulus of Grainex Mar-M 247 and conventionally cast Mar-M 247 specimens removed in the axial, radial, tangential and 45° off-axis orientation.[5]

The metallurgical examination addressed this concern for uniformity in microstructure specifically by:

1. Qualitatively assessing the differences in grain size, structure, and orientation from the NASA disk hub to rim.
2. Determining the extent of porosity in the microstructure from the hub to the rim of the NASA disk.

3.2.2 Procedure

<u>Chord-Slice Preparation</u>

A chord slice of the NASA disk was electro-discharge machined for the metallurgical examination. This included the two halves of the hub section, and 3 sections that accounted for the web and rim of the NASA disk (Figure 3.3 and Figure 3.4).
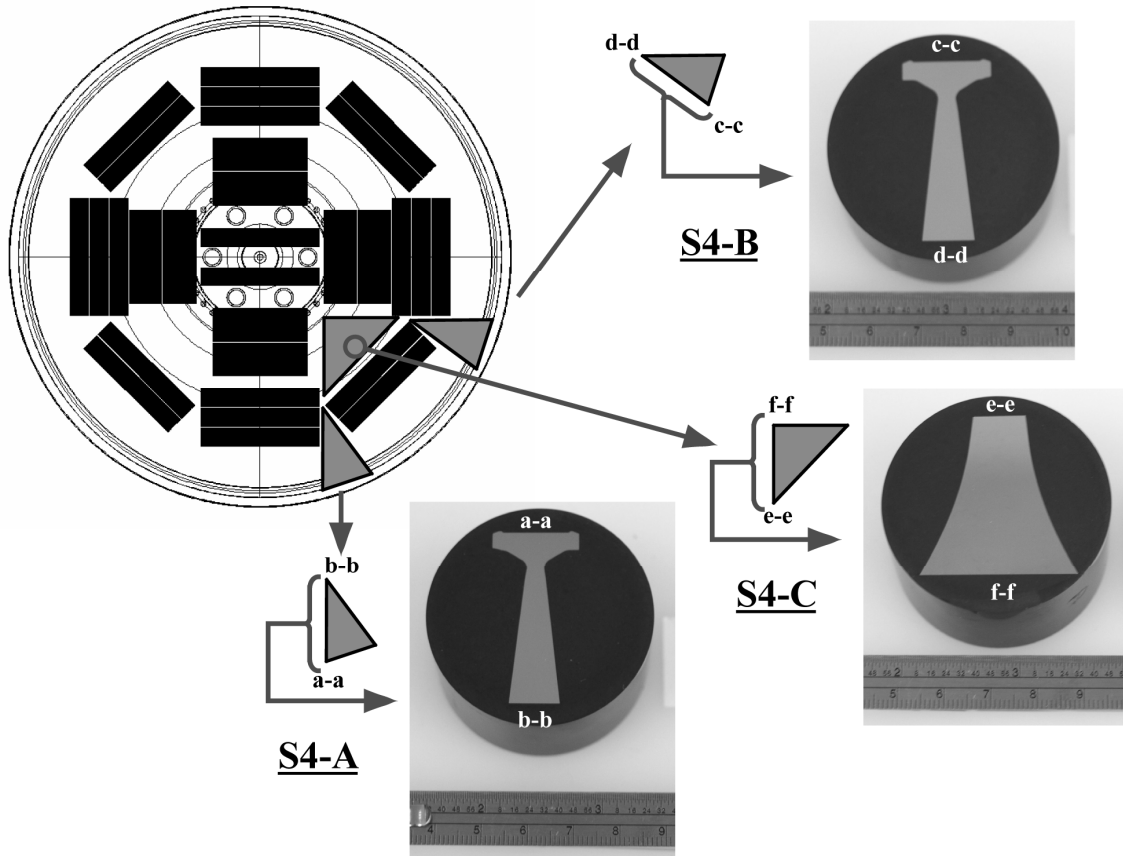
Figure 3.3 Cut-up and orientation of web and rim metallurgical specimens.
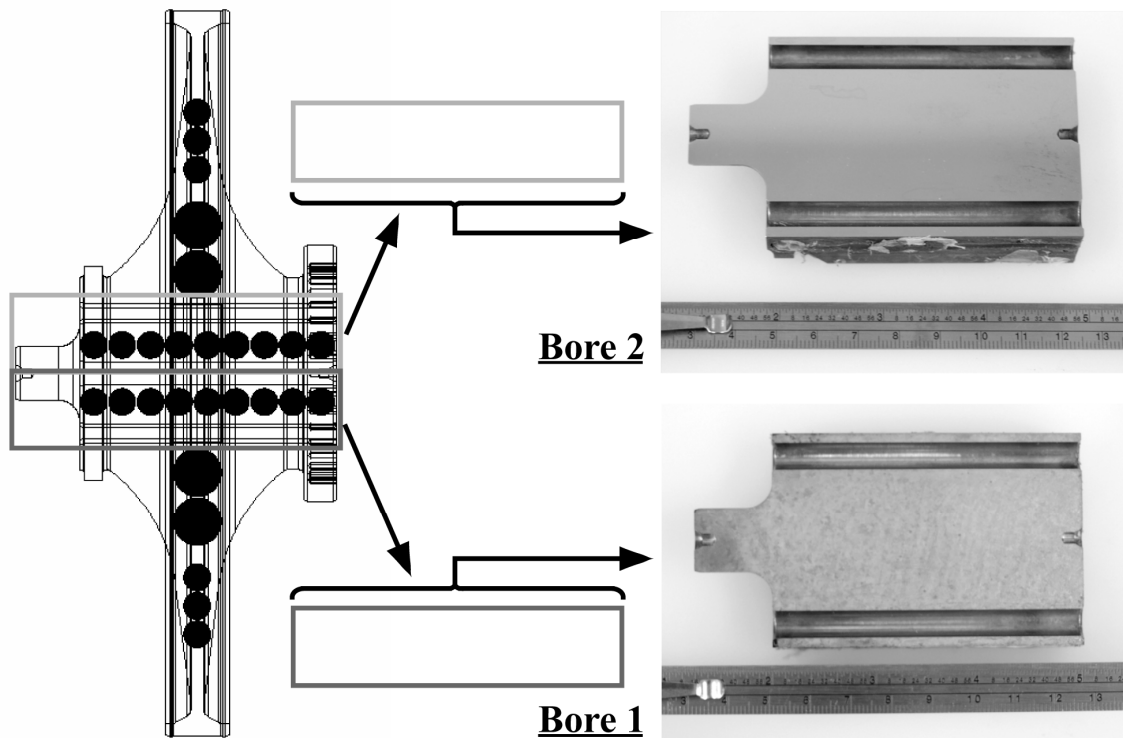
Figure 3.4 Cut-up and orientation of hub section metallurgical specimens.

The three web/rim pieces were mounted in Bakelite. The hub sections were mounted on special fixturing and polished. Polishing was performed following standard metallographic methods. The etchant used was a mixture of acetic acid, nitric acid, deionized water and hydrofluoric acid (HF).

Qualitative Assessment of Grain-Size
A light microscope was used to obtain photomicrographs of the microstructure. The photomicrographs were qualitatively compared with respect to overall grain size and orientation.

Qualitative Assessment of Porosity
Porosity, as defined in Mil-Std-1907, is a specific type of indication. Other types of indications include microstructural discontinuities such as inclusions, cracks, tears, cold shuts, microshrinkage, and phase segregation. Grade A requirements were used per section Mil-Std-1907 Section 4.1.1 for a highly stressed rotating cast component at high temperature.[6] Table 3.1 gives specific indications that were used for comparison.

Table 3.1 Mil-Std-1907 Grade A specifications for castings[6]

Indication	Criteria (mm)	Criteria (inch)
Cracks	reject	Reject
hot tears	reject	Reject
cold shuts	reject	Reject
non-metallic inclusions		
max dia	0.79	0.031
min separation = 3x	2.36	0.093
Shrinkage	6.35	0.250
Microshrinkage		
max dia	1.60	0.063
min separation = 3x	4.80	0.189
phase segregation		
Surface	3.18	0.125
Subsurface	6.35	0.250
gas holes		
max dia	0.79	0.031
min separation = 3x	2.36	0.093

Fluorescent dye penetrant inspection was performed on each chord slice following ASTM E1417, Method C, Level 4.[7] Any oils, dirt, or dust on the specimens were removed with alcohol. After air drying the specimens penetrant was applied and allowed to settle for 20 minutes. Excess penetrant was carefully removed and a developer applied to highlight any possible indications.

3.2.3 Results and Discussion of Chord Slice Examinations

Discussion of Grain Size Results
    The nominal grain size for Grainex Mar-M 247 is reported to range from 0.18 mm to 1.6 mm depending upon relative material thickness at specific locations on cast wheels for engine components (Table 3.2).[5]

Table 3.2 Grain sizes in various sections of Grainex cast integral wheels[5]

	Hub	Rim	Airfoil
Nominal Diameter (mm) (range-mm)	1.2 1.0 – 1.6	1.4 1.2 – 1.6	0.42 0.18 – 0.67
ASTM Macrograin Size Number	M10 – M9	M10 – M9	M15 – M11.5

Qualitative analysis of the grain size of the chord sections (Figure 3.3 and Figure 3.4) showed similar grain size and random orientation between chord sections (Figure 3.5 to Figure 3.7). Grain size was estimated from the photomicrographs to be 1.3 to 1.9 mm (Figure 3.6). The grain size was also comparable to reported data (Table 3.2). A complete set of photomicrographs is given in Appendix A.
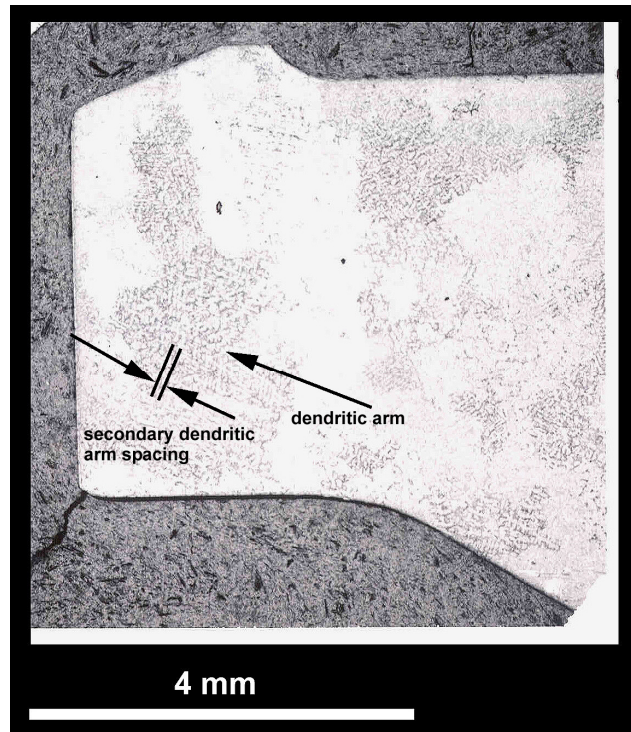
Figure 3.5 Grainex Mar-M 247 rim chord slice (S4B-1) at 16x.
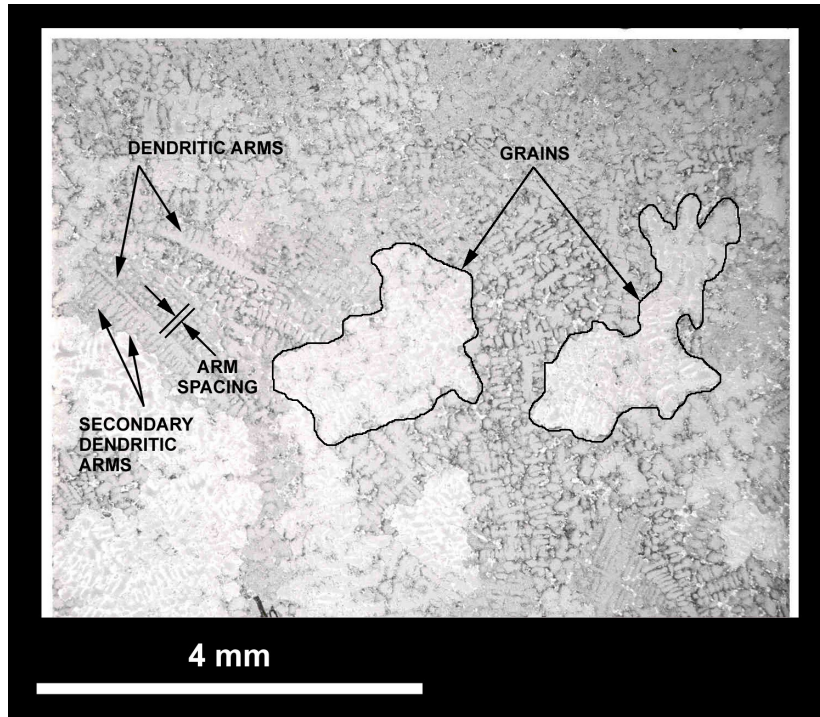
Figure 3.6 Grainex Mar-M 247 web chord slice (S4C-1) at 16x.
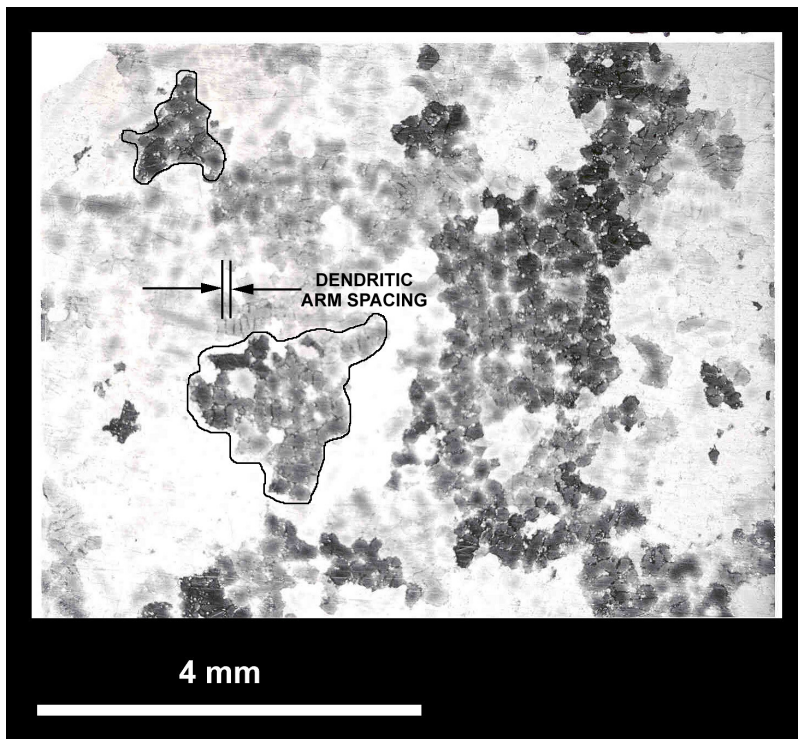
Figure 3.7 Grainex Mar-M 247 hub cross-section (Bore1-2) at 16x.

A major difference in microstructure was observed within the grains where secondary dendritic arm spacings (SDAS) became increasingly larger from the rim to the hub section. The smallest SDAS were found near the rim while the coarsest were found at the hub. An exception was found at the NASA disk boss (see Figure 3.1b) where SDAS sizes were very similar to those found at the rim.

These observations corroborate those observed by Howmet Turbine Components Corporation as shown in Table 3.3.[5] SDAS was observed to become coarser from rim to hub (0.05-0.10 mm). The increase in SDAS from rim to hub can be observed by comparing Figure 3.5 with Figure 3.6 and Figure 3.7.

**Table 3.3 Reported SDAS measurements for Grainex
Mar-M 247 disk/blade sections[5]**

Casting Process	Hub	Rim	Airfoil
Grainex	0.10	0.05	0.03

Discussion of Fluorescent Penetrant Inspection Results

Based upon the criteria given in Table 3.1, no major indications were revealed by the fluorescent penetrant inspection (Figure 3.8). Of particular importance is the fact that no indications were observed along the bolt hole surfaces.
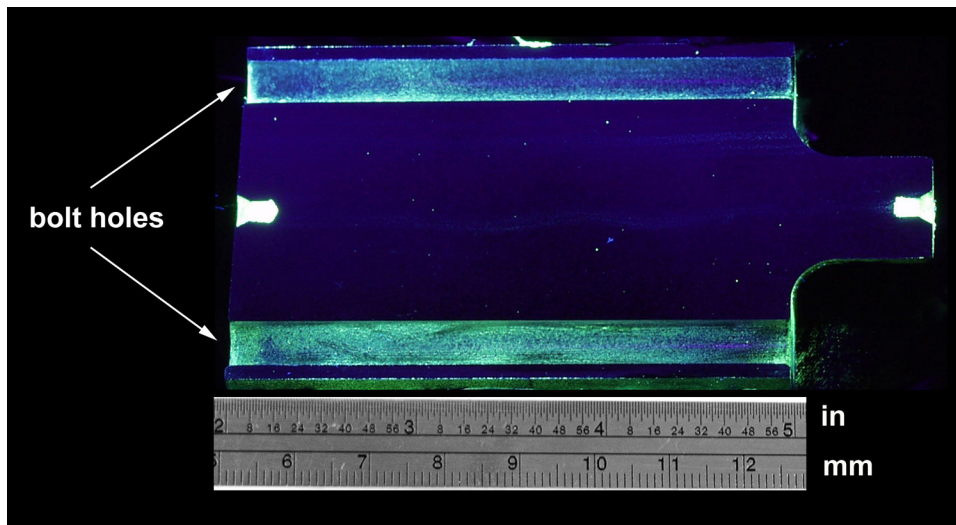
**Figure 3.8 Typical fluorescent penetrant inspection results for hub section
of Grainex Mar-M 247 NASA disk showing negligible indications.**

Chapter 3 Works Cited

1. Keller, Dennis. "Strain-Life Model with Statistics." Real World Quality Systems, Fairview Park. 05-09-01.
2. ASTM Committee E-8 on Fatigue and Fracture. "ASTM E-606 – 92 (Reapproved 1998): Standard Practice for Strain-Controlled Fatigue Testing." <u>Annual Book of ASTM Standards 2001: Section 3 Metals Test Methods and Analytical Procedures: Volume 03.01 Metals—Mechanical Testing; Elevated and Low-Temperature Tests; Metallography</u>. ASTM. West Conshohocken: ASTM, 1998. 543-557.
3. ASTM Committee E-8 on Fatigue and Fracture. "ASTM E-739 – 91 (Reapproved 1998): Standard Practice for Statistical Analysis of Linear or Linearized Stress-Life (S-N) and   Strain-Life (ε-N) Fatigue Data." <u>Annual Book of ASTM Standards 2001: Section 3 Metals Test Methods and Analytical Procedures: Volume 03.01 Metals—Mechanical Testing; Elevated and Low-Temperature Tests; Metallography</u>. ASTM. West Conshohocken: ASTM, 1998. 543-557.
4. Little, R.E. and E.H. Jebe. <u>ASTM STP 588: Manual on Statistical Planning and Analysis for Fatigue Experiments</u>. ASTM, 1975.
5. Howmet Turbine Components Corporation. <u>TB 3000: Grainex Cast Mar-M 247 Alloy</u>. Greenwich: Howmet Turbine Components Corporation.
6. Department of Defense. <u>Mil-Std-1907: Inspection, liquid penetrant and magnetic particle, soundness requirements for materials, parts and weldments. Department of Defense</u>. 7 Sept 1989.
7. ASTM Committee E-7 on Nondestructive Testing. "ASTM E-1417 – 99: Standard Practice for Liquid Penetrant Examination." Annual Book of ASTM Standards 2002: Section 3 Metals Test Methods and Analytical Procedures: Volume 03.03 Nondestructive Testing. ASTM. West Conshohocken: PA, 2002.

4.   Fatigue Strain-Life Behavior of Grainex Mar-M 247

4.1   Introduction

The presence and growth of cracks inside the bolt holes of the Grainex Mar-M 247 NASA disk due to cyclic operation can be monitored and the disk removed from operation to preclude catastrophic disk failure. Both fatigue strain-life behavior and fatigue crack growth behavior will be used to determine a maintenance inspection interval for the bolt holes. This section focuses on the fatigue strain-life behavior of Grainex Mar-M 247.

Strain-life tests will be used to determine the cycles to crack initiation and cycles to failure of the Grainex Mar-M 247 material at maximum NASA disk operating conditions in the turbine seal rig facility. Previous NASA disk analyses showed that the region adjacent the disk bolt hole just enters the plastic region of the stress-strain curve at its maximum operating temperature, pressure, and surface speed (816°C, 1724 KPa, and +300 m/s).[1] Thus, a strain-based approach to fatigue is used to address the local yielding in the material.

The strain-life tests on the Grainex Mar-M 247 NASA disk will be compared to estimates by Tong and Steinetz[1], estimates reported in the literature,[2,3] predictions using the Method of Universal Slopes and the Halford-Nachtigall Method.[4] To predict fatigue strain-life using these methods, tensile tests were conducted at 649°C which is the local NASA disk bolt hole temperature at 816°C test air temperature.

4.2   Materials and Methods: Tensile Behavior

Experiment

Tensile tests were performed at Mar-Test Inc. in Cincinnati, Ohio per ASTM E-8 and ASTM E-21 standards. Tensile testing was conducted on a Mar-Test, Inc. hydraulic servo controlled test system[5], using a box furnace for specimen heating (Figure 4.1).   Load was recorded using a load cell.[5]   Strain was recorded using a Mar-Test fused quartz extensometer with a linear variable differential (LVDT) for sensing deflection. The resolution of the LVDT was the greater of 0.0001 m/m or 0.25% of the measurement (ASTM E83, Class B2).[5]
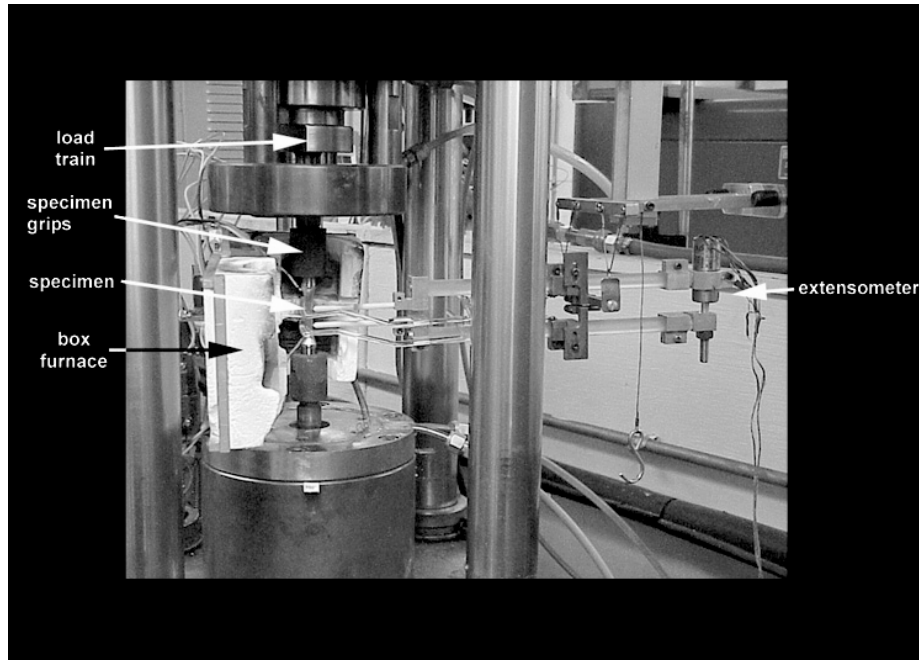
Figure 4.1 A typical tensile test set-up. [5]
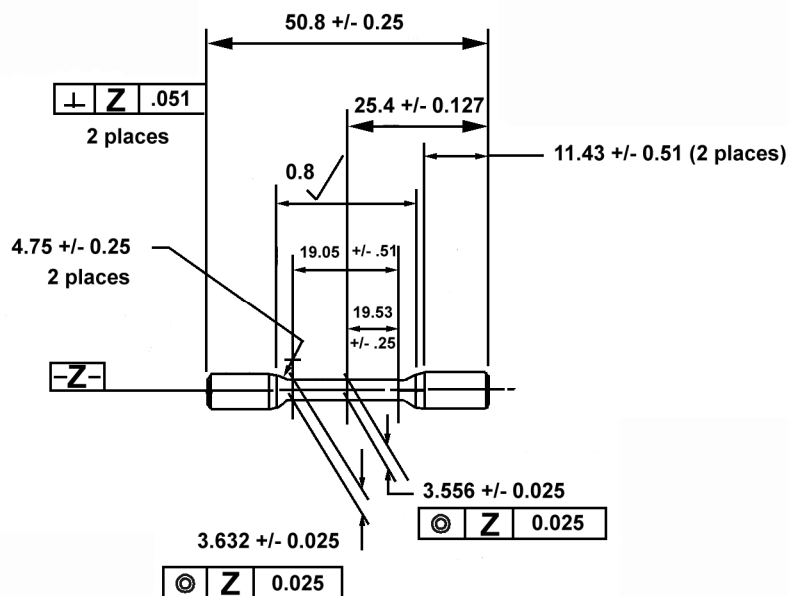
Figure 4.2 Tensile test specimen geometry.[6]

The tensile test specimen geometry was 3.56 mm in diameter by 50.8 mm in length per ASTM E-8 (Figure 4.2). The gage diameter was constant and the grip region was threaded. The gage section diameter of each specimen was measured at 21°C and gage markings were etched at the gage section at a spacing of 14.22 mm. This distance is equal to the uniform section length minus the gage diameter.[5]
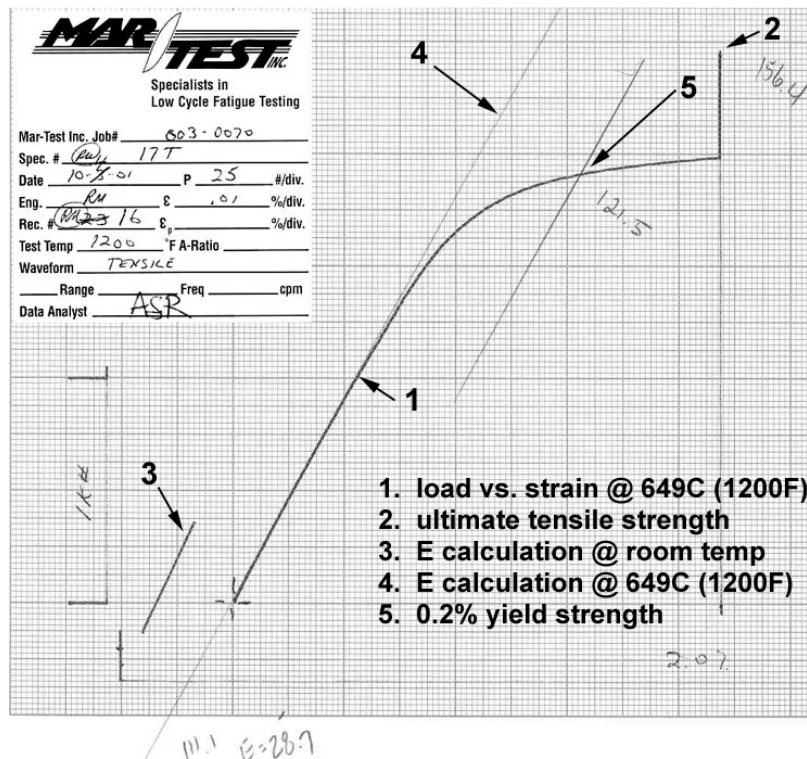
Figure 4.3 A sample tensile test plot. English units are used.

A total of four tensile specimens were tested. Thermocouples were positioned at the transition region to monitor the temperature. Also, extensometer knife edges were positioned at the uniform gage section and held in place with springs. Specimens were then heated to 649°C $\pm$ 1% for testing. Tests were conducted at 649°C at a strain-rate of 2.8x10^{-4} s^{-1}.

For each specimen, plots of load versus strain were obtained (Figure 4.3). After the 0.2% strain was reached, the load rate was increased to finish the test quickly. The final strain was thus not known; this is standard operating procedure for Mar-Test, Inc.[5]

Tensile properties were determined by Mar-Test from strip chart recorder data (Figure 4.3). This included; Young's Modulus, E, at 21°C and at 649°C; the ultimate tensile strength, σ_{UTS}; the 0.2% offset yield strength, $\sigma_{y(0.2\%)}$; percent reduction in area, %RA; and percent elongation, %EL. To calculate E, σ_{UTS}, $\sigma_{y(0.2\%)}$, and %RA, the thermal expansion coefficient, α, for Grainex Mar-M 247 at 649°C (3.32 x 10^{-6} m/m/°C) was used to determine the diameter of the gage section:

$$D_{649°C} = D_{21°C} + D_{21°C} \times \alpha_{649°C} \times \Delta T \qquad \text{Eqn. 4.1}$$

where
$D_{649°C}$ = gage section diameter at 649°C   [mm]
$D_{21°C}$ = gage section diameter at 21°C   [mm]
$\alpha_{649°C}$ = thermal expansion coefficient at 649°C   [m/m/°C]
ΔT = temperature differential from 21°C to 649°C   [°C]

E was obtained by manually identifying the slope of the initial load versus strain behavior for each specimen (Figure 4.3):

$$E = \frac{\sigma}{\varepsilon} = \frac{P/A_{649°C}}{\varepsilon}$$ Eqn. 4.2

where σ = stress [MPa]
  ε = strain [m/m]
  P = load [N]
  $A_{649°C}$ = gage section area at 649°C [m²]

σ_{UTS} was calculated using the ratio of P_{max}, and $A_{649°C}$:

$$\sigma_{UTS} = \frac{P_{max}}{A_{649°C}}$$ Eqn. 4.3

where P_{max} = maximum load [N]

$\sigma_{y(0.2\%)}$, was calculated using the ratio of the load at 0.2% offset strain, $P_{\varepsilon=0.2\%}$, and $A_{649°C}$:

$$\sigma_{y(0.2\%)} = \frac{P(\varepsilon = 0.2\%)}{A_{649°C}}$$ Eqn. 4.4

The reduction in area, %RA was calculated using

$$\%RA = \left(\frac{A_i - A_f}{A_i}\right) \times 100$$ Eqn. 4.5

where A_i is the initial gage section area and A_f is the final gage section area. The percent elongation, %EL, was calculated using

$$\%EL = \left(\frac{L_f - L_i}{L_i}\right) \times 100$$ Eqn. 4.6

where L_f = final gage section length [mm]
  L_i = initial gage section length [mm]

For brittle materials, the engineering fracture stress, σ_f, can be substituted with the ultimate tensile strength, σ_{UTS}.[7] Thus, the true fracture strength, $\tilde{\sigma}_f$, was estimated by :

$$\tilde{\sigma}_f = \frac{P_f}{A_f} = \sigma_f\left(\frac{A_i}{A_f}\right) = \sigma_{UTS}\left(\frac{A_i}{A_f}\right)$$ Eqn. 4.7 (Ref. 7)

Similarly, the true fracture strain, $\tilde{\varepsilon}_f$, was estimated by:

$$\tilde{\varepsilon}_f = \ln \frac{A_i}{A_f} \qquad \qquad \text{Eqn. 4.8 (Ref. 7)}$$

Fractographic Examination

Fracture surfaces from each of the four tested tensile specimens were examined by light stereomicroscopy and scanning electron microscopy. Prior to scanning electron microscopy examination, the specimens were ultrasonically cleaned in acetone for 5 minutes, rinsed in alcohol, and then air dried.

Scanning electron microscopy was performed in both secondary electron (SE) and backscattered electron (BE) modes. SE mode was used to identify general fractographic features such as evidence of brittle or ductile fracture, including necking, and the presence or absence of shear lips while BE mode was used to identify the site of fracture initiation.

4.3 Materials and Methods: Fatigue Strain-Life Behavior

Experimental

Fatigue strain-life tests were performed at Mar-Test Inc. in Cincinnati, Ohio per ASTM E-606 using Mar-Test, Inc. closed loop, servo-hydraulic test systems (Figure 4.4). The extensometer system was identical to that used for the tensile tests. Induction heating was utilized for tests at high temperature.
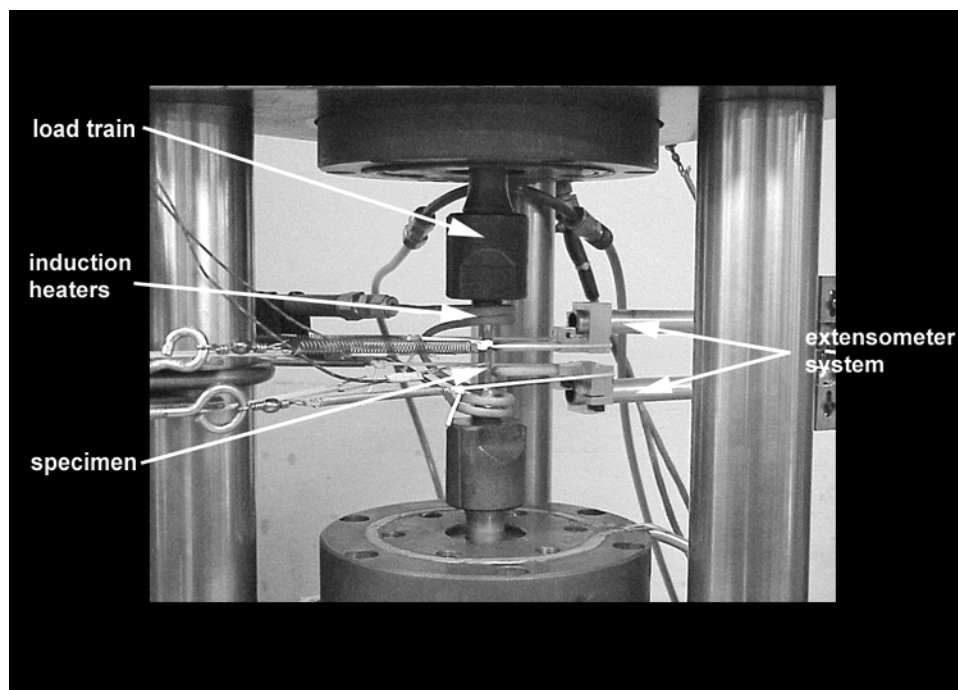
Figure 4.4 Typical fatigue strain-life test set-up.[5]
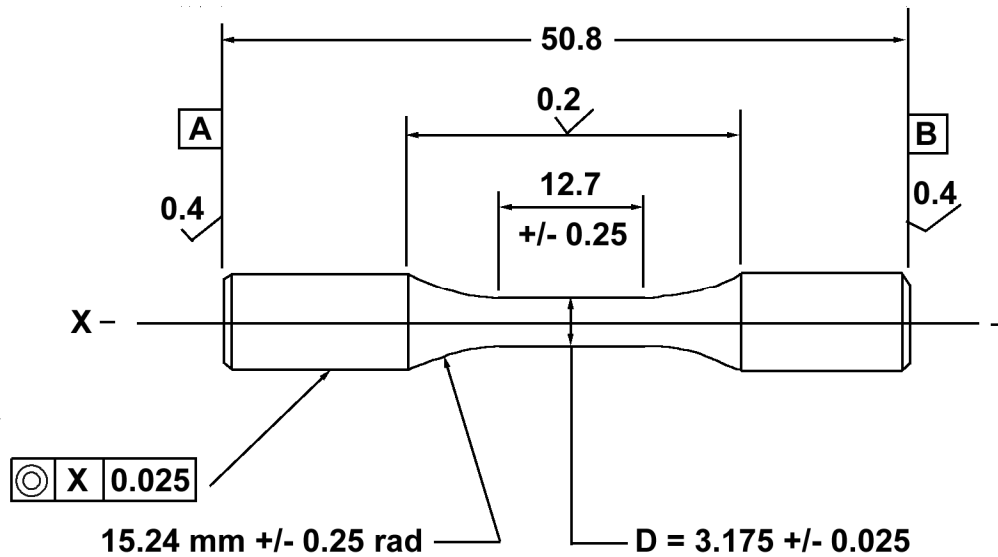
Figure 4.5 Strain-life specimen geometry.[8]

**Table 4.1   Grainex Mar-M 247 strain-life test matrix.
Specimen identifications refer to the NASA disk
location where the specimens were obtained
(Figure 3.1a and Figure 3.1b)**

Specimen Identification	% Strain Range	R_ε
66L, 86L, CB1L	0.50	-1
57L, 76L, CA9L	0.58	-1
47L, CA7L, CB8L	0.67	-1
27L, CA4L, CB6L	0.78	-1
15L, CA2L, CB3L	0.90	-1
67L, 77L, CA8L	0.50	0
56L, 87L, CB2L	0.58	0
46L, CA1L, CB5L	0.67	0
35L, CA3L, CB7L	0.78	0
26L, CA6L, CB9L	0.90	0

The specimen geometry for the strain-life tests followed recommended specimen geometry per ASTM E-606 (Figure 4.5). [9]

A total of 15 fatigue strain-life specimens were obtained from the sacrificial NASA disk. The tests were conducted in air at 649°C at a strain ratio of R_ε = -1 and R_ε = 0 with a frequency of 0.33 Hz using a triangular waveform. Five strain ranges were tested (0.50%, 0.58%, 0.67%, 0.78%, and 0.90%) with three repeats at each strain range (Table 4.1).

Prior to testing the specimen diameter, $D_{21°C}$ for each specimen was measured and A_i was calculated. Using $\alpha_{649°C}$ for Grainex Mar-M 247, (3.32 x 10^{-6} /°C), $D_{649°C}$ and $A_{649°C}$ were calculated. Chromel-alumel thermocouples were then attached at both ends of the gage section for

temperature control with reference thermocouples attached at the ends of the specimen in the grip region.[5] A thermocouple was also attached to the center of the test section to determine the temperature at that point. An optical pyrometer was used to compare the center thermocouple temperature with the temperature of the rest of the uniform section. Adjustments were made to the induction heating coils such that the temperature deviation in the uniform section was less than ±1%.[5]

The specimen was strained elastically to obtain the P versus ε behavior for calculating E at 21°C. The specimen was then heated to the test temperature of 649°C to within ±1%. P versus ε behavior was again recorded to calculate E at 649°C. Strain-controlled fatigue testing was then performed at 0.33 Hz with a triangular waveform.

Plots of load versus strain were recorded at regular intervals during cycling. Cycles to crack initiation, N_i, was subjectively determined when a rapid change in the load versus time history plot occurred (Figure 4.6).[5] Tests were conducted until failure, N_f, which was defined as either specimen fracture or a change in the maximum stress to 30 percent of its original value.

For each specimen, the following parameters were calculated at the start of the test upon reaching the test strain range: cycle, N; stress range, $\Delta\sigma$; maximum stress, σ_{max}; and minimum stress, σ_{min}. At approximately half the specimen life, additional parameters were calculated: elastic modulus, E; the elastic strain range, $\Delta\varepsilon_{el}$; and the inelastic strain range, $\Delta\varepsilon_{in}$. $\Delta\varepsilon$, $\Delta\varepsilon_{el}$, and $\Delta\varepsilon_{in}$ were determined from the load versus strain hysteresis plots following standard methods.[7] N_i and N_f were also obtained from each test.
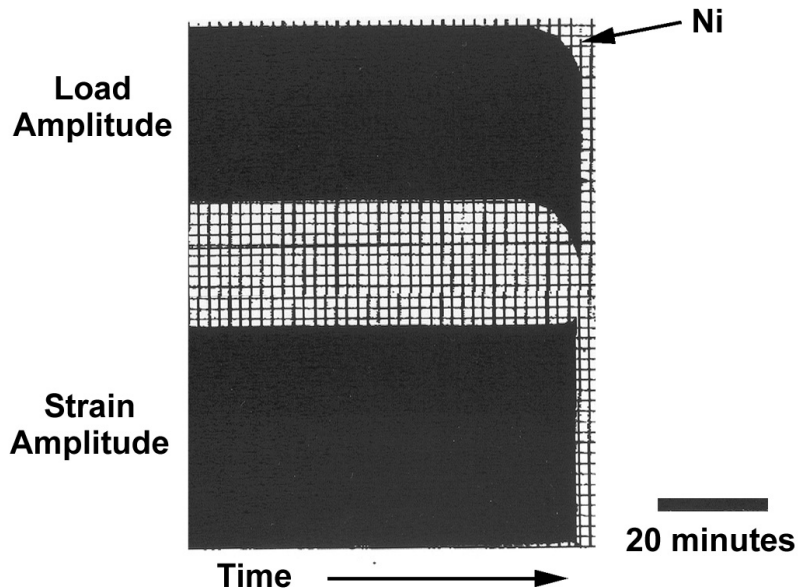
Figure 4.6 Example of crack initiation point in load, strain time history plot.[5]

<u>Statistics</u>

The fatigue strain-life results were evaluated following a simple linear model in log-log coordinates:

$$N_f = Z(\%\Delta\varepsilon)^\varsigma \qquad \text{Eqn. 4.9}$$

where the constant, Z, and exponent, ς, were to be determined and $\%\Delta\varepsilon$ is the percent total strain range. Thus,

$$\log(N_f) = \log Z + \varsigma \log(\%\Delta\varepsilon) \qquad \text{Eqn. 4.10}$$

Linear regression analysis of the log-log transformed fatigue strain-life data was then conducted to determine Z and ς for both $R_\varepsilon = 0$ and $R_\varepsilon = -1$. The linear regressions were tested for significance based upon the null hypothesis method at the 99.95% confidence level.[10] The coefficient of determination, R^2, was also calculated. Normal distribution of the data was checked, data removed, and the regression revised as necessary.[10] A test for lack-of-fit was done to check whether the linear model was correct.[10] Also the Foster-Burr test was performed to check for outliers in the data. [10] Finally 99.95% prediction intervals were calculated for both data sets. [10]

<u>Method of Universal Slopes</u>
The Manson-Hirschberg Method of Universal Slopes[11] (MUS) was used to estimate strain life with zero mean stress based only upon tensile properties:

$$\Delta\varepsilon = \Delta\varepsilon_{el} + \Delta\varepsilon_{in} \qquad \text{Eqn. 4.11 \quad (Ref. 11)}$$

$$\Delta\varepsilon = (C1)N_f^b + (C2)N_f^c \qquad \text{Eqn. 4.12 \quad (Ref. 11)}$$

$$\Delta\varepsilon = 3.5\frac{\sigma_{UTS}}{E}\left(N_{f0}\right)^{-0.12} + \varepsilon_f^{0.6}\left(N_{f0}\right)^{-0.6} \qquad \text{Eqn. 4.13 \quad (Ref. 11)}$$

where   C1, C2 = constant coefficients
N_{f0} = cycles to failure under zero mean stress
ε_f = true fracture ductility

$$= \ln\left(\frac{100}{100 - RA}\right) \qquad \text{Eqn. 4.14 \quad (Ref. 11)}$$

Average tensile properties were calculated based upon the four tensile tests performed. $\Delta\varepsilon_{el}$ and $\Delta\varepsilon_{in}$ were calculated by inserting the averaged tensile properties into Eqn. 4.13. $\Delta\varepsilon$ is the sum of $\Delta\varepsilon_{el}$ (first term) and $\Delta\varepsilon_{in}$ (second term) in Eqn. 4.13. Thus, N_{f0} can be estimated based upon a given $\Delta\varepsilon$.

Halford-Nachtigall Method

To estimate the effect of mean stress on cyclic life, the Halford-Nachtigall Method was used with the MUS:

$$N_{fm}^{-b} = N_{f0}^{-b} - V_{\sigma}$$
Eqn. 4.15 (Ref. 4)

where
N$_{fm}$ = cycles to failure in presence of mean stress
b = fatigue strength exponent
N$_{f0}$ = cycles to failure under zero mean stress
V$_{\sigma}$ = ratio of mean stress to stress amplitude

The relationship is derived from:

$$\Delta\sigma = 2\left(\sigma_f^{'} - \sigma_m\right)N_{fm}^{-b}$$
Eqn. 4.16 (Ref. 4)

where
$\sigma_f^{'}$ = fatigue strength coefficient [MPa]

σ_m = mean stress [MPa]

This is Morrow's original equation (Eqn. 4.14) except that N$_{fm}$ is used instead of 2N$_{fm}$.

The value for b was -0.12 from the MUS. N$_{f0}$ from Eqn. 4.14 was calculated using the ratio of the inelastic strain range and the elastic strain range from the MUS at ratios of 0.3, 0.2, 0.1, 0.08, 0.05, and 0.02. V$_{eff}$ was substituted for V$_{\sigma}$ in Eqn. 4.14 (Ref. 4):

where
$$V_{eff} = k\frac{\sigma_m}{\sigma_a} = kV_{\sigma}$$
Eqn. 4.17 (Ref. 4)

$$k = \exp\left[-70\left(\frac{\Delta\varepsilon_{in}}{\Delta\varepsilon_{el}}\right)^2\right]$$
Eqn. 4.18 (Ref. 4)

V$_{eff}$ = effective ratio of mean stress to stress amplitude
k = transfer function
σ_a = stress amplitude [MPa]

The ratio of the mean stress to stress amplitude is assumed to be unity at the start of each strain-life test. This assumption is correct if the stress-strain hysteresis loop is completely elastic. However, with increasing cyclic plasticity, mean stress relaxation may occur and the ratio of the mean stress to stress amplitude would decrease.

Finally, the variation of mean stress and range of stress was plotted against increasing strain amplitude at the specimen half-life.

Morrow Strain Life Equation
The Morrow Strain-Life equation was used to model $R_\varepsilon = -1$ strain-life data:

$$\frac{\Delta\varepsilon}{2} = \varepsilon_a = \frac{\sigma_f'}{E}(2N_f)^b + \varepsilon_f'(2N_f)^c \qquad \text{Eqn. 4.19 (Ref.12)}$$

where
ε_a = strain amplitude
σ_f' = fatigue strength coefficient [MPa]
b = fatigue strength exponent
ε_f' = fatigue ductility coefficient
c = fatigue ductility exponent

The coefficients and exponents of the Morrow strain-life equation were determined as follows:[13]

1. A plot was made on log-log coordinates of $\frac{\Delta\varepsilon_e}{2}$ versus $2N_f$. By definition, $\frac{\sigma_f'}{E}(2N_f)^b$ is equal to $\frac{\Delta\varepsilon_e}{2}$. Thus, the y-intercept of the regression at $2N_f = 1$ is equal to $\frac{\sigma_f'}{E}$. σ_f' was determined given E. Finally, the slope of the regression is equal to b.

2. A plot was made on log-log coordinates of $\frac{\Delta\varepsilon_p}{2}$ versus $2N_f$. By definition, $\varepsilon_f'(2N_f)^c$ is equal to $\frac{\Delta\varepsilon_p}{2}$. Thus, the y-intercept of the regression at $2N_f = 1$ is equal to the ε_f'. Finally, the slope of the line is equal to c.

Modified Morrow with Mean Stress Effects
The Modified Morrow equation was used to account for mean stress effects in the $R_\varepsilon = 0$ tests:

$$\varepsilon_a = \frac{\sigma_f'}{E}\left(1 - \frac{\sigma_m}{\sigma_f'}\right)(2N_f)^b + \varepsilon_f'\left(1 - \frac{\sigma_m}{\sigma_f'}\right)^{\frac{c}{b}}(2N_f)^c \qquad \text{Eqn. 4.20 (Ref. 7)}$$

The coefficients (σ_f', E, ε_f') and exponents (b and c) initially used were calculated from the Morrow Strain-Life Equation (Eqn. 4.18). For each of the 30 fatigue strain-life tests, the mean stress was determined by the average of the maximum and minimum stress values at the cyclic half-life. ε_a was then calculated for each specimen. Finally, the coefficients and exponents of the Modified Morrow equation were optimized by minimizing the residual between the experimental strain amplitude and the calculated strain amplitude from Eqn. 4.19. Also, constraints were imposed on exponents b and c as follows:

$$-0.12 \leq b \leq -0.05 \qquad \text{Eqn. 4.21 (Ref. 7)}$$

$$-0.9 \leq c \leq -0.5 \qquad \text{Eqn. 4.22 (Ref. 7)}$$

Using these optimized coefficients and exponents, the Modified Morrow equation was then used to plot strain amplitude versus cycles to failure along lines of constant mean stress with values ranging from -345 MPa to 690 MPa. This plot was compared to experimental data.

Fractographic Examination
     The fracture surfaces of fatigued specimens were cleaned in acetone, alcohol rinsed, and air dried to facilitate fractographic examination.
     Surfaces were examined using light stereomicroscopy and scanning electron microscopy (SEM) using secondary electron (SE) and backscattered electron (BE) modes to determine crack initiation sites.

4.4   Results and Discussion: Tensile Behavior

Properties
     Average tensile properties of four tensile tests for the Grainex Mar-M 247 material are shown in Table 4.2. The ultimate tensile strength and 0.2% offset yield stress were found to be 1064 and 821 MPa, respectively.

Table 4.2 Tensile test results for Grainex Mar-M 247 at 649°C

	E [GPa]	σ_{UTS} [MPa]	$\sigma_{y(0.2\%)}$ [MPa]	%RA	%EL	$\tilde{\sigma}_f$ [MPa]	$\tilde{\varepsilon}_f$
Average	194.3	1064.4	821.0	16	6.9	1268	0.177
Standard deviation	12.6	19.8	18.3	1	1.0	31	0.015

The Grainex Mar-M 247 tensile properties determined from the sacrificial NASA disk were within 5 to 10% of values reported from literature (Table 4.3).[2,14] The exception was in the %RA data where the sacrificial NASA disk %RA was 30 to 40% higher than that reported in the literature. The higher values were most likely due to a slight amount of necking observed in the gage sections of the tensile test specimens.

Table 4.3 Comparison of average Grainex Mar-M 247 tensile properties at 649°C with literature

		NASA Disk*	Kaufman*,[2]	Howmet[14]
No. Samples		4	2	N/A
E	[GPa]	194.3	N/A	179.3
σ_{UTS}	[MPa]	1064.4	1011.5	1027.3
$\sigma_{y(0.2\%)}$	[MPa]	821.0	799.1	827.4
%RA		16	9.7	10.7
%EL		6.9	7.1	7.0
* average data				

Fractographic Examination

Crack initiation sites were observed by light stereomicroscopy at the surface of the gage section of the specimens. Little if any necking of the gage section was observed on the tensile specimens. Shear lips were not observed. The overall fracture surface appearance was consistent with brittle fracture (Figure 4.7). Examination of the fracture surfaces by SEM in BE mode did not reveal any evidence of interior initiation, supporting the visual observations that fracture initiated at the surface (Figure 4.8). A complete set of SEM images is given in Appendix B.
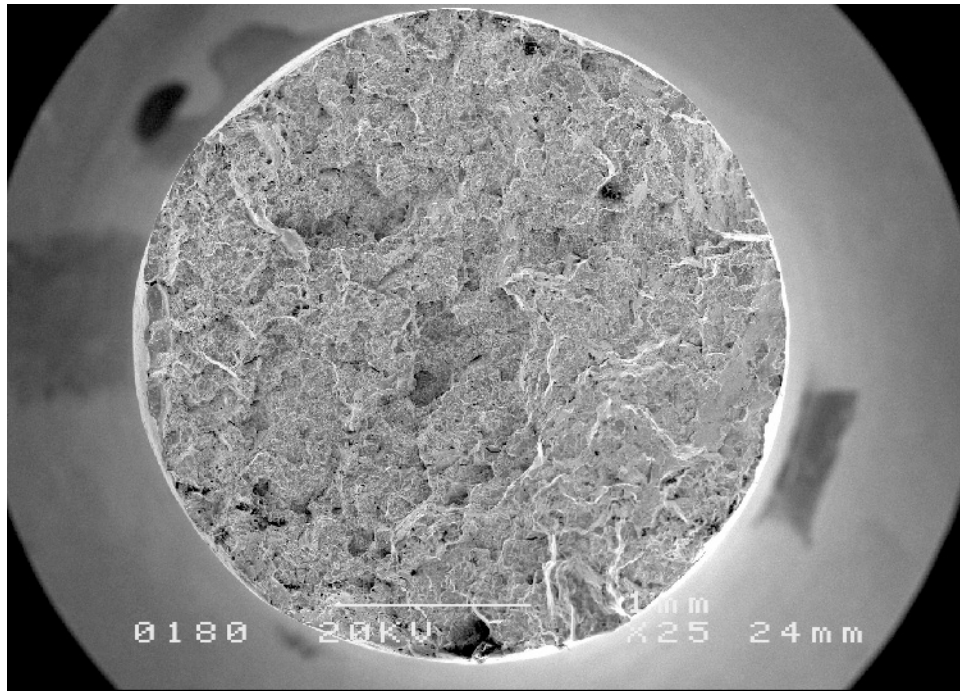
Figure 4.7 Typical SEM (SE mode) image of Grainex Mar-M 247 tensile specimens conducted at 649°C.
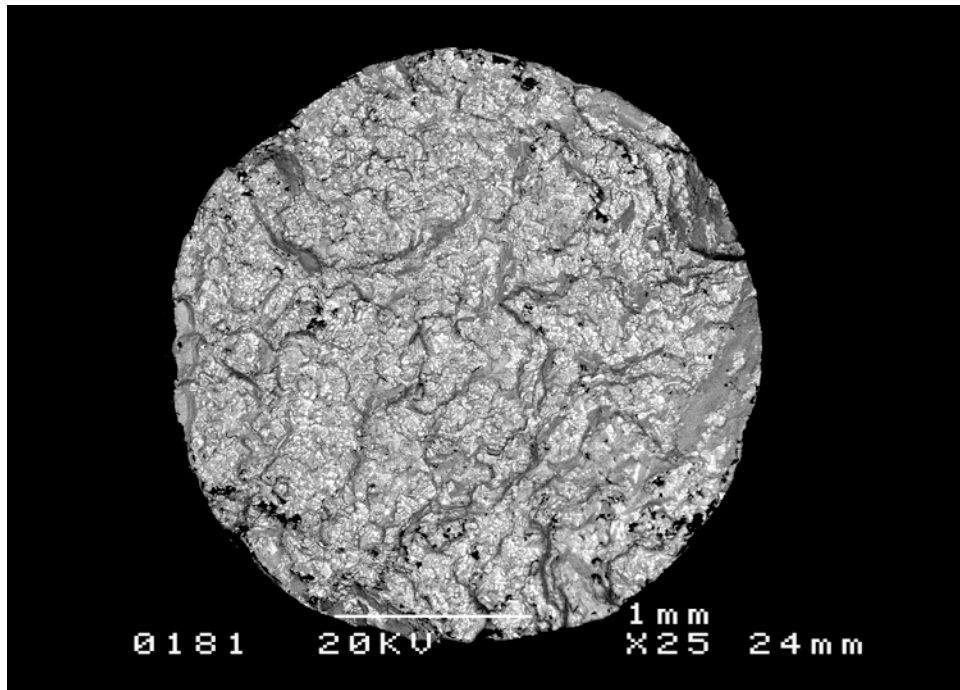
Figure 4.8 Typical SEM (BE mode) image of Grainex Mar-M 247 tensile specimens conducted at 649°C (same fracture surface as in Figure 4.7).

4.5   Results and Discussion: Fatigue Strain-Life Behavior

$\underline{R_\varepsilon = -1}$

N_i and N_f were determined for each of the $R_\varepsilon = -1$ fatigue strain-life tests at 649°C (Table 4.4).

Table 4.4 Grainex Mar-M 247 fatigue strain-life test results at 649°C, $R_\varepsilon = -1$. Specimen identifications refer to the location on the NASA disk where the specimens were obtained (Figure 3.1a and Figure 3.1b)

Specimen Identification	%Δε	N_i	N_f
66L	0.50	*	429420
86L	0.50	*	120171
CB1L	0.50	*	110545
57L	0.58	115737	116335
76L	0.58	31362	31486
CA9L	0.58	43555	44313
47L	0.67	4618	6624
CA7L	0.67	6836	8018
CB8L	0.67	3175	5231
27L	0.78	1464	1668
CA4L	0.78	1004	1586
CB6L	0.78	1773	2279
15L	0.90	192	484
CA2L	0.90	393	875
CB3L	0.90	317	451
*Switched to load-control after approximately 100,000 cycles. No crack-initiation life was available.			

Linear regression analysis of Eqn. 4.9 for the $R_\varepsilon = -1$ total strain life versus N_i data resulted in an exponent, ζ, of -11.49 and a coefficient, Z, of 75.86 with $R^2 = 0.94$. The exponent and coefficient were significant to a 99.95% confidence level. The residuals were normally distributed. A histogram of the residuals found one possible outlier (57L) and subsequent linear regression analysis resulted in an exponent, ζ, of -10.55 and a coefficient, Z, of 91.20 with $R^2 = 0.96$. The exponent and coefficient were again significant to a 99.95% confidence level. The lack-of-fit test showed that the linear model was acceptable to a 99.9% confidence level. The Foster-Burr test showed no outliers in the data to a 99% confidence level. Prediction intervals were calculated to a 99.95% prediction level (Figure 4.9).
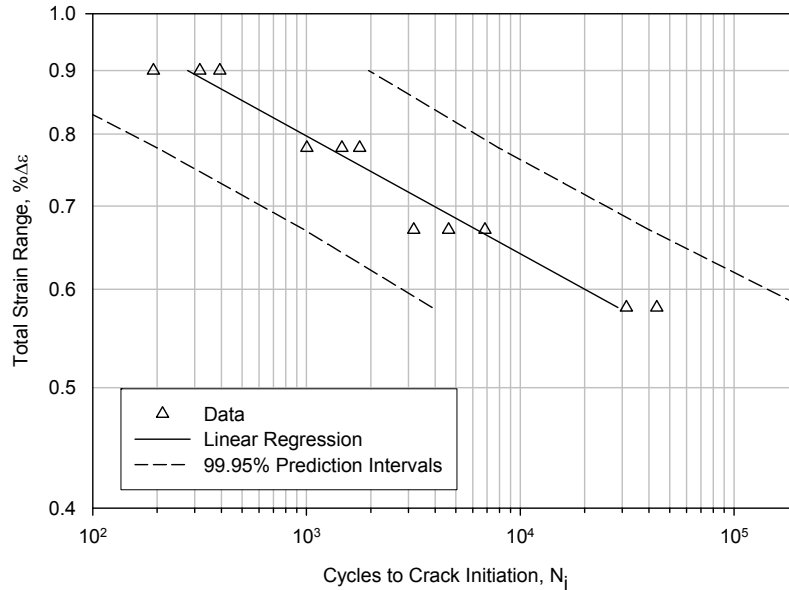
Figure 4.9   Crack initiation strain-life results for Grainex Mar-M 247, R_ε = -1, 649°C, triangular waveform, 0.33 Hz. By convention, N_i was plotted on the abscissa while %$\Delta\varepsilon$ was plotted on the ordinate.

Linear regression analysis of Eqn. 4.9 for the R_ε = -1 total strain life versus N_f data resulted in an exponent, ζ, of -10.10 and a coefficient, Z of 165.96 with R^2 = 0.95. The exponent and coefficient were significant to a 99.95% confidence level. The residuals were normally distributed. A histogram of the residuals found three outliers (57L, 66L, and CA2L) and subsequent linear regression analysis resulted in an exponent, ζ, of -9.53 and a coefficient, Z, of 165.96 with R^2 = 0.99. The exponent and coefficient were again significant to a 99.95% confidence level. The lack-of-fit test showed that the linear model was acceptable to a 99.9% confidence level. The Foster-Burr test showed no outliers in the data to a 99% confidence level. Prediction intervals were calculated to a 99.95% prediction level (Figure 4.10).

A comparison of the outliers found in the R_ε = -1 data (Specimens 66L, 57L, and CA2L) with their respective strain-ranges revealed the following:

1. Crack depth was approximately 1/3 of the gage cross-section regardless of the strain-range.
2. The outlier specimens had a 2x to nearly 4x longer life, N_f, than specimens tested at the same strain range (Table 4.4). Subsequent life predictions would have been non-conservative.
3. Comparing SEM of specimens at the same strain range showed that the outlier specimens had fewer crack initiation sites and that crack growth was limited to fewer facets.
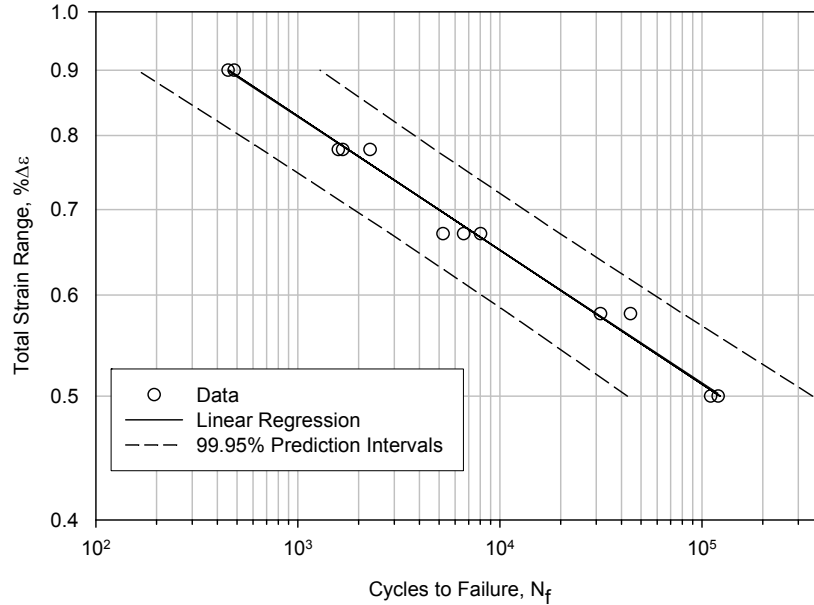
Figure 4.10 Cycles to failure strain-life results for Grainex Mar-M 247, R_ε = -1, 649°C, triangular waveform, 0.33 Hz. By convention, N_f is plotted on the abscissa while %Δε is plotted on the ordinate.

The NASA Grainex Mar-M 247 R_ε = -1 strain-life data at 649°C was compared with available literature at 427°C (Figure 4.11). The data showed that the cyclic life of the Grainex Mar-M 247 sacrificial NASA disk material was similar to that reported by Macha et al.[3] Specifically, data reported by Macha et al. were
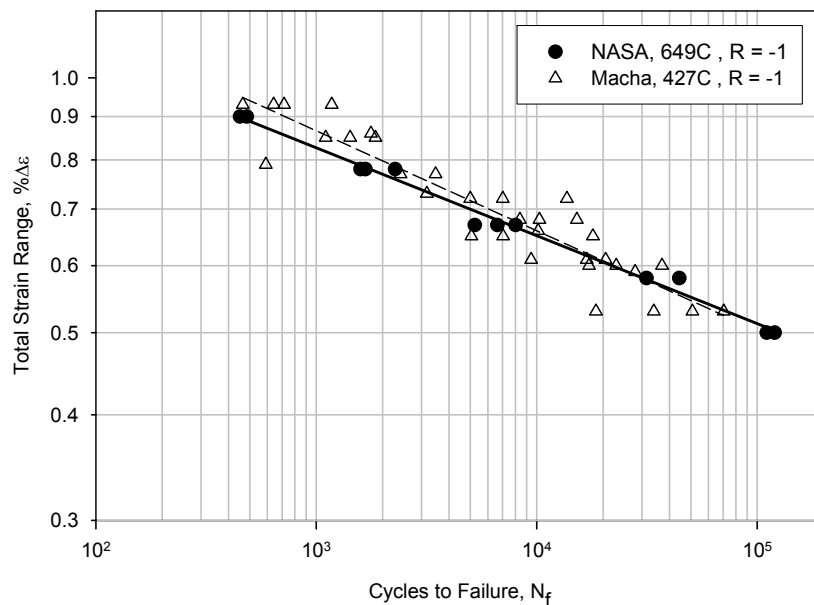
Figure 4.11 Comparison of NASA Grainex Mar-M 247, R_ε = -1 strain-life data with literature.[3]

comparable with the sacrificial NASA disk data at the design point of 0.5% $\Delta\varepsilon$. It should be noted that the values reported by Macha et al. in the early 1980s were when the Grainex process was first introduced and that refinements in the process (i.e., the Grainex examined in this study) appear to have led to equal if not improved strain-life at higher temperatures. Normally, at higher temperatures the strain-life decreases for identical strain ranges. However it was seen that the strain-life at 649°C for the NASA disk Grainex Mar-M 247 material is equal to if not higher than that reported by Macha et al. data at 427°C.

<u>$R_\varepsilon = 0$</u>

N_i and N_f were determined for each of the $R_\varepsilon = 0$ fatigue strain-life tests at 649°C (Table 4.5).

**Table 4.5 Grainex Mar-M 247 strain-life test results at 649°C, $R_\varepsilon = 0$.
Specimen identifications refer to the location on the NASA disk
where the specimens were obtained (Figure 3.1a and Figure 3.1b).**

Specimen Identification	%Δε	N_i	N_f
67L	0.50	*	127523
77L	0.50	25917	26939
CA8L	0.50	9557	10697
56L	0.58	12266	12566
87L	0.58	2450	2842
CB2L	0.58	5910	7970
46L	0.67	2056	3056
CA1L	0.67	3114	3842
CB5L	0.67	1322	2234
35L	0.78	585	723
CA3L	0.78	792	1352
CB7L	0.78	680	1254
26L	0.90	513	889
CA6L	0.90	**	1142
CB9L	0.90	***	554
* Switched to load control after approximately 100,000 cycles.			
** Recorder malfunction. Ni occurred between 415 and 847.			
***Recorder malfunction. Ni occurred between 295 and 500 cycles.			

Linear regression analysis of Eqn. 4.9 for the $R_\varepsilon = 0$ total strain life versus N_i resulted in an exponent, ζ, of -6.48 and a coefficient, Z of 162.18 with $R^2 = 0.86$. The exponent and coefficient were found to be significant to a 99.95% confidence level. The residuals were found to be normally distributed. A histogram showed no outliers. The lack-of-fit test showed that the linear model

was acceptable to a 99.9% confidence level. The Foster-Burr test showed no outliers in the data to a 99% confidence level. Prediction intervals were calculated to a 99.95% prediction level (Figure 4.12).
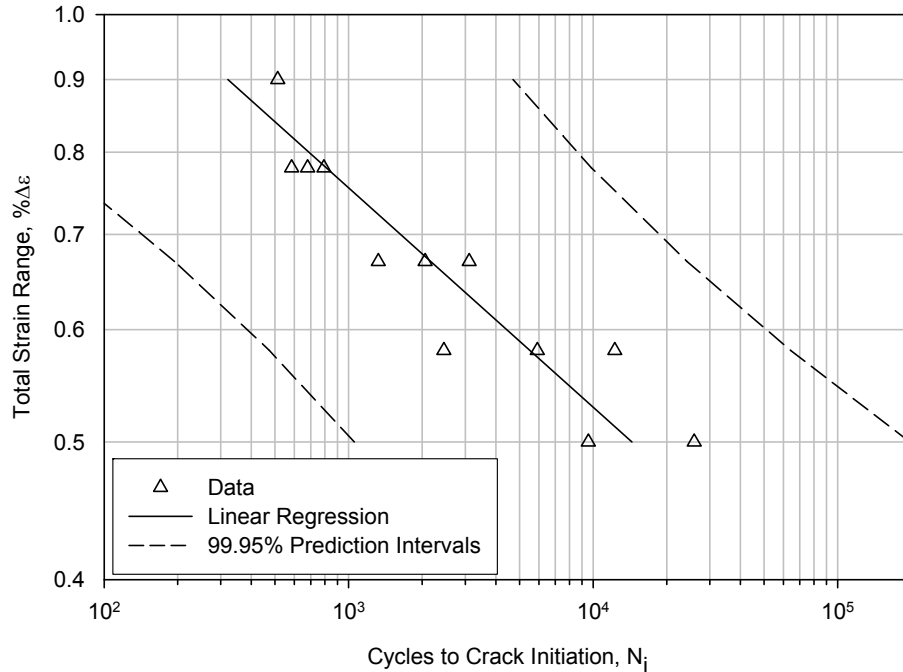
Figure 4.12 Crack initiation strain-life results for Grainex Mar-M 247, R_ε = 0, 649°C, triangular waveform, 0.33 Hz. By convention, N_i was plotted on the abscissa while %$\Delta\varepsilon$ was plotted on the ordinate.

Linear regression analysis of Eqn. 4.9 for the R_ε = 0 total strain life versus N_f resulted in an exponent, ζ, of -6.26 and a coefficient, Z of 295.12 with R^2 = 0.80. The exponent and coefficient were found to be significant to a 99.95% confidence level. The residuals were found to be normally distributed. A histogram of the residuals found two possible outliers (67L and CA6L) and subsequent linear regression analysis resulted in an exponent, ζ, of -5.62 and a coefficient, Z, of 316.23 with R^2 = 0.87. The exponent and coefficient were again significant to a 99.95% confidence level. The lack-of-fit test showed that the linear model was acceptable to a 99.9% confidence level. The Foster-Burr test showed no outliers in the data to a 99% confidence level. Prediction intervals were calculated to a 99.95% prediction level (Figure 4.13).
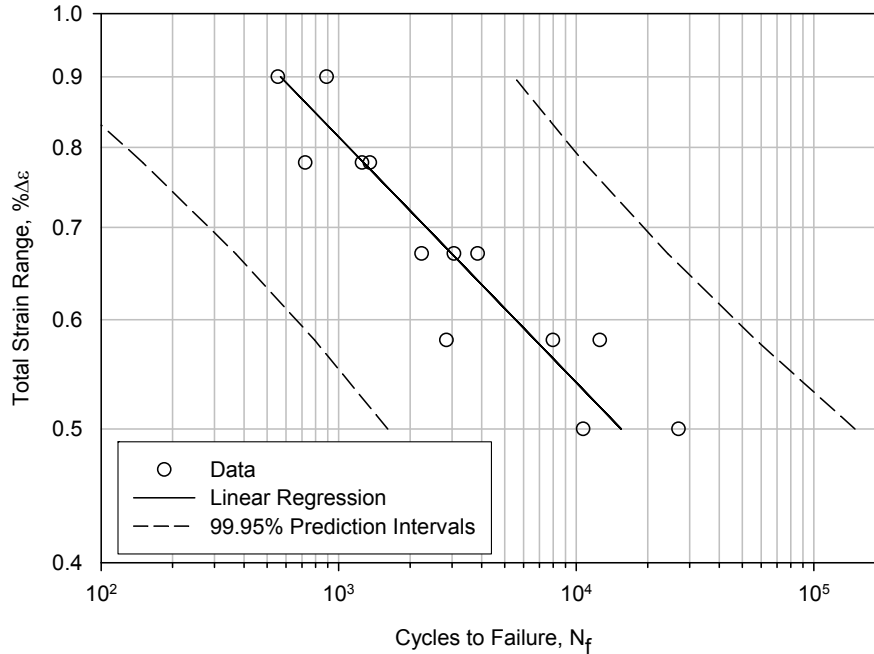
Figure 4.13   Cycles to failure strain-life results for Grainex Mar-M 247, R_ε = 0, 649°C, triangular waveform, 0.33 Hz. By convention, N_f is plotted on the abscissa while %$\Delta\varepsilon$ is plotted on the ordinate.

Testing at R_ε = 0 and 649°C addressed the actual localized conditions the Grainex Mar-M 247 NASA disk bolt holes encounter in the Turbine Seal Test Facility. Specifically, the NASA disk is strained from a zero to maximum strain when the surface speed increases from zero to maximum during testing. The -99.95% prediction interval (1 failure in 2000 samples) on cyclic life was chosen since it was more conservative than the mean cyclic life by a factor of approximately 10 (Table 4.6). As expected, more data scatter was observed at the lower strain ranges. Overall the cyclic life to crack initiation of the Grainex Mar-M 247 NASA disk bolt holes at the 0.5% design strain, R_ε = 0, and -99.95% prediction interval was found to be 1100 cycles (Figure 4.12). This was nearly 6 times less than the cyclic life predicted from previous analyses[1] and more than 10 times less than the cyclic life extrapolated using the R_ε = -1, N_i , -99.95% prediction interval data at %$\Delta\varepsilon$ = 0.5 (see Table 4.6).

Comparison of the NASA Grainex Mar-M 247 R_ε = 0 strain-life data with reported data by Kaufman[2] showed good agreement (Figure 4.14). As observed, the NASA data at 649°C fell in between the 427°C and 760°C data reported by Kaufman.[2]   As expected, cyclic lives decreased with increasing temperature for a constant strain range.
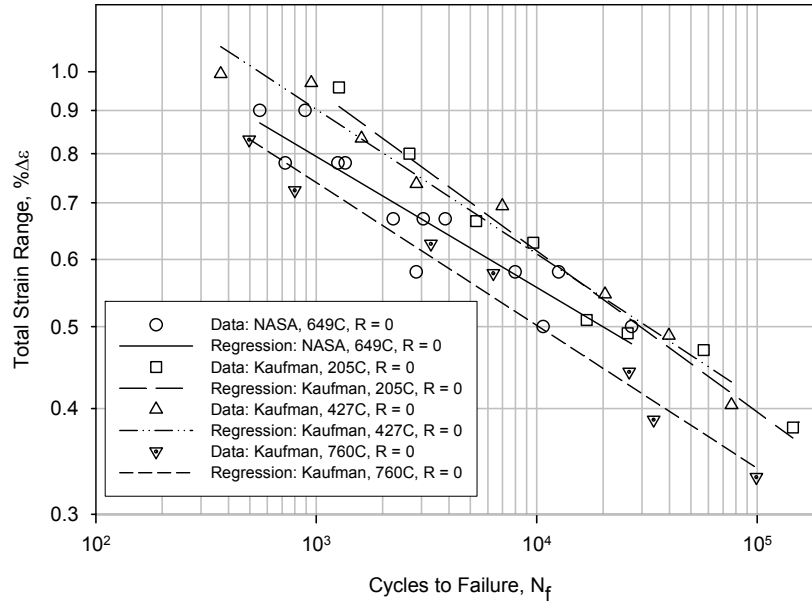
Figure 4.14 Comparison of NASA Grainex Mar-M 247, R_ε = 0 strain-life data with literature.[2]

Table 6 summarizes the mean and -99.95% prediction cyclic life for both R_ε = -1 and R_ε = 0 data at both N_i and N_f at the 0.5% design strain range of the Grainex Mar-M 247 NASA disk (see also Figure 4.9, Figure 4.10, Figure 4.12, Figure 4.13).

Table 4.6 Grainex Mar-M 247 mean and -99.95% cyclic life predictions at 649°C, %$\Delta\varepsilon$ = 0.5.

$R_\varepsilon \rightarrow$	-1		0	
Statistic $\rightarrow$	Mean	-99.95%	Mean	-99.95%
N_i (cycles)	>100000	14500	14500	1100
N_f (cycles)	>100000	40000	15500	1600

Method of Universal Slopes

The estimated N_f was plotted against $\Delta\varepsilon$ for the Grainex Mar-M 247 material using tensile data (Table 4.2) as input for the MUS (Figure 4.15). The plastic and elastic strain lines were also plotted. N_t was found to be 400 cycles to failure.
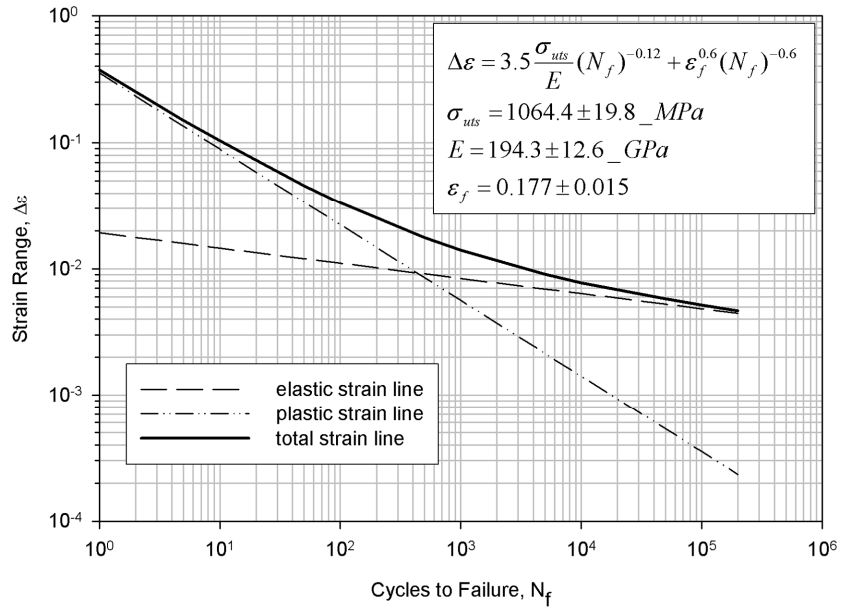
Figure 4.15   Method of Universal Slopes equation using Grainex Mar-M 247 Tensile Data at 649°C.

The equation shown in the figure:

$$\Delta\varepsilon = 3.5\frac{\sigma_{uts}}{E}(N_f)^{-0.12} + \varepsilon_f^{0.6}(N_f)^{-0.6}$$

$$\sigma_{uts} = 1064.4 \pm 19.8\_MPa$$

$$E = 194.3 \pm 12.6\_GPa$$

$$\varepsilon_f = 0.177 \pm 0.015$$

Halford-Nachtigall Method

Comparison of the Halford-Nachtigall Method with the MUS, $R_\varepsilon = 0$ data, and $R_\varepsilon = -1$ data for the Grainex Mar-M 247 material is shown (Figure 4.16).
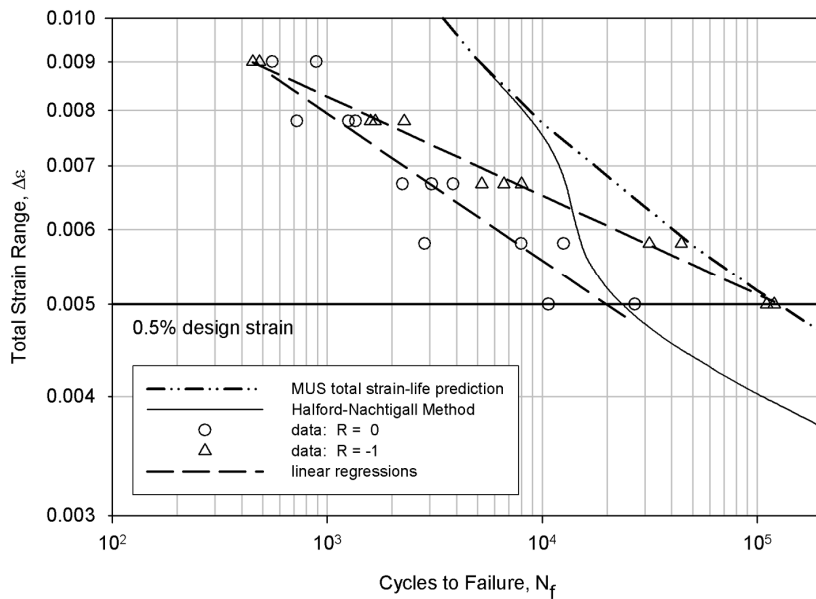
Figure 4.16   Comparison of MUS, Halford-Nachtigall method, and data for Grainex Mar-M 247 at 649°C.

Assuming the ratio of mean to alternating stress was equal to 1 at the start of the strain-life tests, V_σ (Eqn. 4.15) was compared at the beginning and approximate half-life for each test (Table 4.7). The variation of mean stress and range of stress was then compared with increasing strain amplitude Figure 4.17). Point P1 through point P2 defines elastic behavior. Point P2 defines where the mean stress and range of stress are equal. Point P3 defines the point of zero mean stress. Finally, point P3 to P4 is the region of zero mean stress.

Table 4.7 Comparison of V_σ at N_f = 1 and $N_f/2$ for Grainex Mar-M 247 at 649°C, R_ε = 0

strain range	at N = 1	at $N_f/2$		at $N_f/2$
	V_σ	σ_m [MPa]	σ_a [MPa]	V_σ
0.50	1	344.1	463.3	0.74
0.50	1	281.0	472.7	0.59
0.58	1	295.1	513.7	0.57
0.58	1	247.9	562.3	0.44
0.58	1	265.8	556.1	0.48
0.67	1	227.5	598.5	0.38
0.67	1	206.9	600.6	0.34
0.67	1	180.6	608.1	0.30
0.78	1	100.3	745.0	0.13
0.78	1	153.8	669.5	0.23
0.78	1	106.9	706.7	0.15
0.90	1	88.6	734.7	0.12
0.90	1	60.0	781.2	0.08
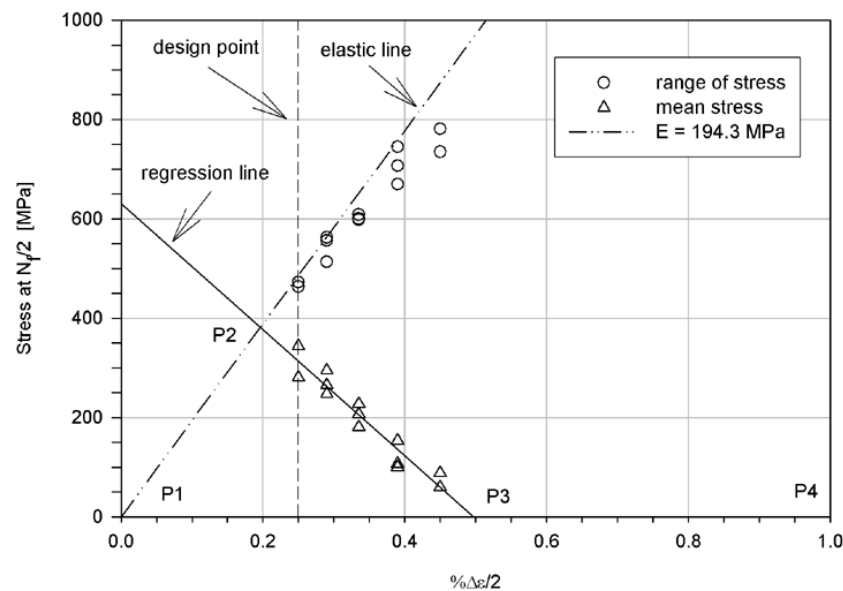
Figure 4.17 Variation of mean stress and range of stress with strain amplitude at $N_f/2$ for Grainex Mar-M 247 at 649C, R_ε = 0.[15]

Comparison between MUS, Halford-Nachtigall, and Data

Both the MUS and the Halford-Nachtigall method provide a means to predict fatigue strain-life by use of only tensile data. It was expected that the MUS would over-predict the $R_\varepsilon = 0$ data (Figure 4.16) since the MUS is generally used in predicting $R_\varepsilon = -1$ data. At the design point of 0.5% total strain, the MUS predicted N_{f0} at 100,000 cycles. This is 5 times greater than the average $R_\varepsilon = 0$ data at 0.5% total strain of approximately 20,000 cycles. In comparison, the Halford-Nachtigall method predicted a life of approximately 23,500 cycles. Thus, a more accurate prediction was found at the 0.5% total strain design point using only tensile data and modifying the MUS with the Halford-Nachtigall Method to account for mean stress effects.

Morrow Strain-Life Equation

σ_f' and b were determined from a plot of $\dfrac{\Delta\varepsilon_{el}}{2}$ versus $2N_f$ (Figure 4.18). A linear regression of the $R_\varepsilon = -1$ data resulted in a y-intercept at $2N_f = 1$ of -2.09 in log-log coordinates. In linear coordinates the y-intercept was 8.13×10^{-3} $\left(=\dfrac{\sigma_f'}{E}\right)$.

Given an average E of 186 GPa, calculated from the $R_\varepsilon = -1$ data, σ_f' was calculated as 1510 MPa. The fatigue strength exponent, b, was -0.0928.
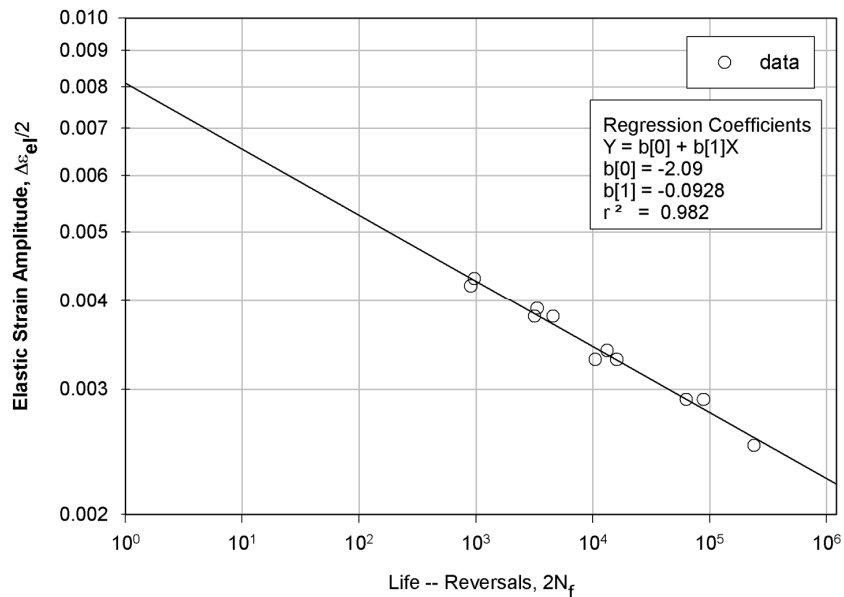
Figure 4.18 Grainex Mar-M 247 elastic strain-amplitude data, $R_\varepsilon = -1$, 649°C.

ε_f' and c were determined from a plot of $\dfrac{\Delta\varepsilon_{in}}{2}$ versus $2N_f$ (Figure 4.19). A linear regression of the $R_\varepsilon = -1$ data resulted in a y-intercept of -1.78 in log-log coordinates. In linear coordinates the y-intercept was 0.0166 (= ε_f'). The fatigue ductility exponent, c, was -0.628.
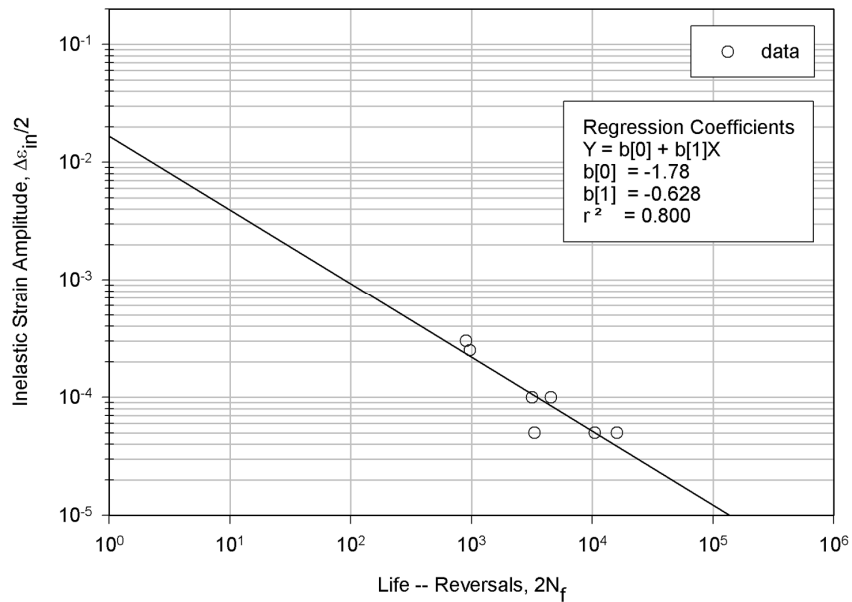
Figure 4.19   NASA Grainex Mar-M 247inelastic Strain-Amplitude Data, $R_\varepsilon = -1$, 649°C.

Thus, the Morrow strain-life equation was determined to be

$$\varepsilon_a = 8.13 \times 10^{-3} \left(2N_f\right)^{-0.0928} + 0.0166\left(2N_f\right)^{-0.628} \qquad \text{Eqn. 4.23}$$

and was compared with $R_\varepsilon = -1$ data (Figure 4.20).

$$\varepsilon_a = 8.13 \times 10^{-3} \left(2N_f\right)^{-0.0928} + 0.0166 \left(2N_f\right)^{-0.628}$$
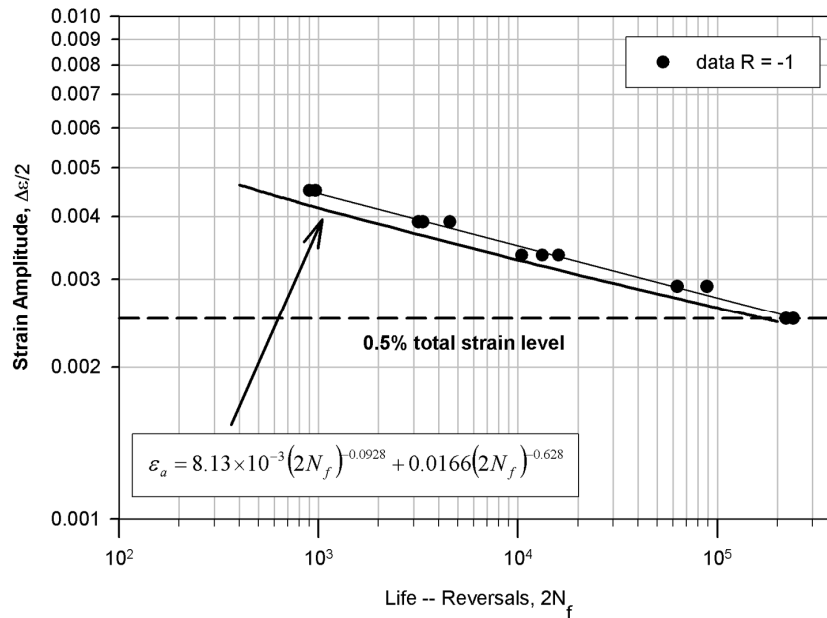
Figure 4.20 Comparison of Morrow Strain-Life equation with Grainex Mar-M 247 data at 649°C.

The Morrow Equation conservatively predicted the cyclic life when compared to the strain-life data at R_ε = -1 and 649°C. At 0.9% total strain range ($\Delta\varepsilon/2$ = 0.0045) the predicted reversal to failure, $2N_f$, was 400 which was 2 times lower than that given by the R_ε = -1 data ($2N_f$ = 950). At the design strain ($\Delta\varepsilon$ = 0.5%), the difference between predicted (155,000) and experimental data (240,000) is nearly 100,000 reversals. One source of error was the low resolution in the plastic strain data used to calculate the fatigue ductility coefficient and exponent. This was due to the low resolution of the pen plotter used to plot the cyclic load versus strain curves for each of the strain-life tests.

Modified Morrow with Mean Stress Effects

Optimization of the coefficients and exponents for the Modified Morrow equation resulted in an R^2 value of 0.928. The coefficients and exponents (Table 4.8) were used in the Modified Morrow equation. The results of the Modified Morrow equation were compared to experimental Grainex Mar-M 247 strain-amplitude data (Figure 4.21).

**Table 4.8 Optimized coefficient and
exponent values for the Modified Morrow
Equation for Grainex Mar-M 247 at 649°C**

Coefficients	original	optimized
$\sigma_f^{'}$ (MPa)	1507	1507
$\varepsilon_f^{'}$	0.117	0.027
Exponents		
b	-0.0928	-0.090
C	-0.628	-0.627
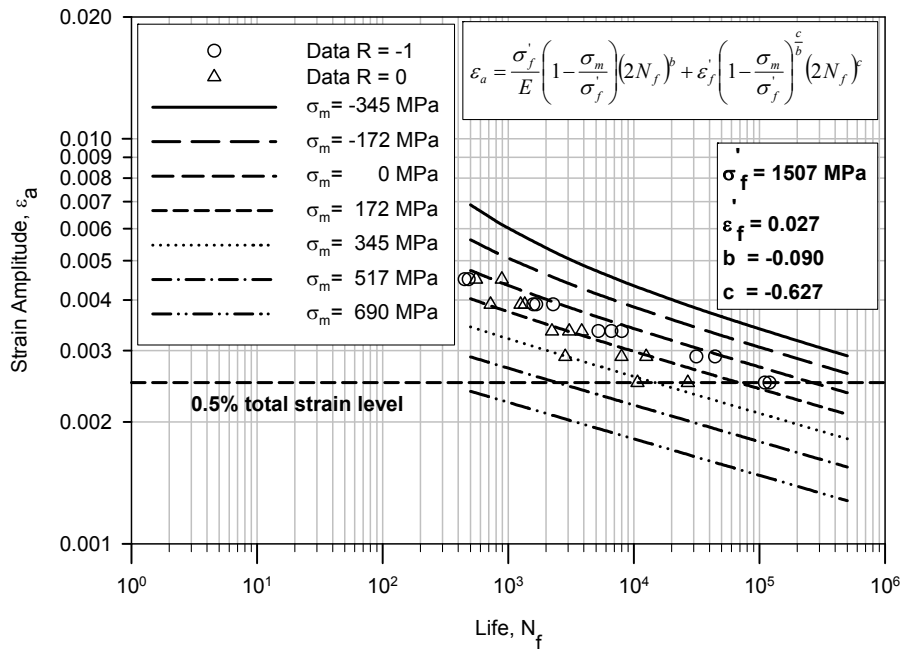
**Figure 4.21 Comparison of NASA Grainex Mar-M 247 data at 649°C with
predictions from the Modified Morrow equation.**

As expected, higher mean stresses were observed at lower strain levels while lower mean stresses were observed at higher strain levels (see also Figure 4.17).[15] This is because the larger the strain range, the greater the degree of relaxation of the initial mean stress imposed by the $R_\varepsilon = 0$ strain condition. The effect of mean stress on cyclic life was more pronounced at lower strain levels (Table 4.7). For example, at the design strain level of 0.5% total strain, the average mean stress was 313 MPa, while at 0.9% total strain, the average mean stress was 74 MPa.

Also, cyclic life decreased as mean stress increased for constant strain amplitude. For example, at the design point of $\Delta\varepsilon = 0.5\%$ ($\varepsilon_a = 0.0025$) the difference in cyclic life between the $\sigma_m = 0$ MPa line and the $\sigma_m = 172$ MPa line was nearly a factor of four. The $R_\varepsilon = 0$ data were observed to trend towards a zero mean stress at the highest strain range ($\varepsilon_a = 0.0045$). Finally, as expected, compressive mean stresses predict an increase in cyclic life.

Fractographic Examination

The majority of the crack initiation sites were observed at or near the surface of the gage cross-section perimeter and initiated at carbides. The fracture surfaces exhibited 3 areas of cracking – crack initiation, propagation, and overload.

The crack initiation site could be traced by following river patterns which point back to the crack initiation site (Figure 4.22 - Figure 4.24).[16] By contrast, the overload surfaces were faceted in appearance at low magnification (Figure 4.25 and Figure 4.26).

No relationship was determined between crack initiation direction on the fracture surface in relation to the specimen's location in the NASA disk, to R_ε, level or $\%\Delta\varepsilon$. Dual crack initiation sites (Figure 4.25) were observed in most specimens tested at higher strain ranges, which is in agreement with literature[17].
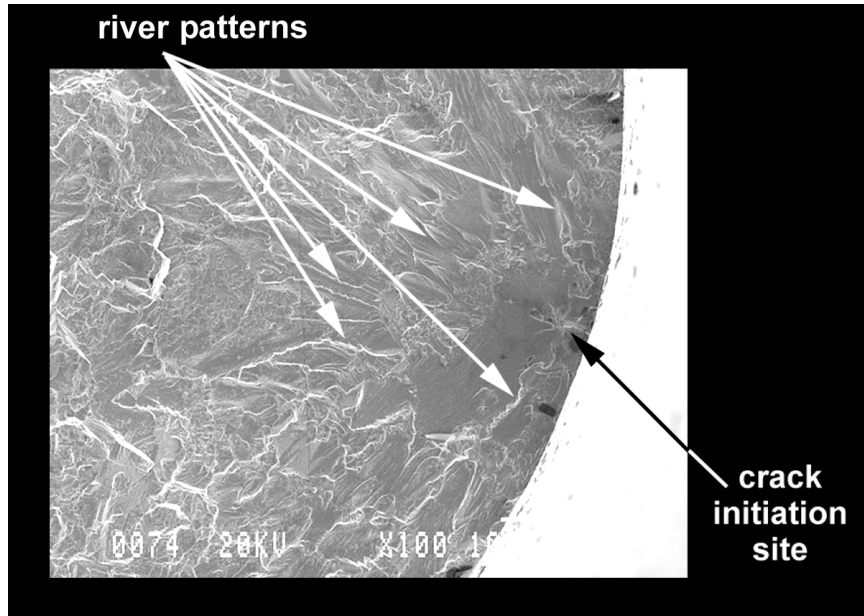
Figure 4.22 SEM Micrograph SE mode for specimen 77L at 100x. River patterns pointing back to crack initiation site.
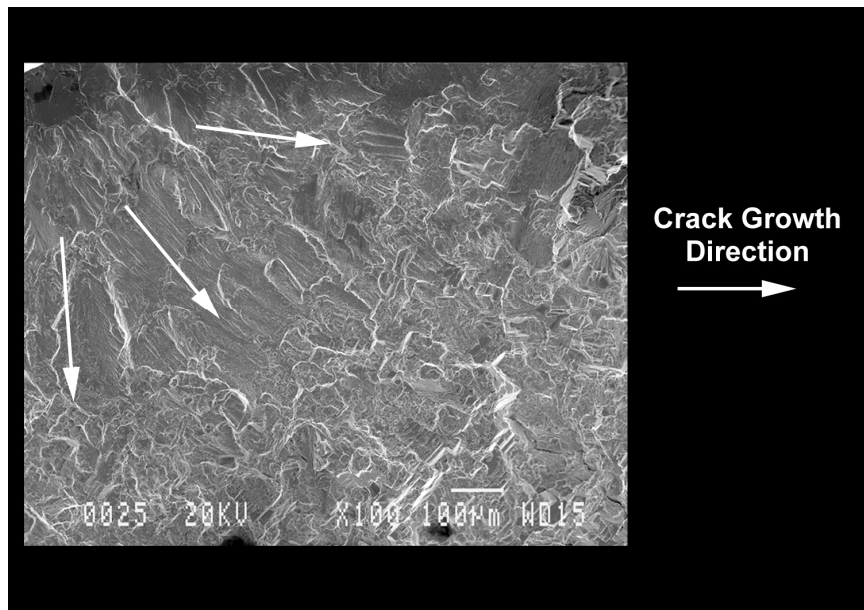
Figure 4.23   SEM (SE mode), 87L, 100x. River patterns pointing back to crack initiation site.
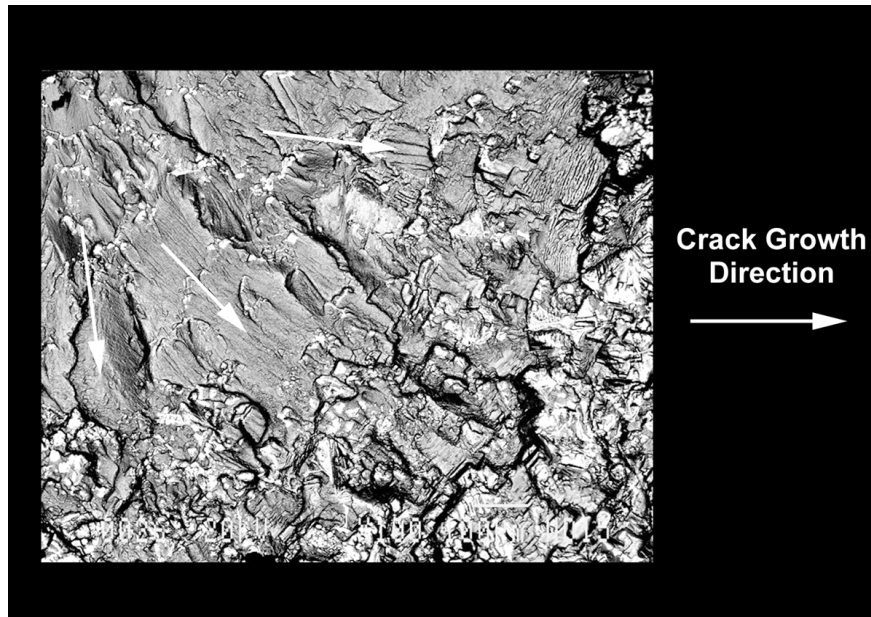
Figure 4.24 SEM (BE mode), 87L, 100x. Crack propagation showing river patterns pointing back to crack initiation site. (See also Figure 4.23)
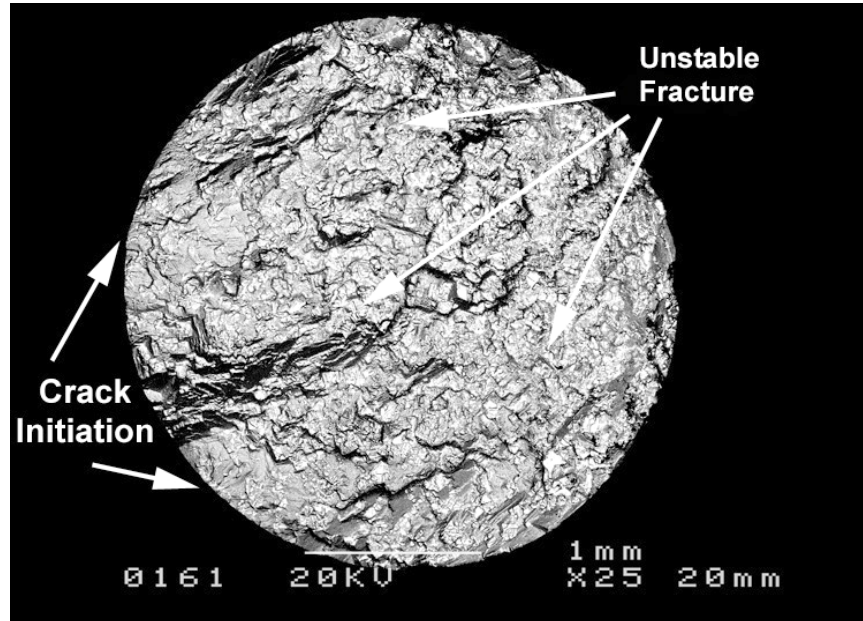
Figure 4.25 SEM Micrograph in backscattered electron mode for specimen 26L at 25x. Unstable fracture with dual crack initiation sites.
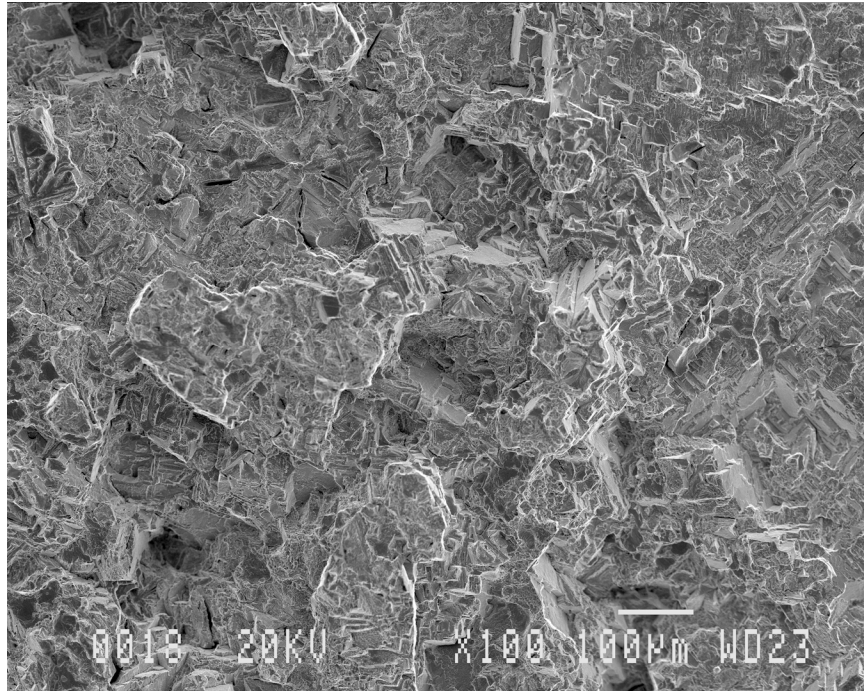
Figure 4.26 SEM (SE), 86L, 100x. Typical overload fracture.

Of the 30 fracture surfaces examined, 25 exhibited surface crack initiation. Twenty-one of the 25 surface initiated cracks occurred at a carbide (Figure 4.27). Three of the remaining 4 specimens with surface initiated cracks contained voids (Figure 4.28). SEM examination of the complementary surface of the specimens may determine if a carbide was present. One specimen with surface initiated cracks (Specimen 47L) showed both a void and a carbide at surface locations. Five of the 25 surface initiated cracks that started at a carbide also showed evidence of grain boundary cracking (Figure 4.29). Five of the original 30 surfaces showed subsurface crack initiation. Four of the 5 initiated at carbides (Figure 4.30 and Figure 4.31) while the last (Specimen 15L) was indeterminate. Table 4.9 summarizes specimen crack, void and carbide locations. A complete set of SEM images is given in Appendix C.
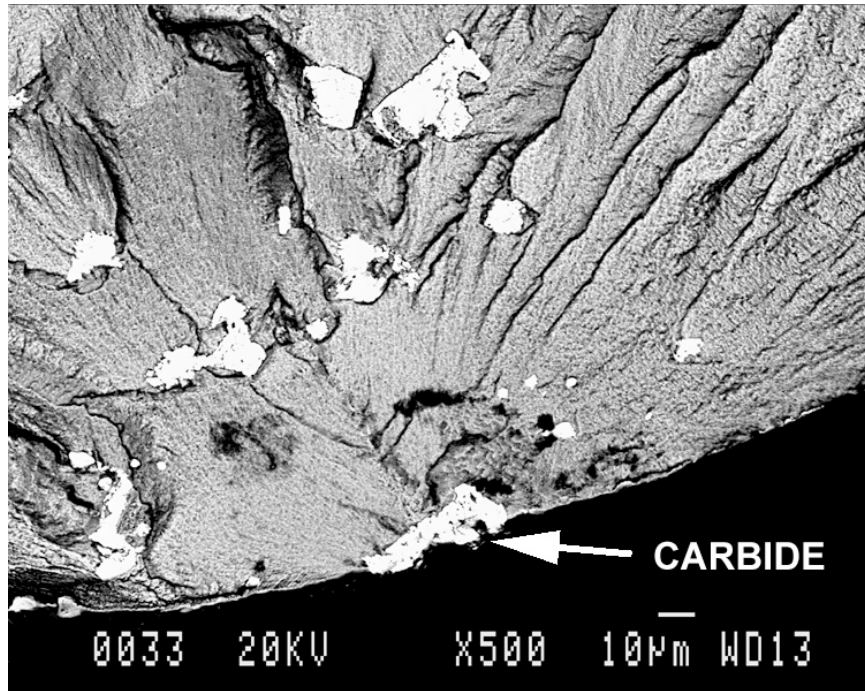
Figure 4.27 SEM (BE), CA1L, 500x showing surface carbide crack initiation.
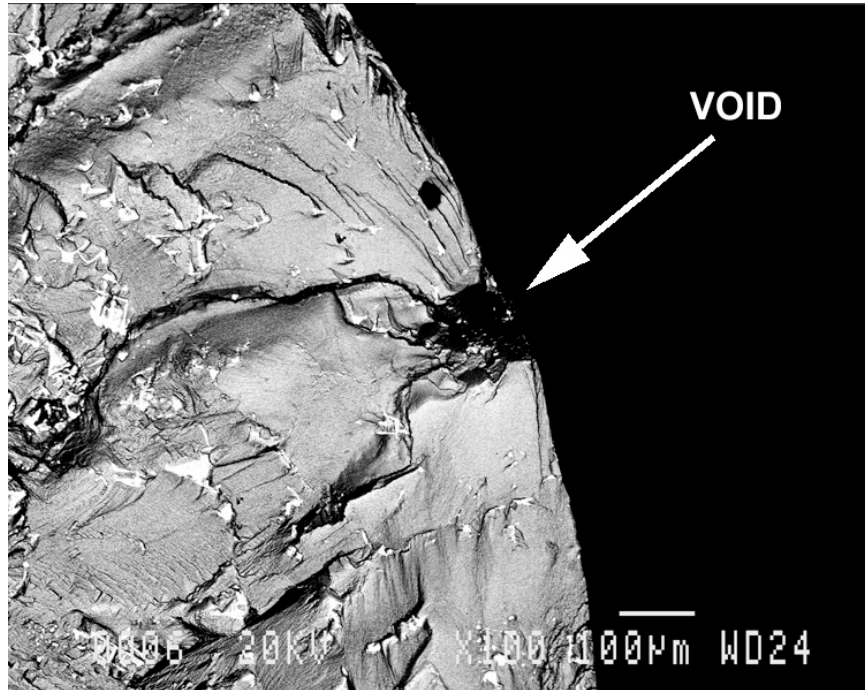
Figure 4.28 SEM (BE), 86L, 100x showing void at surface crack initiation site.
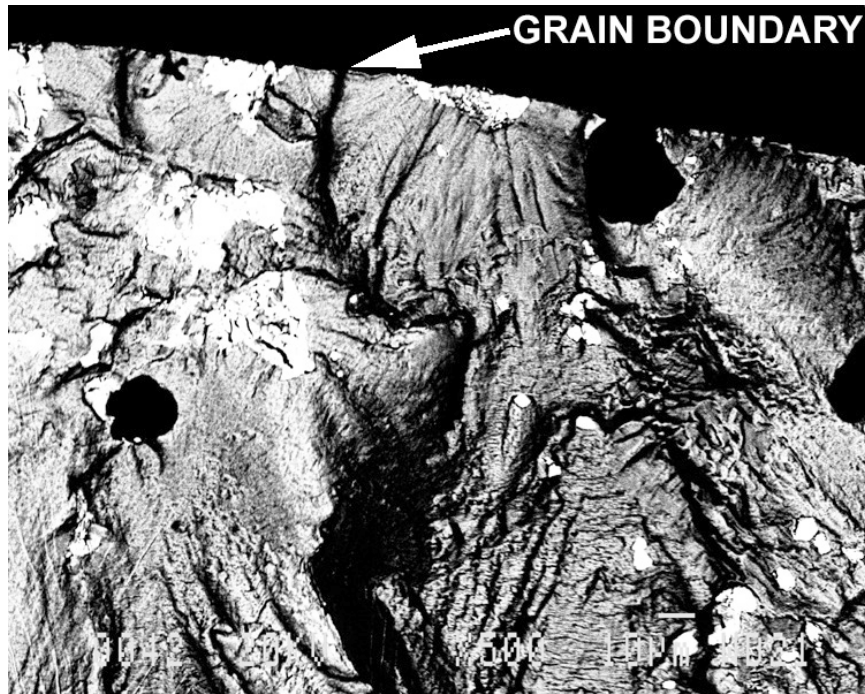
Figure 4.29 SEM (BE), CA3L, 500x. Observed grain boundary cracking.
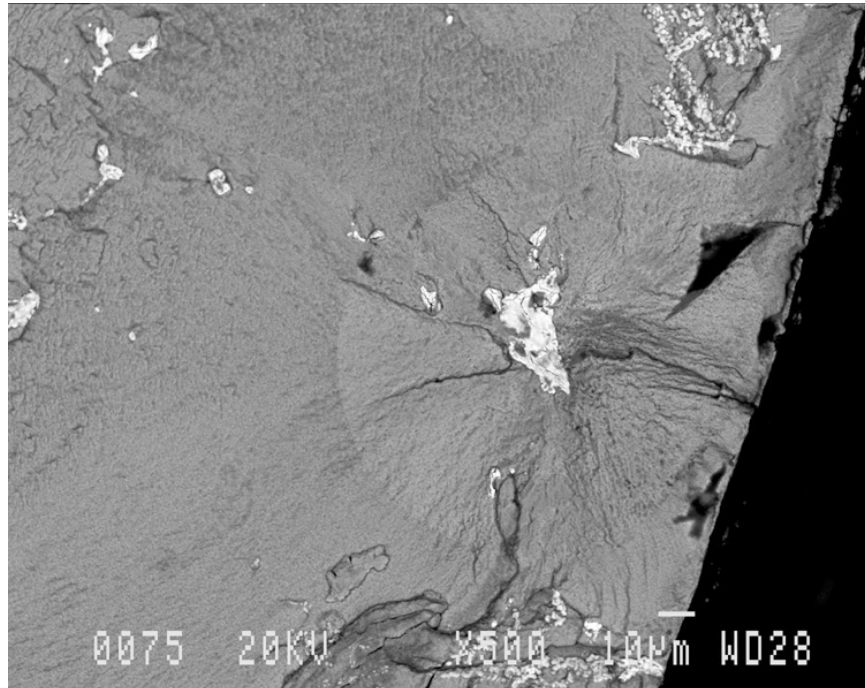
**Figure 4.30   SEM (BE), 77L, 500x. Subsurface carbide crack initiation
occurring at a carbide.**
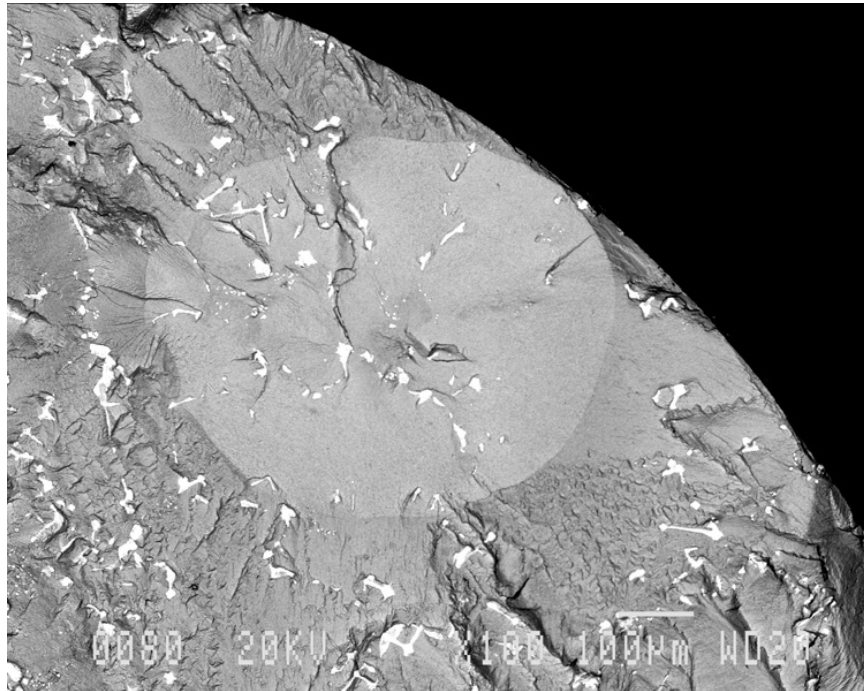
Figure 4.31 SEM (BE), CA9L, 100x. Carbide cracking within grain.

Table 4.9 Summary of scanning electron microscope results for Grainex Mar-M 247 strain-life specimens at 649°C

Specimen	R_ε	$\%\Delta\varepsilon$	N_f	Crack Information 'clock' location, surface/subsurface, carbide/void
CB1L	-1	0.50	104433	0200, surface, no carbide present
86L	-1	0.50	120171	0230, surface, void
66L	-1	0.50	429420	0900, surface, void
76L	-1	0.58	31486	0900, surface, carbide
CA9L	-1	0.58	44313	0100, subsurface, carbide within grain
57L	-1	0.58	116335	0930, surface, void
CB8L	-1	0.67	5231	0530, surface, carbide
47L	-1	0.67	6624	Crack 1, 1100, surface, carbide Crack 2, 1100, surface, void
CA7L	-1	0.67	8018	0800, surface ,carbide
CA4L	-1	0.78	1586	0430, surface, carbide + boundary, 0730, surface, multiple carbides
27L	-1	0.78	1668	Crack 1, 1000, surface, carbide Crack 2, 1200, surface, multiple carbides
CB6L	-1	0.78	2279	0800, surface, carbide
CB3L	-1	0.90	451	0730, surface, carbide
15L	-1	0.90	484	Indeterminate, surface likely, carbide likely
CA2L	-1	0.90	875	Crack 1, 0300, surface, carbide Crack 2, 1200, surface, multiple carbides
CA8L	0	0.50	10697	0500, surface, void
77L	0	0.50	26939	0400, subsurface, carbide
67L	0	0.50	127523	middle, within grain, carbide
87L	0	0.58	2842	1100, surface, carbide + boundary
CB2L	0	0.58	7970	0900, surface, carbide
56L	0	0.58	12566	0700, subsurface, carbide
CB5L	0	0.67	2234	0130, surface, carbide
46L	0	0.67	3056	0900, surface, carbide
CA1L	0	0.67	3842	0500, surface, carbide
35L	0	0.78	723	0900, surface, multiple carbides & voids
CB7L	0	0.78	1254	1030, surface, carbide
CA3L	0	0.78	1352	0100, surface, carbide + grain boundary
CB9L	0	0.90	554	0230, surface, carbide + grain boundary
26L	0	0.90	889	Crack 1, 0700, surface, multiple carbides Crack 2, 0900, surface, multiple carbides
CA6L	0	0.90	1142	1030, surface, carbide + grain boundary

<u>Discussion Summary</u>

Tensile properties for the Grainex Mar-M 247 NASA disk at 649°C were presented and compared with literature data. Fatigue strain life data for the same material were also presented at 649°C at strain ranges of 0.50%, 0.58%, 0.67%, 0.78%, and 0.90%. Both the tensile and $R_\varepsilon = 0$ strain-life data were comparable with literature.

Evaluation of mean stress effects showed a large effect on cyclic life. The Halford-Nachtigall Method used with the MUS was practical for predicting $R_\varepsilon = 0$ life using only tensile data at 649°C. A difference of only 18% in cyclic life was observed between predicted and experimental lives at the design point of 0.5% strain range. The 10,000 cycle limit suggested by the Modified Morrow analysis at the 0.5% design strain range can be reduced accordingly to 1500 cycles using an equivalent -3σ reduction factor and probabilistic accounting for the 6 bolt holes using Eqn. 1.1.

During operation, the NASA disk is generally cycled at zero to maximum strain conditions ($R_\varepsilon = 0$). At the design strain of $\Delta\varepsilon = 0.5\%$ the $R_\varepsilon = 0$ results lead to, at the -99.95% prediction level, a cyclic crack initiation life of 1100 cycles which is nearly 6 times less than the initial predicted cycles to failure obtained previously by Tong and Steinetz.[1] Probabilistic accounting for the 6 bolt holes by using Eqn. 1.1 gives the most conservative result of 665 cycles with 6 bolt holes.

Thus, using the experimental data at a -99.95% prediction level and the presence of 6 bolt holes it was found that the NASA disk should be inspected for surface cracks after 665 cycles based on a total strain range of 0.50% at 649°C.

Chapter 4 Works Cited

1. Tong, Mike and Bruce Steinetz. "Mar-M 247 Disk Finite Element Thermal and Stress Analysis", NASA Glenn Research Center, Cleveland. 30 January 1997.
2. Kaufman, M. "Properties of Cast Mar-M-247 for Turbine Blisk Applications." Superalloys 1984. Ed. Maurice Gell et al. Warrendale: Metallurgical Society of AIME, 1984. 43-52.
3. Macha, D.E., G.R. Cole, and J.A. Butzer. "Fine Grain, Investment-Cast Integral Turbine Wheels." Grain Refinement in Castings and Welds. Ed. G.J. Abbaschian and S.A. David. New York: The Metallurgical Society of AIME, 1983. 197-219.
4. Halford, G.R., and A.J. Nachtigall. "Strainrange Partitioning Behavior of an Advanced Gas Turbine Disk Alloy AF2-1DA." Journal of Aircraft, 17.8 (1980) 598-604.
5. Mar-Test. "Tensile and Strain-Life Test Descriptions" email to Irebert Delgado. 15 Oct. 2003.
6. Mar-Test. "Tensile Test Specimen Geometry." Fax to Irebert Delgado. 03 May 2001.
7. Dowling, Norman E. Mechanical Behavior of Materials : engineering methods for deformation, fracture, and fatigue. Upper Saddle River: Prentice-Hall, Inc., 1999.
8. Neugebauer, Bob. "Mar-Test Strain-Life Specimen Geometry." Personal communication by Irebert Delgado. 22 September 2000.
9. ASTM Committee E-8 on Fatigue and Fracture. "ASTM E-606 – 92 (Reapproved 1998): Standard Practice for Strain-Controlled Fatigue Testing." Annual Book of ASTM Standards 2001: Section 3 Metals Test Methods and Analytical Procedures: Volume 03.01 Metals—Mechanical Testing; Elevated and Low-Temperature Tests; Metallography. ASTM. West Conshohocken: ASTM, 1998. 543-557.
10. Keller, Dennis. Introduction to Regression: Theory, Methods, Applications. Fairview Park: RealWorld Quality Systems.
11. Manson, S.S. "Fatigue: A Complex Subject." Experimental Mechanics. 5.7 (1965) 193-226.
12. Manson, S.S. "Predictive Analysis of Metal Fatigue in the High Cyclic Life Range." Methods for Predicting Material Life in Fatigue. Ed. W.J. Ostergren and J.R. Whitehead. New York: ASME, 1979.
13. Lapointe, N.R. "Monotonic and Fatigue Characterizations of Metals," Proceedings of The SAE Fatigue Conference P-109. Warrendale: Society of Automotive Engineers, Inc., 1982.
14. Howmet Turbine Components Corporation. TB 3000: Grainex Cast Mar-M 247 Alloy. Greenwich: Howmet Turbine Components Corporation.

15. Conway, Joseph B., and Lars H. Sjodahl. <u>Analysis and Representation of Fatigue Data</u>. Materials Park: ASM International, 1991.

16. Kerlins, Victor, and Austin Phillips. "Modes of Fracture." <u>Metals Handbook Volume 12 Fractography</u>. 9th ed. Metals Park: ASM International. 1987.

17. Hertzberg, Richard W. <u>Deformation and Fracture Mechanics of Engineering Materials</u>. 3rd ed. New York: John Wiley & Sons, Inc. 1989.

5.   Fatigue Crack Growth Behavior of Grainex Mar-M 247

5.1   Introduction

The possibility exists that surface cracks would develop over time in the bolt holes of the Grainex Mar-M 247 NASA disk (Figure 1.1, Figure 3.1a, and Figure 3.1b) used in NASA's Turbine Seal Test Facility. An inspection interval of the bolt holes can be implemented using strain-life data and fatigue crack growth data to preclude catastrophic NASA disk failure. The present chapter focuses on the fatigue crack growth behavior of the Grainex Mar-M 247 material.

The purpose for characterization of the fatigue crack growth behavior is to predict the cycles to failure of a surface crack growing from an initial flaw to a critical crack length.

5.2   Materials and Methods

Experiment

Tests were conducted at 649°C, at a load ratio of R = 0.05, with a sinusoidal waveform at a cyclic frequency of 0.33 Hz. A surface flaw (or K_b) specimen (Figure 5.1) was used to simulate the growth of a flaw within a disk bolt hole. The K_b specimen was first developed by Coles et. al.[1] for evaluating turbine engine components.

The K_b specimen was fabricated by electro-discharge machining (EDM) a cylinder from the sacrificial Grainex Mar-M 247 NASA disk that was 41 mm long by 14 mm in diameter. A total of 8 fatigue crack growth specimens were fabricated from the sacrificial NASA disk (Figure 3.1a). The cylinders were removed at locations adjacent to the NASA disk bolt holes and oriented perpendicular to the bolt hole axis. This oriented the machined surface flaw on the K_b specimen perpendicular to the applied cyclic stress, since cracks tend to initiate within bolt holes from circumferential and radial disk stresses during rotation.[2] The axial direction is parallel with the bolt holes of the NASA disk (Figure 3.1b).

Inconel 718 cylinders were inertia-welded to both ends of the Grainex Mar-M 247 cylinders. The ends of the resultant specimen were machined to a buttonhead for gripping by the fatigue testing machine. The surface flaw was plunge EDM'd on one side of the rectangular gage section in the shape of a half-circle (Figure 5.2). Note that the depth and width of the surface flaw were approximately doubled from those dimensions shown in Figure 5.2 after failures outside the gage section occurred in initial tests. Thus, the final surface flaw size that was used was 0.46 mm in depth by 0.91 mm in width. This enlargement of the EDM notch was necessary to encourage crack growth at the surface flaw. All fatigue crack growth specimens (Figure 5.3) were fabricated at Mar-Test in Cincinnati, Ohio.
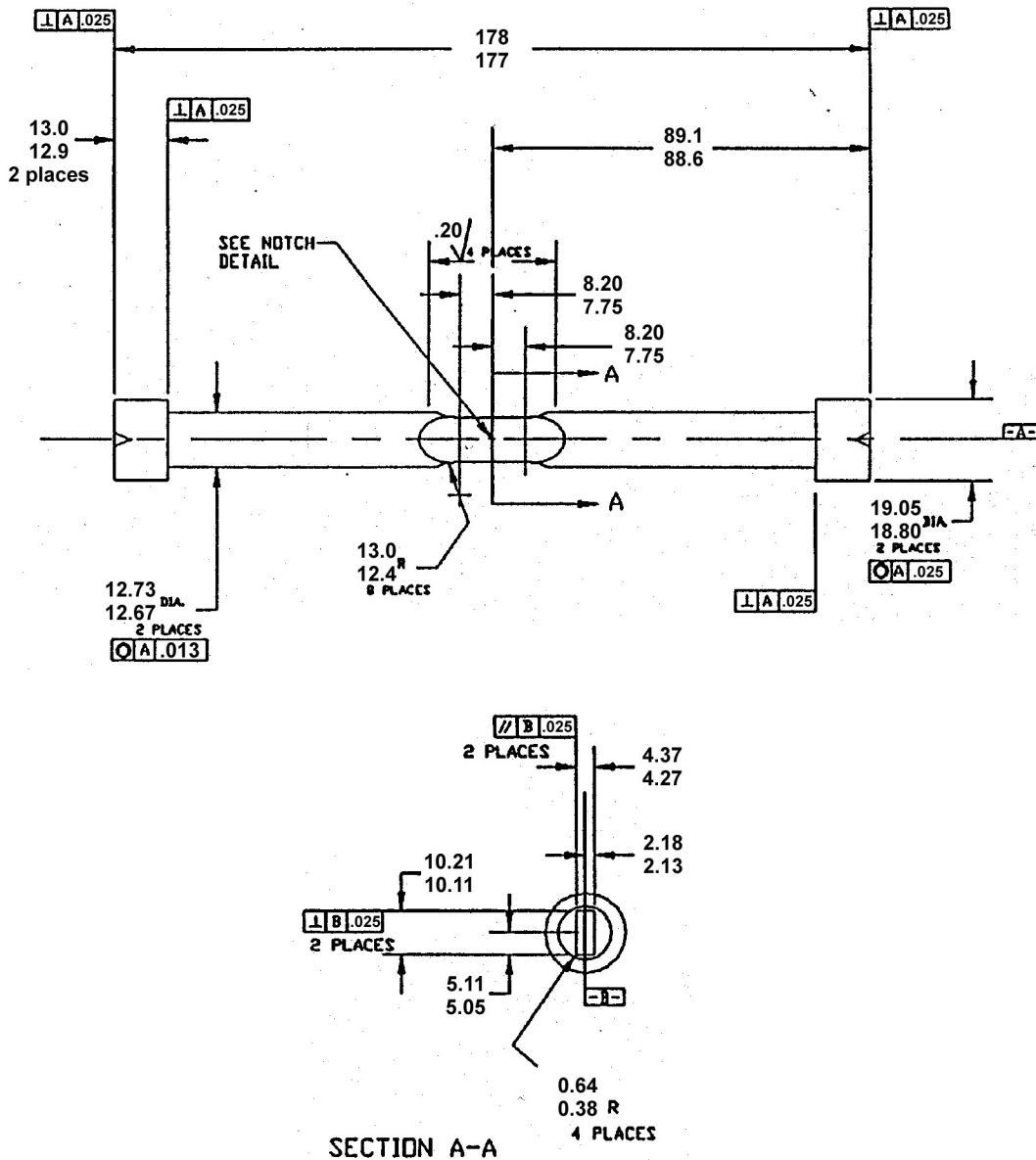
Figure 5.1 Surface flaw (K$_b$) specimen geometry for the Grainex Mar-M 247 fatigue crack growth tests at 649°C. [3] **Dimensions are in millimeters.**
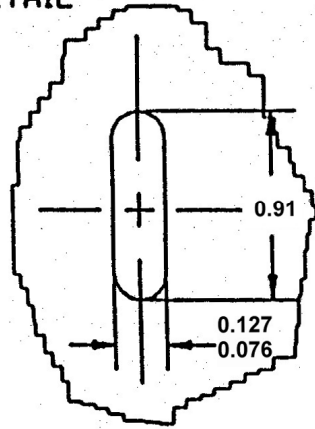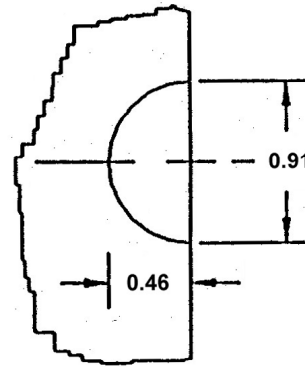
Figure 5.2 Surface flaw geometry for the K_b specimen.[3] Dimensions are in millimeters. See also Figure 5.1 for location of notch on K_b specimen.
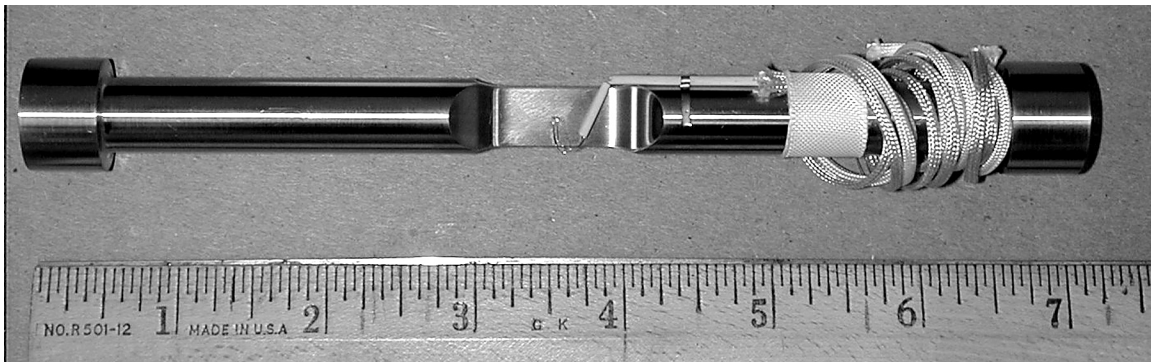
Figure 5.3 K_b specimen with alumel wire attachments for potential drop crack growth measurement.

Fatigue crack growth tests were performed at the NASA Glenn Research Center fatigue and fracture laboratories. A Materials Test System 810 (MTS Corporation, Minneapolis, Minnesota) was utilized (Figure 5.4). The system is computer-controlled by a custom program, MATE (Material Analysis and Test Environment), which also acquires the raw fatigue crack growth data.[4] Crack length computations for the K_b specimen are based on a closed-form analytical model by Gangloff et.al. that has been experimentally confirmed.[5,6,7]

Fatigue crack growth of the K_b specimen was measured using the direct current electrical potential difference (dcEPD) method. The method was initially developed by Gangloff[8] for small surface cracks in hour-glass shaped specimens. The method was modified by Vanstone and Richardson[9] for specimens having rectangular cross sections with semi-circular EDM notches. Fatigue crack growth in a semi-circular crack is related to voltage through an analytical model developed by Roe and Coffin[8]. To facilitate potential drop measurements, 0.13 mm diameter alumel wires were tack-welded to either side of the EDM notch (Figure 5.5).
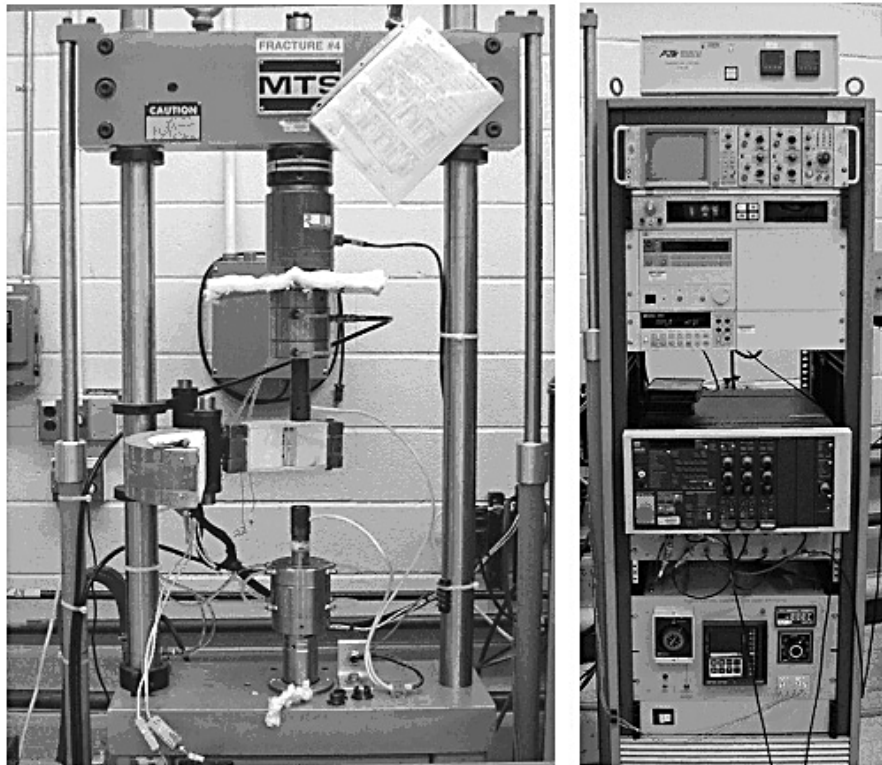
Figure 5.4 Fatigue crack growth test equipment and controls at NASA's fatigue and fracture laboratories.
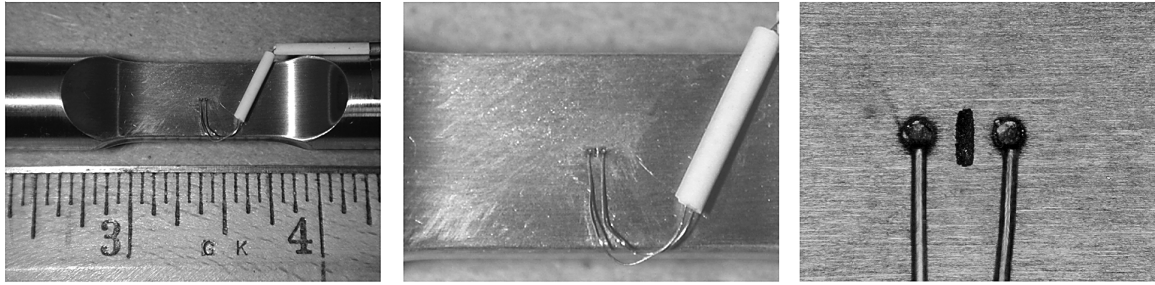
Figure 5.5 Alumel wire location at the notch area of the K_b specimen.

Key
$2b_c$	crack height
$2c_c$	crack width
$2L_p$	potential probe spacing

Nominal Measurements [mm]
$2b_c$	0.152
$2c_c$	0.953
$2L_{pmin}$	0.523
$2L_{pctr}$	0.732
$2L_{pmax}$	0.955
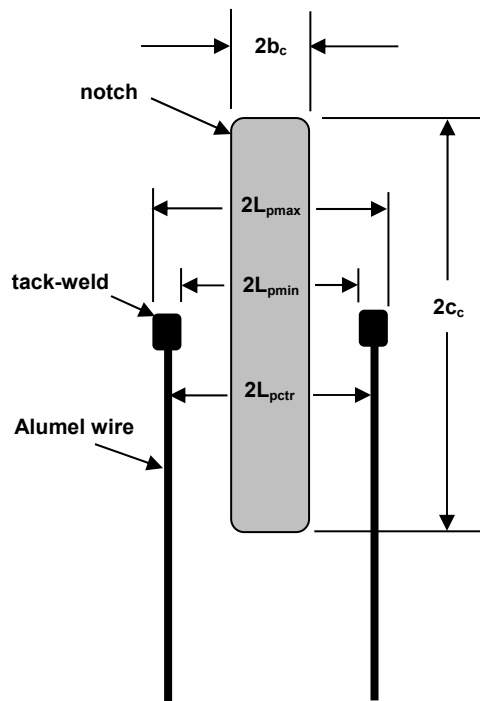
Figure 5.6 Nominal fatigue crack growth pre-test measurements for the K_b specimen surface flaw geometry.

Measurements of the EDM notch geometry were taken prior to installing the K_b specimen in the load frame (Figure 5.6). Measurements were taken with a Nikon Measurescope 10 (Nikon, Tokyo, Japan) and a Nikon SC-102 X-Y digital readout (Nikon, Tokyo, Japan). The Measurescope has an accuracy of ±0.0025 mm.

The measurements were used as input into MATE to calculate crack length, maximum load, and dcEPD voltage during the test. An assumption on the EDM crack depth was initially inputted into MATE, based on original EDM notch specifications, and was subsequently corrected for in post-test calculations.

The K_b specimen was installed into the MTS load frame with 12-gage copper leads attached to the buttonheads. A constant 10 amps was applied to the leads, forming a circuit through the specimen having a voltage across the Alumel wire locations (Figure 5.5). The voltage increased with increasing crack length and depth. Baseline voltage measurements were taken to adjust for thermoelectric influences.[10]

Prior to starting the pre-cracking portion of the test, initial voltages were taken at 0 N and 17.8 KN axial load on the K_B specimen. The specimen was pre-cracked at room temperature to grow the notch to approximately 0.81 mm in depth. Pre-cracking was conducted to ensure that fatigue crack growth occurred beyond the recast layer resulting from the EDM notch. Pre-cracking was performed with a sinusoidal waveform at 3 Hz, and R = 0.05 (P_{max} = 25.8 KN). Both crack length voltages and number of cycles were acquired. After pre-cracking, reference voltage measurements (V_N) were again taken at 0 N and 17.8 KN axial load. These voltages were used to correct for voltage drift and for normalizing the acquired crack length voltages for data reduction. Reference voltages were taken prior to the pre-crack test and the actual crack-growth test at 649°C.

Three type-K thermocouples were tack-welded to the gage section of the K_b specimen (Figure 5.7). Thermocouple 1 (T/C 1) measured the K_b specimen test temperature. T/C 2 and T/C 3, spaced 6.35 mm from the center thermocouple, were used for temperature control.

Two half-section resistance furnaces (Figure 5.4) were then positioned around the K_b specimen. The specimen was heated to 649 ± 1°C at zero load with the K_b surface temperature read out through a digital meter. Initial voltage potentials were measured at axial loads of 0 N and 17.8 KN. An initial voltage was also taken to account for thermoelectric influences. The test was conducted with a sinusoidal waveform at 0.33 Hz, and a ratio of R = 0.05 (P_{max} = 27.4 KN).
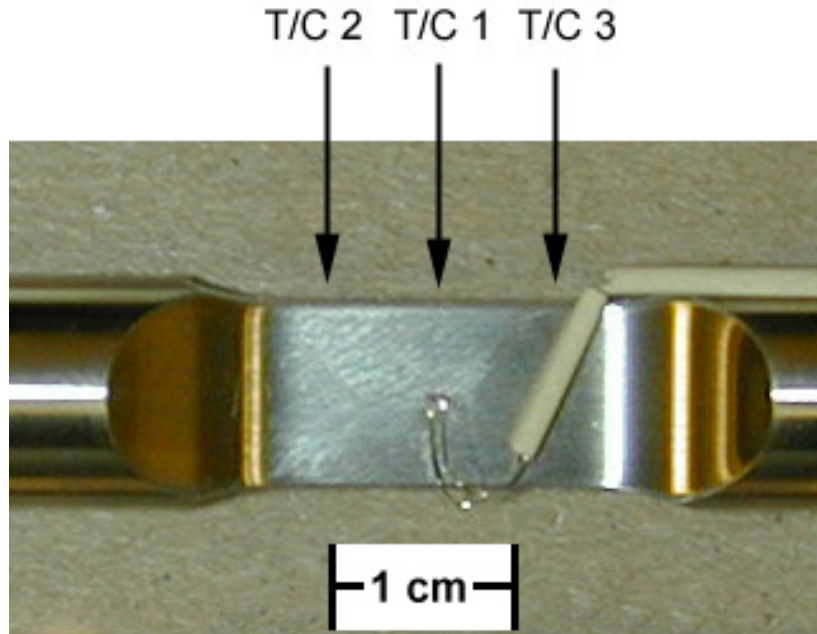
Figure 5.7 Thermocouple locations on the K_b specimen gage section indicated by the arrows. Thermocouples not shown.

For each acquisition, MATE recorded the cycle count, total crack length, maximum load, corrected dcEPD voltage, number of dcEPD points acquired, thermoelectrically induced voltage, and input load ratio. Data was taken approximately every 0.0508 mm of crack extension.[11] For back-up, voltage and load history were recorded with a strip chart recorder and data acquired by MATE was printed.

The crack was allowed to grow to 2.54 mm. This crack length limitation was due to the 4.32 mm gage thickness. Experience has shown that crack length voltage accuracy begins to drop off for crack lengths at approximately 65% of the gage thickness.[12] Final voltages were again taken at axial loads of 0 N and 17.8 KN. At the conclusion of the test, the test specimen was brought to failure by monotonically increasing the load to failure.

<u>Data Reduction</u>

   Crack depth data was corrected based on post-test measurements of the fracture surface (Figure 5.8 and Figure 5.9).
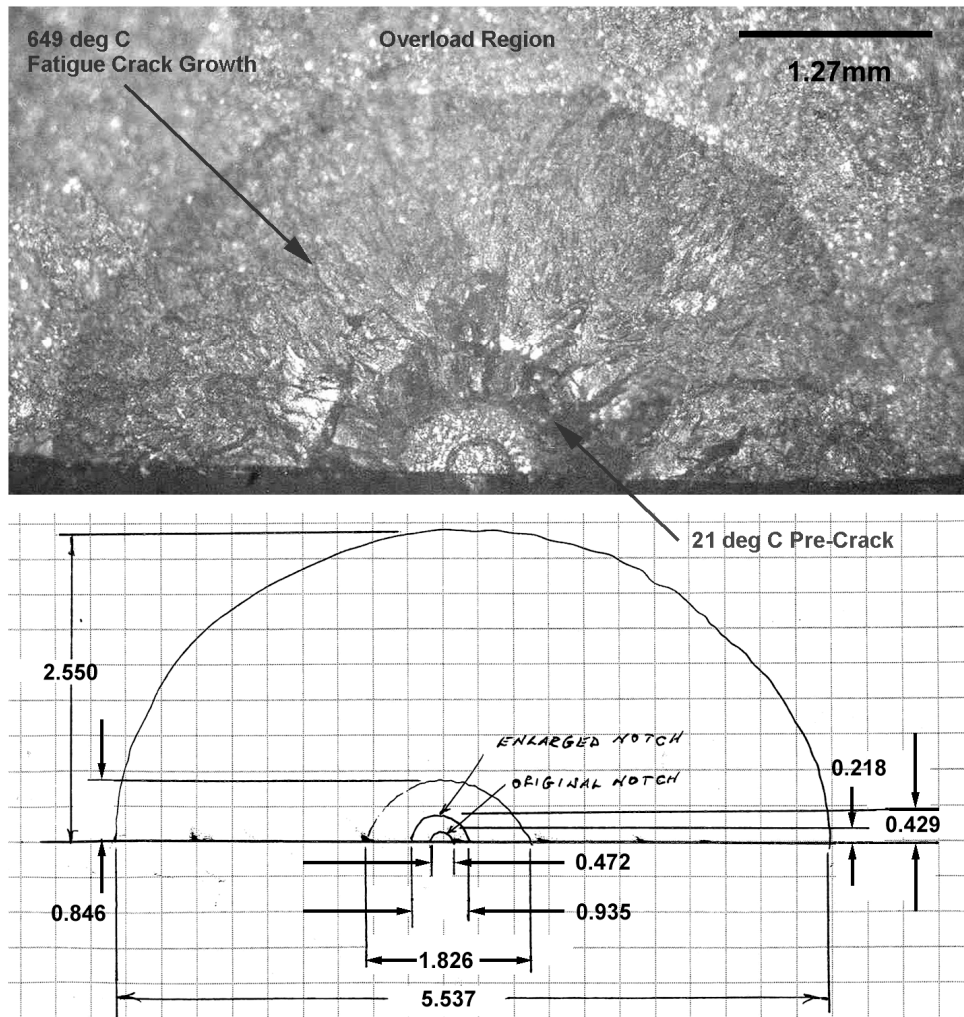
Figure 5.8   Fracture surface measurements for the Grainex Mar-M 247 K_b specimen (13K). Dimensions are in millimeters.
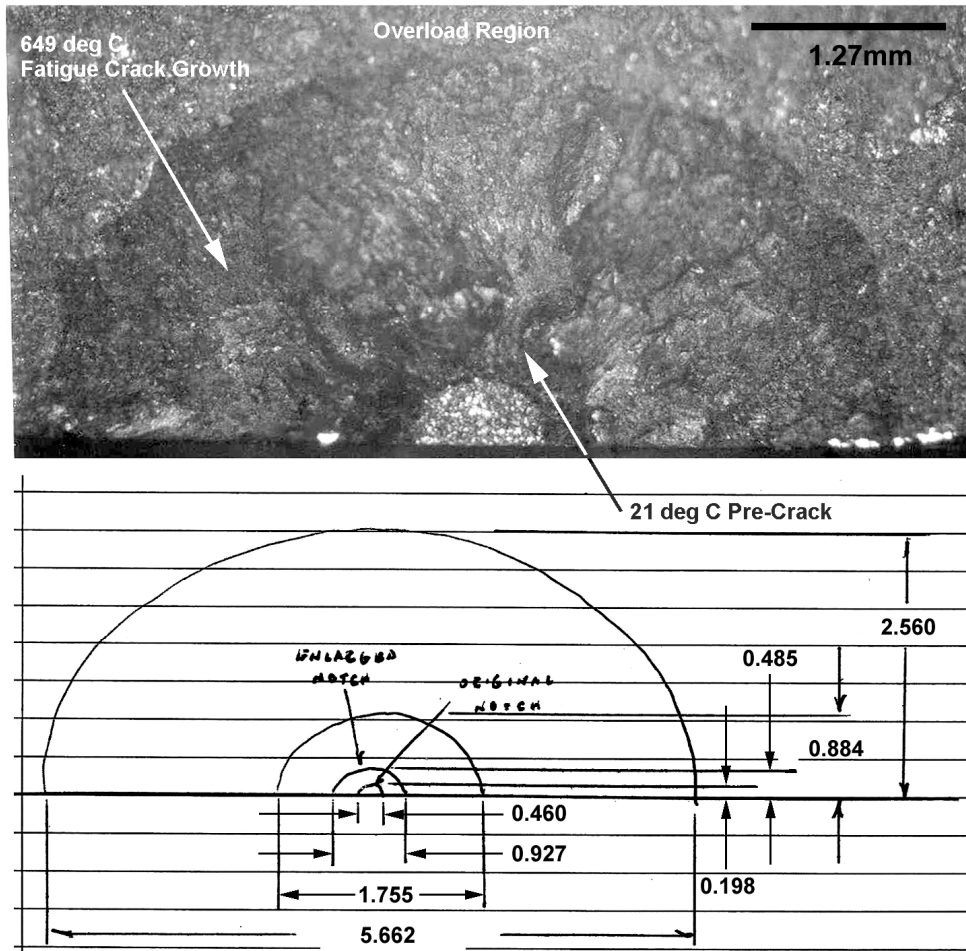
Figure 5.9 **Fracture surface measurements for the Grainex Mar-M 247 K$_b$ specimen (32K). Dimensions are in millimeters.**

The solution was automated within the MATE program where iterations were performed which compared the measured voltage for a calculated crack depth to the voltage predicted by the Roe-Coffin potential solution[9] for a semi-elliptical surface notch.

The Roe-Coffin solution, given by Gangloff,[8] has the form

$$V/_{V_N} = f(a_c, b_c, c_c, a_n, b_n, c_n, L_p) \qquad \text{Eqn. 5.1 (Ref.8)}$$

where
V	= crack length voltage	[volts]
V$_N$	= reference voltage	[volts]
a$_c$	= crack depth	[mm]
b$_c$	= crack half-height	[mm]
c$_c$	= crack surface half-width	[mm]
a$_n$	= initial EDM crack depth	[mm]

$$b_n = \text{initial crack half-height} \qquad\qquad \text{[mm]}$$
$$c_n = \text{initial crack surface half-width} \qquad \text{[mm]}$$
$$L_p = \text{potential probe spacing half-width} \qquad \text{[mm]}$$

The crack depth and length were iterated within the MATE program such that the difference between the measured and predicted voltages of the crack depth and length were minimized. This was done by holding constant $V\!/\!V_N$, a_n, b_n, c_n, and L_p, and holding constant the aspect ratio, $c_c\!/\!a_c$, for each increment of crack depth acquired during the test. Thus, crack depth was generated for each cycle.

The crack growth rate, $\dfrac{da_c}{dN}$, was calculated using the incremental polynomial method, per ASTM E647.[13] The stress intensity range, ΔK, was calculated within MATE using stress-intensity factor equations developed by Newman and Raju [14] for a semi-elliptical surface crack subjected to tensile loading:

$$K_I = s\sqrt{\pi\frac{a_c}{Q}}F_S(\frac{a_c}{c_c},\frac{a_c}{t},\frac{c_c}{b_c},\Phi) \qquad \text{Eqn. 5.2 \quad (Ref.14)}$$

where

$$K_I = \text{stress-intensity factor (Mode I)} \qquad [\text{MPa}\sqrt{m}\,]$$
$$s = \text{remote uniform tensile stress} \qquad [\text{MPa}]$$
$$Q = \text{shape factor}$$
$$F_s = \text{boundary correction factor}$$
$$t = \text{through thickness of test specimen} \qquad [\text{mm}]$$
$$\phi = \text{ellipse parametric angle} \qquad [\text{radians}]$$

K_{max} was determined by inputting the maximum recorded load at each data point into Eqn. 5.2, which is programmed into MATE. Finally, ΔK was calculated using

$$\Delta K = K_{max}(1-R) \qquad \text{Eqn. 5.3 \quad (Ref. 15)}$$

where

$$\Delta K = \text{stress intensity range} \qquad [\text{MPa}\sqrt{m}\,]$$
$$K_{max} = \text{maximum stress intensity factor} \qquad [\text{MPa}\sqrt{m}\,]$$
$$R = \text{stress ratio}$$

The resultant $\dfrac{da_c}{dN}$ versus ΔK data were then plotted on log-log coordinates.

The fatigue crack growth behavior over the entire range of data that was collected was modeled using:

$$\frac{da_c}{dN} = C(\Delta K)^m$$

Eqn. 5.4 (Ref.15)

where

$\frac{da_c}{dN}$ = fatigue crack growth rate [mm/cycle]

C = coefficient $\left[\frac{mm/cycle}{\left(MPa\sqrt{m}\right)^m}\right]$

m = exponent

This relationship was used to estimate fatigue crack growth life of the Grainex Mar-M 247 material. The entire range of data was evaluated with this relationship to provide a conservative estimate of fatigue crack growth life.

Statistics

Linear regression analysis was conducted to evaluate the log-log transformed data:

$$\log\left(\frac{da_c}{dN}\right) = \log(C) + m\log(\Delta K)$$

Eqn. 5.5

A statistical comparison between regression lines was performed to determine if the individual slopes and intercepts were statistically similar at a confidence level of 95%. A test of equal variances on the error terms for each regression line was first done to validate a comparison between regression lines.[16] To test for similar slopes and intercepts, a reduced statistical model was determined which combined data sets from successful fatigue crack growth tests. The reduced statistical model was:

$$Y_{ij} = \beta_0 + \beta_1 X_{ij} + \varepsilon_{ij}$$

Eqn. 5.6 (Ref.16)

where

Y_{ij} = predicted value

β_0 = intercept of reduced model

β_1 = slope of reduced model

X_{ij} = independent variable

ε_{ij} = error term

A test statistic, F*, was calculated and compared with the F value determined from F-tables based on significance level and degrees of freedom. F* is defined as:

$$F* = \frac{SSE(R) - SSE(F)}{2} \div \frac{SSE(F)}{n_1 + n_2 - 4} \qquad \text{Eqn. 5.7 \quad (Ref.16)}$$

where

	SSE(R)	=	sum squared error of reduced model
	SSE(F)	=	sum squared error of full model
	n_1	=	number of data points for data set 1
	n_2	=	number of data points for data set 2

For F* ≤ F(1-a; 2, n_1 + n_2 - 4) a conclusion can be made that the slopes and intercepts of both regression lines are equal. Note that "a" is the desired percentile level.

Small Crack Growth Behavior

Because of the small size of the EDM notch dimensions (Figure 5.2) with respect to the Grainex Mar-M 247 grain size (1.6 mm, See Chapter 3), it was possible that fatigue crack growth would occur in the small crack growth regime. Small cracks are defined as having dimensions equal to or smaller than the dimension of greatest microstructural significance, such as grain size.[15] Small cracks are characterized by higher growth rates and their ability to grow at ΔK values below the threshold stress intensity range, ΔK_{th} (Figure 5.10). Small cracks may decelerate and arrest or approach a minimum in fatigue crack growth rate, then accelerate, and merge with long crack growth behavior. Thus, the fatigue crack growth behavior and respective crack size relative to the grain size was evaluated to determine if fatigue crack growth followed small crack behavior.
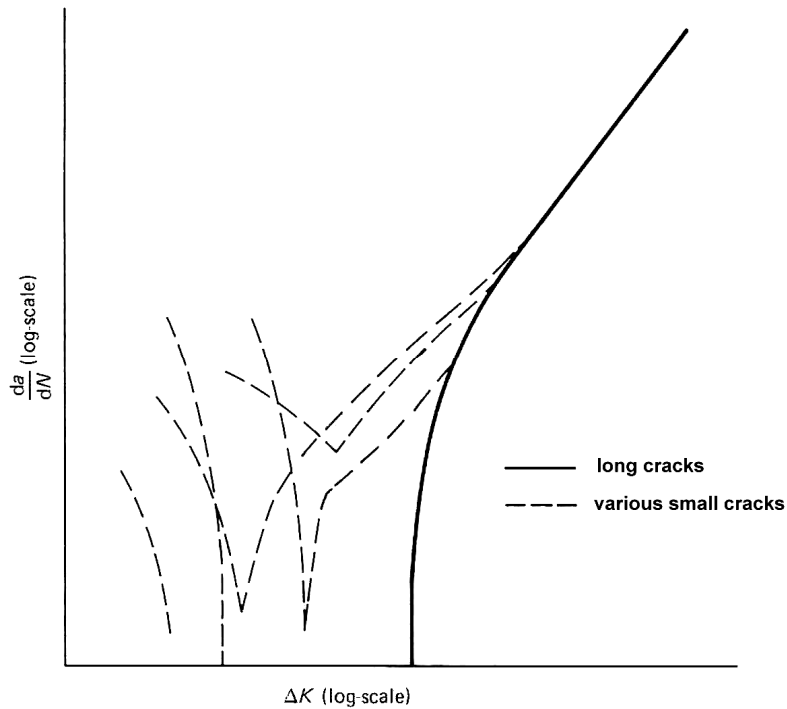
Figure 5.10 Typical small-crack growth behavior.[17]

Linear-Elastic Fracture Mechanics (LEFM)

An assessment of the validity of linear-elastic fracture mechanics (LEFM) was made based on specimen geometry. LEFM limitations were compared to specimen geometry based on

$$a_c, (t - a_c), h \geq \frac{4}{\pi} \left(\frac{K_{max}}{\sigma_{y(0.2\%)}} \right)^2 \qquad \text{Eqn. 5.8 (Ref. 15)}$$

where a_c =   crack depth   [mm]
          t   =   through thickness of the test specimen   [mm]
          h   =   half-height of the K_b specimen gage section
                      from the EDM notch   [mm]

Plastic-Zone Size

The plastic zone size was compared with the average grain size of Grainex Mar-M 247. The plastic zone size for plane stress conditions, $2r_{0\sigma}$, was estimated by:

$$2r_{0\sigma} = \frac{1}{\pi} \left(\frac{K_{max}}{\sigma_{y(0.2\%)}} \right)^2 \qquad \text{Eqn. 5.9 (Ref.15)}$$

Fractographic Examination

Fatigue crack propagation surfaces from each specimen were prepared for examination by carefully removing the gage section with a cut-off wheel. The surface was cleaned and then mounted. Fracture surfaces were examined using a light microscope and a scanning electron microscope (SEM) under secondary electron (SE) and backscattered electron (BE) modes.

Fracture surface features were identified including: initial and final EDM notches; pre-crack region; low ΔK (= 23.3 to 26.4 MPa $\sqrt{m}$) and high ΔK (= 35.7 to 39.1 MPa $\sqrt{m}$) regions; and the overload region. SEM micrographs of the low and high ΔK regions were taken, respectively, at 1.00 – 1.25 mm and 2.00 to 2.25 mm from the EDM notch origin. A comparison was made between crack growth rate and crack depth. The microscopic crack growth rate was determined for the low and high ΔK regions by measurement of striation spacings.

A comparison was made between the experimentally applied ΔK and the calculated ΔK based on striation spacings at the low and high ΔK fracture surface regions using the Bates and Clark relationship[18]:

$$\text{striation spacing} = 6\left(\frac{\Delta K}{E}\right)^2 \qquad \text{Eqn. 5.10 (Ref.18)}$$

where Young's modulus, E, was taken to be 194 GPa (see Chapter 4). The experimental ΔK used to compare with the Bates and Clark relationship was taken from the averaged ΔK determined from the low ΔK regime (24.85 MPa $\sqrt{m}$) and high ΔK regime (37.40 MPa $\sqrt{m}$).

5.3   Results and Discussion

Test Summary

Of the original eight K_b specimens, two tests (13K and 32K) were successfully conducted after doubling the EDM notch width and depth. Four K_b specimens, previously tested, failed prematurely outside the EDM notch. The remaining two were untested. Hereafter, the results pertain only to K_b specimens 13K and 32K.

Experimental Data

The fatigue crack growth behavior for the two tests specimens is shown in Figures 5.11 and 5.12 and the coefficient, C, and exponent, m, from Eqn. 5.4 are given for each specimen in Table 5.1.
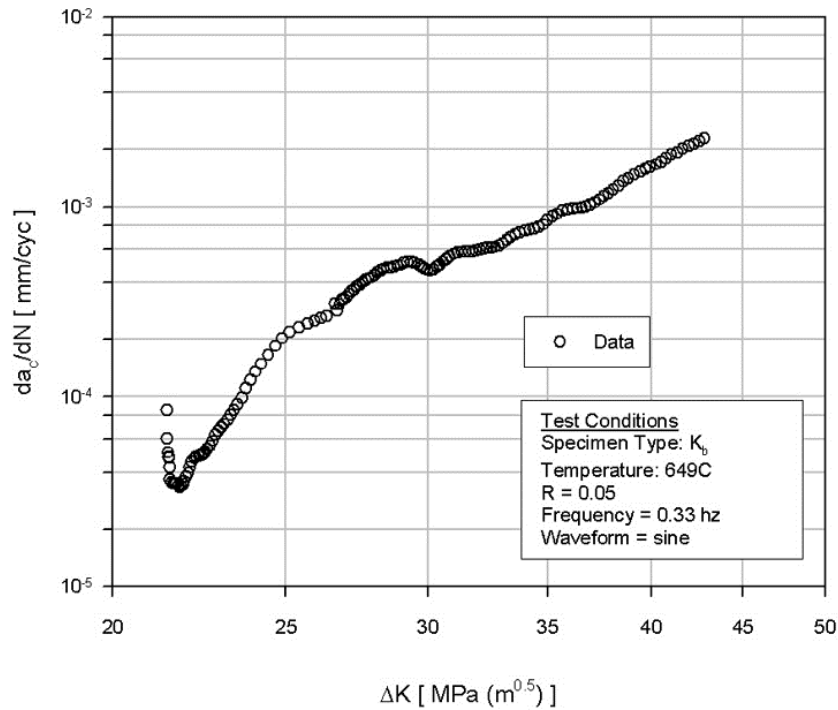
Figure 5.11   Fatigue crack growth behavior for Grainex Mar-M 247 at 649°C (K_b specimen 13K).
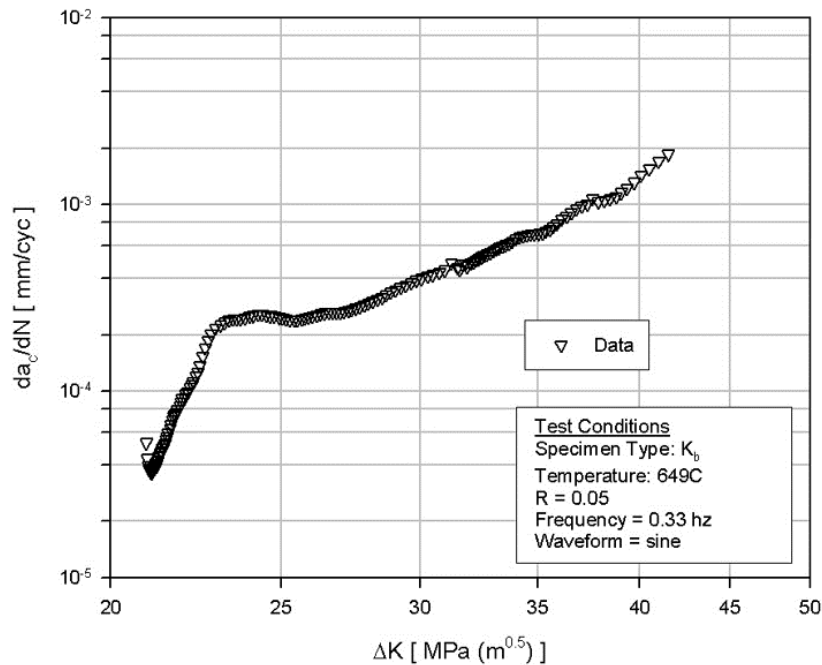
Figure 5.12   Fatigue crack growth behavior for Grainex Mar-M 247 at 649°C (K_b specimen 32K).

Table 5.1 Regression results of Eqn. 5.4 for fatigue crack growth behavior of Grainex Mar-M 247 K_b specimens at 649°C for the entire stress intensity range tested (13K and 32K)

Specimen	intercept	slope	R^2	constant C	exponent m
13K	-11.98	5.80	0.93	1.05×10^{-12}	5.80
32K	-10.53	4.82	0.90	2.94×10^{-11}	4.82

The deceleration and then acceleration of the da_c/dN data in the low ΔK region may be due to the crack approaching microstructural barriers such as grain boundaries or due to crack closure.[17,21] This small crack growth behavior generally transitions into long crack growth behavior at higher ΔK values[19], and this appears to have been the case in this study.

<u>Statistics</u>

Fatigue crack growth data with regressions from both data sets were analyzed for similarity. The variances between the individual regressions were found to be equivalent to a 95% confidence level. Thus a comparison between the regressions for similarity was valid. The reduced model (Eqn. 5.6) was determined with $\beta_0 = -11.20$ and $\beta_1 = 5.28$. Finally, F* (Eqn. 5.7) was calculated as -72.56. From standard F-tables, F(0.999, 2, 120) was 7.32. Thus F*≤ F and the slopes and intercepts were equal to within a 99.9% confidence level. The data from the two specimens were thus combined into one data set and an overall coefficient, C, and exponent, m, were determined (Figure 5.13).
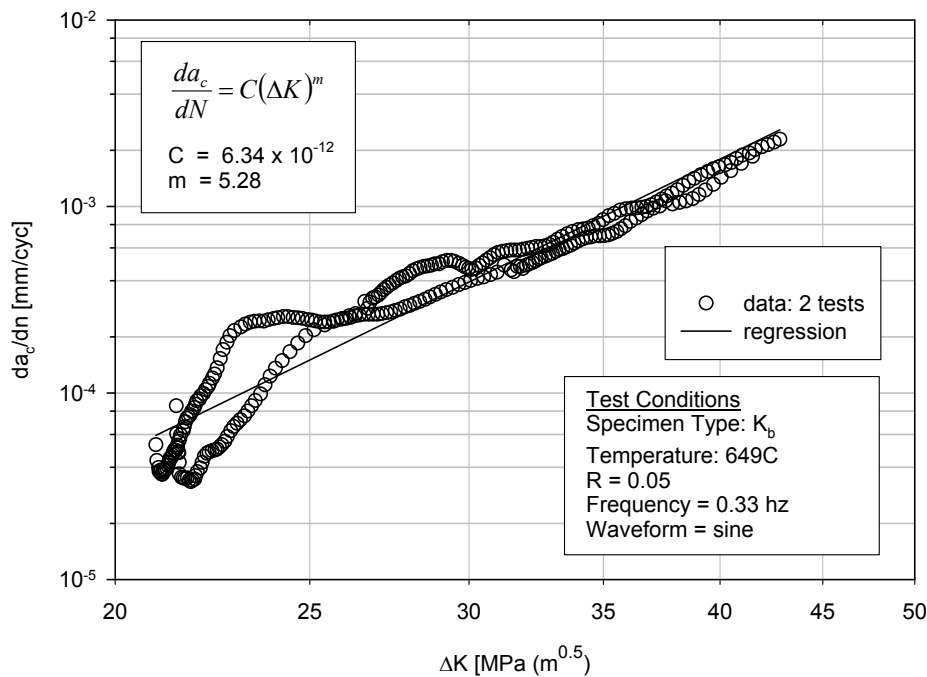
Figure 5.13   Regression results using both specimen data sets for Grainex Mar-M 247 fatigue crack-growth K_b data.

To be conservative in predicting fatigue crack growth life, both data sets (13K and 32K) were used with regression analysis over the entire experimentally determined range. The steeper da_c/dN versus ΔK slope in both data sets at low ΔK was thus taken into account as well as the shallower slope at high ΔK. This is appropriate since a conservative inspection interval is needed for the turbine seal rig facility (see Chapter 6).

Small Crack Growth Behavior

Small crack growth behavior (Figure 5.10) was observed for both fatigue crack growth specimens (Figure 5.11 and Figure 5.12). That is, the crack growth rate for both specimens was observed to initially decelerate to a minima and then to transition into the long crack growth regime.

In this study, the transition from small crack growth to long crack growth appeared to occur at approximately $\Delta K = 30$ MPa $\sqrt{m}$ ($da_c/dN = 4e\text{-}4$ mm/cycle) for both fatigue crack growth tests (Figure 5.13), based on the similarity in da_c/dN versus ΔK behavior above the transition. Consistent with this, the corresponding range of crack depths at that stress intensity was between 1.55 and 1.65 mm (see Figure 5.17 below). This coincides with reported Grainex Mar-M 247 average grain sizes of 1.6 mm. In other words, once the crack grows larger than the grain size, long crack growth behavior is expected.

Linear Elastic Fracture Mechanics, LEFM

Initial and final crack lengths for both fatigue crack growth test specimens were compared to the K_b specimen geometry to determine LEFM applicability using Eqn. 5.8 (Table 5.2). Initial crack lengths did not meet LEFM criteria for either specimen. Final crack lengths and remaining gage specimen thickness (i.e. $t - a_c$) also did not meet LEFM criteria.

Table 5.2 Comparison of initial and final crack lengths to K_b specimen geometry (13K and 32K) for LEFM applicability (Eqn. 5.8) at 649°C

Initial	13K	13K Criteria	Pass/Fail	Initial	32K	32K Criteria	Pass/Fail
a_c [mm]	0.846	0.963	Fail	a_c [mm]	0.884	0.919	Fail
$(t - a_c)$ [mm]	3.472	0.963	Pass	$(t - a_c)$ [mm]	3.434	0.919	Pass
h [mm]	7.976	0.963	Pass	h [mm]	7.976	0.919	Pass
Final	**13K**	**13K Criteria**	**Pass/Fail**	**Final**	**32K**	**32K Criteria**	**Pass/Fail**
a [mm]	2.550	3.840	Fail	a_c [mm]	2.560	3.607	Fail
$(t - a_c)$ [mm]	1.768	3.840	Fail	$(t - a_c)$ [mm]	1.758	3.607	Fail
h [mm]	7.976	3.840	Pass	h [mm]	7.976	3.607	Pass

The use of an LEFM approach for fatigue crack growth tests assumes that plasticity is limited to a local region that is small compared to the specimen dimensions.[15] Predicted gross yielding of the specimen calls into question the use of an LEFM approach. In this study, during fatigue crack growth testing, the initial maximum stress level at the gage section, calculated using the uncracked ligament, was approximately 79% of the 0.2% offset yield stress at 649°C. The final maximum stress level at the gage section, calculated using the uncracked ligament, was nearly 118% of the 0.2% offset yield stress. Thus, the fatigue crack growth behavior in these tests may have been influenced by gross yielding in the gage region. This suggests that the fatigue crack growth behavior of Grainex Mar-M 247 may be worse than the experimentally-obtained data. Fatigue crack propagation tests of Grainex Mar-M 247 using a specimen geometry that meets LEFM criteria would help answer this question.   Because of the uncertainty in the data, a safety factor of 2 is used to predict fatigue crack growth life (see Chapter 6).

Plastic Zone Size

The initial and final plane stress plastic zone sizes for both specimens 13K and 32K (Eqn. 5.9) can be found in Table 5.3.

Table 5.3 Initial and final plastic zone sizes for Grainex Mar-M 247 K_b fatigue crack growth specimens, 13K and 32K, for plane stress conditions at 649°C

Specimen	Plane Stress Plastic Zone Size	
	Initial [mm]	Final [mm]
13K	0.241	0.960
32K	0.230	0.902

The final plane stress plastic zone size did not exceed the average grain size of 1.6 mm determined from results in Chapter 3 (Material Cut-Up and Characterization). Thus, the recorded da_c/dN versus ΔK behavior was likely microstructurally-sensitive.[20]

Fractographic Examination

The fracture surface of specimen 13K is shown in SE mode (Figure 5.14 and Figure 5.15) Fracture surface features for K_b specimen 32K were similar.
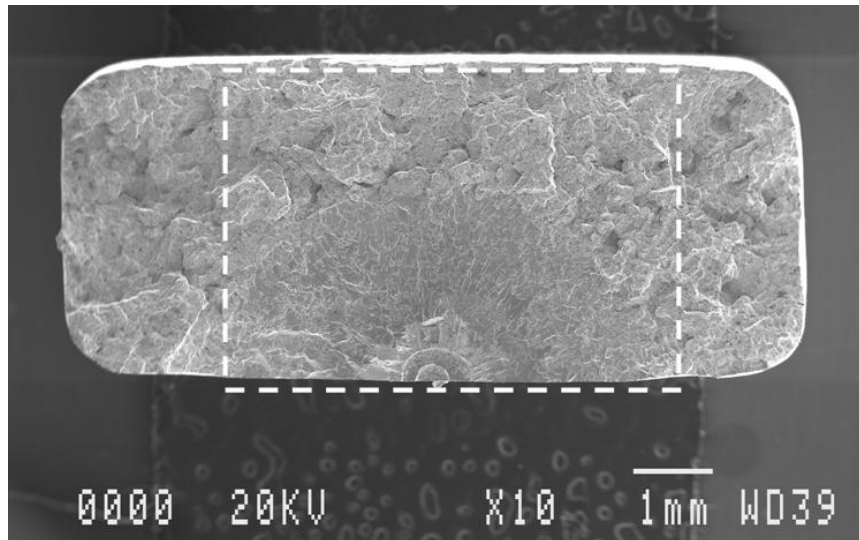
Figure 5.14   Grainex Mar-M 247 fatigue crack growth fracture surface for Kb specimen 13K (649°C). Dotted area enlarged in Figure 5.15
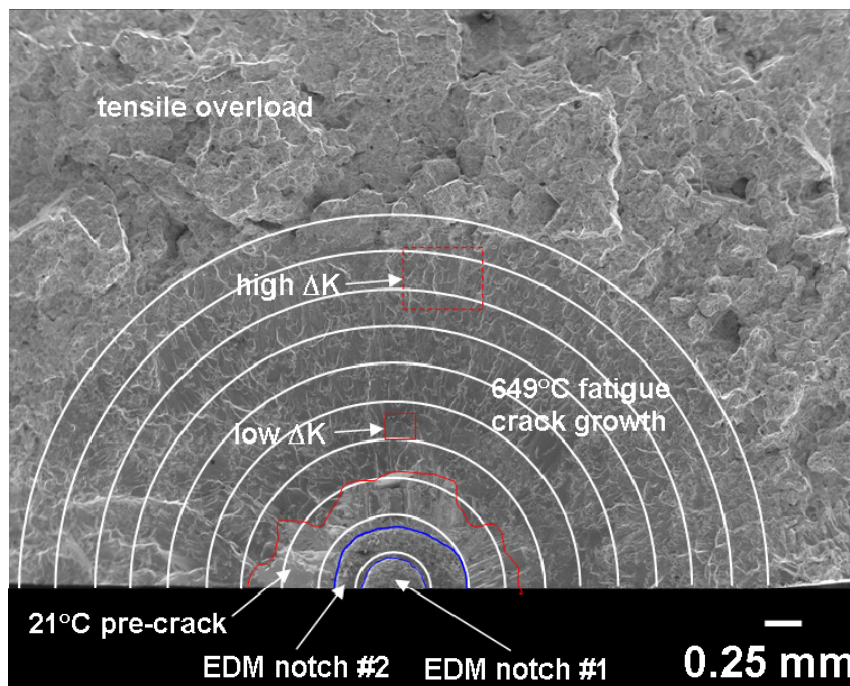
Figure 5.15   Close-up of Grainex Mar-M 247 fatigue crack growth fracture surface features for Kb specimen 13K at 649°C. Low ΔK region: 23.3 to 26.4 MPa$\sqrt{m}$. High ΔK region: 35.7 to 39.1 MPa$\sqrt{m}$.   SEM (SE mode). The initial EDM notches are indicated in blue and the initial pre-crack region (conducted at 649°C) is indicated in red.
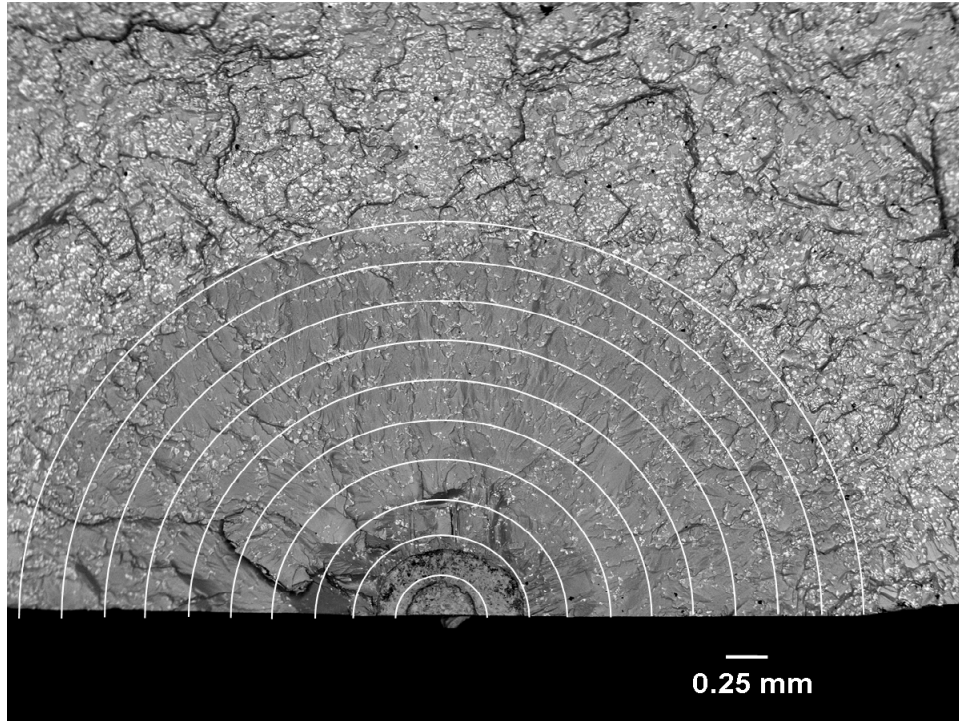
Figure 5.16 Grainex Mar-M 247 fatigue crack growth fracture surface for K$_b$ specimen 13K at 649°C showing grain boundary near beginning of fatigue crack growth (SEM – BE mode)

Under BE mode, grain boundaries were observed in the fatigue crack propagation region beginning between 0.75 and 1.00 mm radii from the EDM notch origin (Figure 5.16). Note that the 649°C fatigue crack growth began at approximately 0.82 mm from the EDM notch origin.

The decreasing crack growth rate at low ∆K (Figure 5.11) at a crack depth between 0.85 and 0.90 mm may be related to the grain boundary (Figure 5.16) between 0.75 and 1.50 mm from the notch origin. This deceleration in crack growth rate may be due to the crack front encountering a microstructural barrier such as a grain boundary. In fact, the minima in the fatigue crack growth rate was found to correspond to a crack depth of 0.88 mm (Figure 5.17) for specimen 13K. This is consistent with findings by Taylor[17] and Suresh et.al. [21]
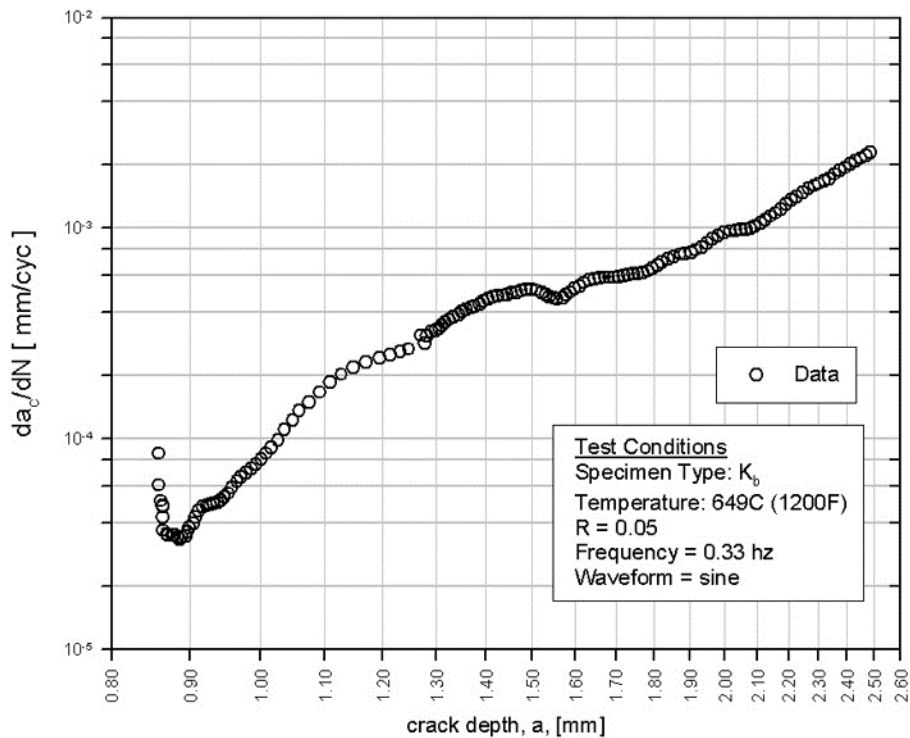
Figure 5.17 Fatigue crack growth rate versus crack depth for Grainex Mar-M 247 K$_b$ specimen (13K) at 649°C.

The low ΔK region (Figure 5.18) of specimen 13K between 1.00 to 1.25 mm from the EDM notch origin showed pockets of fatigue striations. The microstructural fatigue crack growth rate per cycle was approximately 2.5 x 10^{-3} mm/cycle (Figure 5.17). In contrast, the high ΔK region (Figure 5.19) shows more organized and delineated striations and the microstructural fatigue crack growth rate is approximately 5 x10^{-3} mm/cycle (Figure 5.17). Specimen 32K showed similar results. A complete set of SEM images is given in Appendix D.
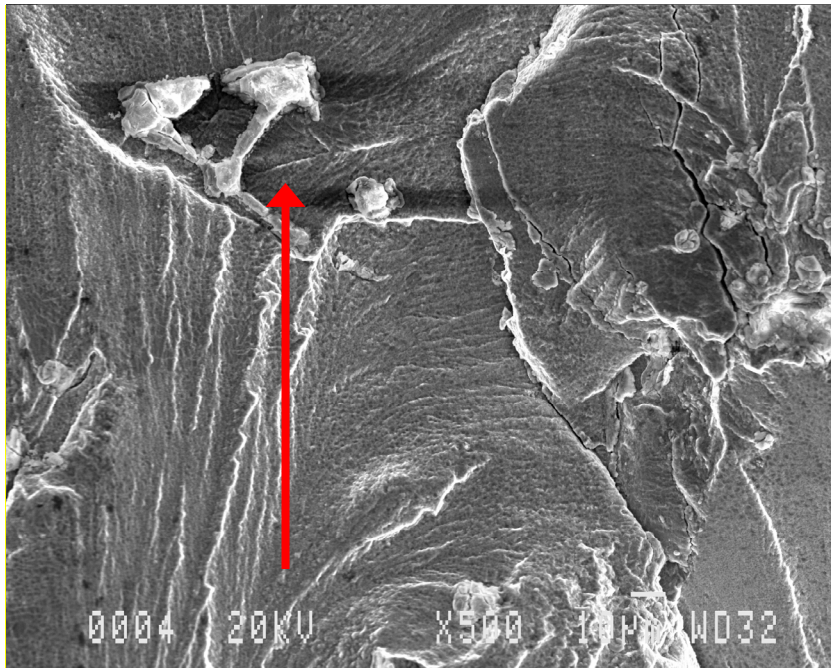
Figure 5.18 Low ΔK fatigue striations of Grainex Mar-M 247 fatigue crack growth fracture surface for K$_b$ specimen 13K at 649°C (SEM – SE mode) (See also Figure 5.15). ΔK range from 23.3 to 26.4 MPa$\sqrt{m}$. Arrow indicates crack growth direction.
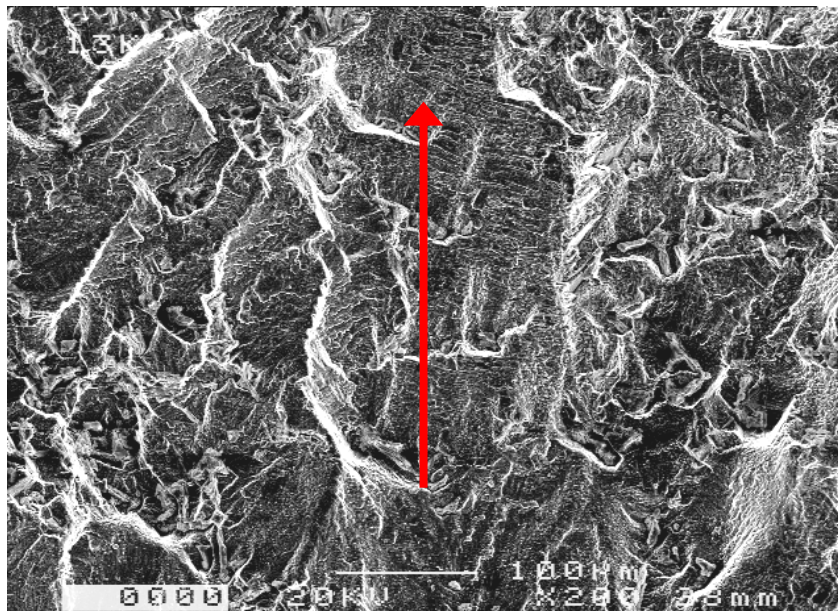
Figure 5.19 High ΔK fatigue striations of Grainex Mar-M 247 fatigue crack growth fracture surface for K$_b$ specimen 13K at 649°C (SEM – SE mode) (See also Figure 5.15). ΔK range from 35.7 to 39.1 MPa$\sqrt{m}$. Arrow indicates crack growth direction.

Table 5.4 compares the experimentally applied ΔK and the calculated ΔK based on striation spacings taken from the low and high ΔK regions. The stress intensity ranges were overestimated by the Bates and Clark relationship, (Eqn. 5.10), by a factor of 5 for both low and high ΔK regions.

Table 5.4 Comparison between experimental ΔK and calculated ΔK from striation spacing measurements for Grainex Mar-M 247 at 649°C

ΔK region	ΔK (experimental)* [MPa $\sqrt{m}$]	Striation Spacing [mm/cycle]	ΔK (Bates & Clark[18]) [MPa $\sqrt{m}$]
Low	24.85	2.5×10^{-3}	125.2
High	37.40	5.0×10^{-3}	177.1
*average			

Adjusting Eqn. 5.10 by the percent striated area of the fracture surface may result in better agreement between the experimental and calculated ΔK.[18] A rigorous survey of the fractographic area would be needed to determine if the Bates and Clark relationship would be a reliable predictor of cyclic stress intensity.

Comparison of Data to Literature

The regression of the combined experimental data was compared to literature at 426°C and 538°C (Figure 5.20 and Table 5.5). The fatigue crack growth rate increases with test temperature at constant cyclic stress-intensity. Data reported by Macha et. al. [22,], MacIntyre et.al. [23], Helmink et.al. [24], and Alloy Digest[,25] support this observation. The data from this study had the highest fatigue crack growth rate, since tests were conducted at the highest test temperature, 649°C.
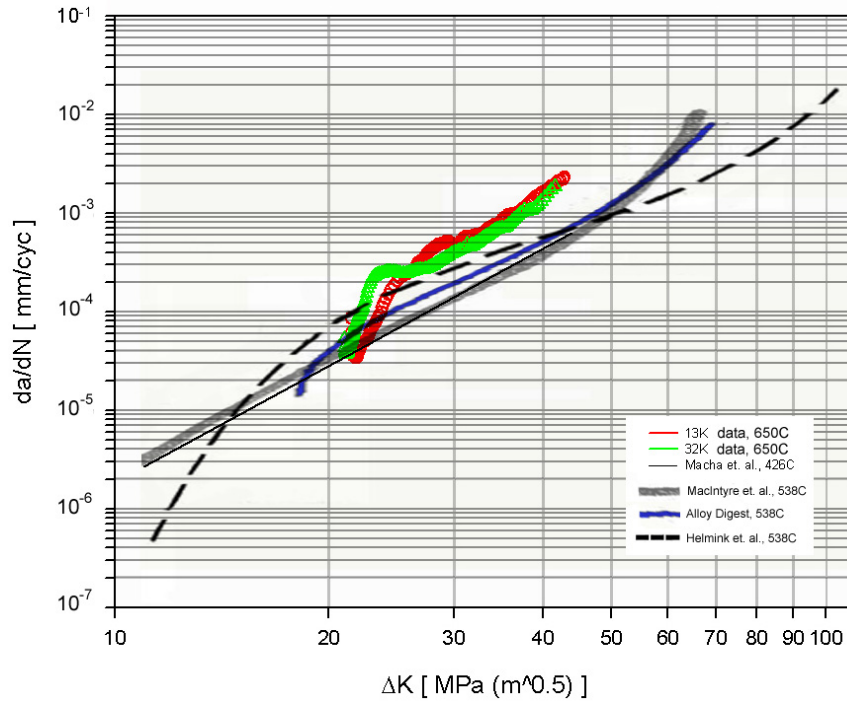
Figure 5.20 Comparison of Grainex Mar-M 247 to literature.[22,23,24,25]

Table 5.5 Comparison of experimental Grainex Mar-M 247 test parameters with reported data from available literature.[22,23, 24,25]

	This Study	Macha	MacIntyre	Alloy Digest	Helmink
Specimen Type	K_b	C-T	unknown	unknown	Unknown
Temp [°C]	649	426	538	538	538
Frequency [Hz]	0.33	30	0.33	unknown	Unknown
Load Ratio	0.05	0.1	0.05	0.05	Unknown
Waveform	sine	sine	unknown	unknown	Unknown

Summary

Small crack growth behavior observed by minima in the fatigue crack growth rate was likely related to microstructural barriers such as grain boundaries. The data transitioned towards long crack growth behavior at higher ΔK. The fatigue crack growth behavior is likely microstructurally sensitive because the final plane stress plastic zone size was predicted to be smaller than the average grain size.

Data sets from both fatigue crack growth tests were combined to account for the higher crack growth rates in the low ΔK region. However, since gross yielding was predicted at the fracture surfaces and LEFM criteria were not met, this may indicate a more severe da_c/dN versus ΔK behavior than given by the data. Thus, an arbitrary factor of 2 safety was used for determining fatigue crack growth life (see Chapter 6).

Chapter 5 Works Cited

1. Coles, A., R.E. Johnson, and H.G. Popp. "Utility of Surface-Flawed Tensile Bars in Cyclic Life Studies." Journal of Engineering Materials and Technology. 98 (1976) 305–315.
2. Diez, Andrew. "Crack formation in bolt holes." Personal communication by Irebert Delgado. 03 August 2000.
3. Kantzos, Pete. "K_b specimen geometry." Personal communication by Irebert Delgado. 31 March 2000.
4. Hartman, G.A., and N.E. Ashbaugh. "A Fracture Mechanics Test Automation System for a Basic Research Laboratory." Applications of Automation Technology to Fatigue and Fracture Testing, ASTM STP 1092. Eds. Braun, A.A., N.E. Ashbaugh, and F.M. Smith. Philadelphia, ASTM, 1990. 95-110.
5. Ashbaugh, N. and G. Hartman. "Direct Current Electric Potential Workshop." MATE Workshop. University of Dayton Research Institute.
6. Gangloff, R. P., D. C. Slavik, R. S. Piascik, and R. H. Van Stone. "Direct Current Electrical Potential Measurement of the Growth of Small Cracks." Small-Crack Test Methods, ASTM STP 1149. Eds. Larsen, J. M., and J.E. Allison. Philadelphia: ASTM, 1992. 116-168.
7. Hartman, George. "Questions on MATE program." Personal communication by Irebert Delgado. 17 September 2002.
8. Gangloff, R.P. "Electric Potential Monitoring of Crack Formation and Subcritical Growth from Small Defects." Fatigue of Engineering Materials and Structures. 4.1 (1981) 15-33.
9. VanStone, R.H., and T.L. Richardson. "Potential-Drop Monitoring of Cracks in Surface-Flawed Specimens." Automated Test Methods for Fracture and Fatigue Crack Growth, ASTM STP 877. Eds. Cullen, W.H., R.W. Landgraf, L.R. Kaisand, and J.H. Underwood. Philadelphia: ASTM, 1985. 148-166.

10. Shannon, Brian. "Accounting for thermoelectric influences." Personal communication by Irebert Delgado. 07 August 2000.

11. Shannon, Brian. "FCG data acquisition rate." Personal communication by Irebert Delgado. 24 July 2003.

12. Telesman, Jack. "Crack growth limitations." Personal communication by Irebert Delgado. 07 September 2002.

13. ASTM Committee E-8 on Fatigue and Fracture. "ASTM E-647-95a Standard Test Method for Measurement of Fatigue Crack Growth Rates." Annual Book of ASTM Standards 2001: Section 3 Metals Test Methods and Analytical Procedures: Volume 03.01 Metals—Mechanical Testing; Elevated and Low-Temperature Tests; Metallography. ASTM. West Conshohocken: ASTM, 1998. 577-613.

14. Newman, J.C., Jr., and I.S. Raju. "Stress-Intensity Factor Equations for Cracks in Three-Dimensional Finite Bodies." Fracture Mechanics: Fourteenth Symposium—Volume I: Theory and Analysis, ASTM STP 791. Eds. Lewis, J.C., and G. Sines. Philadelphia: ASTM, 1983. I-238 - I-265.

15. Dowling, Norman E. Mechanical Behavior of Materials : engineering methods for deformation, fracture, and fatigue. Upper Saddle River: Prentice-Hall, Inc., 1999.

16. Neter, John, and William Wasserman. Applied Linear Statistical Models. Homewood: Richard D. Irwin, Inc. (1974).

17. Taylor, David. Fatigue Thresholds. London: Butterworths, 1989.

18. Bates, R.C., and W.G. Clark Jr. "Fractography and Fracture Mechanics." ASM Transactions Quarterly. 62.2 (1969) 380-389.

19. Taylor, D. A Compendium of Fatigue Thresholds and Growth Rates. London: Chameleon Press LTD. (1985).

20. Hertzberg, Richard W. Deformation and Fracture Mechanics of Engineering Materials. 3rd Ed. New York: John Wiley and Sons, Inc. (1989).

21. Suresh, S., and Ritchie, R. O. "Propagation of short fatigue cracks." International Metals Reviews. 29.6 (1984) 445-476.

22. Macha, D.E., G.R. Cole, and J.A. Butzer. "Fine Grain, Investment-Cast Integral Turbine Wheels." Grain Refinement in Castings and Welds. Ed. G.J. Abbaschian and S.A. David. New York: The Metallurgical Society of AIME, 1983. 197-219.

23. MacIntyre, Cal A. and P. Neil Agarwal. "Development of Fine Grain Cast Mar-M 247 Axial and Radial Turbine Wheels." Advanced Aerospace Materials Technology: SP-597. Warrendale: Society of Automotive Engineers, Inc., 1984. 35-45.

24. Helmink, R.C. et. al. "Advanced Superalloys and Tailored Microstructures for Integrally Cast Turbine Wheels." Superalloys 2000. Ed. T.M Pollock et al. Warrendale: TMS, 2000. 171-179.

25. "Microcast-X Mar-M 247." Alloy Digest May 1995.

6. Determination of the NASA Disk Inspection Interval

6.1 Introduction

As discussed in Chapter 1, eddy-current inspections are used to examine the NASA disk bolt holes after a set number of cycles at maximum operating conditions. In general, engine companies use eddy current inspection or other non-destructive evaluation procedures for turbine disks, such as the Grainex Mar-M 247 NASA disk, to prevent disk failure by growth of an existing crack to a critical crack length, a_{crit}. The inspection interval is based on a critical crack length, a_{crit}, determined at a specific cyclic life from K_{IC} tests at a specific test temperature, stress level, and detectable threshold crack size.

This chapter discusses the eddy-current inspection interval determined for the Grainex Mar-M 247 NASA disk based on strain-life and fatigue crack growth results from previous chapters.

6.2 Methods

Although the da_c/dN versus ΔK behavior was estimated in Chapter 5, a critical crack length was not determined because of a lack of valid K_{IC} tests. However, an estimate of the critical crack length at failure is required to predict cyclic life. Data reported by Kaufman[1] indicates that the plane-strain fracture toughness, K_{IC}, for Grainex Mar-M 247 is greater than 55 MPa $\sqrt{m}$ at 760°C. The maximum ΔK value of 40.83 MPa $\sqrt{m}$, attained at the end of the fatigue crack growth tests, can be used as a conservative estimate of K_{IC}. This is reasonable since the fatigue crack growth behavior was observed to be well-behaved at the end of the test (i.e. stable crack growth rate).

Assuming K_{IC} to be approximately 40 MPa $\sqrt{m}$, the critical crack length, a_{crit}, for a cyclic stress intensity range of 40 MPa $\sqrt{m}$ was determined. Using the regression values for coefficient, (C = 6.34x10^{-12}), and exponent, (m = 5.28), for the combined data (Chapter 5, Figure 5.13) with an initial crack size of 0.381 mm (the threshold level for eddy-current inspection[2]), the crack length versus cycles can be calculated iteratively and plotted.[3] Assuming the initial crack length, a_i, occurs at cycle 1, the following crack length at cycle 2 is calculated as follows:

1. Calculate ΔK based on $\Delta K = \hat{F} \Delta \sigma \sqrt{\pi a_i}$. $\Delta \sigma$ is 699 MPa from analyses by Tong and Steinetz.[4] $\hat{F}$ is 1.12 for a half-elliptical surface crack.[5]
2. Calculate da_c/dN per Eqn. 5.4 (Chapter 5) using the values for C and m found for the combined data set.
3. Recalculate the crack length for cycle 2 by adding the previous crack length, a_i, to the value da_c/dN calculated in step 2. The estimated crack growth length for the following cycle is da_c/dN.
4. Repeat steps 1 – 3 until ΔK is approximately 40 MPa $\sqrt{m}$.

6.3 Results and Discussion

The calculated critical crack length was 0.831 mm at 734 cycles at $\Delta K = 40$ MPa $\sqrt{m}$ (Figure 6.1). An average crack growth of 0.016 mm per 50 cycles was calculated from cycle 0 to approximately cycle 350.

An arbitrary safety factor of 2 on cyclic fatigue crack growth life was used since results from Chapter 5 indicate that LEFM conditions were not met and gross yielding was predicted at the gage section. Thus, the calculated cyclic life of 734 cycles is reduced, by half, to 367 cycles. Also, the corresponding crack depth is reduced from 0.831 mm to a crack depth of 0.501 mm.

The total fatigue life of a material often encompasses approximately 90% fatigue strain-life and 10% fatigue crack growth life.[6] Recall Figure 4.12 which gives the $R_\varepsilon = 0$ fatigue strain-life crack initiation curve at 649°C. At the design strain of 0.5% the mean life to crack initiation is approximately 15,000 cycles. Combining this with the predicted fatigue crack propagation cycles to failure, 734, in Figure 6.1 gives a total life of 15,734 cycles. This approach suggests that, for the Grainex Mar-M 247 NASA disk operating at 649°C air temperature, crack initiation represents 95% of the cyclic life of the NASA disk while the remaining 5% is used to propagate the crack to failure.
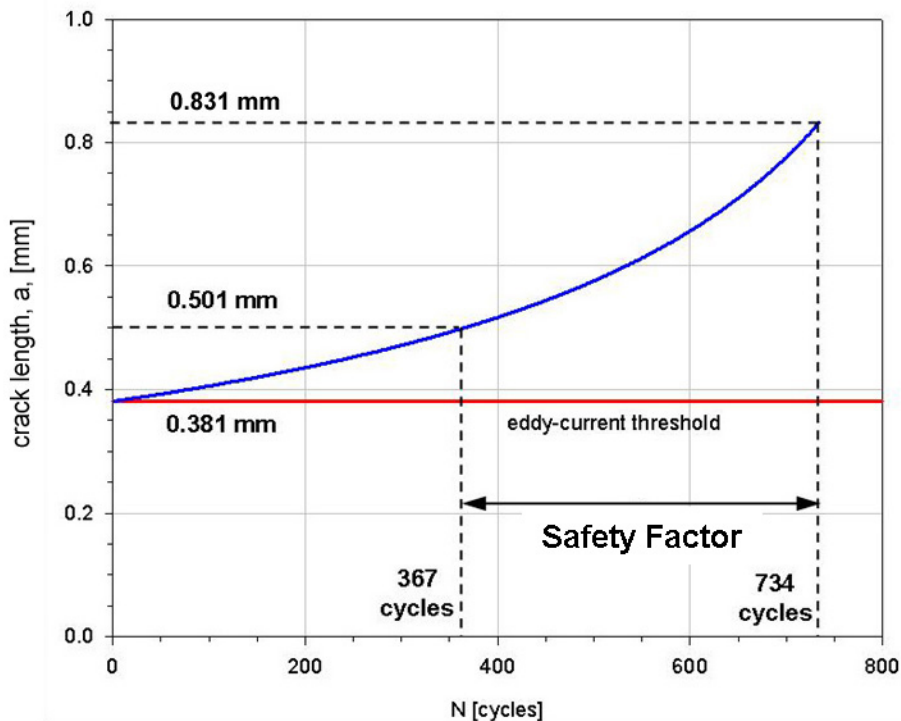
Figure 6.1   **Grainex Mar-M 247 NASA disk fatigue crack growth rate with increasing cycles at 649°C.**

However, considering the environment in which the NASA disk is used and the safety required for personnel and equipment, statistical and other safety factors must be used to estimate the inspection interval. Specifically, using the -99.95% prediction interval shown in Figure 4.12, the cyclic life to crack initiation, with statistically 1 failure in 2000, is 1100 cycles at the design strain of 0.5% at 649°C. Accounting for the 6 bolt holes using the system life analysis as previously discussed in Chapter 1, the resultant crack initiation life is 665 cycles. Combining this with the predicted fatigue crack propagation cycles of 367 cycles (using a factor of safety of 2) gives a total cyclic life for the Grainex Mar-M 247 NASA disk bolt holes of 1032 cycles at a crack length of 0.501 mm at maximum disk operating conditions.

Since the eddy-current detection threshold is currently 0.381 mm, an initial NASA disk bolt hole inspection is recommended starting at approximately 665 cycles to detect crack initiation. Inspection intervals are then recommended approximately every 50 cycles thereafter to adequately monitor fatigue crack growth. The NASA disk should be retired from service upon attaining either 1032 cycles or a crack depth of 0.501 mm (Figure 6.2). One possible implementation plan is given in Figure 6.3.
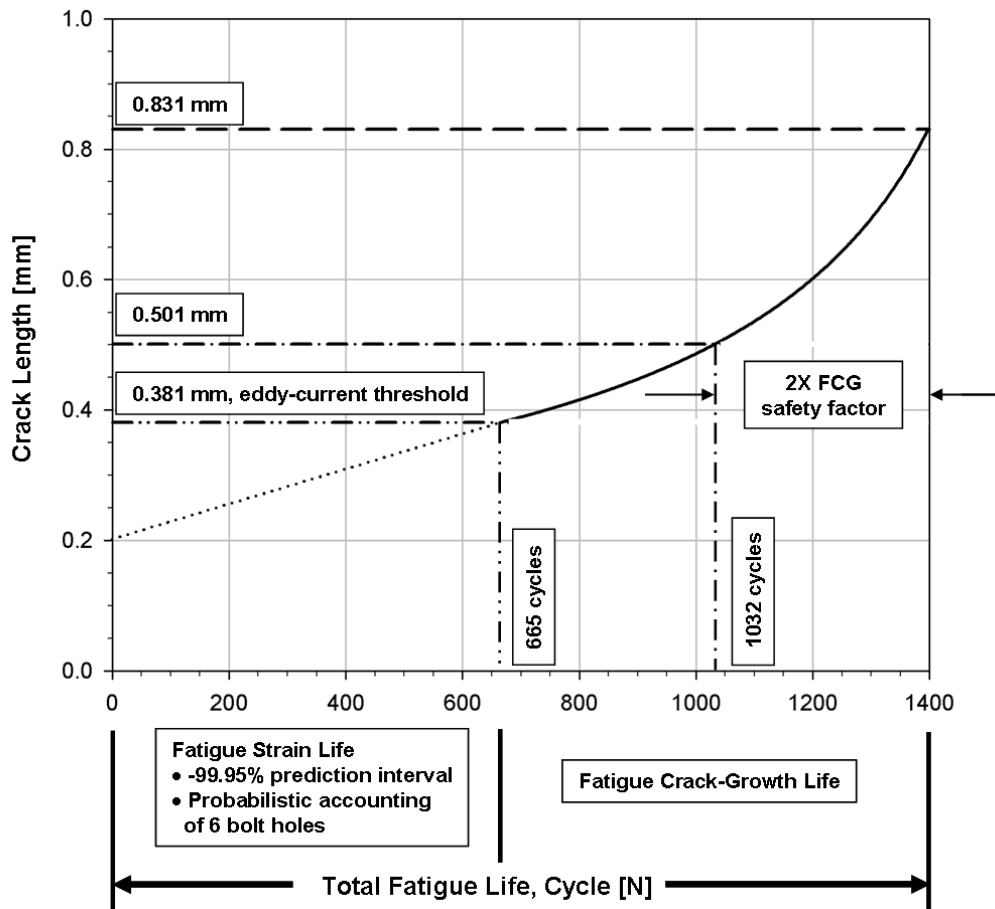
Figure 6.2   Total fatigue life of Grainex Mar-M 247 at maximum operating conditions of the NASA Turbine Seal Test Rig.
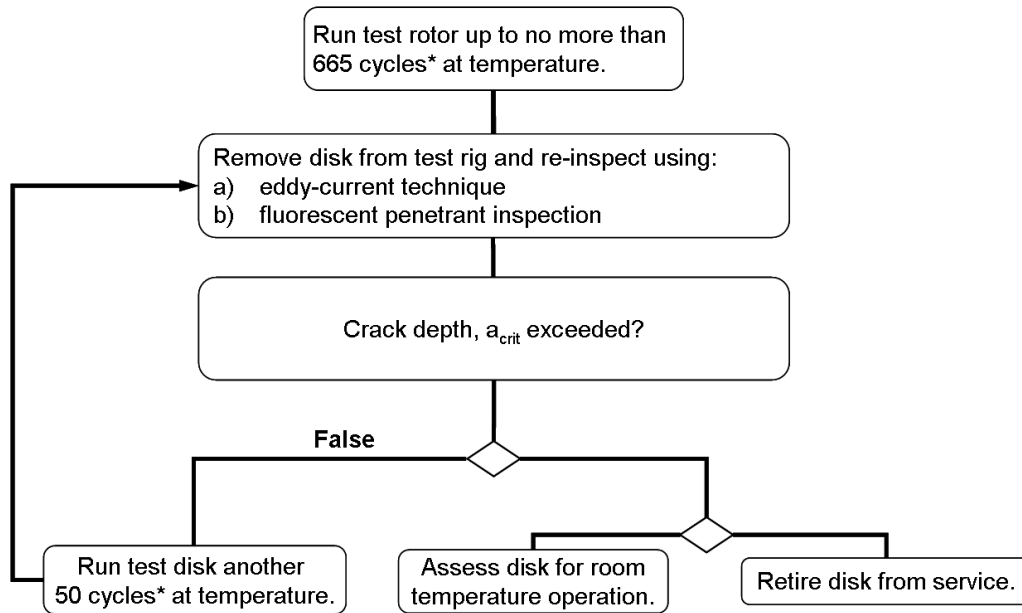
Figure 6.3   Decision tree for implementing eddy-current inspection interval for Grainex Mar-M 247 NASA disk.

Chapter 6 Works Cited

1. Kaufman, M. "Properties of Cast Mar-M-247 for Turbine Blisk Applications." Superalloys 1984. Ed. Maurice Gell et al. Warrendale: Metallurgical Society of AIME, 1984. 43-52.

2. Curtis Industries, Inc. "Reference Standard Calibration for GX Mar-M 247." Inspection report for reference standard. Curtis Industries, Inc., Pennsylvania. 12 May 2003.

3. Broek, David. Elementary Engineering Fracture Mechanics. 3rd ed. Hingham: Kluwer Boston, Inc., 1984.

4. Tong, Mike and Bruce Steinetz. "Mar-M 247 Disk Finite Element Thermal and Stress Analysis", NASA Glenn Research Center, Cleveland. 30 January 1997.

5. Dowling, Norman E. Mechanical Behavior of Materials : engineering methods for deformation, fracture, and fatigue. Upper Saddle River: Prentice-Hall, Inc., 1999.

6. Kerlins, Victor, and Austin Phillips. "Modes of Fracture." Metals Handbook Volume 12 Fractography. 9th ed. Metals Park: ASM International. 1987.

7. Future Work

7.1 Effect of Material limitations

The size and number of test specimens (tensile, strain-life, and fatigue crack growth) were limited due to the single Grainex Mar-M 247 NASA disk available for cut-up. This also limited preferential cutting planes for microstructural examination of the NASA disk from the rim to the centerline.

Priorities were set on the specimens taken out of the NASA disk based on the data that was needed. For example, fatigue crack growth specimens were taken near the bolt hole locations since they were the structural feature most limiting in terms of fatigue strain-life per analyses by Tong and Steinetz.[1] A large number of strain-life specimens were taken out of the NASA disk to obtain a statistical prediction of the cyclic crack initiation life at design conditions with a high degree of confidence (i.e. 99.95%). Tensile specimens numbered the fewest because the results were used to confirm previous data and to make general comparisons to fatigue strain-life prediction models. Finally, specimen cut-out plans were necessary to ensure that an adequate cross-section of the NASA disk was available for metallurgical analysis.

The biggest disadvantage to having limited materials for test specimens was that fracture toughness tests could not be carried to out to determine K_{IC}. Even with available material for fatigue crack growth tests, size limits on K_b test specimen thicknesses brought into question the applicability of LEFM for these fatigue crack growth analyses to predict a fatigue crack growth life. Further tests are needed to determine K_{IC} from adequately sized fracture toughness specimens.

Finally, because of inherent differences in processing from casting to casting, the Grainex Mar-M 247 material study was limited to the set of disks (7 total including sacrificial disk) used at NASA's Glenn Research Center Turbine Seal Test Facility.

7.2 Effect of Test Parameter Limitations

Tests were limited to the 649°C bolt hole temperature as predicted from analysis.[1] This was based on the limited material available and because the bolt hole region had the lowest predicted strain-life limits in terms of maximum operating temperature and stress.

Strain-life specimens were limited to two strain ratios with 5 strain-levels at each R-ratio. Work with statisticians aided in setting the proper number of repeats (three) at each strain-level to ensure a statistical analysis could be carried out for each R value. Other parameters were held constant, such as frequency and waveform and thus limited the study accordingly. Further, cumulative fatigue damage effects were not tested.

Fatigue crack growth tests were also limited to one set condition (R = 0.05, waveform = sine, temperature = 649°C, frequency = 0.33 Hz). Thus effects of these parameters were not within the scope of the study. Hold-times were also not considered nor was threshold limit testing.

7.3 Eddy-Current Limitations

Eddy-current threshold crack size limits (0.381 mm) currently place limitations on the detectable defect size. Thus, -99.95% prediction intervals were placed for the strain-life cycles to crack initiation. Also, an arbitrary safety factor of 2 was imposed for the fatigue crack growth critical crack size.

7.4 Recommendations for Further Research or Improvements

Material availability for K_{IC} testing would improve on the predicted critical crack length to failure calculation. Conclusions made on the fatigue crack growth study were done in consideration of the available literature data and specifically on the range of ΔK tested.

Characterization of the material microstructure would benefit from a complete chord slice from the NASA disk rim to the disk center. Also, Grainex Mar-M 247 disks used in the turbine seal test facility that would eventually be retired from service could possibly be used to study the effects of temperature and stress over time on the microstructure.

Finally, strain-life and fatigue crack growth as well as creep tests from material at the NASA disk rim should be considered. These areas experience higher operating temperatures but not necessarily the same magnitude of stress seen at the hub location. Nevertheless, creep is an additional issue and would complement the work done on characterizing the bolt hole location on the Grainex Mar-M 247 NASA disk.

Chapter 7 Works Cited

1. Tong, Mike and Bruce Steinetz. "Mar-M 247 Disk Finite Element Thermal and Stress Analysis", NASA Glenn Research Center, Cleveland. 30 January 1997.

8. Bibliography

Ashbaugh, N. and G. Hartman. "Direct Current Electric Potential Workshop." MATE Workshop. University of Dayton Research Institute.

ASM International Handbook Committee. "Eddy-Current Inspection." Metals Handbook 9th Edition Volume 17: Nondestructive Evaluation and Quality Control. Metals Park: ASM International, 1989. 164+.

ASTM Committee E-8 on Fatigue and Fracture. "ASTM E-606 – 92 (Reapproved 1998): Standard Practice for Strain-Controlled Fatigue Testing." Annual Book of ASTM Standards 2001: Section 3 Metals Test Methods and Analytical Procedures: Volume 03.01 Metals—Mechanical Testing; Elevated and Low-Temperature Tests; Metallography. ASTM. West Conshohocken: ASTM, 1998. 543-557.

ASTM Committee E-8 on Fatigue and Fracture. "ASTM E-647-95a Standard Test Method for Measurement of Fatigue Crack Growth Rates." Annual Book of ASTM Standards 2001: Section 3 Metals Test Methods and Analytical Procedures: Volume 03.01 Metals—Mechanical Testing; Elevated and Low-Temperature Tests; Metallography. ASTM. West Conshohocken: ASTM, 1998. 577-613.

ASTM Committee E-8 on Fatigue and Fracture. "ASTM E-739 – 91 (Reapproved 1998): Standard Practice for Statistical Analysis of Linear or Linearized Stress-Life (S-N) and Strain-Life (ε-N) Fatigue Data." Annual Book of ASTM Standards 2001: Section 3 Metals Test Methods and Analytical Procedures: Volume 03.01 Metals—Mechanical Testing; Elevated and Low-Temperature Tests; Metallography. ASTM. West Conshohocken: ASTM, 1998. 543-557.

ASTM Committee E-7 on Nondestructive Testing. "ASTM E-1417 – 99: Standard Practice for Liquid Penetrant Examination." Annual Book of ASTM Standards 2002: Section 3 Metals Test Methods and Analytical Procedures: Volume 03.03 Nondestructive Testing. ASTM. West Conshohocken: PA, 2002.

Bates, R.C., and W.G. Clark Jr. "Fractography and Fracture Mechanics." ASM Transactions Quarterly. 62.2 (1969) 380-389.

Broek, David. Elementary Engineering Fracture Mechanics. 3rd ed. Hingham: Kluwer Boston, Inc., 1984.

Coles, A., R.E. Johnson, and H.G. Popp. "Utility of Surface-Flawed Tensile Bars in Cyclic Life Studies." Journal of Engineering Materials and Technology. 98 (1976) 305–315.

Conway, Joseph B., and Lars H. Sjodahl. Analysis and Representation of Fatigue Data. Materials Park: ASM International, 1991.

Cowie, William D. "Fracture Control Philosophy." <u>Metals Handbook 9th Edition Volume 17: Non-Destructive Evaluation and Quality Control</u>. Metals Park: ASM International, 1989. 666+.

Curtis Industries, Inc. "Reference Standard Calibration for GX Mar-M 247." Inspection report for reference standard. Curtis Industries, Inc., Pennsylvania. 12 May 2003.

Davis, Joseph R., ed. <u>Heat Resistant Materials</u>. Materials Park: ASM International, 1997.

Department of Defense. <u>Mil-Std-1907: Inspection, liquid penetrant and magnetic particle, soundness requirements for materials, parts and weldments. Department of Defense</u>. 7 Sept 1989.

Diez, Andrew. "Crack formation in bolt holes." Personal communication by Irebert Delgado. 03 August 2000.

Dowling, Norman E. <u>Mechanical Behavior of Materials : engineering methods for deformation, fracture, and fatigue</u>. Upper Saddle River: Prentice-Hall, Inc., 1999.

Freeman, William R., Jr. "Investment Casting." <u>Superalloys II</u>. Ed. Chester T. Sims et al. New York: John Wiley & Sons, Inc., 1987. 411-439.

Gangloff, R.P. "Electric Potential Monitoring of Crack Formation and Subcritical Growth from Small Defects." <u>Fatigue of Engineering Materials and Structures</u>. 4.1 (1981) 15-33.

Gangloff, R. P., D. C. Slavik, R. S. Piascik, and R. H. Van Stone. "Direct Current Electrical Potential Measurement of the Growth of Small Cracks." <u>Small-Crack Test Methods, ASTM STP 1149</u>. Eds. Larsen, J. M., and J.E. Allison. Philadelphia: ASTM, 1992. 116-168.

Halford, G.R., and A.J. Nachtigall. "Strainrange Partitioning Behavior of an Advanced Gas Turbine Disk Alloy AF2-1DA." <u>Journal of Aircraft</u>, 17.8 (1980) 598-604.

Hartman, G.A., and N.E. Ashbaugh. "A Fracture Mechanics Test Automation System for a Basic Research Laboratory." <u>Applications of Automation Technology to Fatigue and Fracture Testing, ASTM STP 1092.</u> Eds. Braun, A.A., N.E. Ashbaugh, and F.M. Smith. Philadelphia, ASTM, 1990. 95-110.

Hartman, George. "Questions on MATE program." Personal communication by Irebert Delgado. 17 September 2002.

Helmink, R.C. et. al. "Advanced Superalloys and Tailored Microstructures for Integrally Cast Turbine Wheels." <u>Superalloys 2000</u>. Ed. T.M Pollock et al. Warrendale: TMS, 2000. 171-179.

Hertzberg, Richard W. Deformation and Fracture Mechanics of Engineering Materials. 3rd ed. New York: John Wiley & Sons, Inc. 1989.

Howmet Turbine Components Corporation. TB 3000: Grainex Cast Mar-M 247 Alloy. Greenwich: Howmet Turbine Components Corporation.

Kantzos, Pete. "Kb specimen geometry." Personal communication by Irebert Delgado. 31 March 2000.

Kaufman, M. "Properties of Cast Mar-M-247 for Turbine Blisk Applications." Superalloys 1984. Ed. Maurice Gell et al. Warrendale: Metallurgical Society of AIME, 1984. 43-52.

Keller, Dennis. Introduction to Regression: Theory, Methods, Applications. Fairview Park: RealWorld Quality Systems.

Keller, Dennis. "Strain-Life Model with Statistics." Real World Quality Systems, Fairview Park. 05-09-01.

Kerlins, Victor, and Austin Phillips. "Modes of Fracture." Metals Handbook Volume 12 Fractography. 9th ed. Metals Park: ASM International. 1987.

Lapointe, N.R. "Monotonic and Fatigue Characterizations of Metals," Proceedings of The SAE Fatigue Conference P-109. Warrendale: Society of Automotive Engineers, Inc., 1982.

Little, R.E. and E.H. Jebe. ASTM STP 588: Manual on Statistical Planning and Analysis for Fatigue Experiments. ASTM, 1975.

Ludwig, Lawrence P., and Robert C. Bill. "Gas Path Sealing in Turbine Engines." ASLE Transactions 23.1 (1978):1-5.

Macha, D.E., G.R. Cole, and J.A. Butzer. "Fine Grain, Investment-Cast Integral Turbine Wheels." Grain Refinement in Castings and Welds. Ed. G.J. Abbaschian and S.A. David. New York: The Metallurgical Society of AIME, 1983. 197-219.

MacIntyre, Cal A. and P. Neil Agarwal. "Development of Fine Grain Cast Mar-M 247 Axial and Radial Turbine Wheels." Advanced Aerospace Materials Technology: SP-597. Warrendale: Society of Automotive Engineers, Inc., 1984. 35-45.

Manson, S.S. "Fatigue: A Complex Subject." Experimental Mechanics. 5.7 (1965) 193-226.

Manson, S.S. "Predictive Analysis of Metal Fatigue in the High Cyclic Life Range." Methods for Predicting Material Life in Fatigue. Ed. W.J. Ostergren and J.R. Whitehead. New York: ASME, 1979.

Mar-Test. "Tensile and Strain-Life Test Descriptions" email to Irebert Delgado. 15 Oct. 2003.

Mar-Test. "Tensile Test Specimen Geometry." Fax to Irebert Delgado. 03 May 2001.

Melis, M.E., E.V. Zaretsky, and R. August. "Probabilistic Analysis of Aircraft Gas Turbine Disk Life and Reliability." Journal of Propulsion and Power, 15.5 (1999) 658-666

"Microcast-X Mar-M 247." Alloy Digest May 1995.

Neter, John, and William Wasserman. Applied Linear Statistical Models. Homewood: Richard D. Irwin, Inc. (1974).

Neugebauer, Bob. "Mar-Test Strain-Life Specimen Geometry." Personal communication by Irebert Delgado. 22 September 2000.

Newman, J.C., Jr., and I.S. Raju. "Stress-Intensity Factor Equations for Cracks in Three-Dimensional Finite Bodies." Fracture Mechanics: Fourteenth Symposium—Volume I: Theory and Analysis, ASTM STP 791. Eds. Lewis, J.C., and G. Sines. Philadelphia: ASTM, 1983. I-238 - I-265.

Ott, James. "JT8D Hub Failure Sparks Intense Inquiry." Aviation Week & Space Technology, 15 July 1996: 29+.

Ross, Earl W., Chester T. Sims. "Nickel-Base Alloys." Superalloys II. Ed. Chester T. Sims et al. New York: John Wiley & Sons, Inc., 1987. 97-133.

Shannon, Brian. "Accounting for thermoelectric influences." Personal communication by Irebert Delgado. 07 August 2000.

Shannon, Brian. "FCG data acquisition rate." Personal communication by Irebert Delgado. 24 July 2003.

Suresh, S., and Ritchie, R. O. "Propagation of short fatigue cracks." International Metals Reviews. 29.6 (1984) 445-476.

Taylor, D. A Compendium of Fatigue Thresholds and Growth Rates. London: Chameleon Press LTD. (1985).

Taylor, David. Fatigue Thresholds. London: Butterworths, 1989.

Telesman, Jack. "Crack growth limitations." Personal communication by Irebert Delgado. 07 September 2002.

Tong, Mike and Bruce Steinetz. "Mar-M 247 Disk Finite Element Thermal and Stress Analysis", NASA Glenn Research Center, Cleveland. 30 January 1997.

United States Patent and Trademark Office. <u>Trademark: Grainex, Registration No. 121275</u>. By Howmet Turbine Components Corporation. 1982.

United States Patent and Trademark Office. <u>U.S. Patent 3720509: Nickel Base Alloy</u>. By Danesi, Wilbert P. and Rudolph H. Thielemann. 1973.

VanStone, R.H., and T.L. Richardson. "Potential-Drop Monitoring of Cracks in Surface-Flawed Specimens." <u>Automated Test Methods for Fracture and Fatigue Crack Growth, ASTM STP 877</u>. Eds. Cullen, W.H., R.W. Landgraf, L.R. Kaisand, and J.H. Underwood. Philadelphia: ASTM, 1985. 148-166.

9. Appendix A.—Grainex Mar-M 247 NASA Disk Photomicrographs

Specimen ID	Comments	Page
Hub 1, Hub 2	Overall location relative to disk	104
S4A, S4B, S4C	Overall chord slices relative to disk	105
S4B-1	rim tip, 16x	106
S4B-2	web, 16x	107
S4B-3	web, 16x	108
S4B-4	web, 200x	109
S4C-1	web, 16x	110
S4C-2	web, 16x	111
Hub 1-1	hub near boss, 16x	112
Hub 1-2	mid-hub, 16x	113
Hub 1-3	hub opposite boss, 16x	114
Hub 2-1	hub near boss, 16x	115
Hub 2-2	mid-hub, 16x	116
Hub 2-3	hub near boss, 200x	117
Hub 2-4	mid-hub, 200x	118

Hub 2

Hub 1

S4-B

S4-C

S4-A
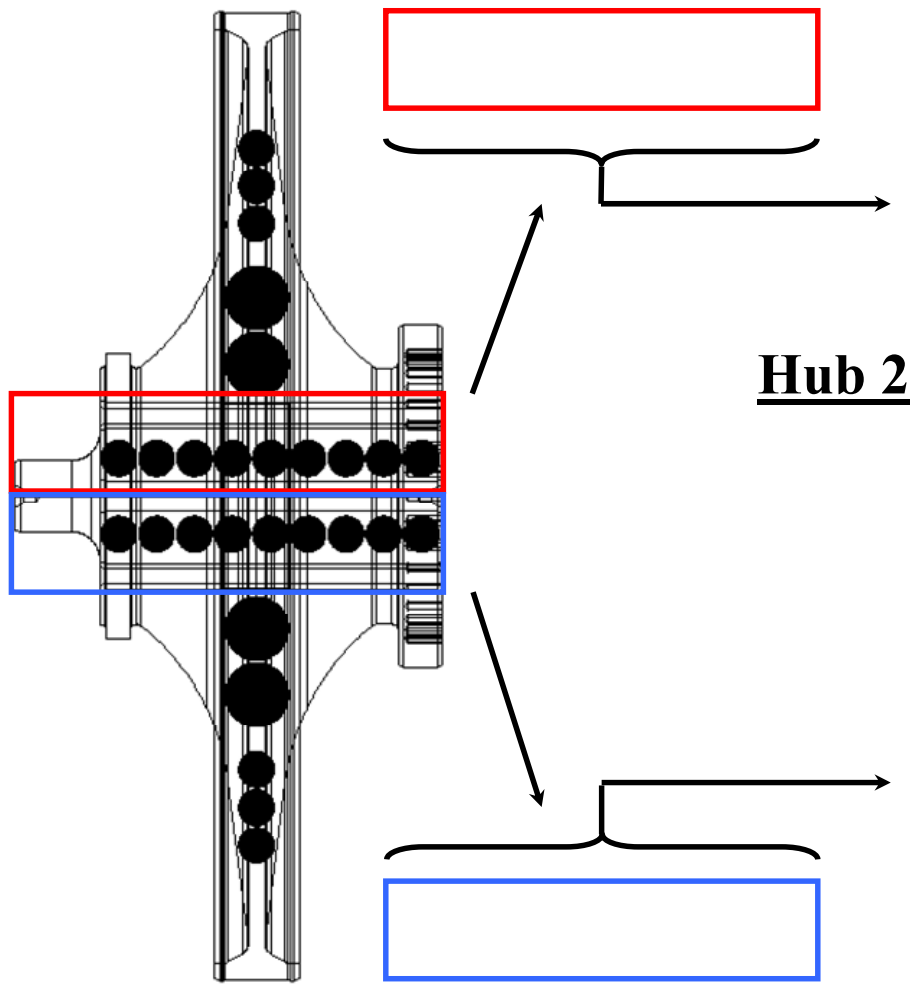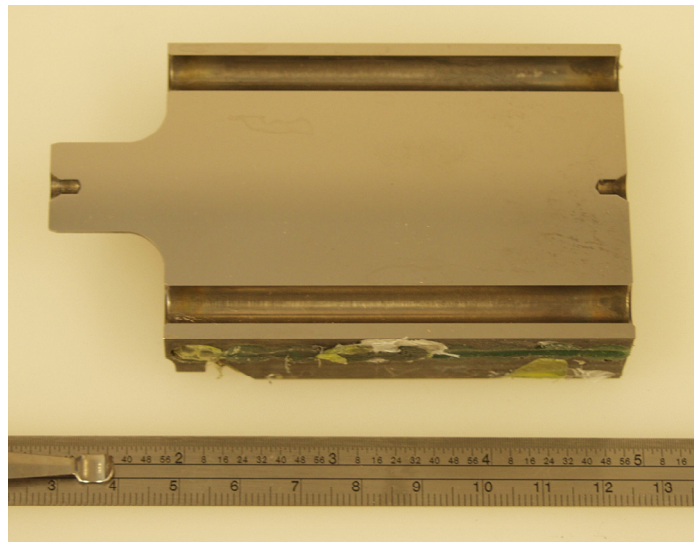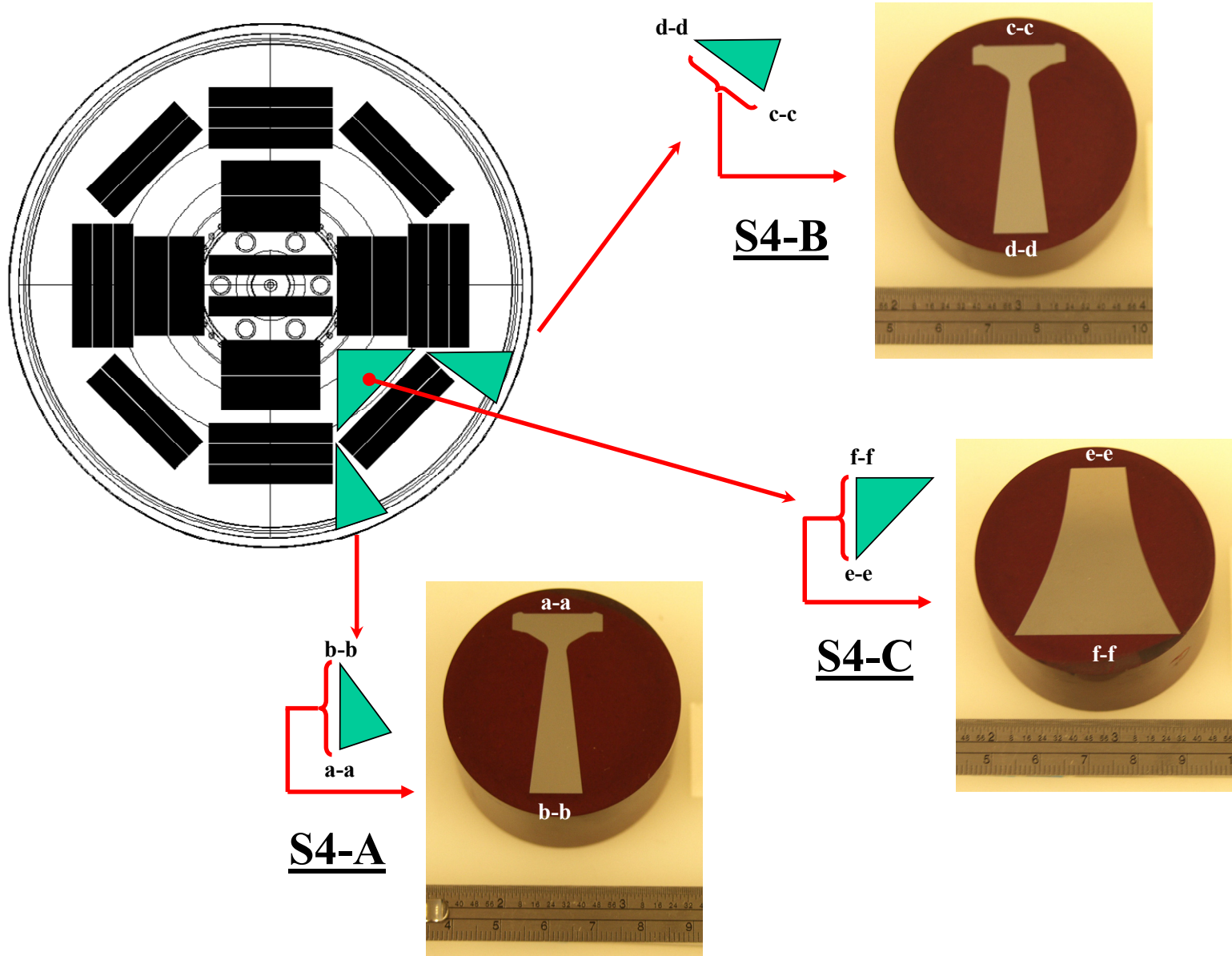
S4B-1 16x
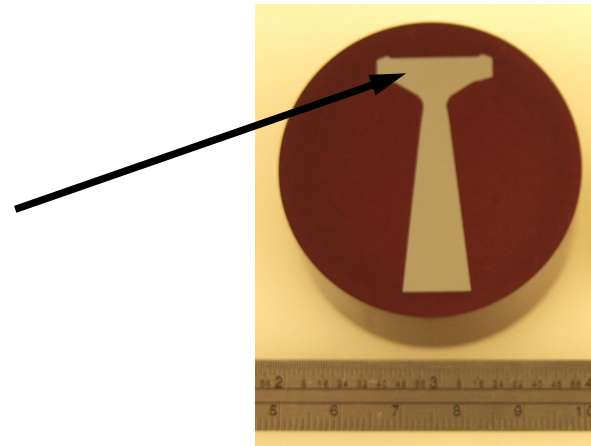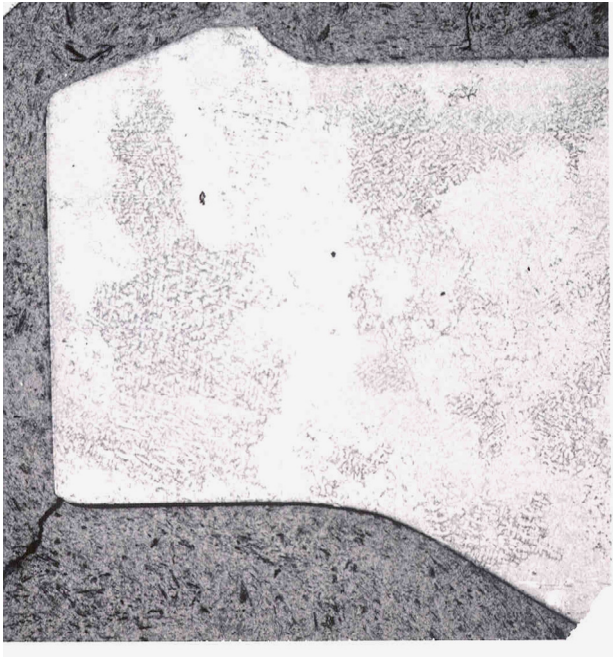
S4B-2 16x
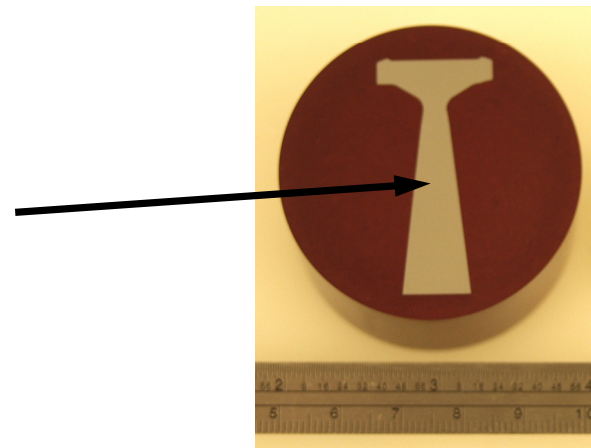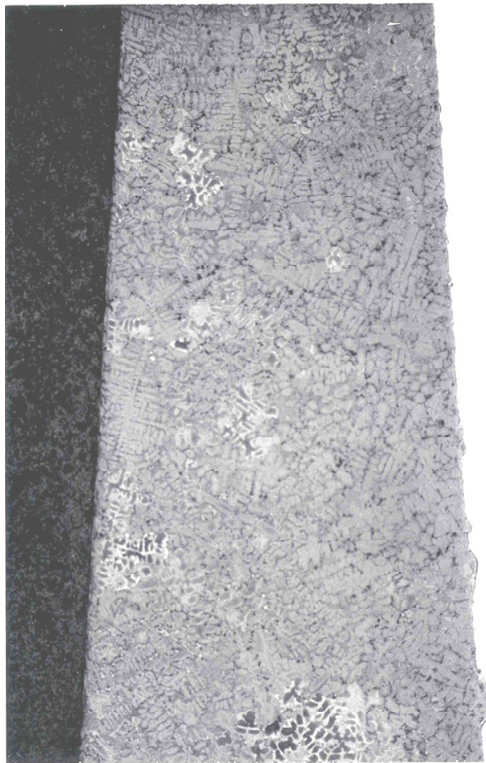
S4B-3 16x
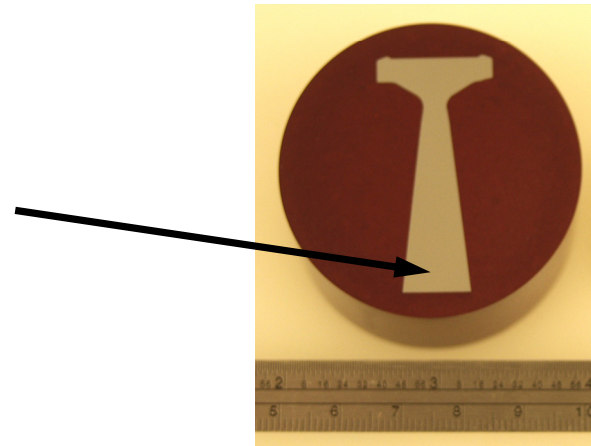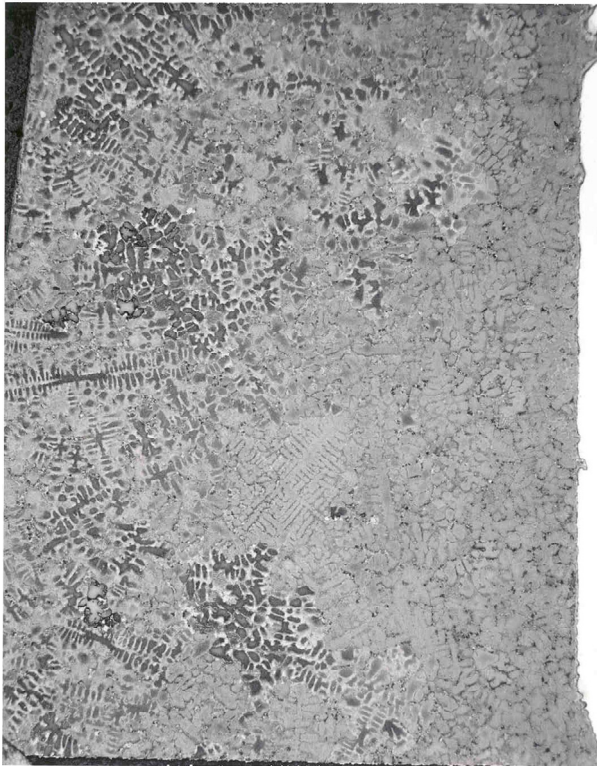
S4B-4 200x
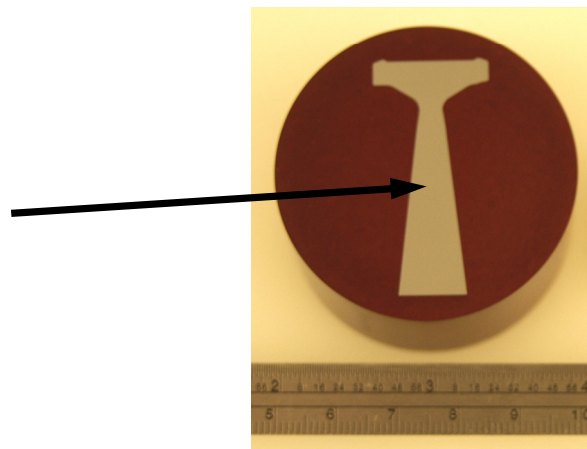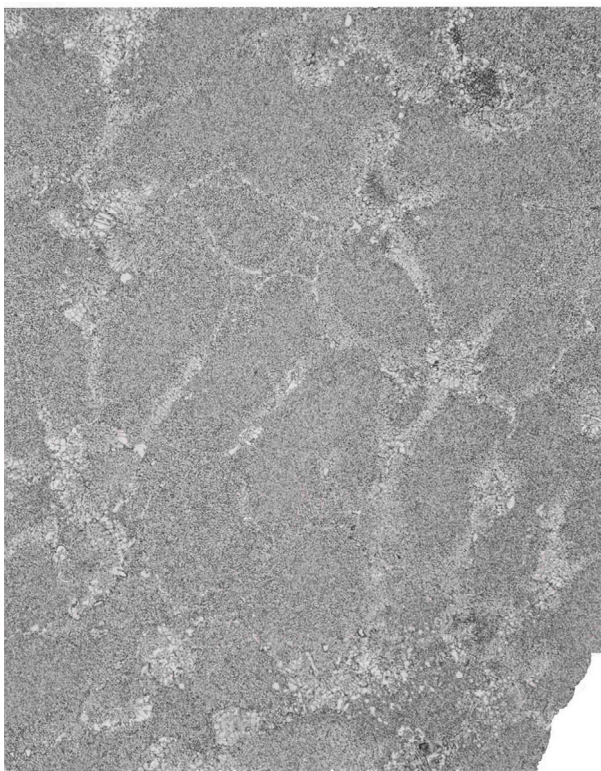
S4C-1 16x
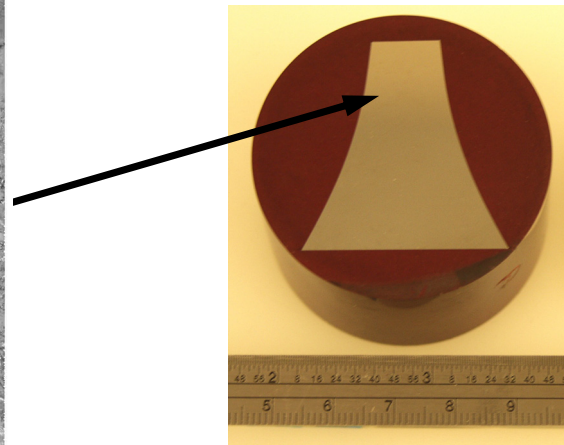
S4C-2 16x
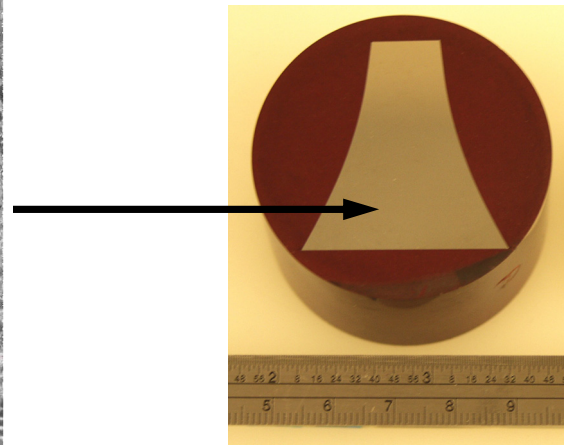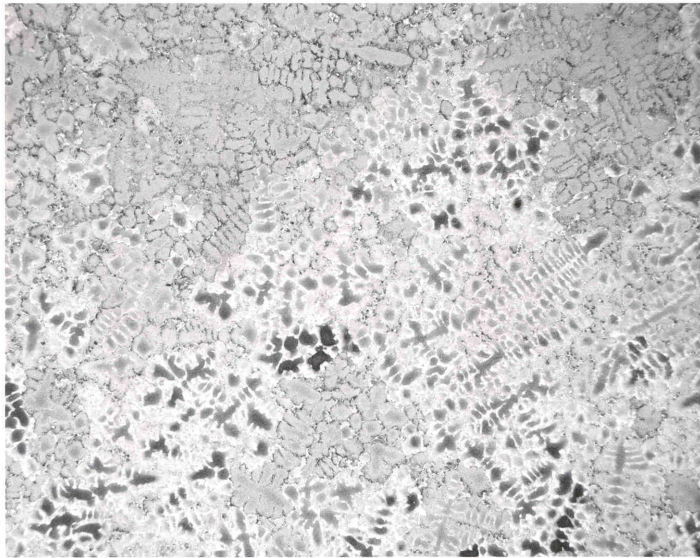
Hub1-1 16x
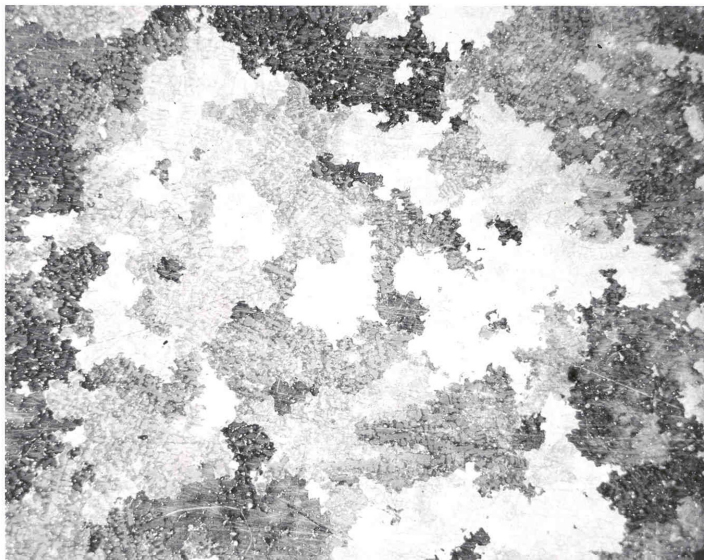
Hub1-2 16x
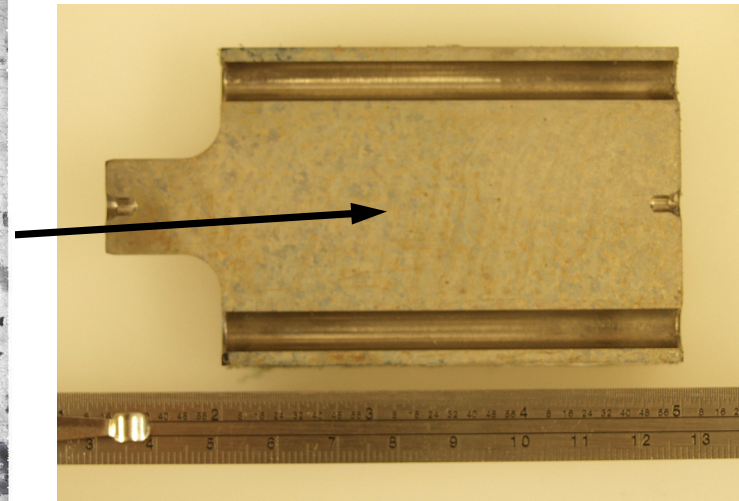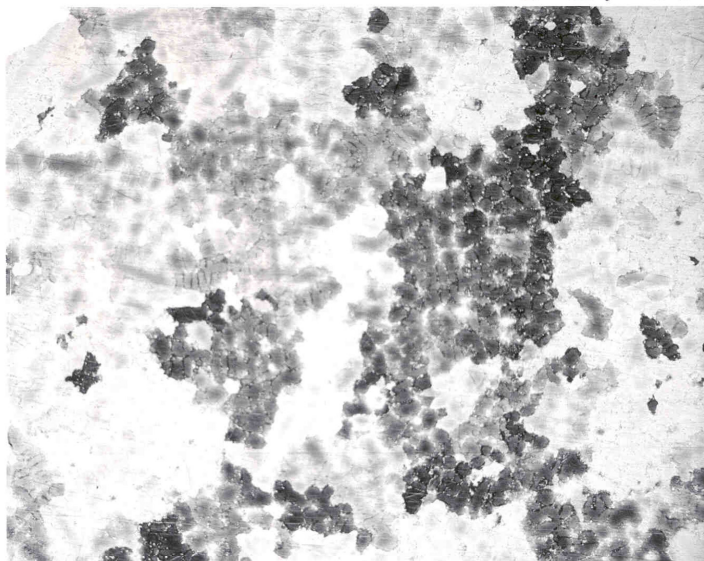
Hub1-3 16x
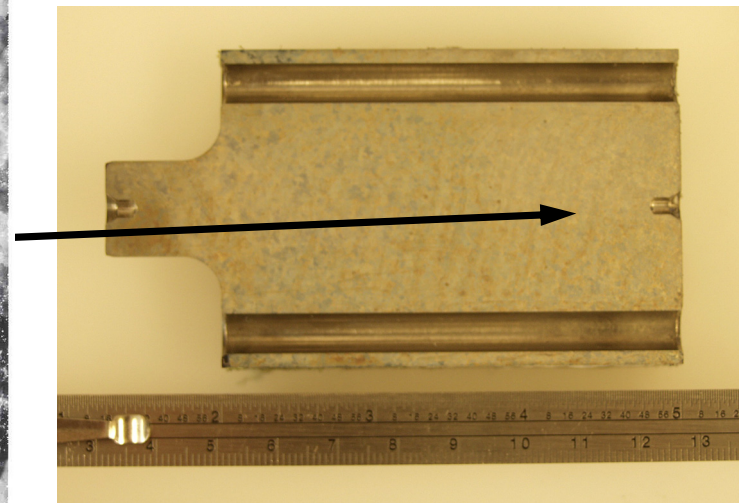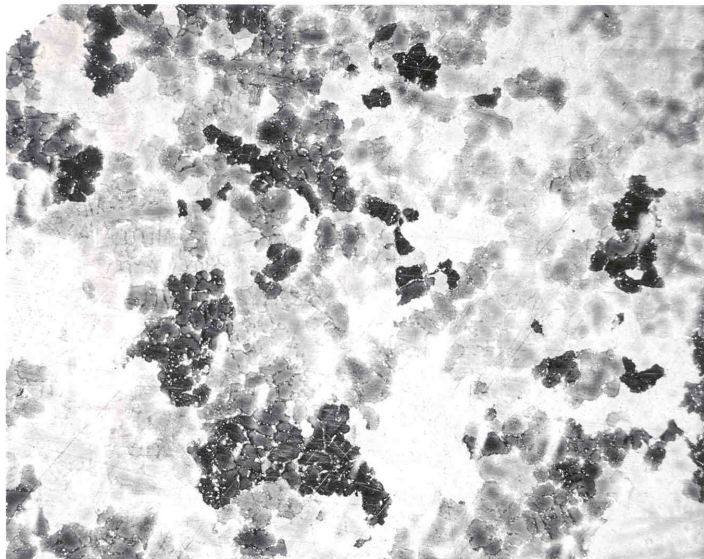
Hub 2-1 16x
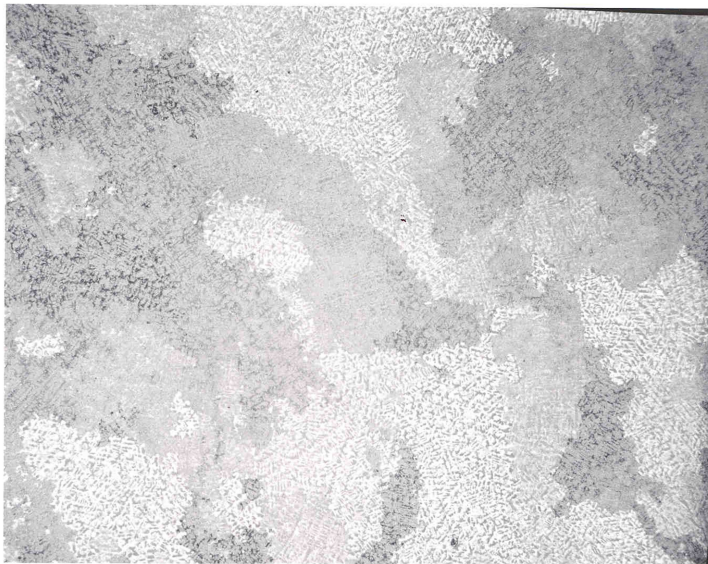
Hub 2-2 16x
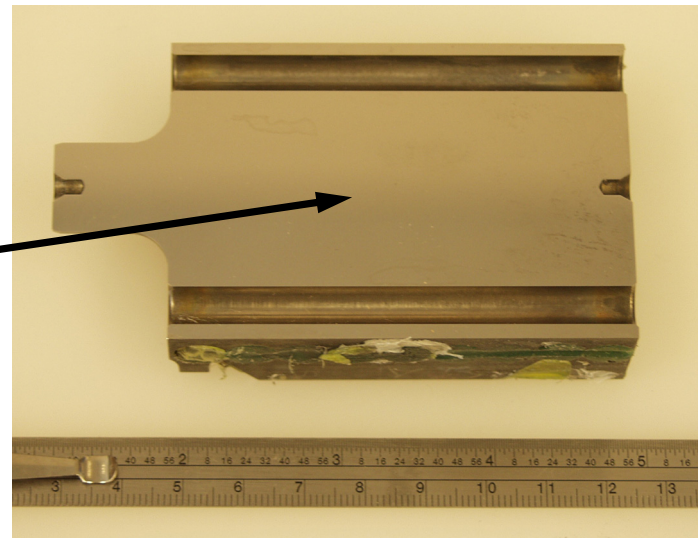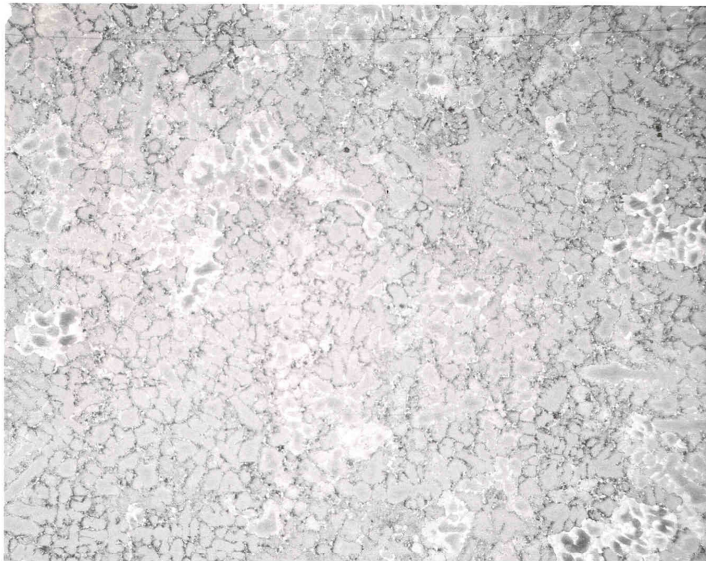
Hub 2-3 200x
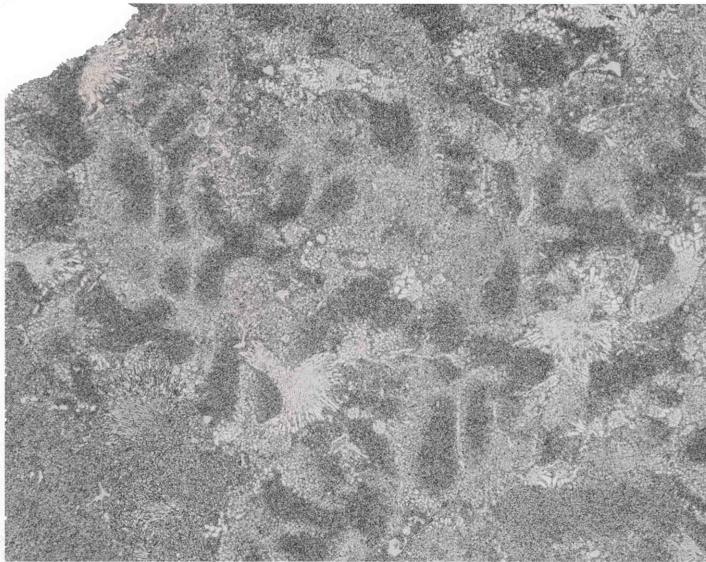
Hub 2-4 200x
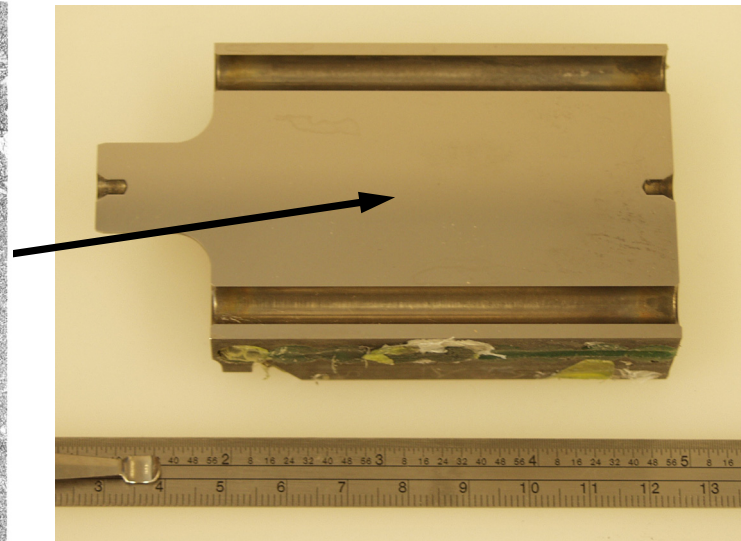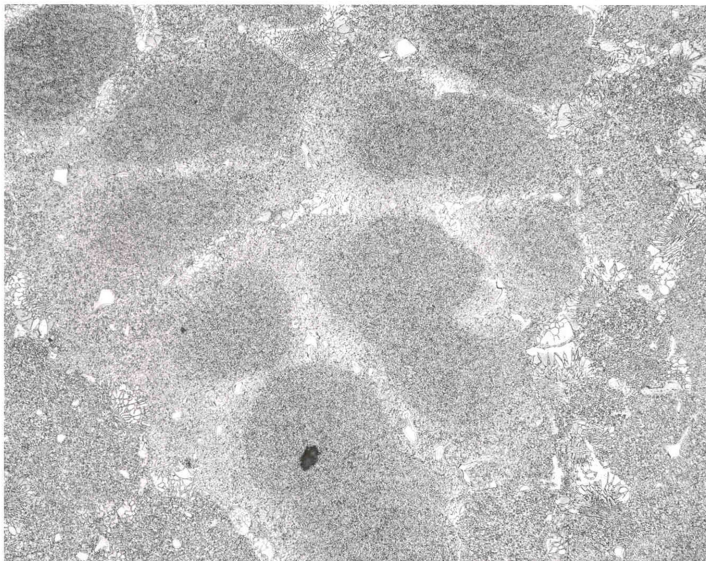
10. Appendix B.—Grainex Mar-M 247 Tensile Specimen SEM Images

Specimen ID	Temp [°C]	Comments	Page
17T	649	SE, BE	120
36T	649	SE, BE	121
55T	649	SE, BE	122
CB4T	649	SE, BE	123

Tensile Specimen 17T, 649°C
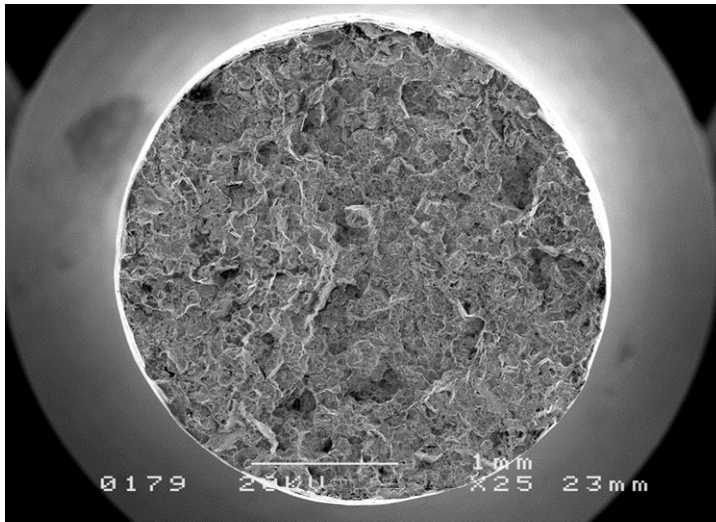
SE - mode
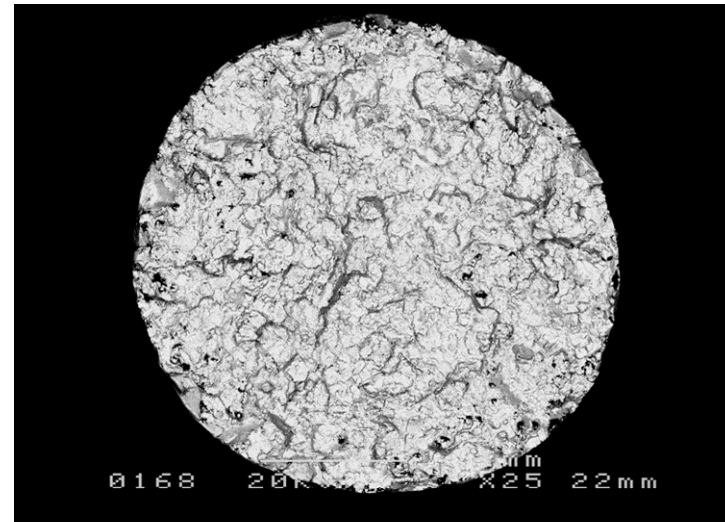
BE - mode

Tensile Specimen 36T, 649°C
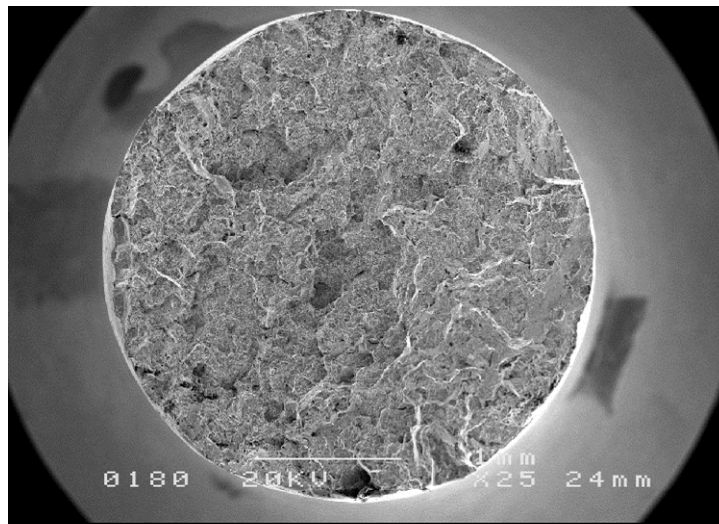
SE - mode
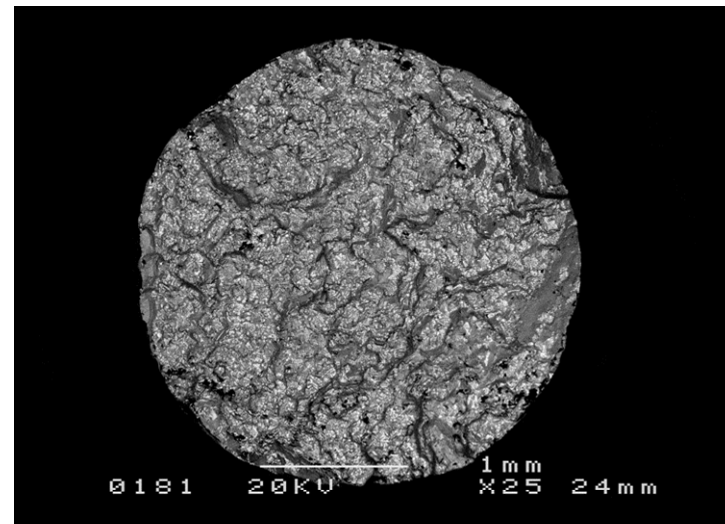
BE - mode

Tensile Specimen 55T, 649°C
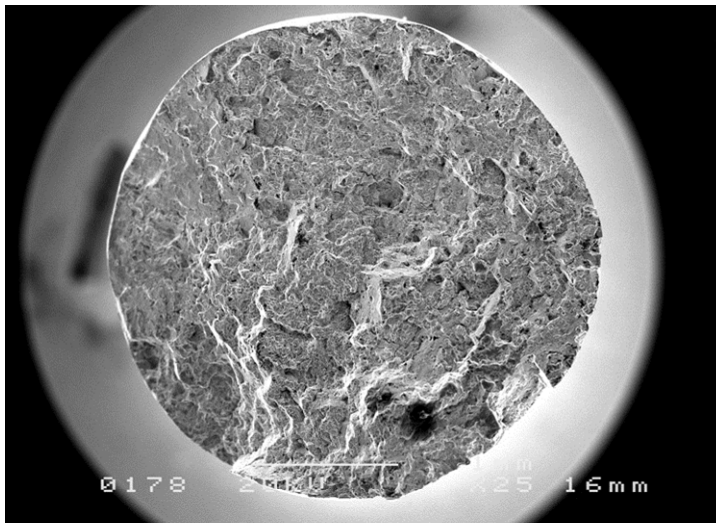
SE - mode
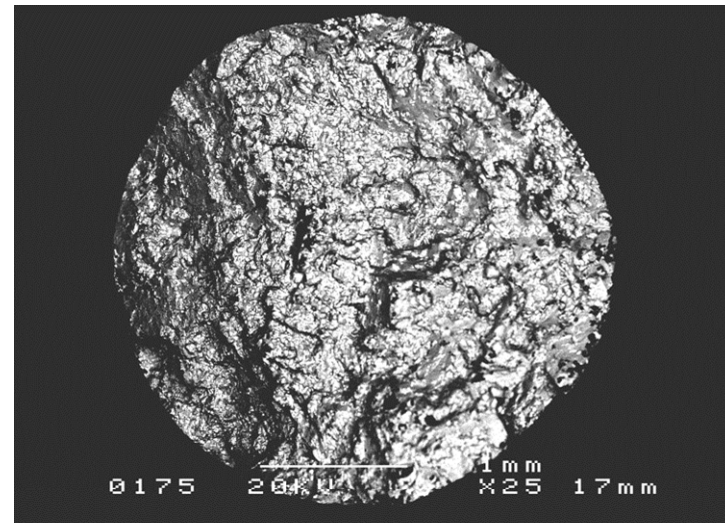
BE - mode

Tensile Specimen CB4T, 649°C
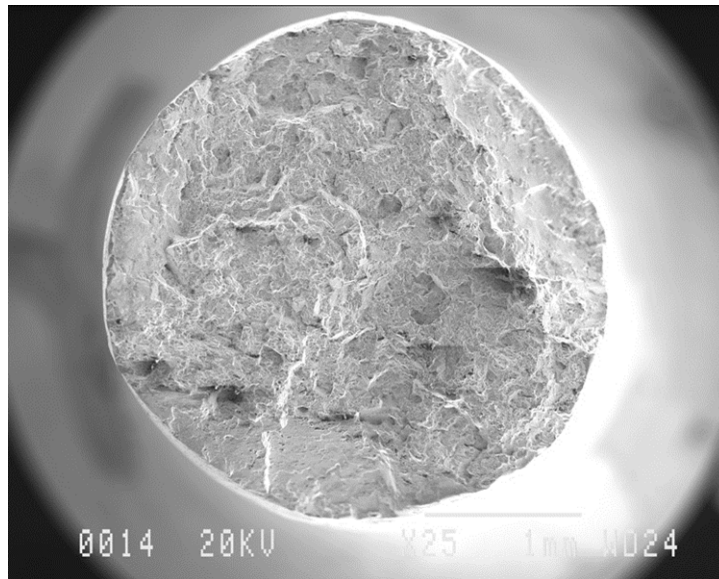
SE - mode
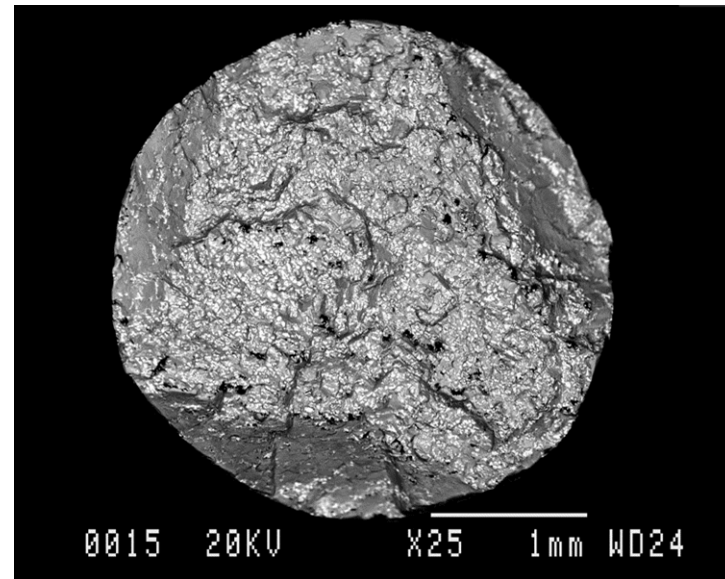
BE - mode

11. Appendix C.—Grainex Mar-M 247 Low Cycle Fatigue Specimen SEM Images

SpecimenID	R	Δε[%]	Mag [x]	Comments	Page	Specimen ID	R	Δε [%]	Mag [x]	Comments	Page
15L	-1	0.90	25	SE, BE	127	57L	-1	0.58	100	SE, BE	149
15L	-1	0.90	100	BE	128	57L	-1	0.58	500	SE, BE	150
26L	0	0.90	25	SE, BE	129	66L	-1	0.50	25	SE, BE	151
26L	0	0.90	100	SE, BE, Crack 1	130	66L	-1	0.50	100	SE, BE	152
26L	0	0.90	100	SE, BE, Crack 2	131	66L	-1	0.50	500	SE, BE	153
26L	0	0.90	500	SE, BE, Crack 1	132	67L	0	0.50	25	SE, BE	154
27L	-1	0.78	25	SE, BE	133	67L	0	0.50	100	SE, BE	155
27L	-1	0.78	100	SE, BE, Crack 1	134	67L	0	0.50	500	SE, BE	156
27L	-1	0.78	100	SE, BE, Crack 2	135	77L	0	0.50	25	SE, BE	157
27L	-1	0.78	500	SE, BE, Crack 1	136	77L	0	0.50	100	SE, BE	158
35L	0	0.78	25	SE, BE	137	77L	0	0.50	500	SE, BE	159
35L	0	0.78	100	SE, BE	138	76L	-1	0.58	25	SE, BE	160
46L	0	0.67	25	SE, BE	139	76L	-1	0.58	100	SE, BE, Crack 1	161
46L	0	0.67	100	SE, BE	140	76L	-1	0.58	100	SE, BE, Crack 2	162
46L	0	0.67	500	SE, BE	141	76L	-1	0.58	500	SE, BE, Crack 1	163
47L	-1	0.67	25	SE, BE	142	76L	-1	0.58	500	SE, BE, Crack 2	164
47L	-1	0.67	100	SE, BE	143	86L	-1	0.50	25	SE, BE	165
47L	-1	0.67	500	SE, BE	144	86L	-1	0.50	100	SE, BE	166
56L	0	0.58	25	SE, BE	145	86L	-1	0.50	500	SE, BE	167
56L	0	0.58	100	SE, BE	146	86L	-1	0.50	100	SE, Overload	168
56L	0	0.58	500	SE, BE	147	86L	-1	0.50	500,1500	SE, Overload	169
57L	-1	0.58	25	SE, BE	148	87L	0	0.58	25	SE, BE	170

Specimen ID	R	Δε[%]	Mag [x]	Comments	Page	Specimen ID	R	Δε [%]	Mag [x]	Comments	Page
87L	0	0.58	100	SE, BE	171	CA9L	-1	0.58	500	SE, BE	198
87L	0	0.58	500	SE, BE	172	CB1L	-1	0.50	25	SE, BE	199
87L	0	0.58	100	stage II/III crack prop.	173	CB1L	-1	0.50	100	SE, BE	200
CA1L	0	0.67	25	SE, BE	174	CB1L	-1	0.50	500	SE, BE	201
CA1L	0	0.67	100	SE, BE	175	CB2L	0	0.58	25	SE, BE	202
CA1L	0	0.67	500	SE, BE	176	CB2L	0	0.58	100	SE, BE	203
CA2L	-1	0.90	25	SE, BE	177	CB2L	0	0.58	500	SE, BE	204
CA2L	-1	0.90	100	SE, BE, Crack 1	178	CB3L	-1	0.90	25	SE, BE	205
CA2L	-1	0.90	100	SE, BE, Crack 2	179	CB3L	-1	0.90	100	SE, BE	206
CA3L	0	0.78	25	SE, BE	180	CB3L	-1	0.90	500	SE, BE	207
CA3L	0	0.78	100	SE, BE	181	CB5L	0	0.67	25	SE, BE	208
CA3L	0	0.78	500	SE, BE	182	CB5L	0	0.67	100	SE, BE	209
CA4L	-1	0.78	25	SE, BE	183	CB5L	0	0.67	500	SE, BE	210
CA4L	-1	0.78	100	SE, BE, Crack 1	184	CB6L	-1	0.78	25	SE, BE	211
CA4L	-1	0.78	100	SE, BE, Crack 2	185	CB6L	-1	0.78	100	SE, BE	212
CA4L	-1	0.78	500	SE, BE, Crack 1	186	CB6L	-1	0.78	500	SE, BE	213
CA6L	0	0.90	25	SE, BE	187	CB7L	0	0.78	25	SE, BE	214
CA6L	0	0.90	100	SE, BE	188	CB7L	0	0.78	100	SE, BE	215
CA6L	0	0.90	500	SE, BE	189	CB7L	0	0.78	500	SE, BE, Crack 1	216
CA7L	-1	0.67	25	SE, BE	190	CB7L	0	0.78	500	SE, BE, Crack 2	217
CA7L	-1	0.67	100	SE, BE	191	CB8L	-1	0.67	25	SE, BE	218
CA7L	-1	0.67	500	SE, BE	192	CB8L	-1	0.67	100	SE, BE	219
CA8L	0	0.50	25	SE, BE	193	CB8L	-1	0.67	500	SE, BE	220
CA8L	0	0.50	100	SE, BE	194	CB9L	0	0.90	25	SE, BE	221
CA8L	0	0.50	500	SE, BE	195	CB9L	0	0.90	100	SE, BE	222
CA9L	-1	0.58	25	SE, BE	196	CB9L	0	0.90	500	SE, BE	223
CA9L	-1	0.58	100	SE, BE	197						

15L, R = -1, Δε = 0.90%, 25x
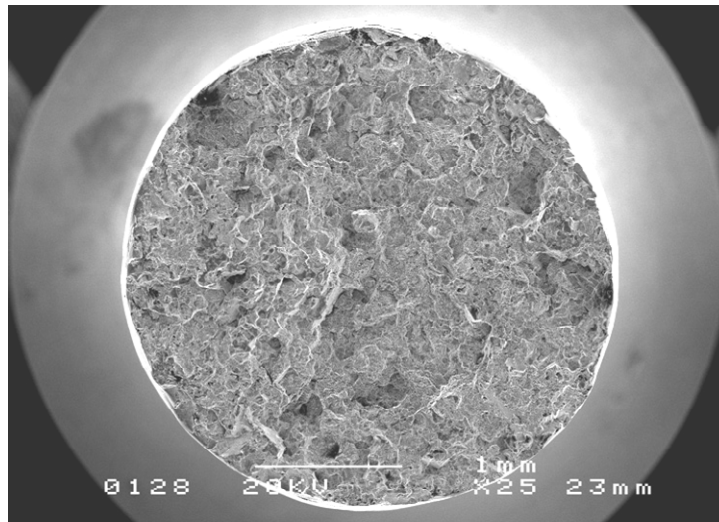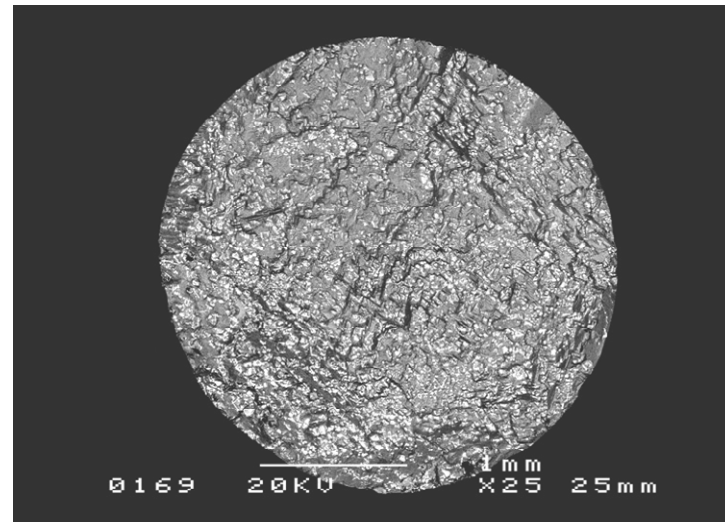
SE mode

BE mode

15L, R = -1, $\Delta\varepsilon$ = 0.90%, 100x
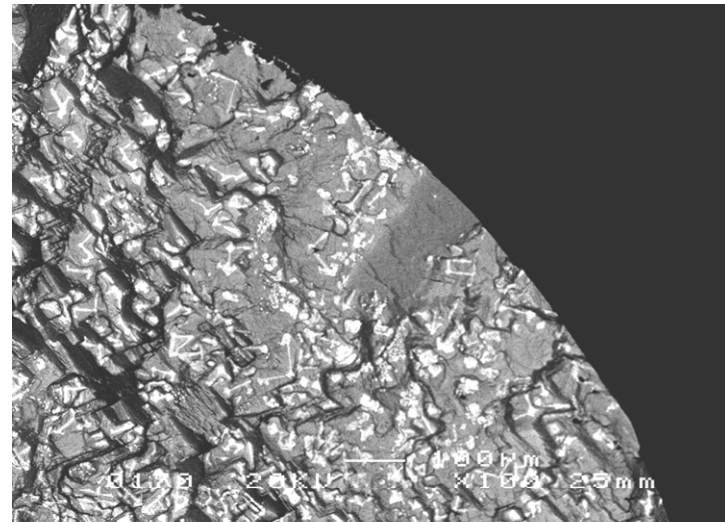
BE mode

26L, R = 0, $\Delta\varepsilon$ = 0.90%, 25x
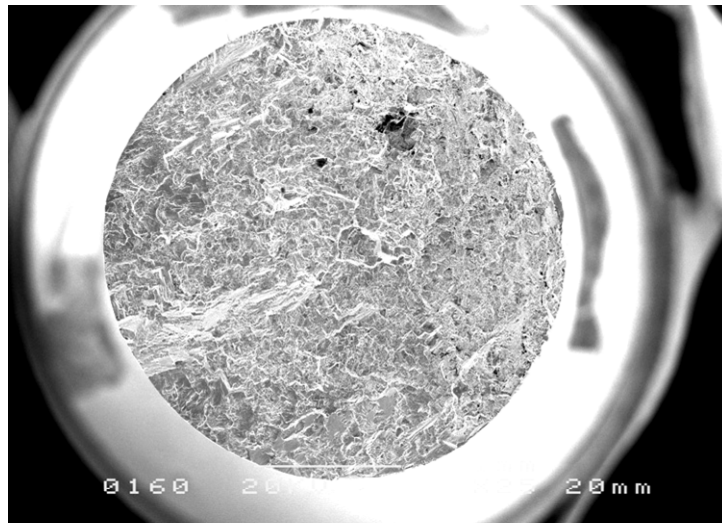
SE mode   BE mode
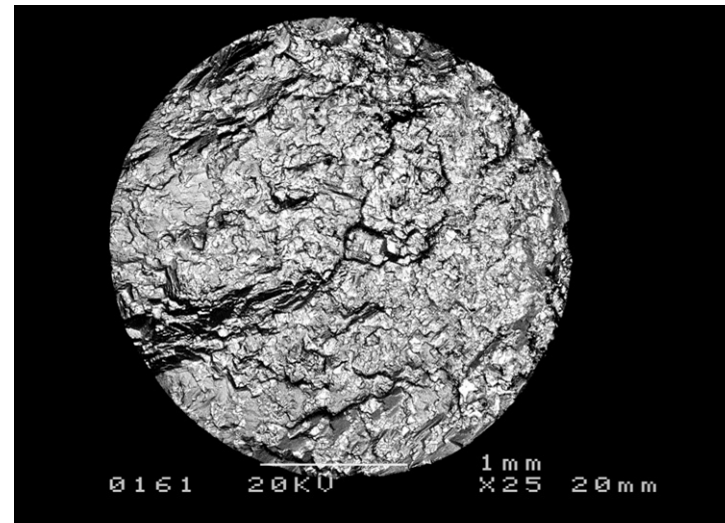
26L, R = 0, $\Delta\varepsilon$ = 0.90%, 100x

Crack 1
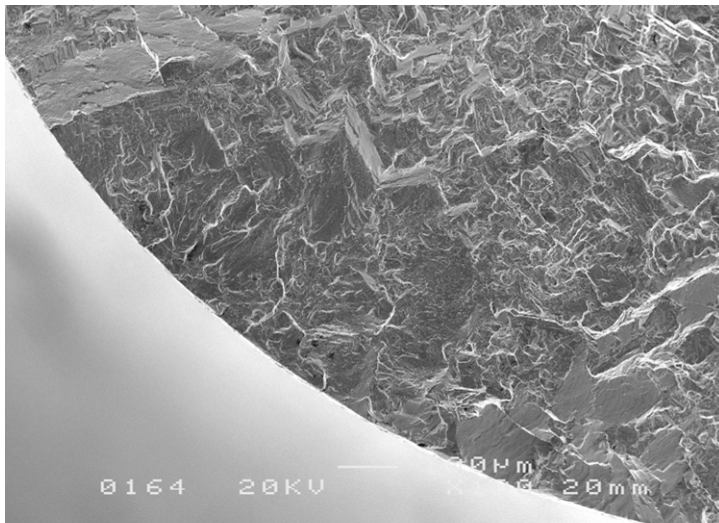
SE mode
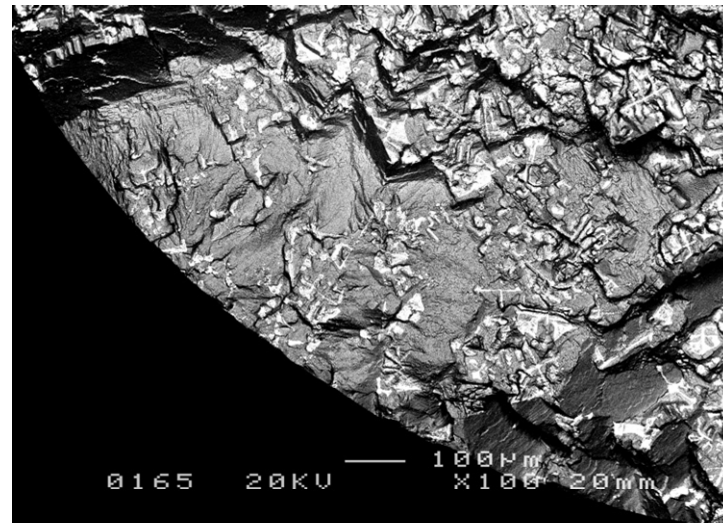
BE mode

26L, R = 0, $\Delta\varepsilon$ = 0.90%, 100x

Crack 2
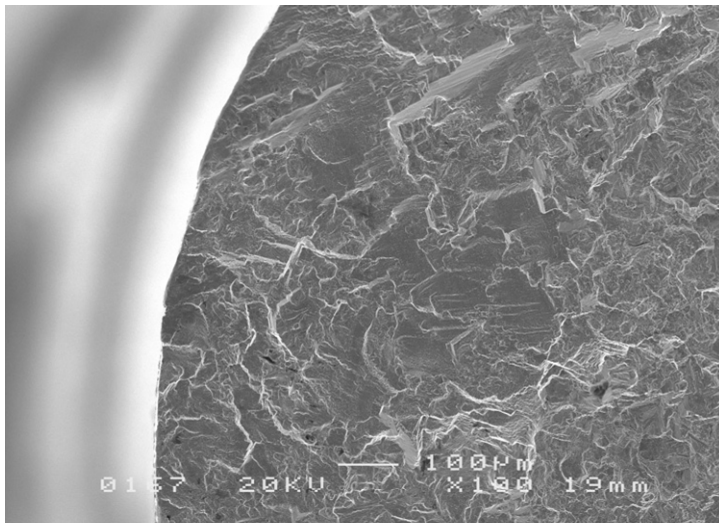
SE mode
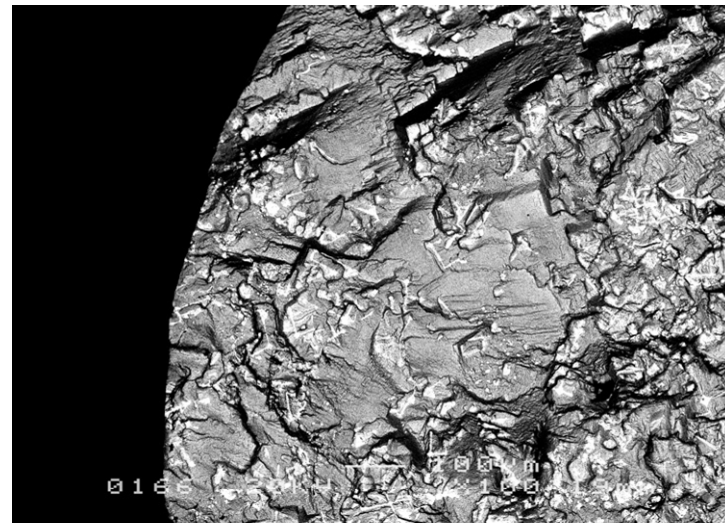
BE mode

26L, R = 0, $\Delta\varepsilon$ = 0.90%, 500x

Crack 1

SE mode   BE mode
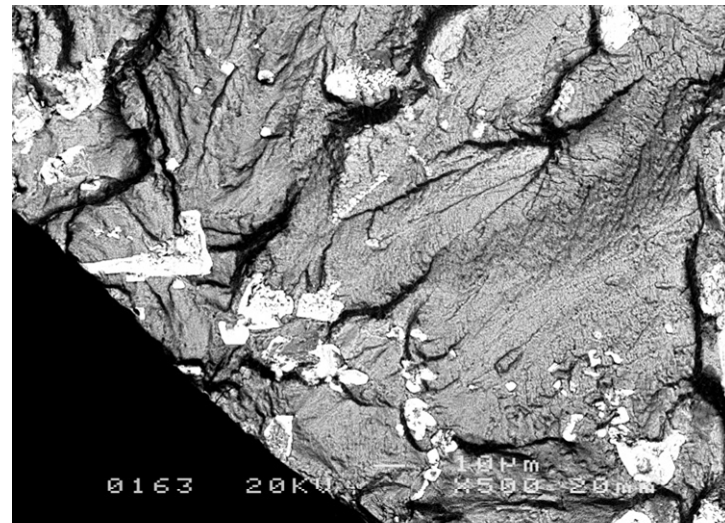
27L, R = -1, Δε = 0.78%, 25x
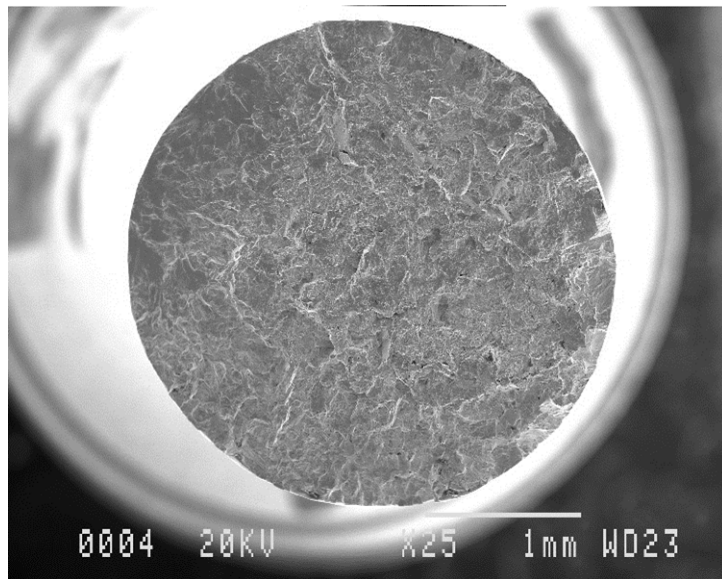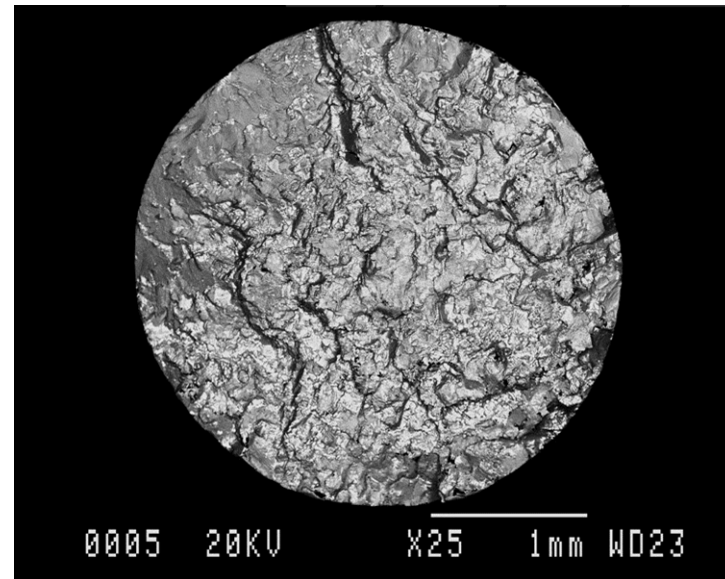
SE mode

BE mode

27L, R = -1, $\Delta\varepsilon$ = 0.78%, 100x

Crack 1

SE mode   BE mode

27L, R = -1, Δε = 0.78%, 100x

Crack 2

SE mode   BE mode

27L, R = -1, Δε = 0.78%, 500x
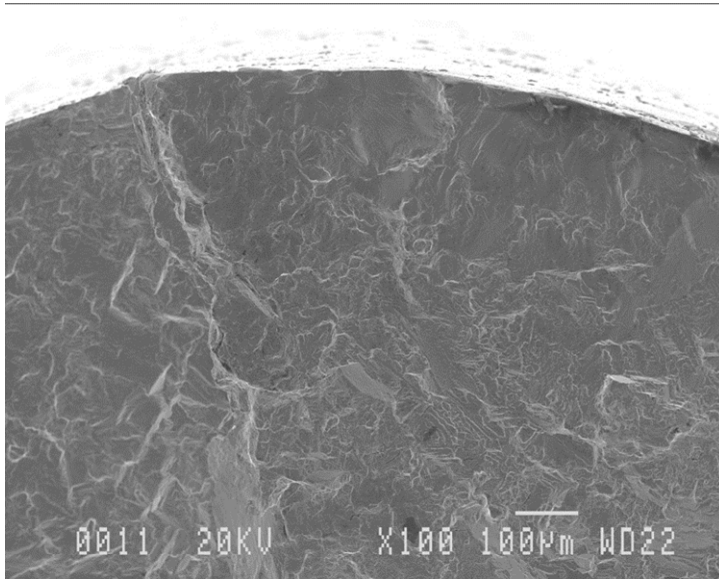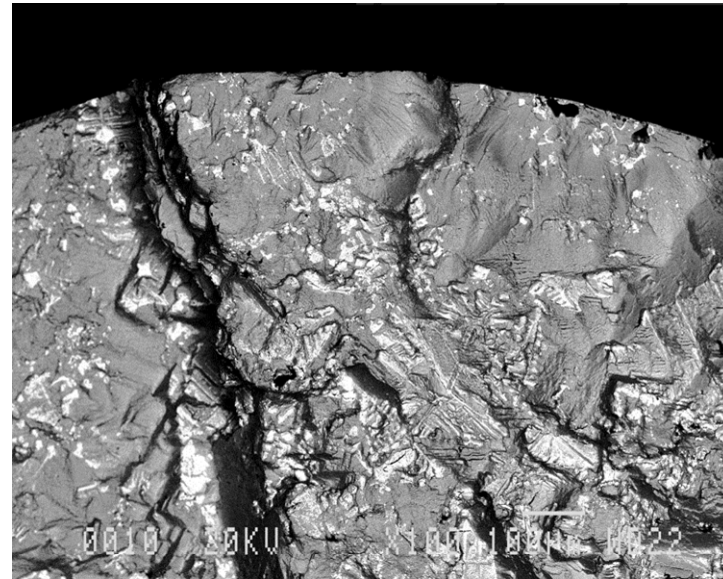
Crack 1
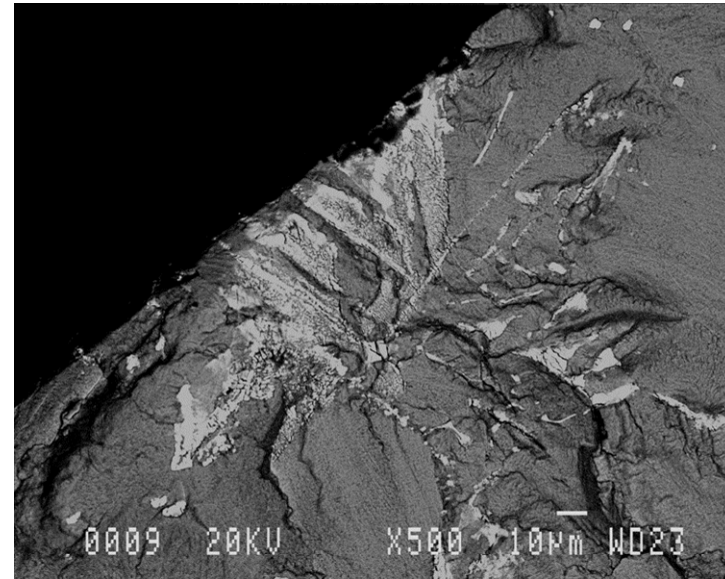
SE mode

BE mode

35L, R = 0, Δε = 0.78%, 25x

SE mode

BE mode
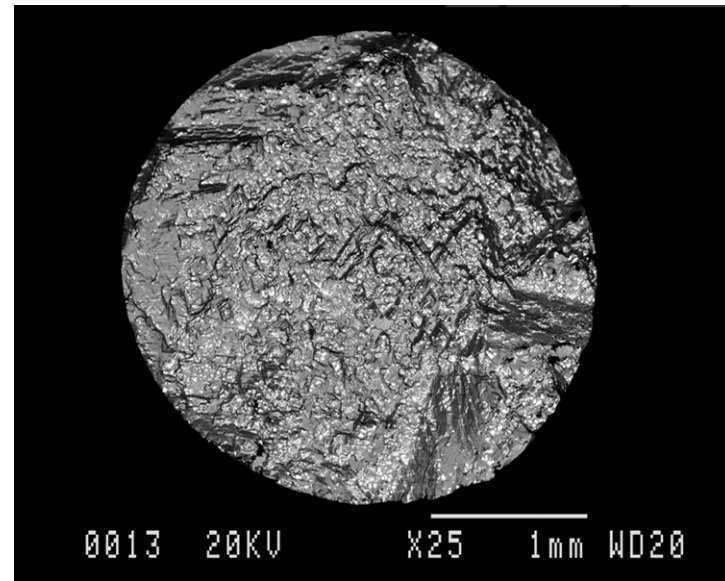
35L, R = 0, $\Delta\varepsilon$ = 0.78%, 100x

SE mode
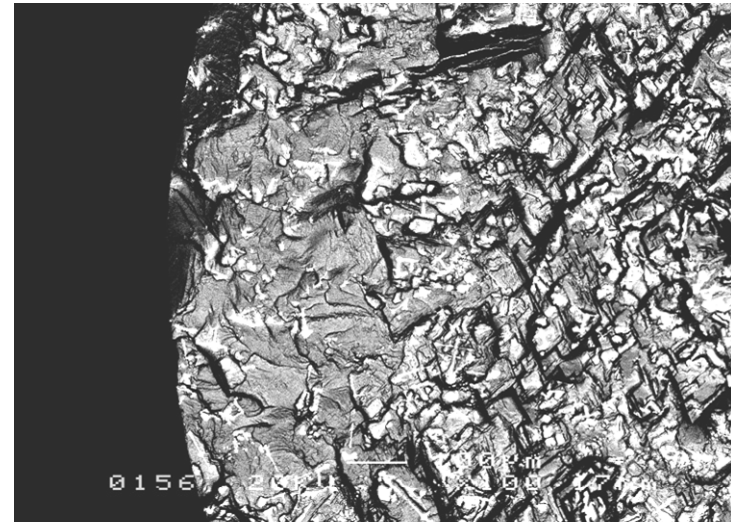
BE mode

46L, R = 0, Δε = 0.67%, 25x

SE mode   BE mode

# 46L, R = 0, Δε = 0.67%, 100x
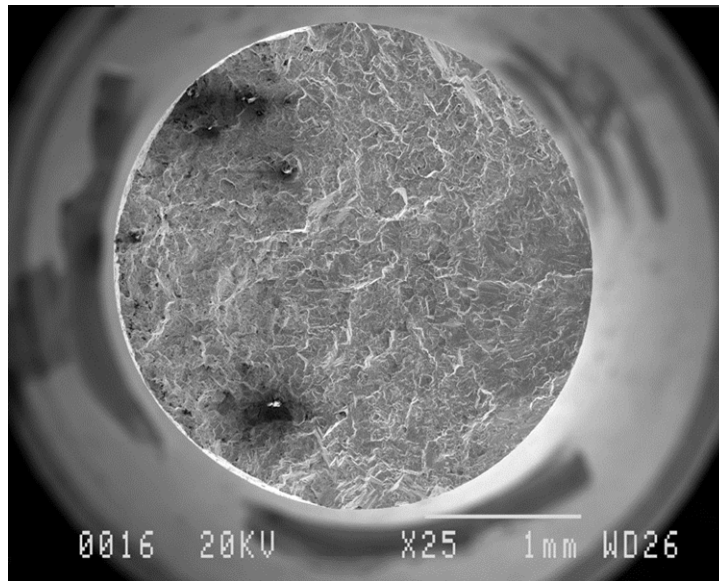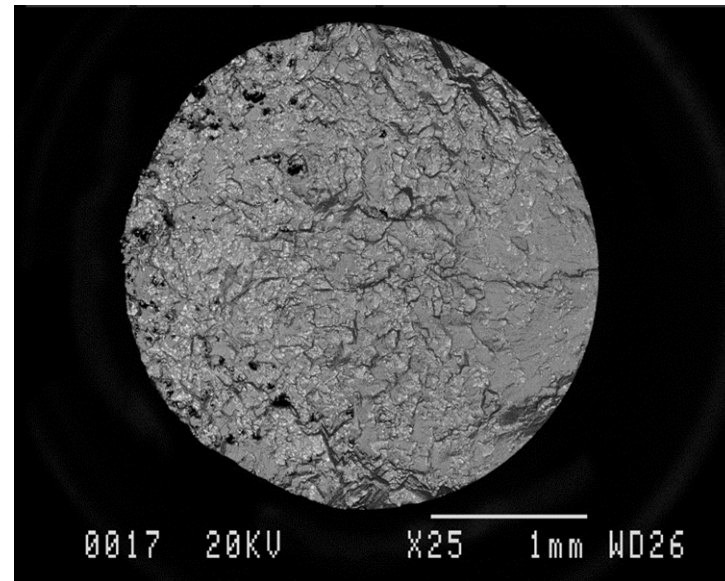
SE mode   BE mode
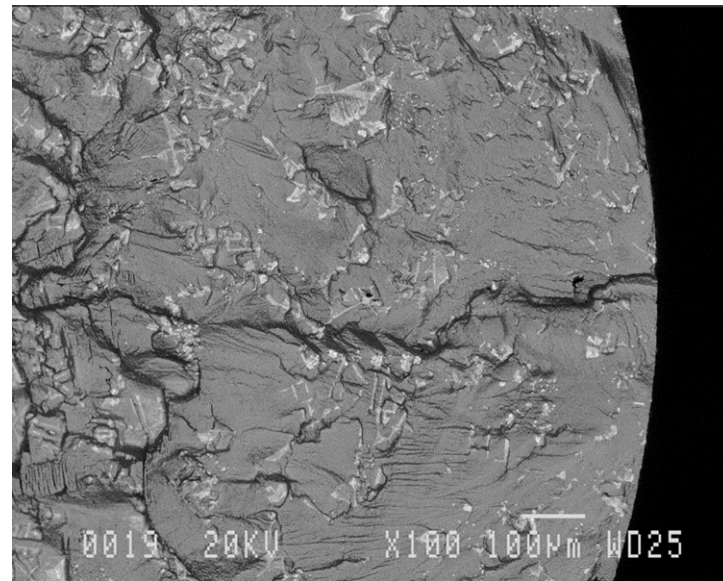
46L, R = 0, $\Delta\varepsilon$ = 0.67%, 500x
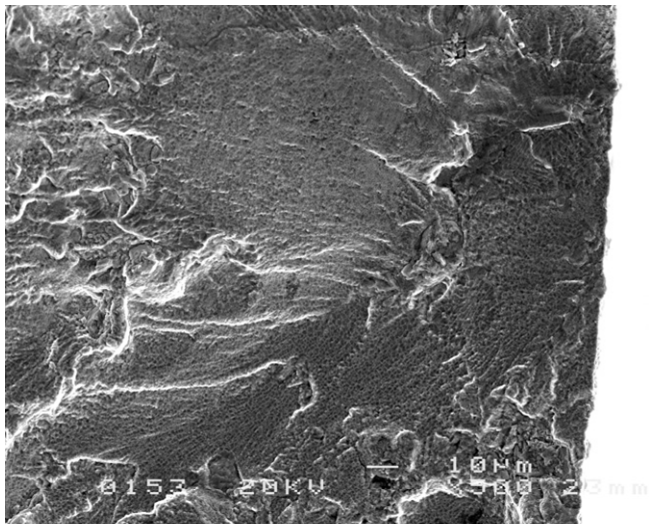
SE mode
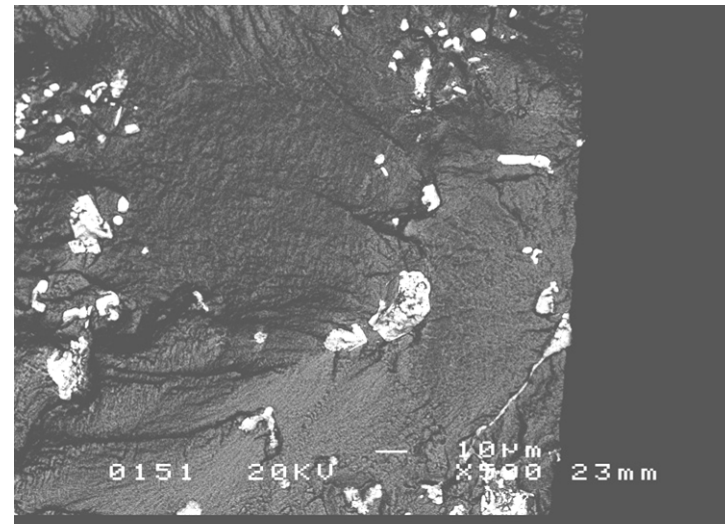
BE mode

47L, R = -1, Δε = 0.67%, 25x

SE mode

BE mode

47L, R = -1, Δε = 0.67%, 100x

SE mode

BE mode
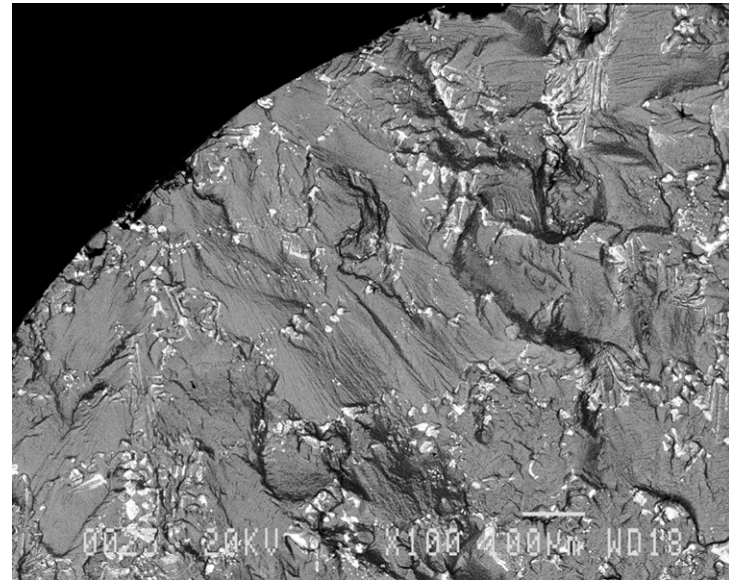
47L, R = -1, $\Delta\varepsilon$ = 0.67%, 500x
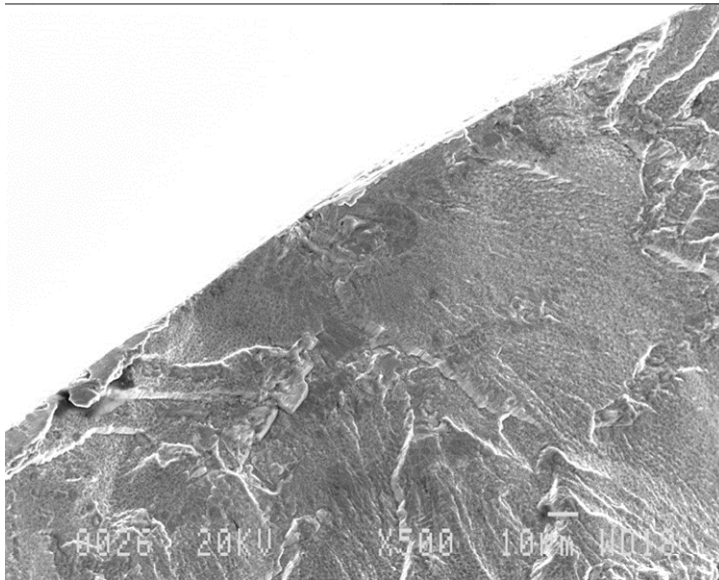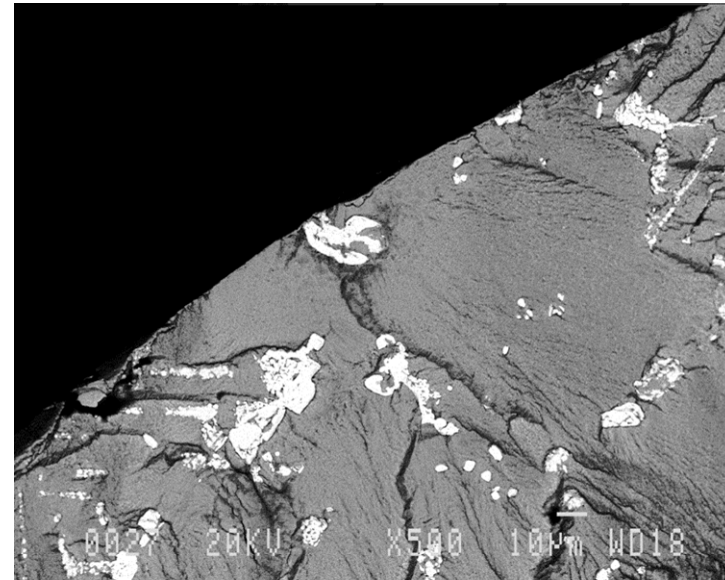

SE mode   BE mode

56L, R = 0, $\Delta\varepsilon$ = 0.58%, 25x
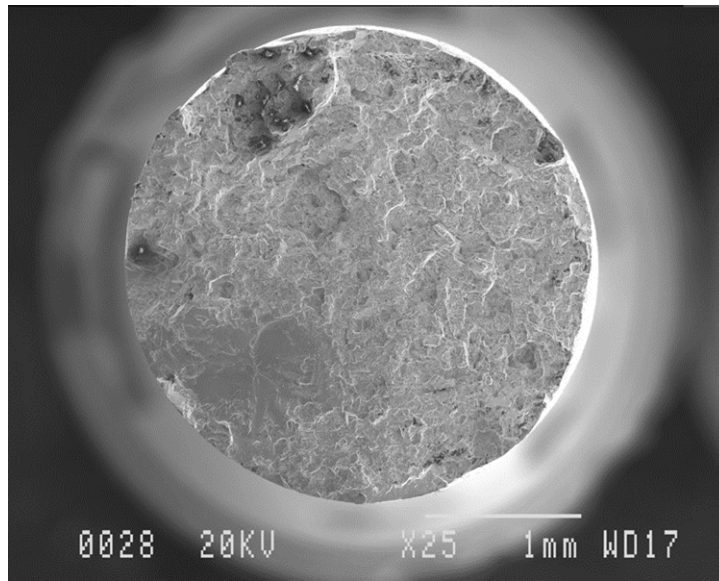

SE mode
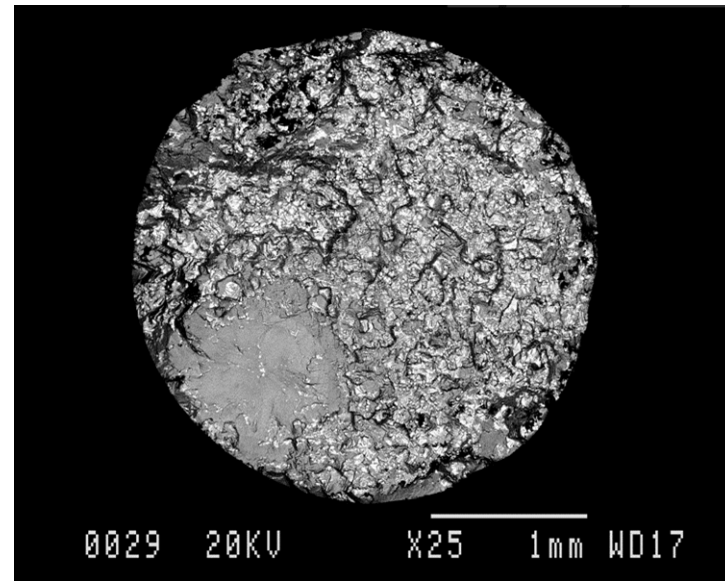
BE mode

56L, R = 0, $\Delta\varepsilon$ = 0.58%, 100x
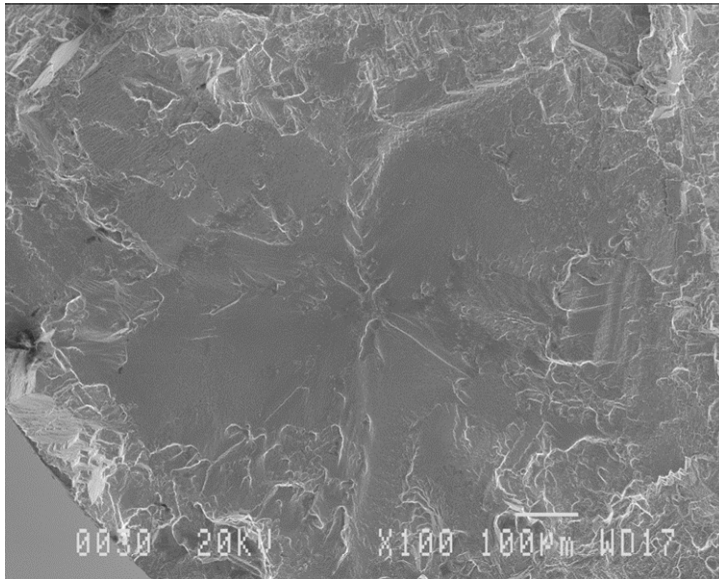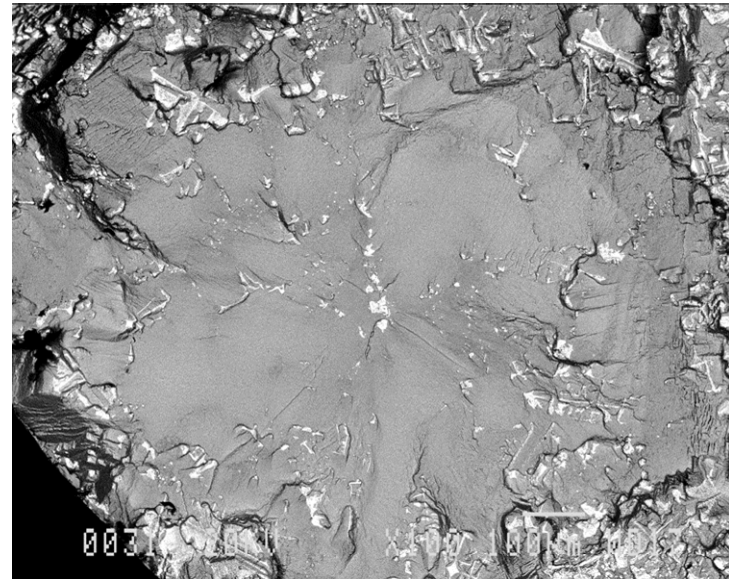

SE mode   BE mode

56L, R = 0, $\Delta\varepsilon$ = 0.58%, 500x

SE mode
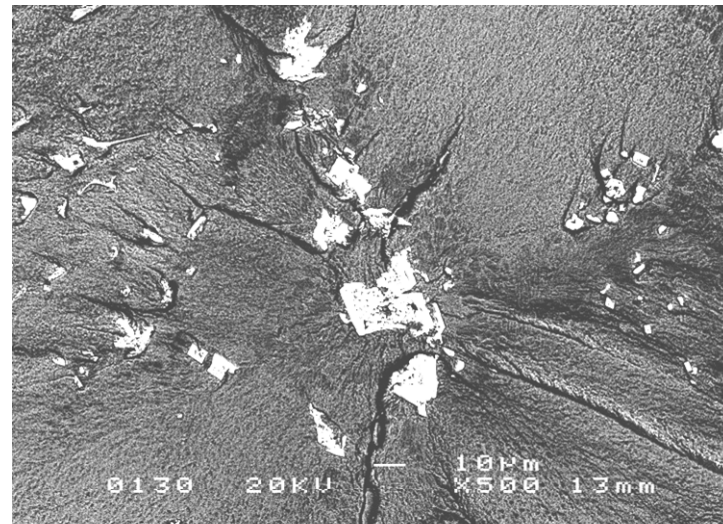
BE mode

57L, R = -1, Δε = 0.58%, 25x

SE mode

BE mode
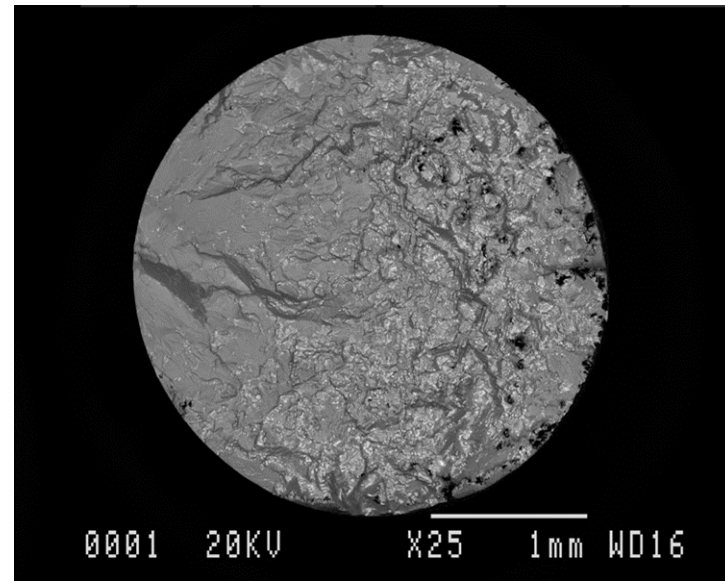
57L, R = -1, $\Delta\varepsilon$ = 0.58%, 100x

SE mode

BE mode

57L, R = -1, Δε = 0.58%, 500x
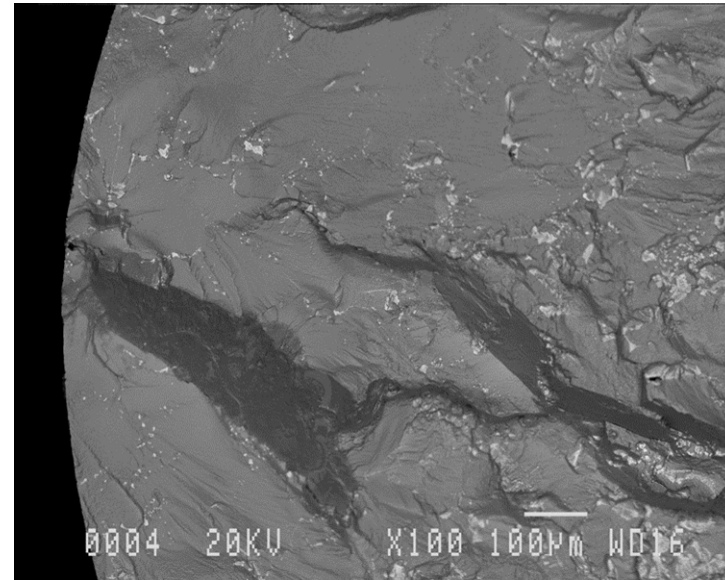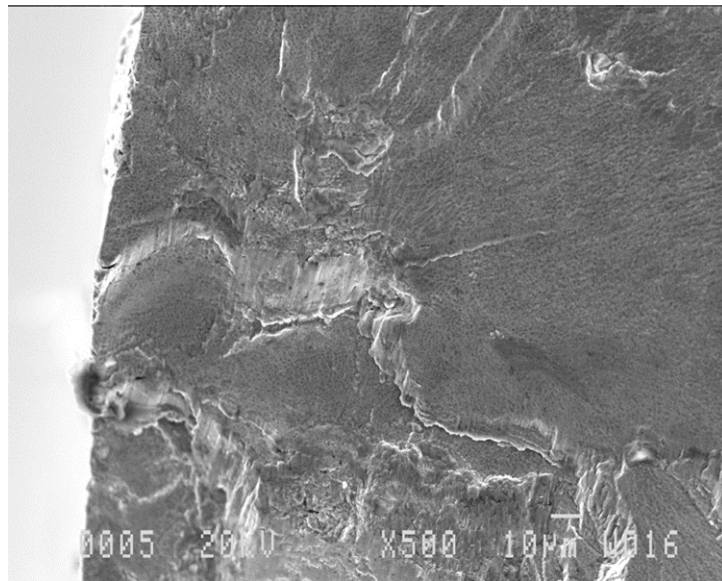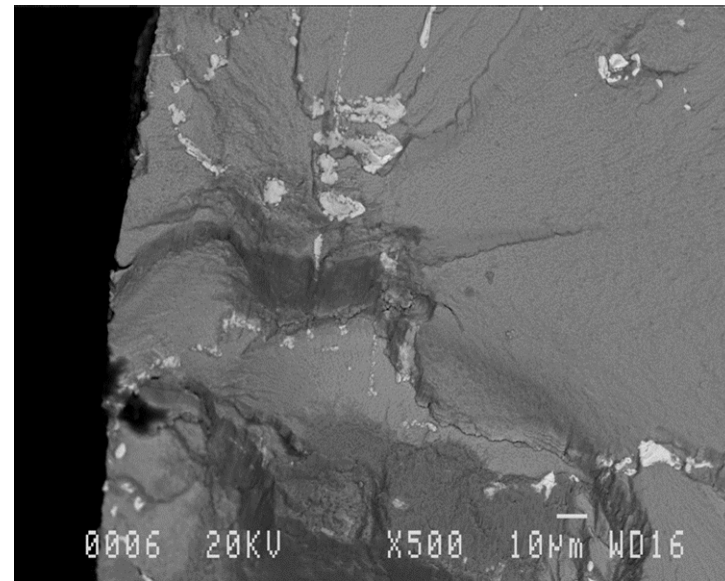
SE mode

BE mode

66L, R = -1, Δε = 0.50%, 25x

SE mode   BE mode

66L, R = -1, Δε = 0.50%, 100x
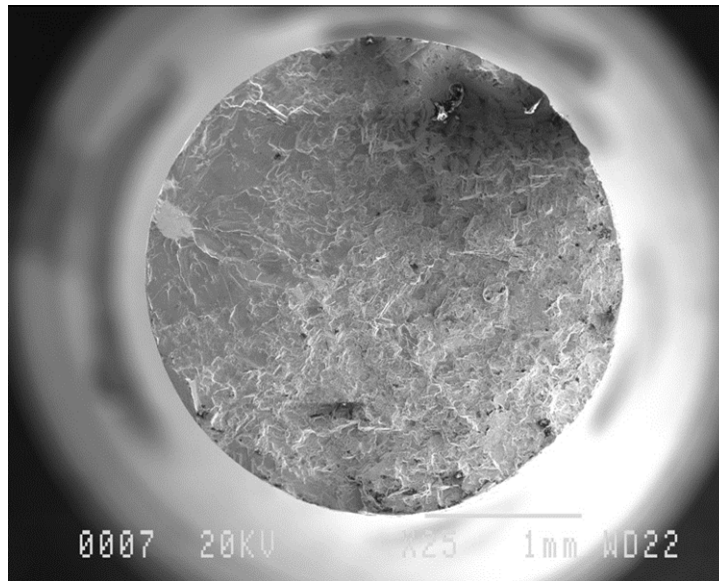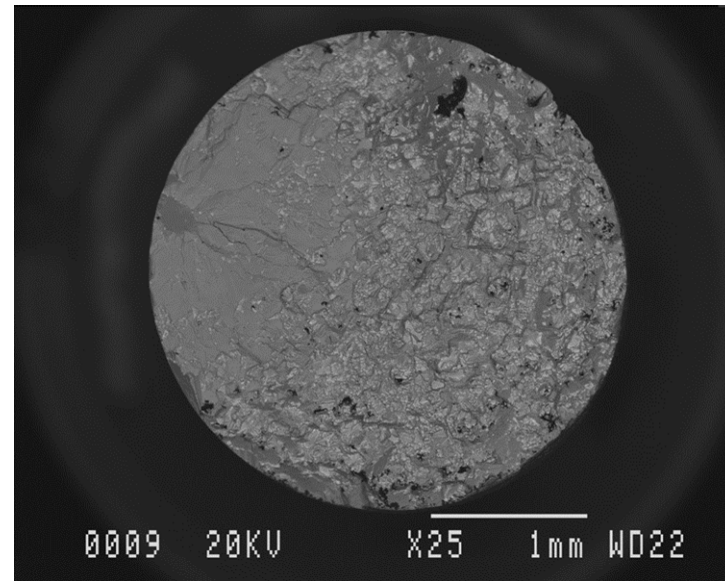
SE mode

BE mode
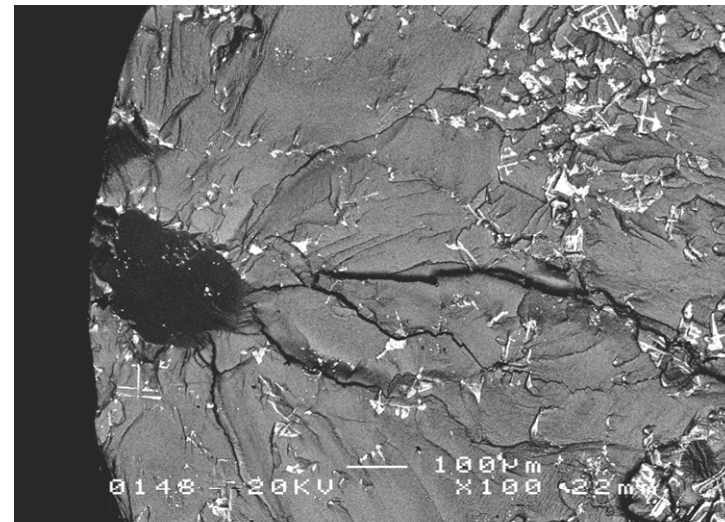
66L, R = -1, $\Delta\varepsilon$ = 0.50%, 500x

SE mode
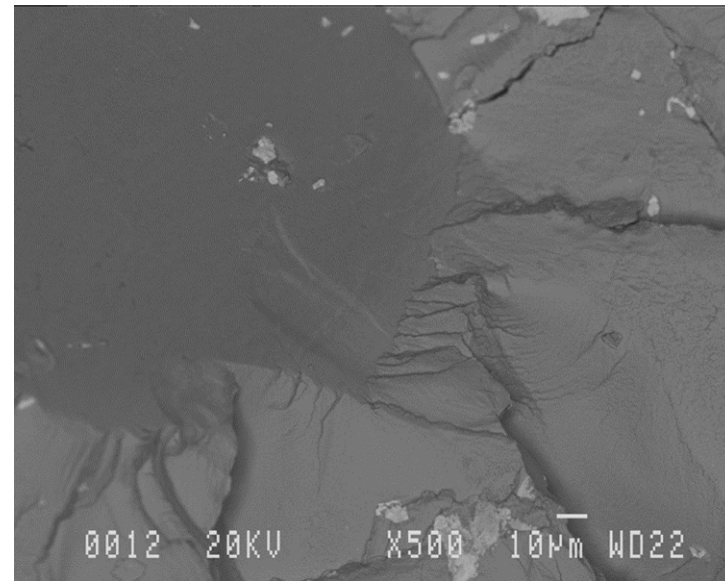
BE mode

67L, R = 0, Δε = 0.50%, 25x

SE mode

BE mode
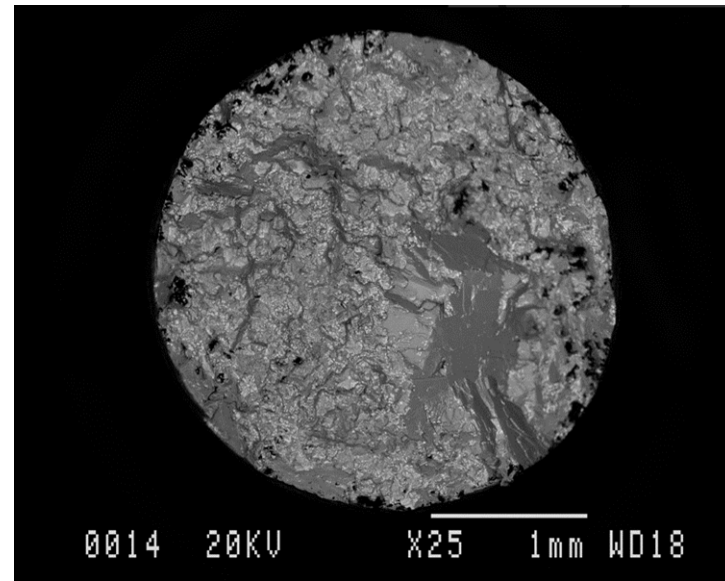
67L, R = 0, $\Delta\varepsilon$ = 0.50%, 100x

SE mode

BE mode

67L, R = 0, Δε = 0.50%, 500x
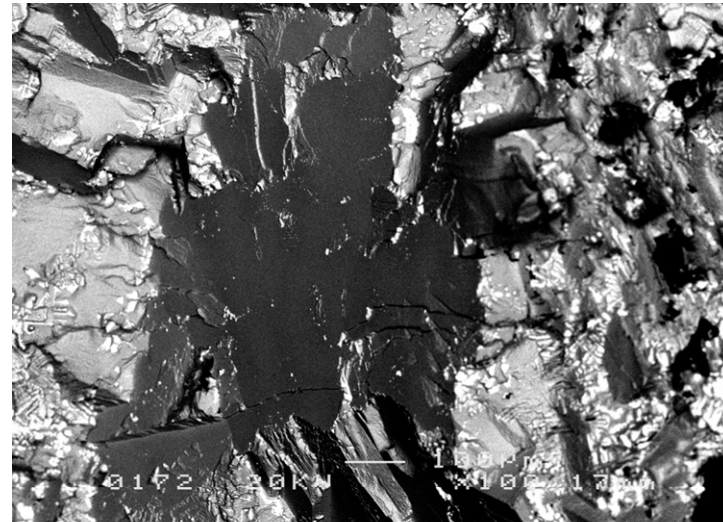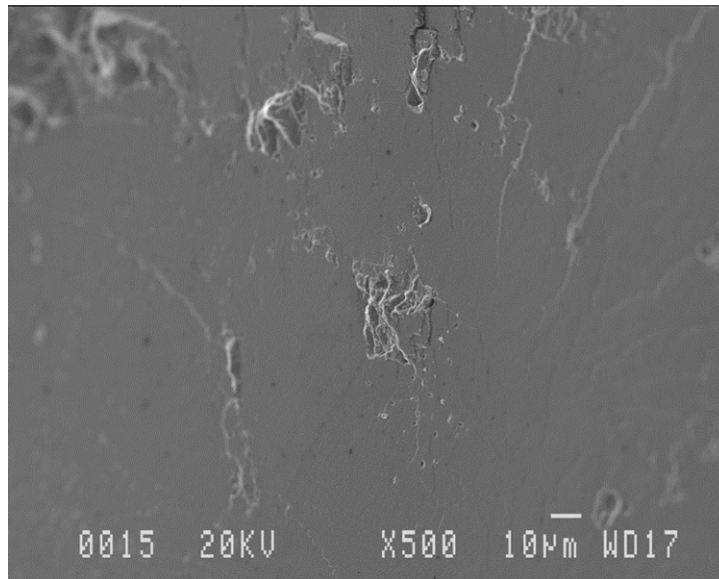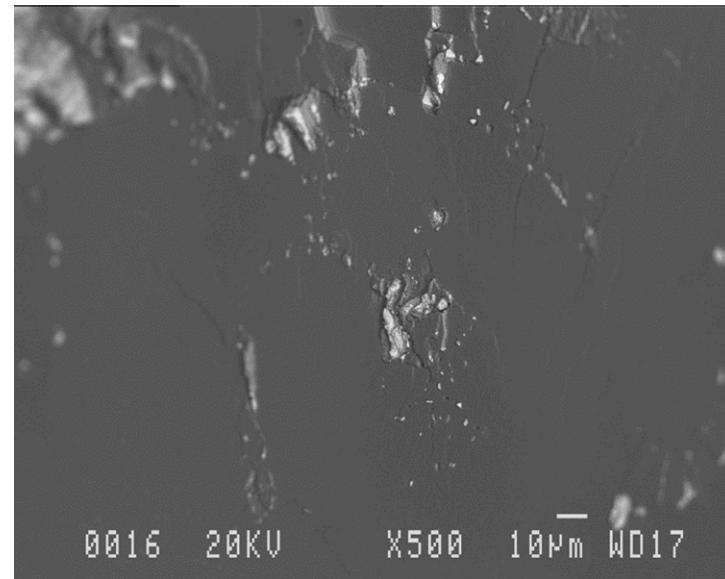
SE mode

BE mode

77L, R = 0, $\Delta\varepsilon$ = 0.50%, 25x
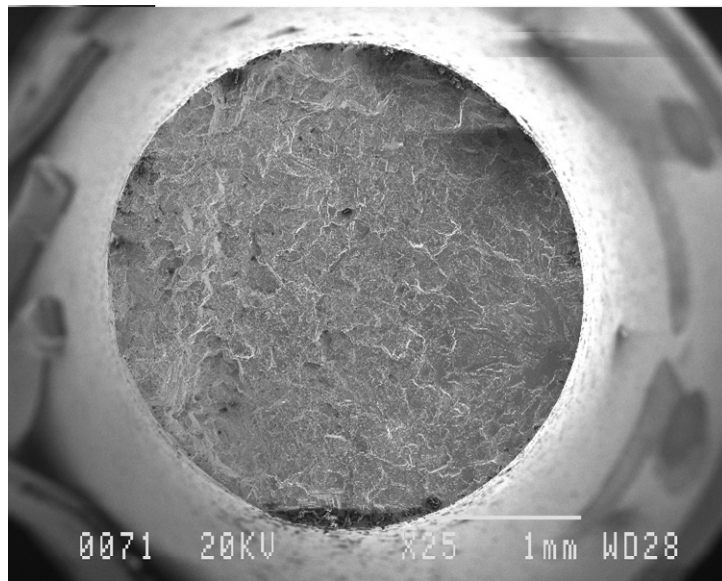
SE mode
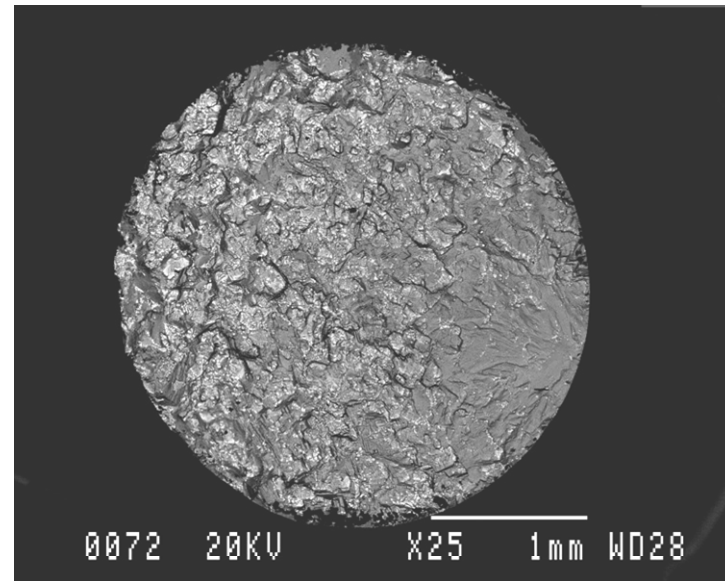
BE mode

77L, R = 0, $\Delta\varepsilon$ = 0.50%, 100x

SE mode


BE mode

77L, R = 0, Δε = 0.50%, 500x
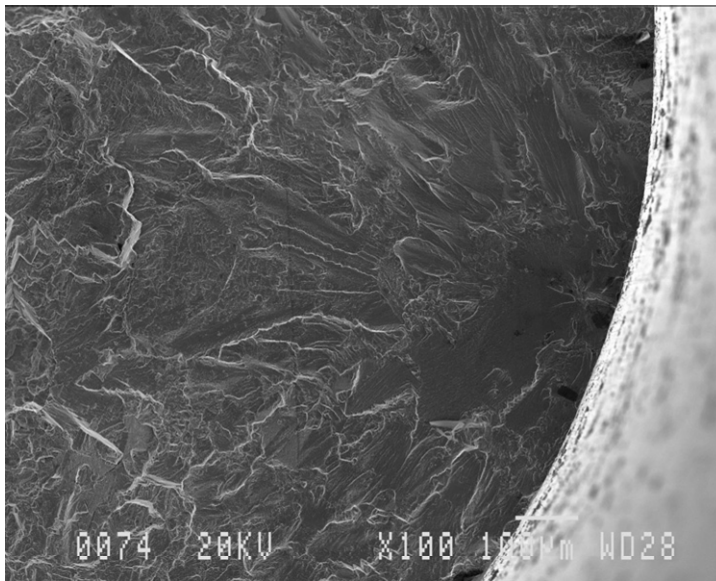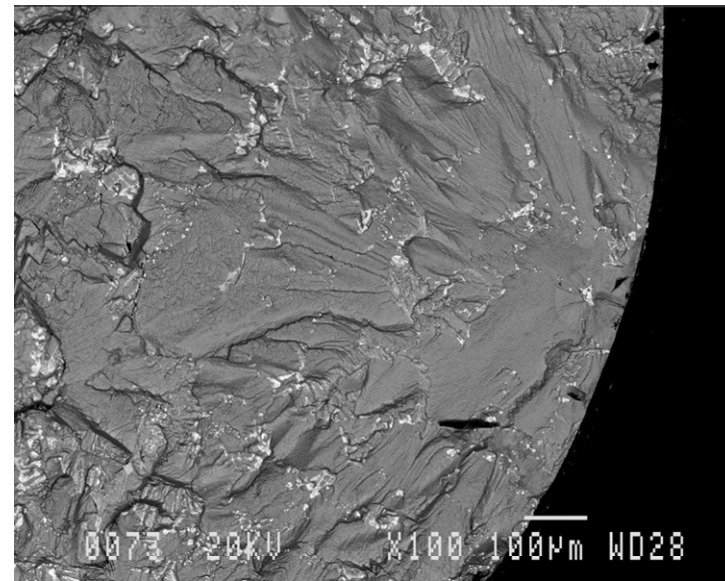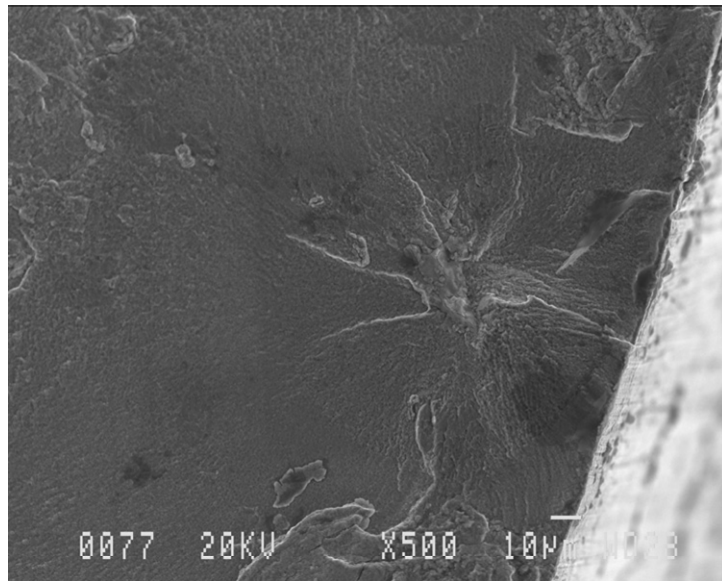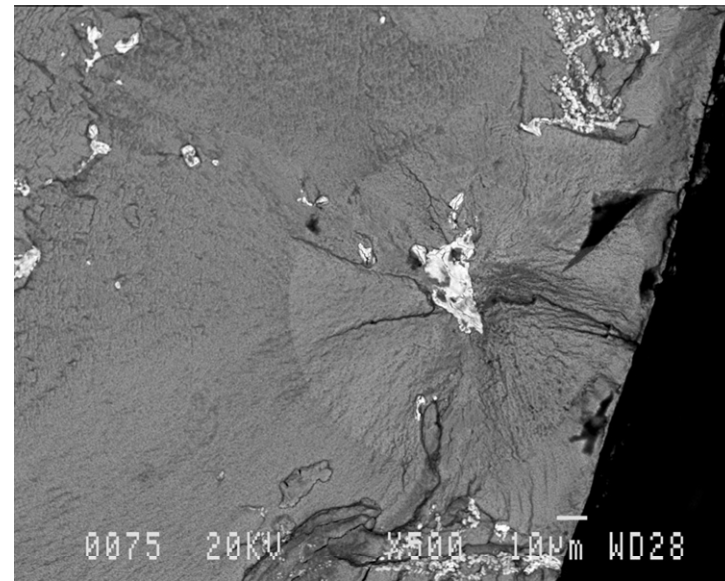
SE mode

BE mode

# 76L, R = -1, $\Delta\varepsilon$ = 0.58%, 25x
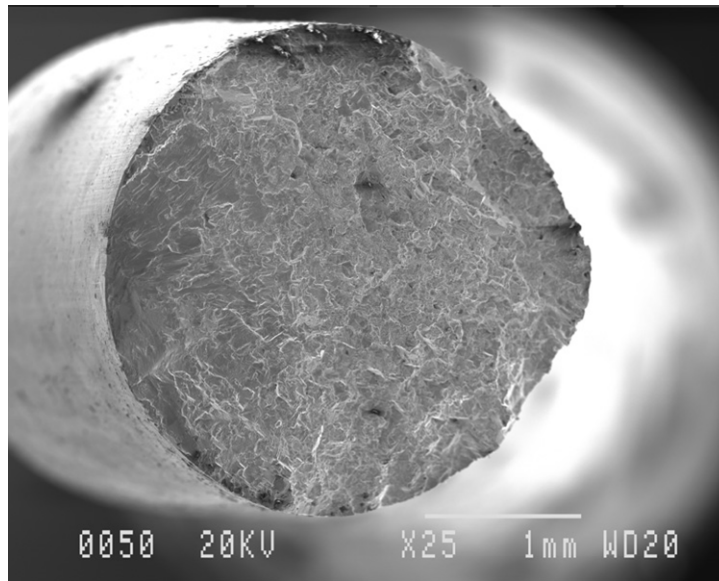
SE mode
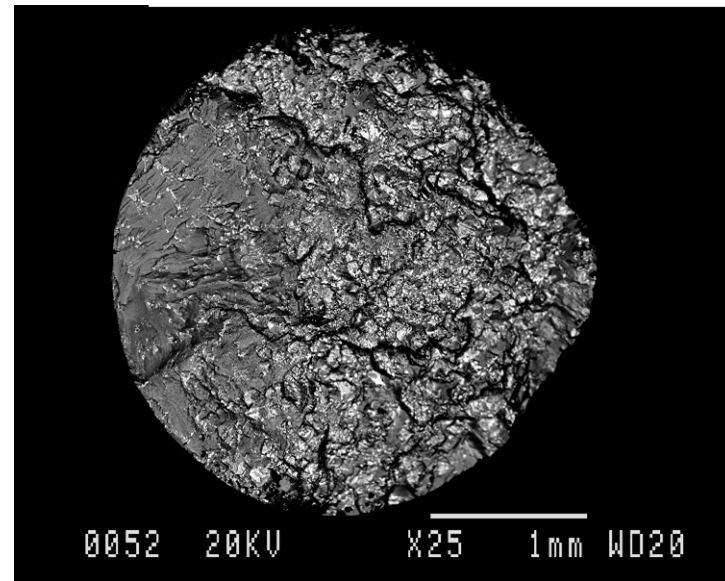
BE mode

# 76L, R = -1, $\Delta\varepsilon$ = 0.58%, 100x
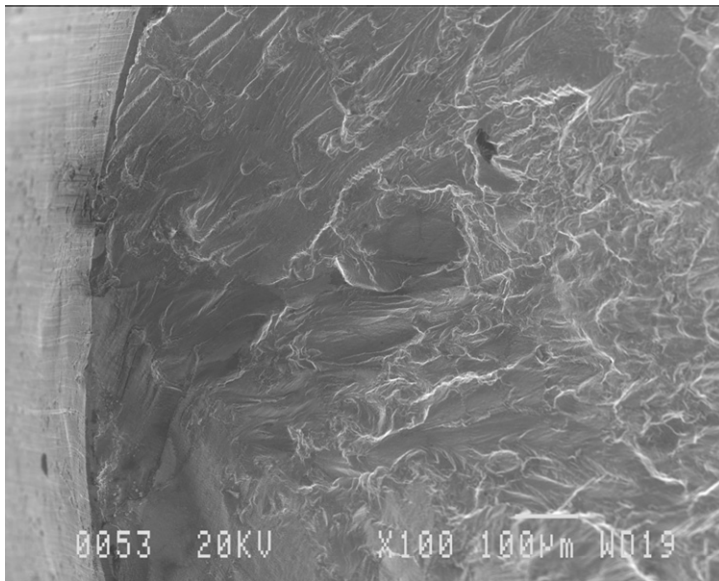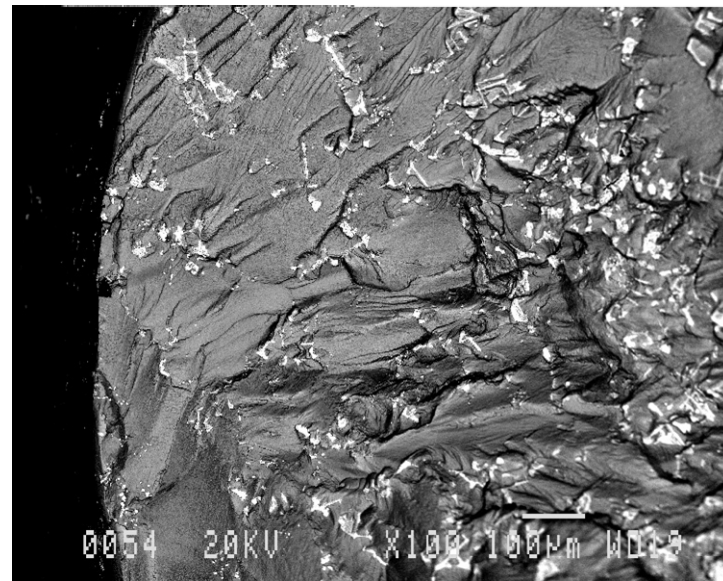
SE mode

BE mode
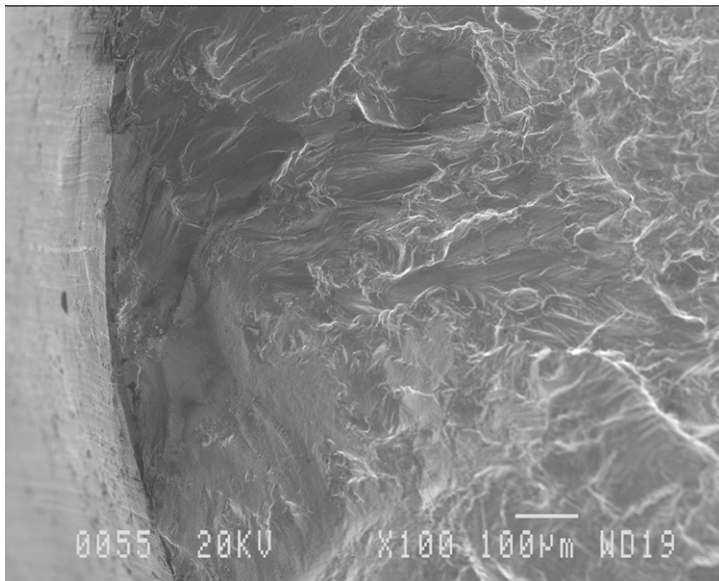
# 76L, R = -1, $\Delta\varepsilon$ = 0.58%, 100x
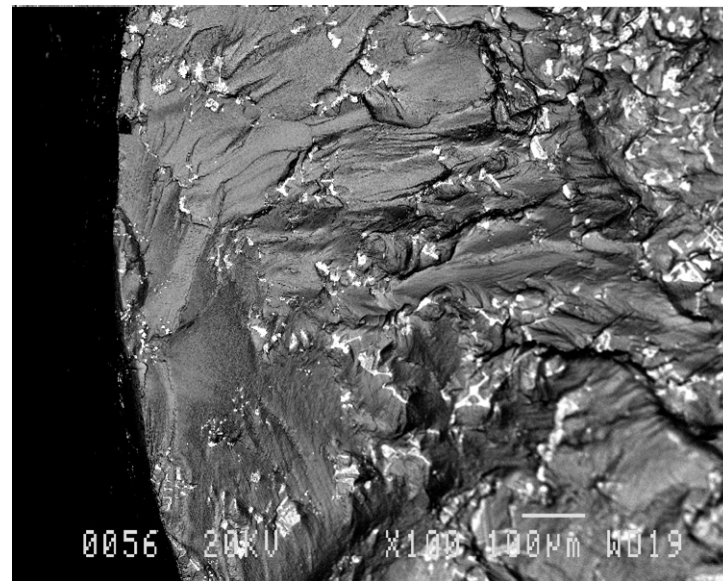
SE mode

BE mode

76L, R = -1, $\Delta\varepsilon$ = 0.58%, 500x

SE mode

BE mode

76L, R = -1, Δε = 0.58%, 500x
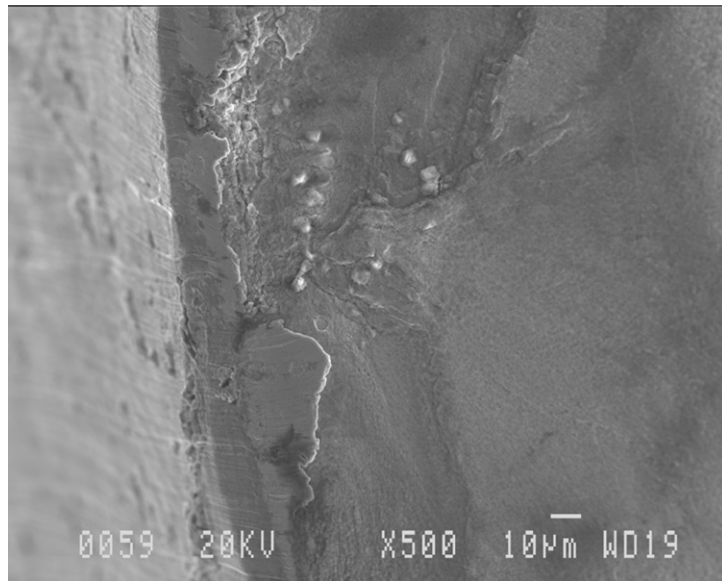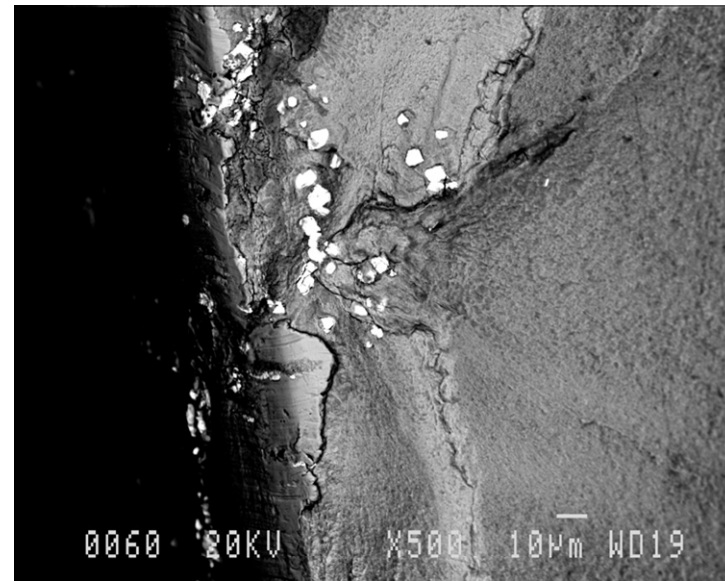
SE mode

BE mode

86L, R = -1, Δε = 0.50%, 25x
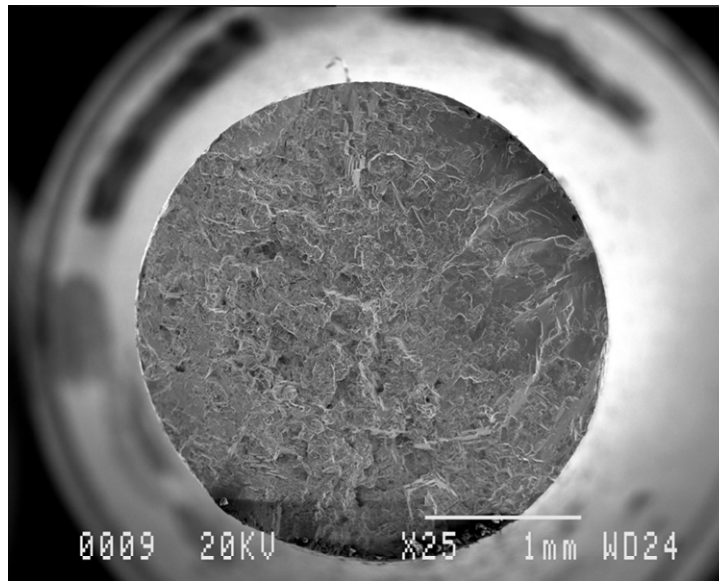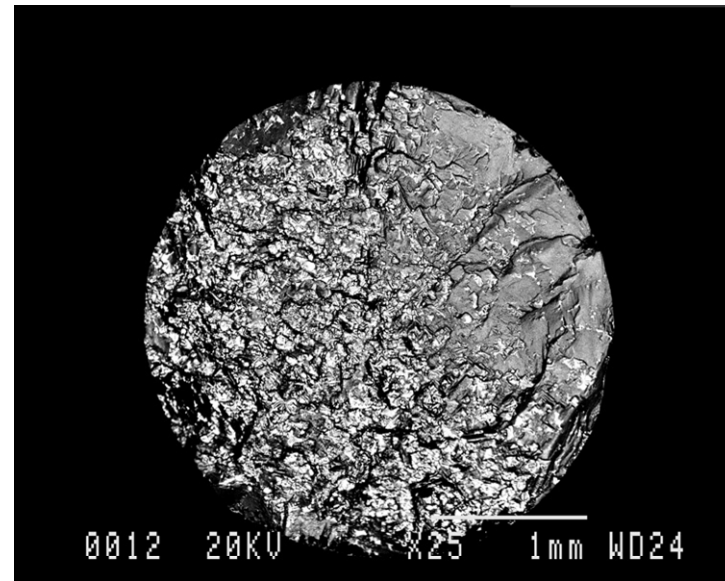
SE mode   BE mode

# 86L, R = -1, $\Delta\varepsilon$ = 0.50%, 100x
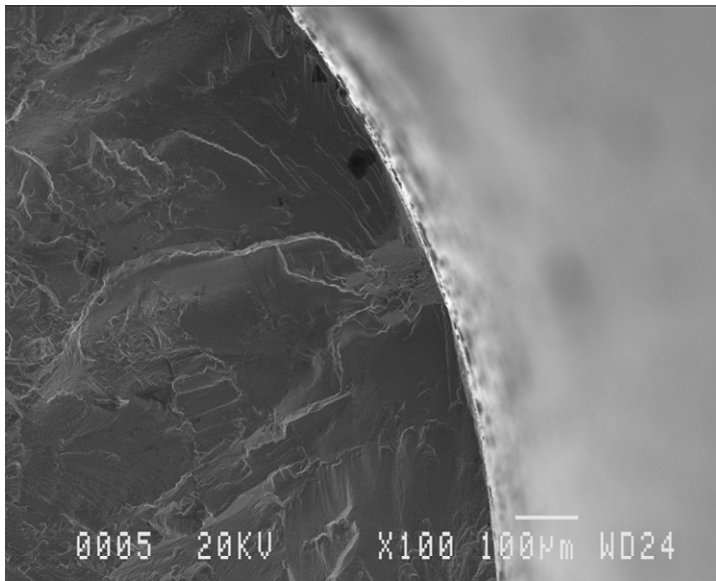
SE mode
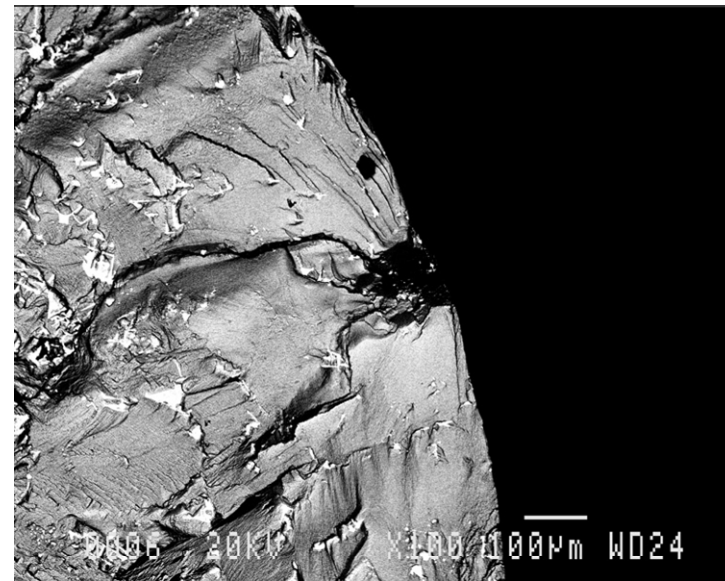
BE mode

# 86L, R = -1, $\Delta\varepsilon$ = 0.50%, 500x
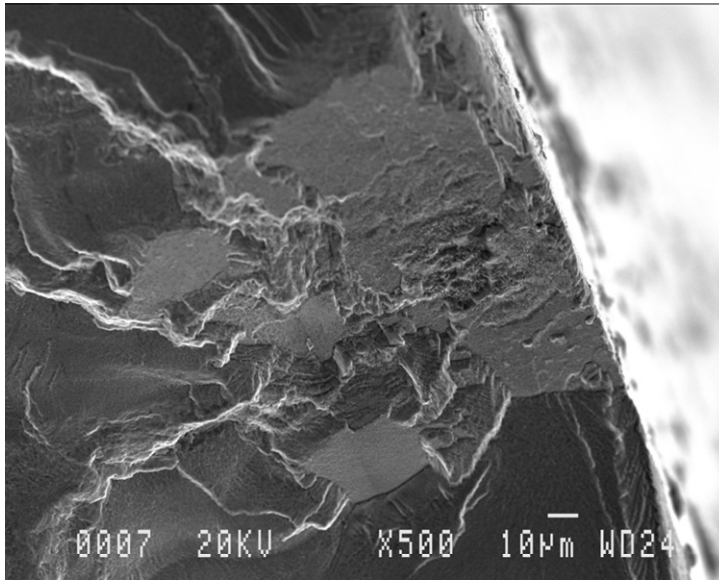
SE mode
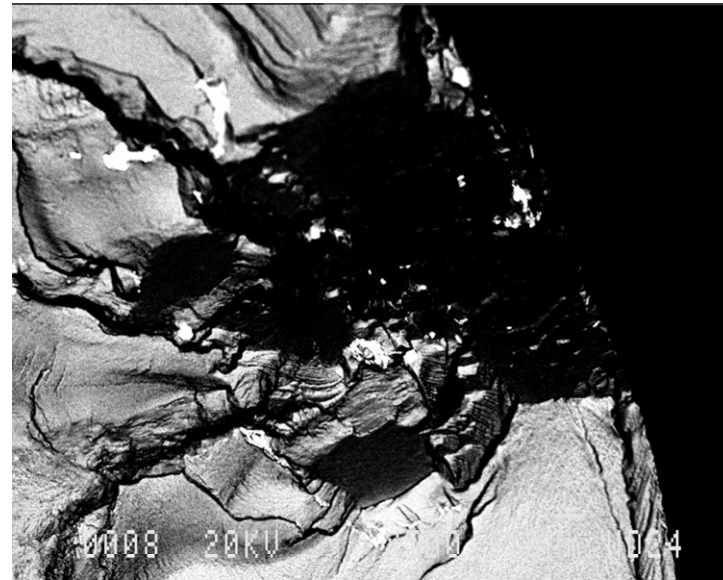
BE mode

86L, R = -1, $\Delta\varepsilon$ = 0.50%, 100x

Location: Overload Zone
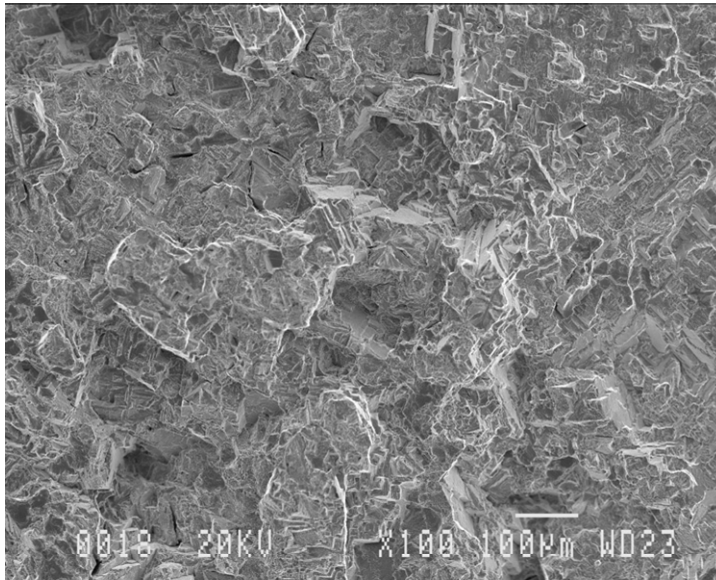
Typical Overload Morphology
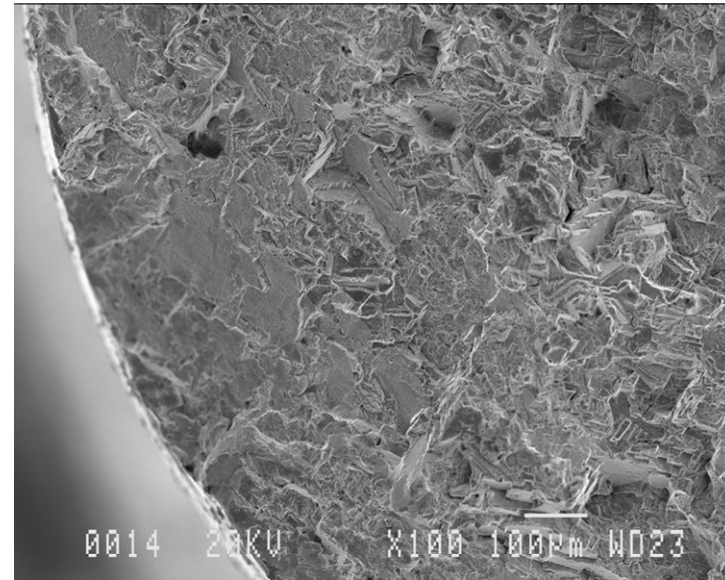
Failure Site

86L, R = -1, Δε = 0.50%

Location: Overload Zone
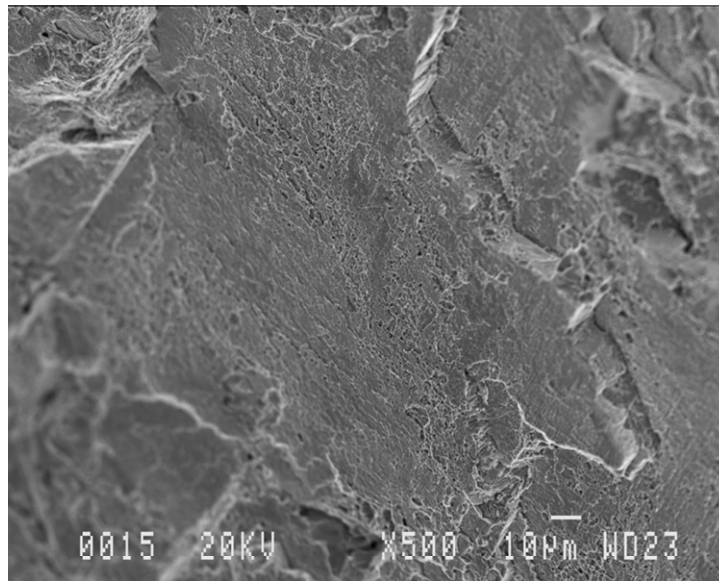
Localized ductile failure 500x   Localized ductile failure 1500x
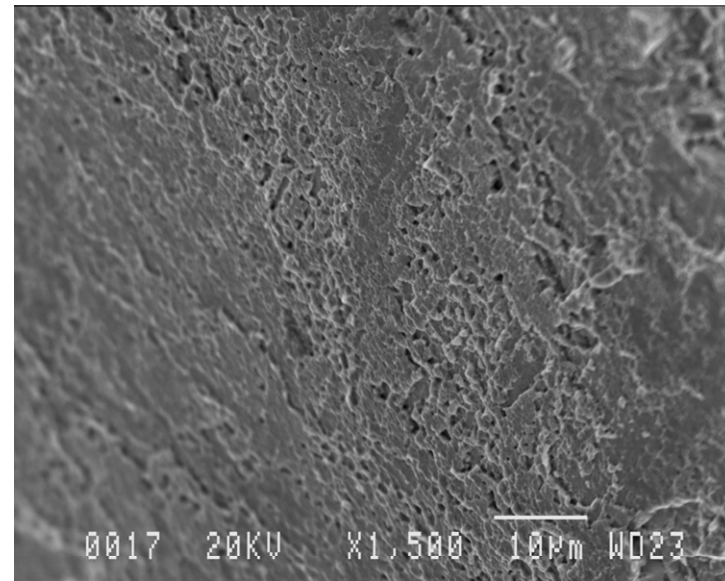
87L, R = 0, $\Delta\varepsilon$ = 0.58%, 25x

SE mode

BE mode

87L, R = 0, Δε = 0.58%, 100x

SE mode

BE mode

87L, R = 0, Δε = 0.58%, 500x
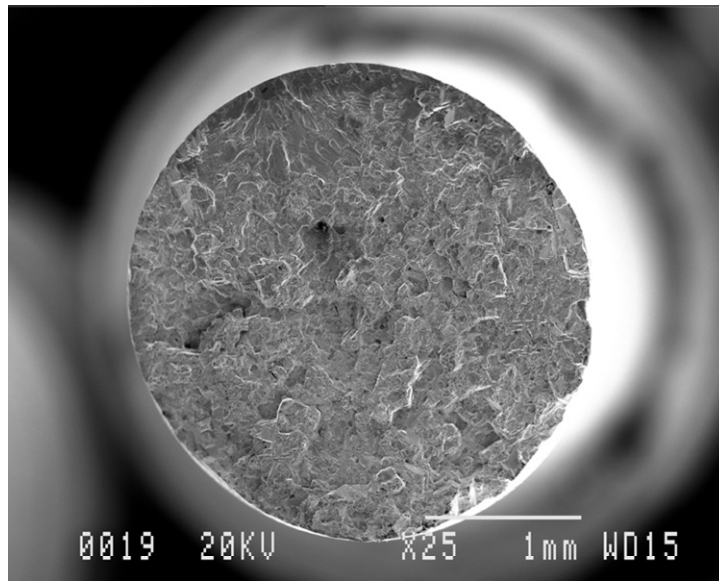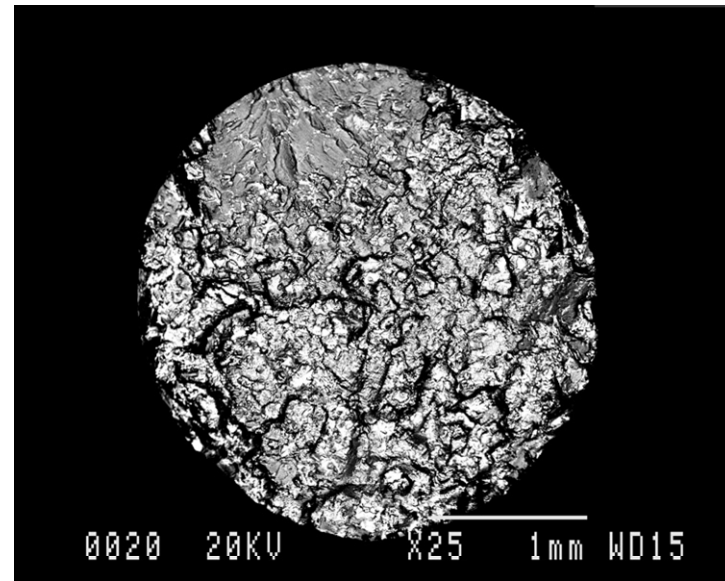
SE mode

BE mode

87L, R = 0, $\Delta\varepsilon$ = 0.58%, 100x

Stage II (Crack Propagation) to Stage III (Overload)
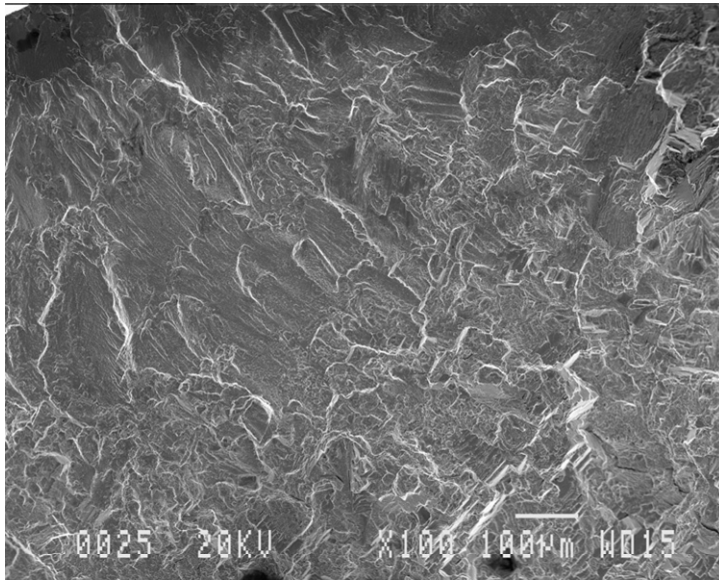
SE mode
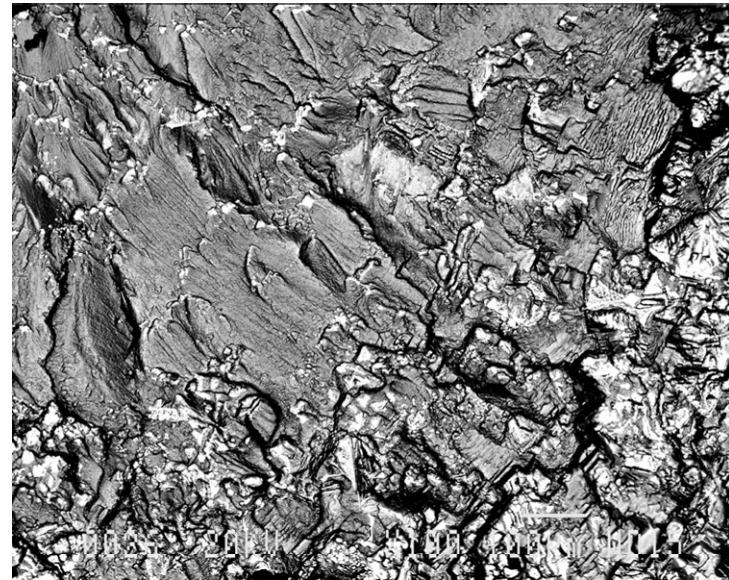
BE mode

# CA1L, R = 0, $\Delta\varepsilon$ = 0.67%, 25x
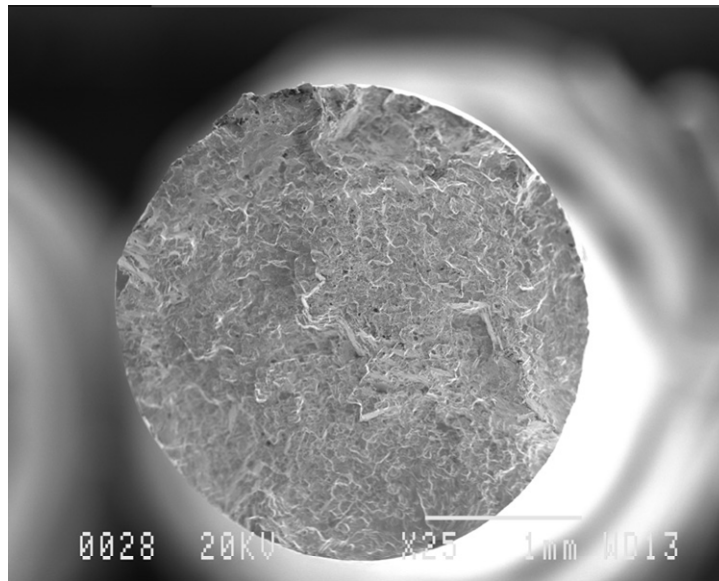
SE mode
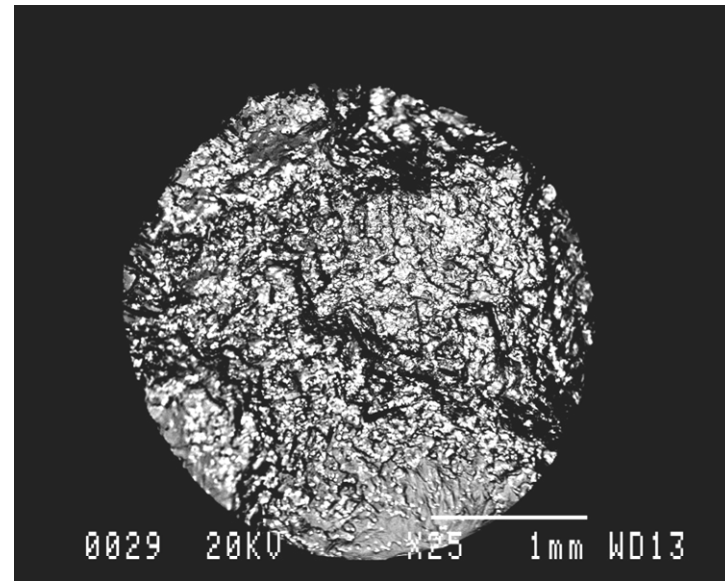
BE mode

CA1L, R = 0, $\Delta\varepsilon$ = 0.67%, 100x
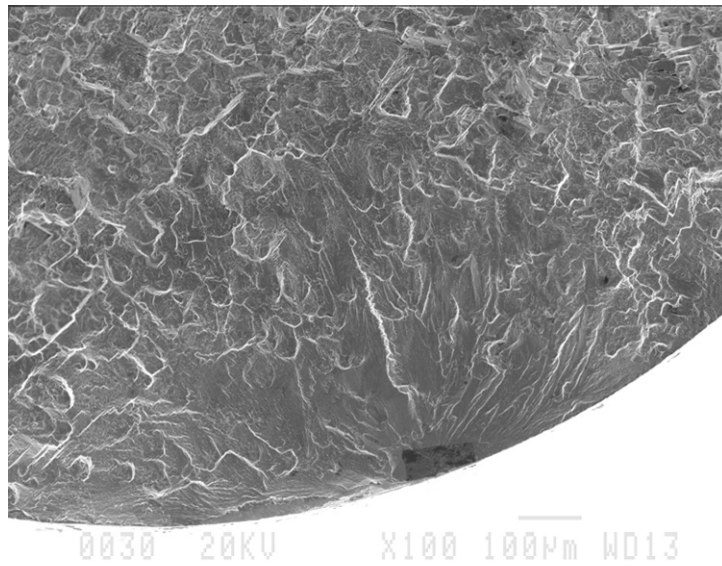
SE mode
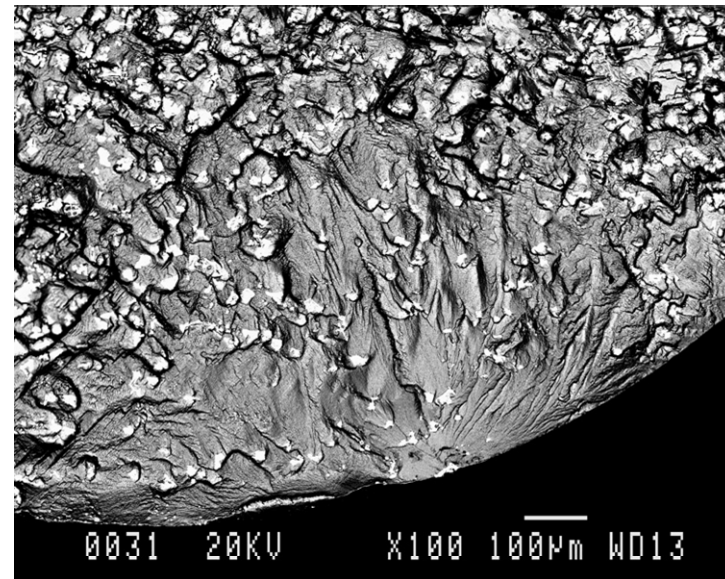
BE mode

# CA1L, R = 0, $\Delta\varepsilon$ = 0.67%, 500x
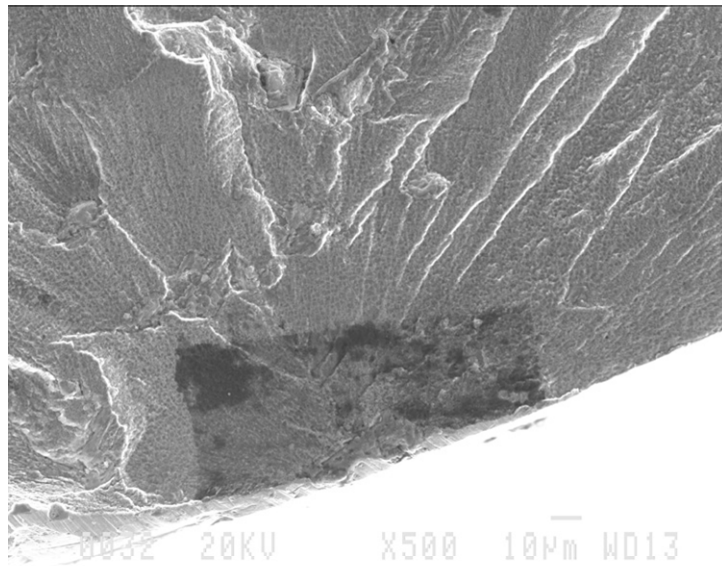
SE mode
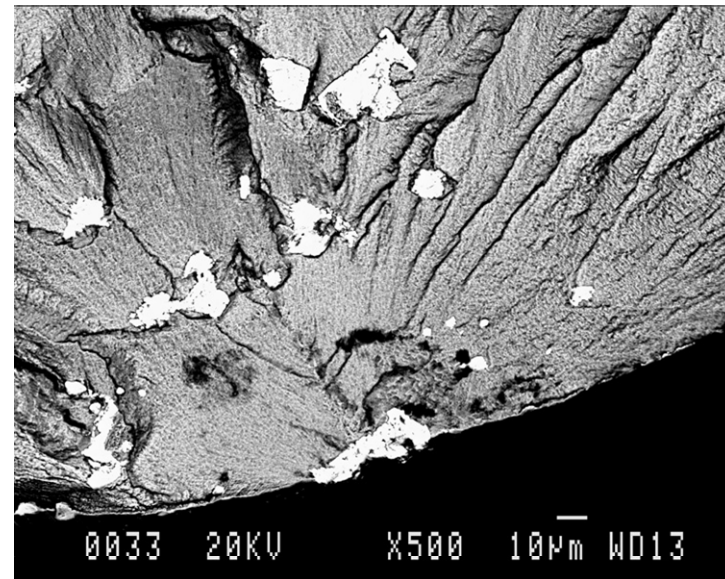
BE mode

CA2L, R = -1, $\Delta\varepsilon$ = 0.90%, 25x

SE mode

BE mode

CA2L, R = -1, Δε = 0.90%, 100x
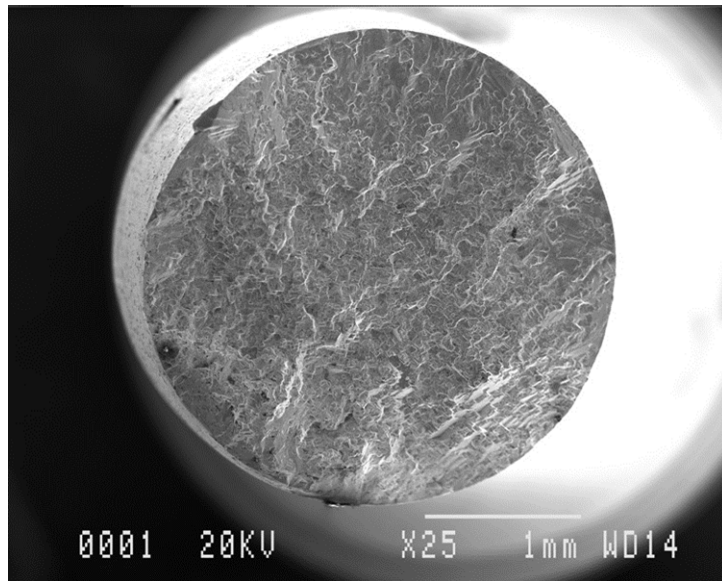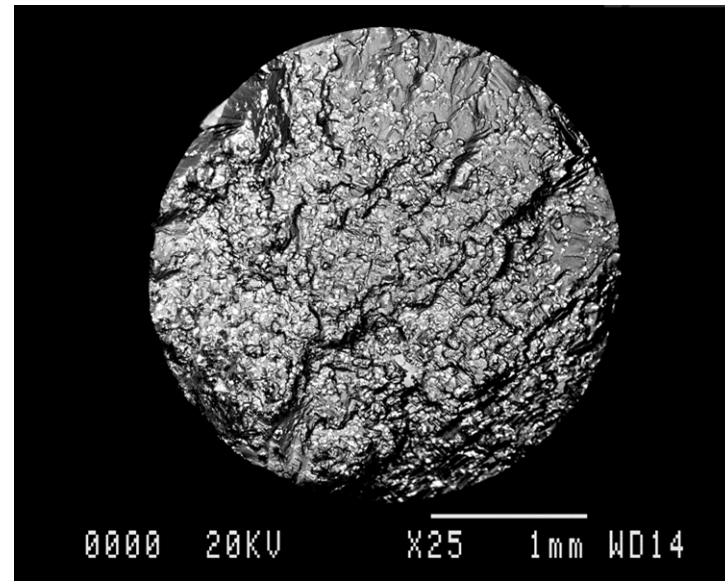
Crack 1

SE mode

BE mode

CA2L, R = -1, Δε = 0.90%, 100x
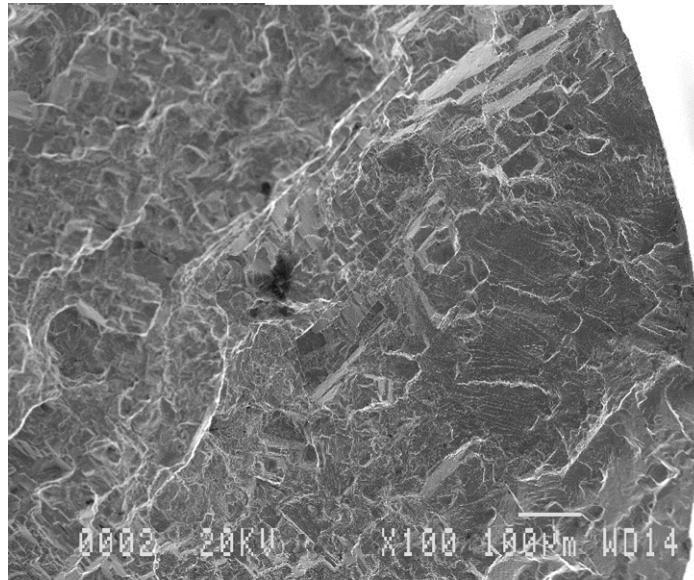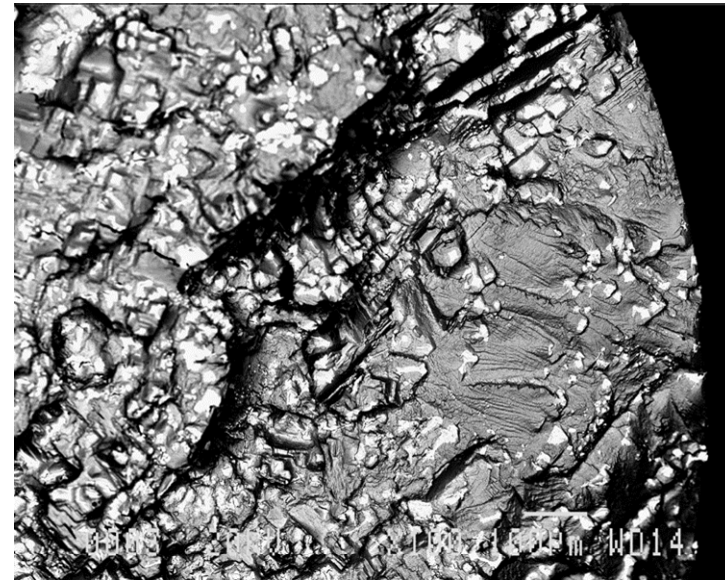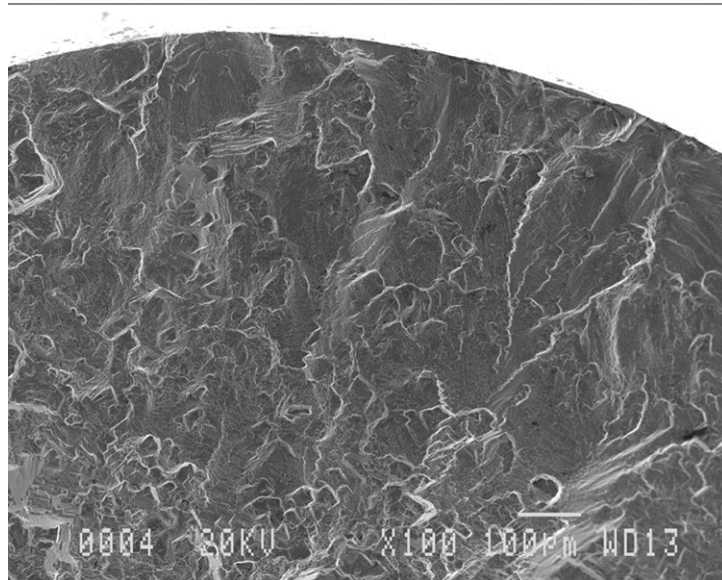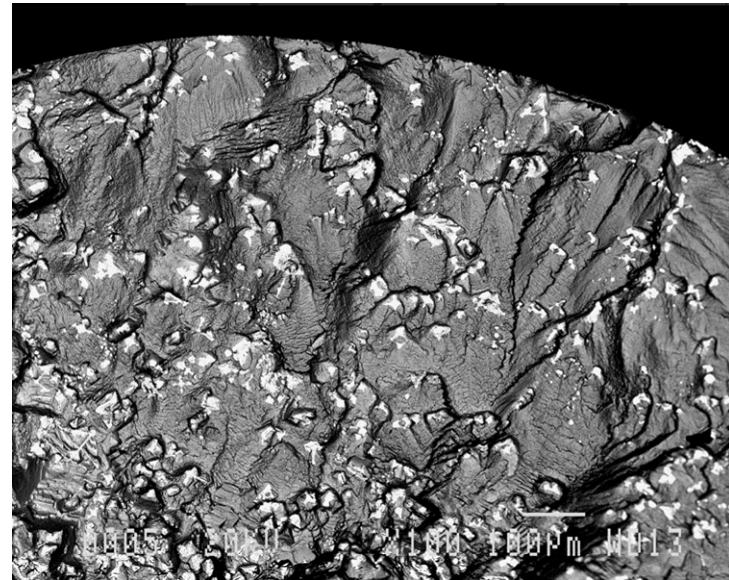
Crack 2

SE mode

BE mode

CA3L, R = 0, $\Delta\varepsilon$ = 0.78%, 25x
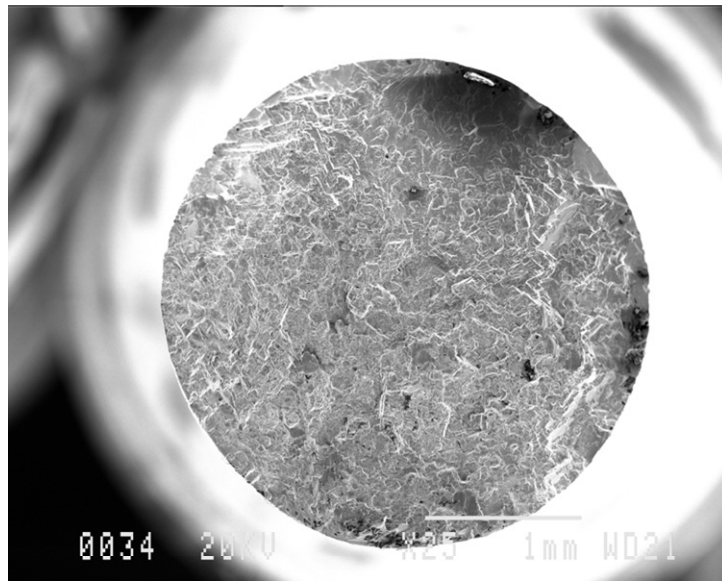
SE mode
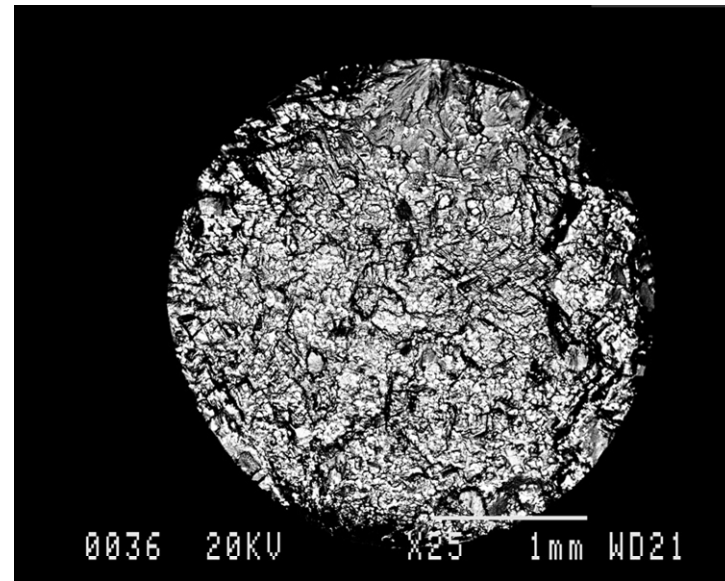
BE mode

CA3L, R = 0, $\Delta\varepsilon$ = 0.78%, 100x
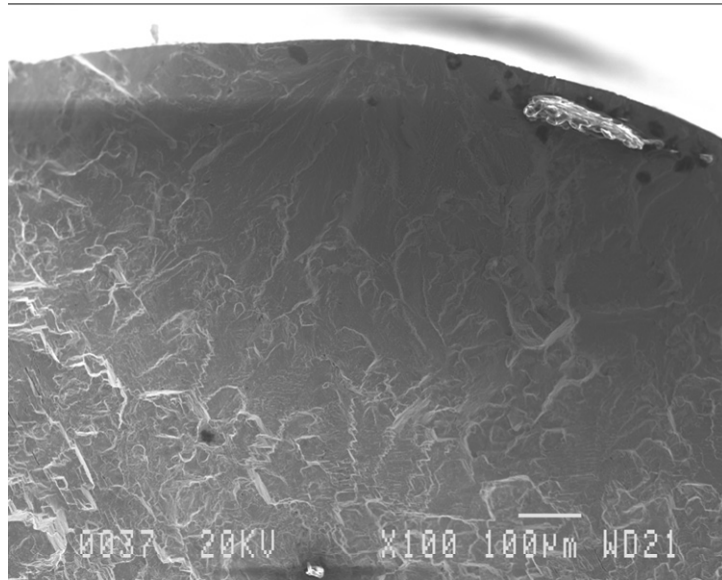
SE mode
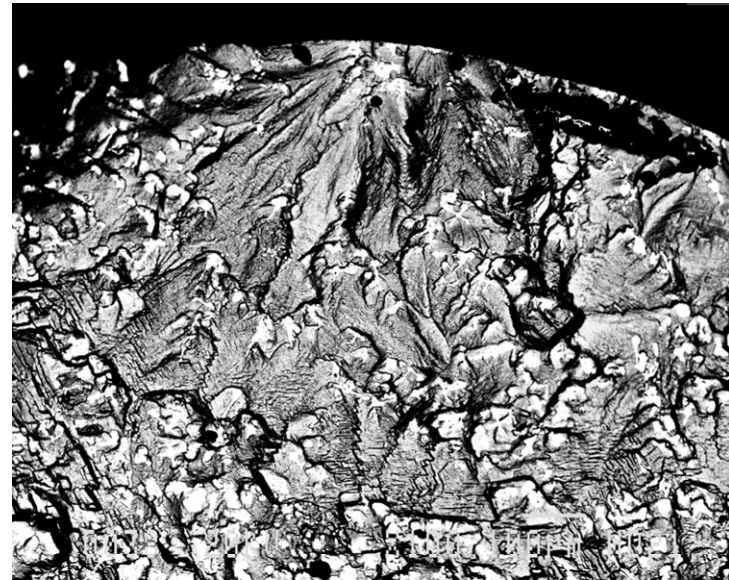
BE mode

# CA3L, R = 0, $\Delta\varepsilon$ = 0.78%, 500x
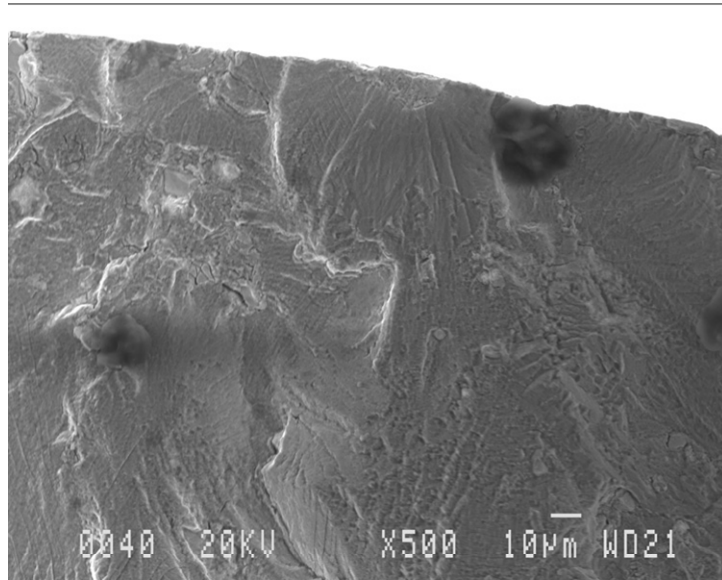
SE mode
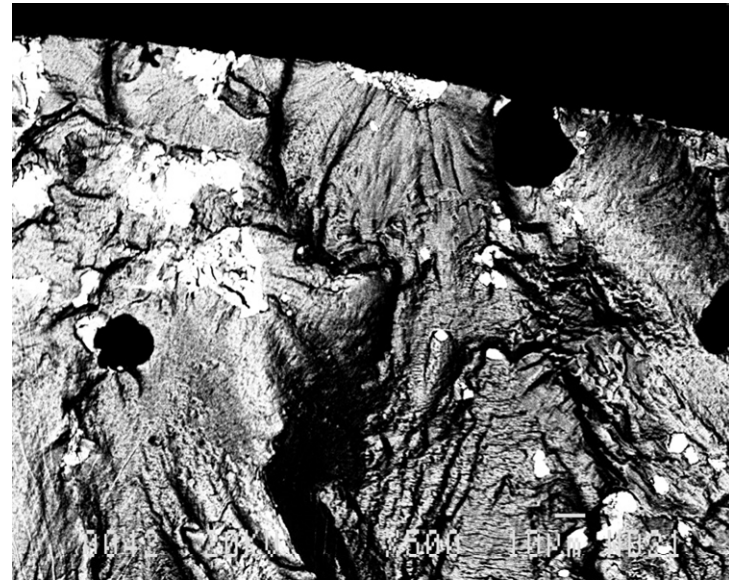
BE mode

CA4L, R = -1, $\Delta\varepsilon$ = 0.78%, 25x
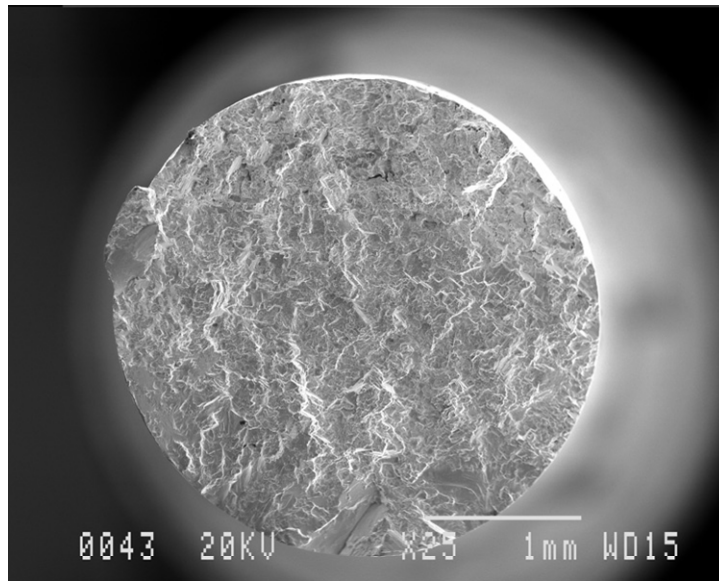
SE mode
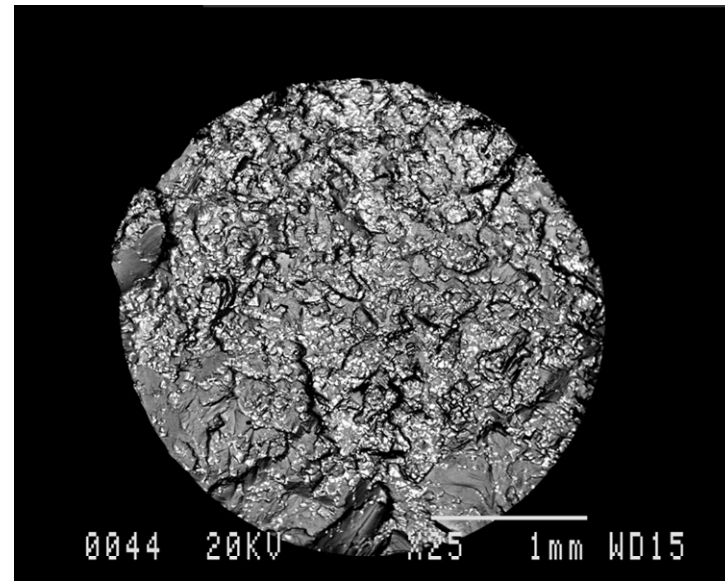
BE mode

CA4L, R = -1, $\Delta\varepsilon$ = 0.78%, 100x
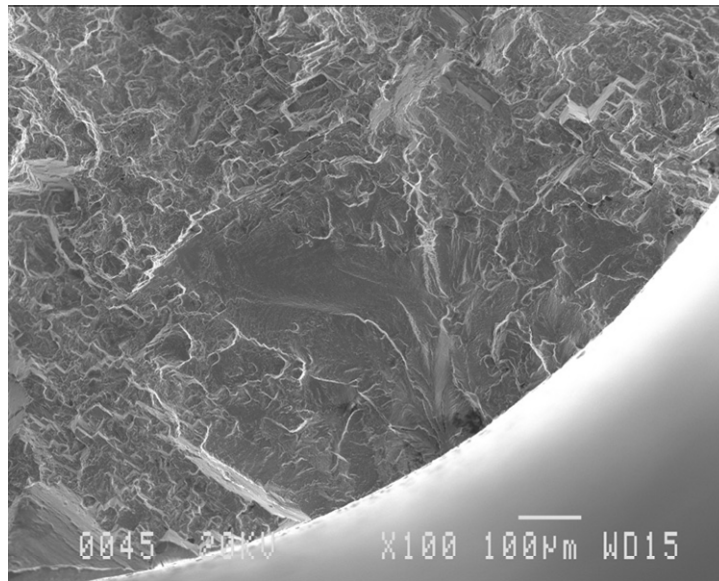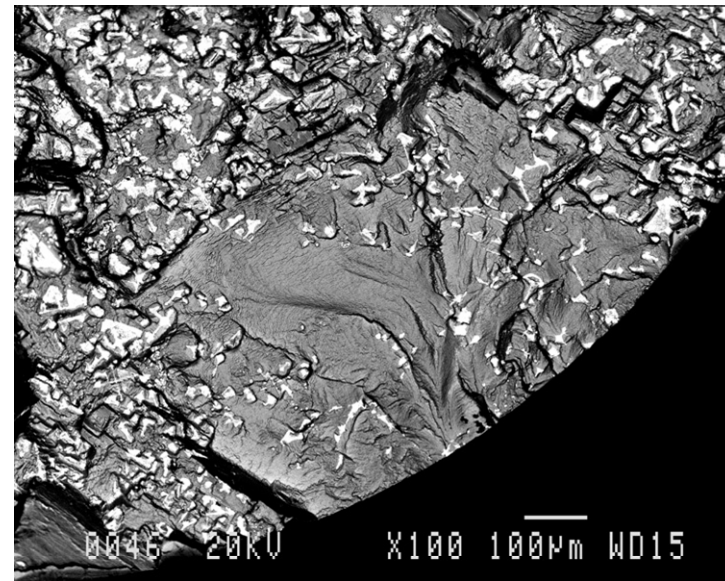
Crack 1

SE mode

BE mode

CA4L, R = -1, $\Delta\varepsilon$ = 0.78%, 100x

Crack 2
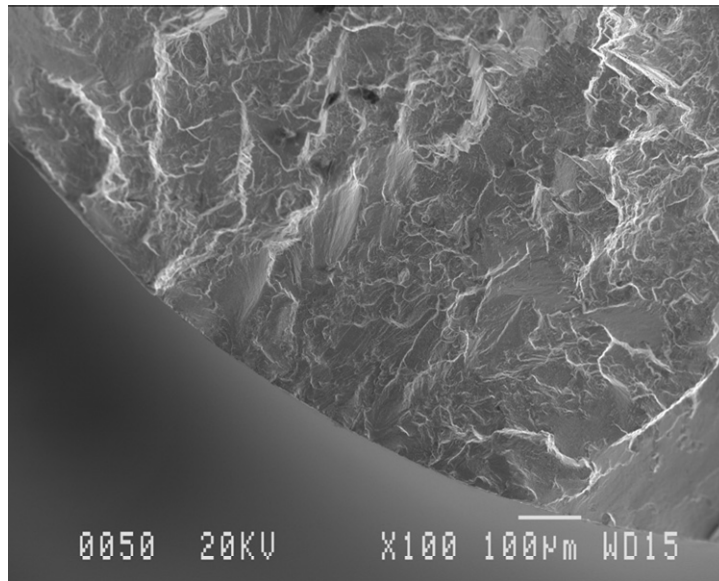
SE mode
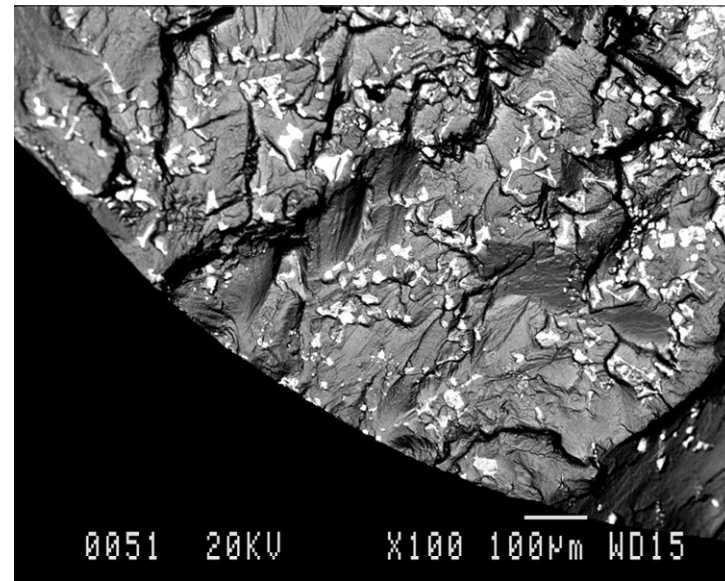
BE mode

CA4L, R = -1, $\Delta\varepsilon$ = 0.78%, 500x

Crack 1
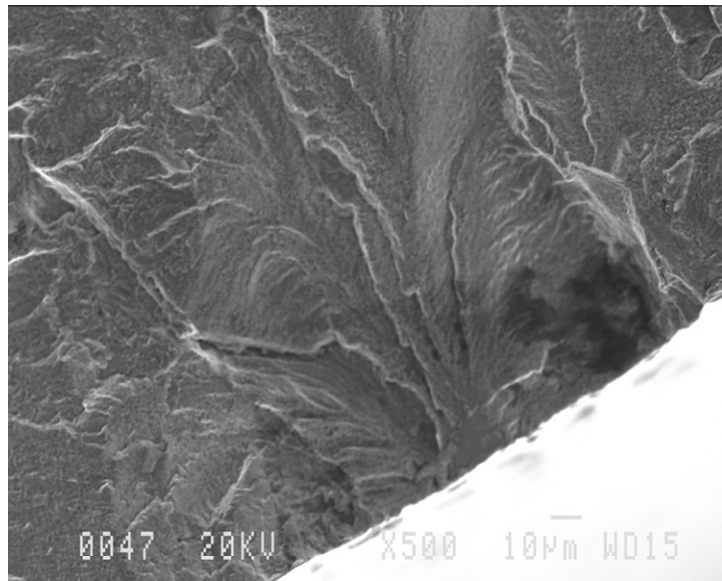
SE mode
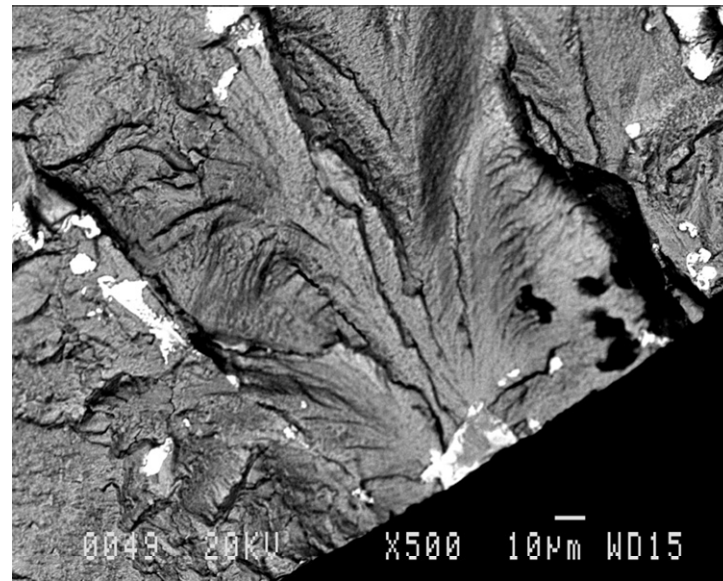
BE mode

CA6L, R = 0, $\Delta\varepsilon$ = 0.90%, 25x
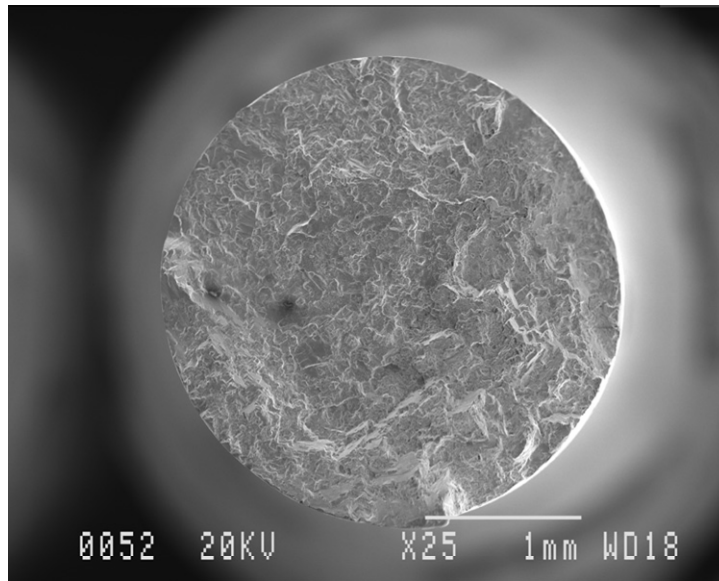
SE mode
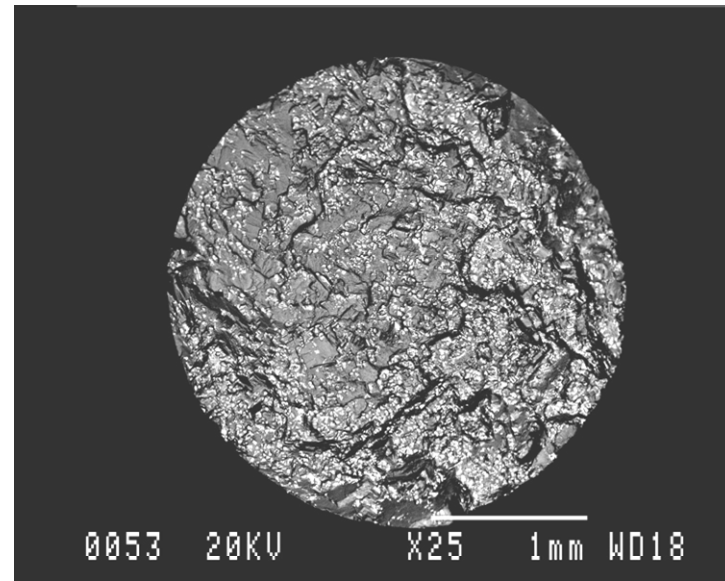
BE mode

CA6L, R = 0, $\Delta\varepsilon$ = 0.90%, 100x
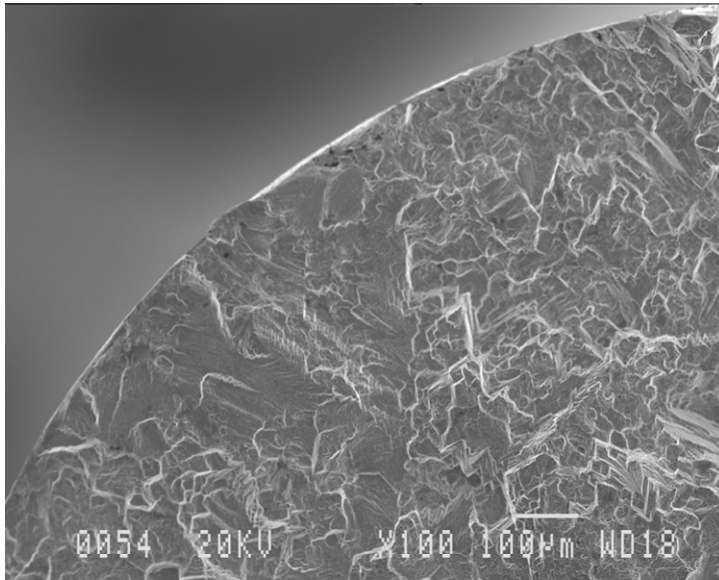
SE mode
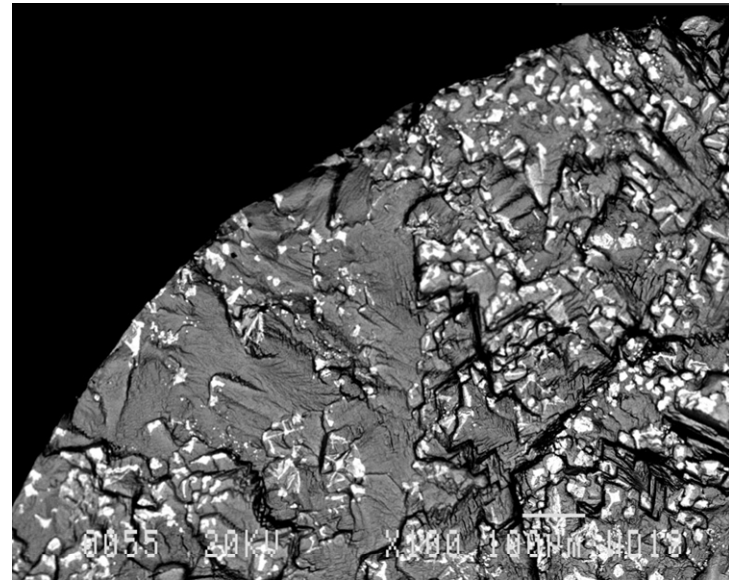
BE mode

CA6L, R = 0, $\Delta\varepsilon = 0.90\%$, 500x
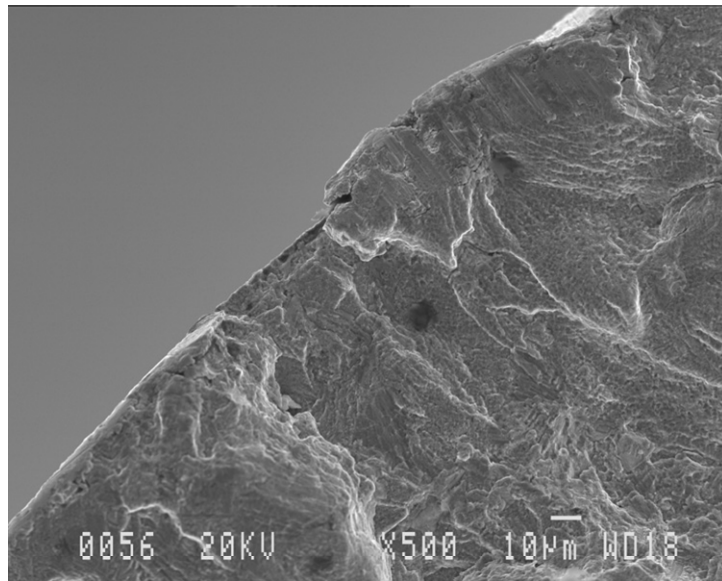
SE mode
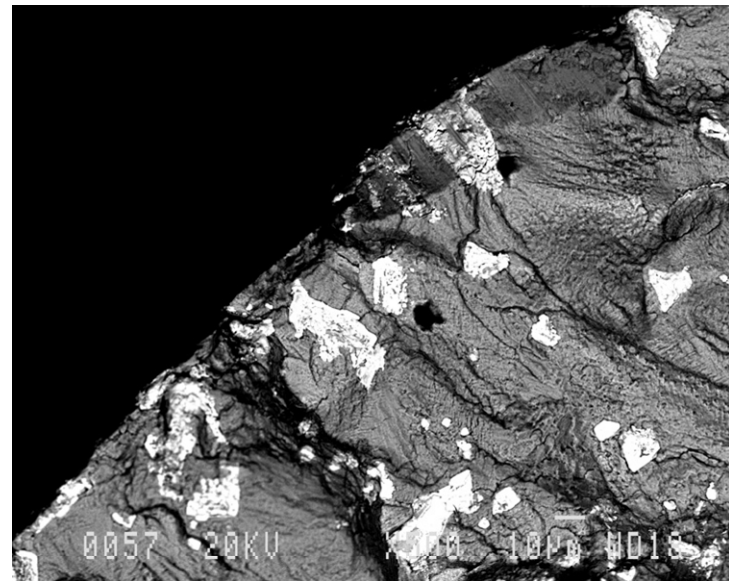
BE mode

CA7L, R = -1, $\Delta\varepsilon$ = 0.67%, 25x
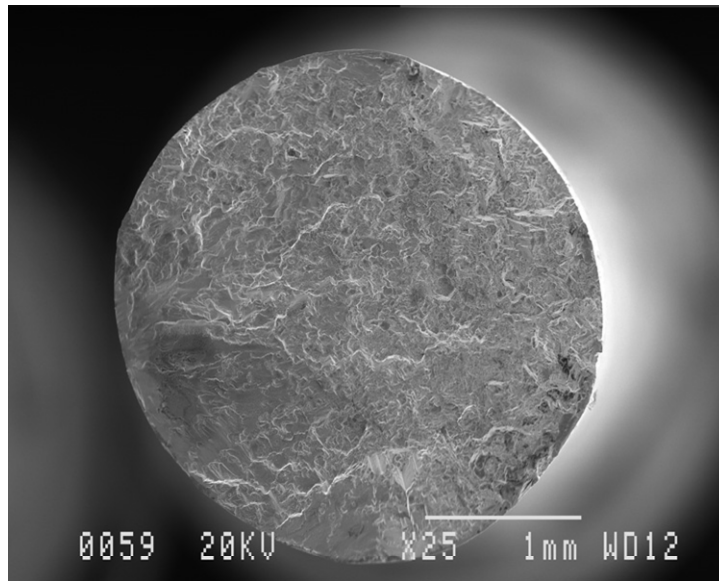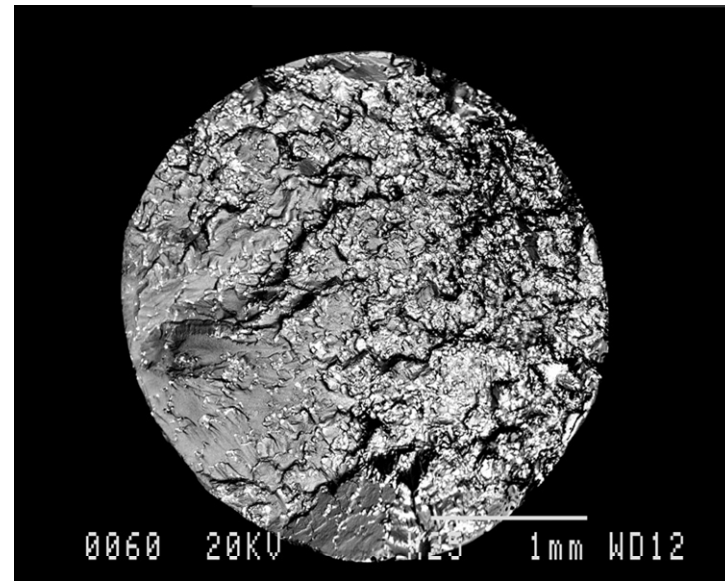
SE mode   BE mode

# CA7L, R = -1, $\Delta\varepsilon$ = 0.67%, 100x
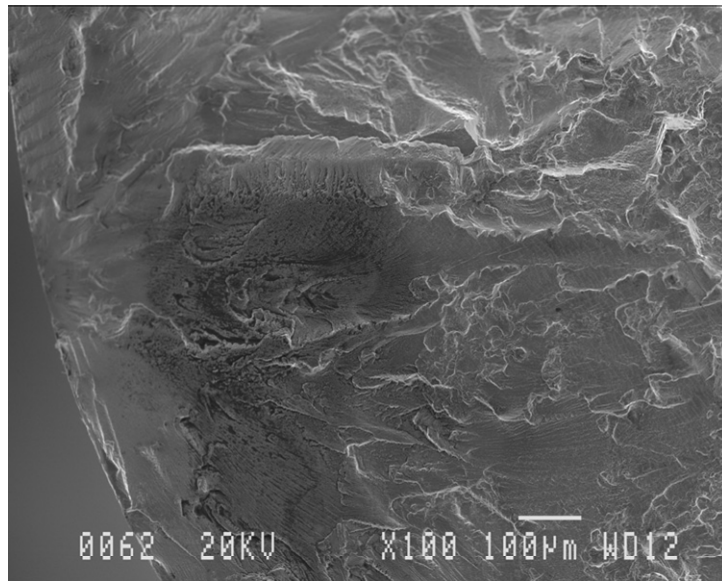
SE mode
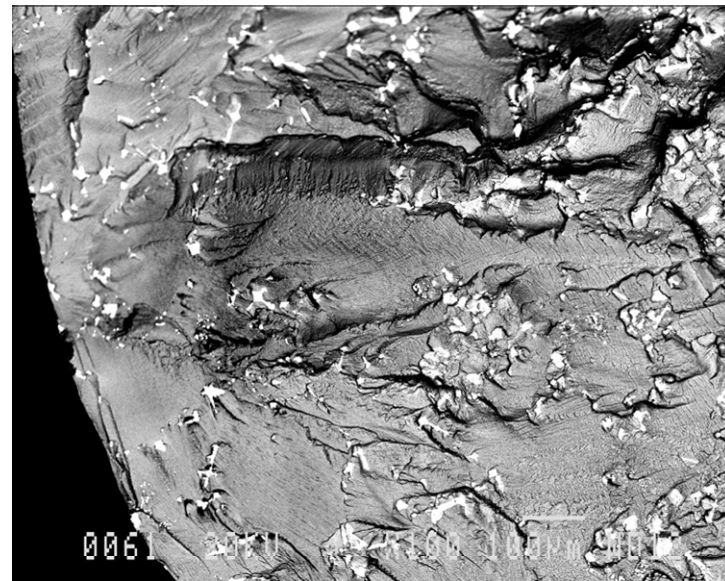
BE mode

CA7L, R = -1, $\Delta\varepsilon$ = 0.67%, 500x
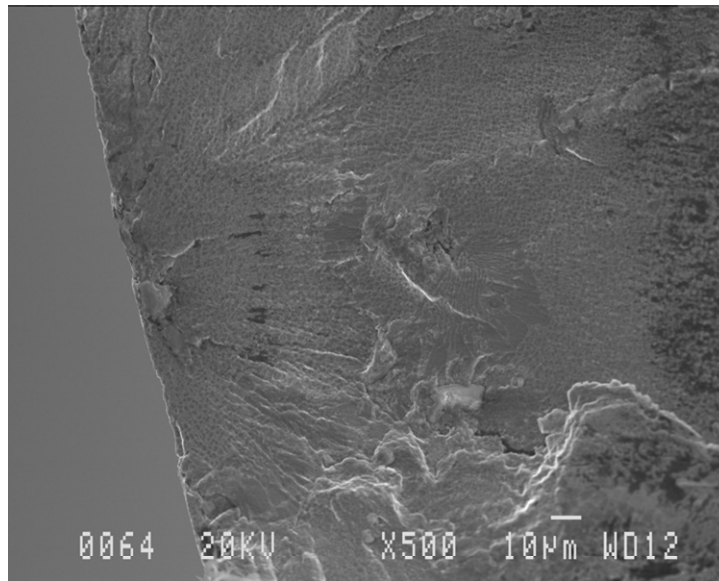
SE mode
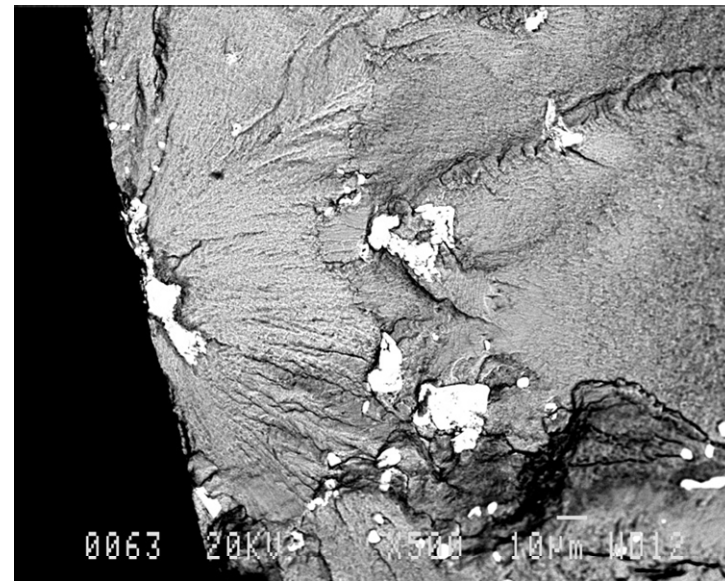
BE mode

CA8L, R = 0, $\Delta\varepsilon$ = 0.50%, 25x
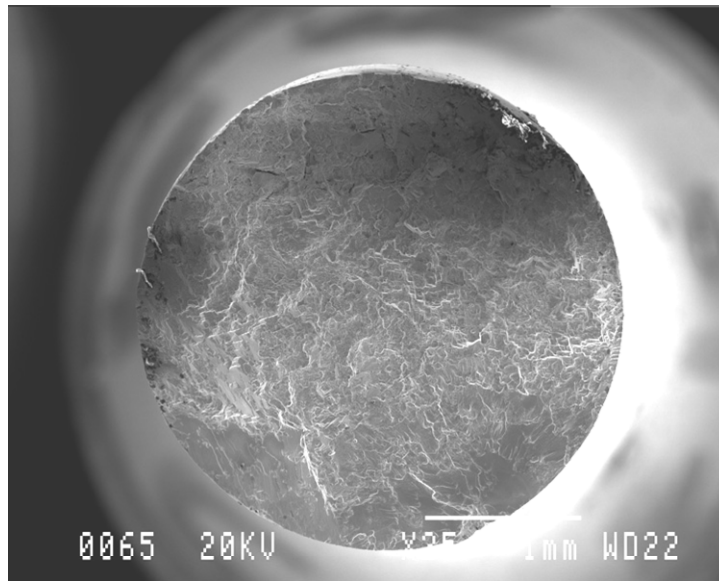
SE mode
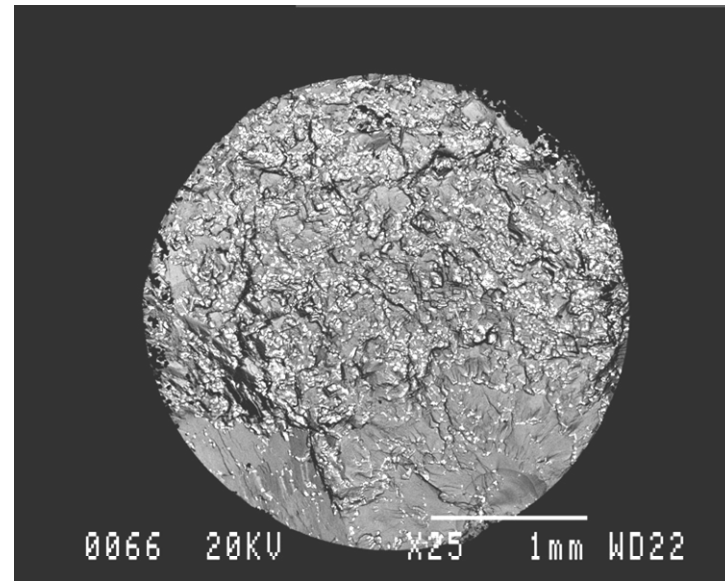
BE mode

CA8L, R = 0, $\Delta\varepsilon$ = 0.50%, 100x
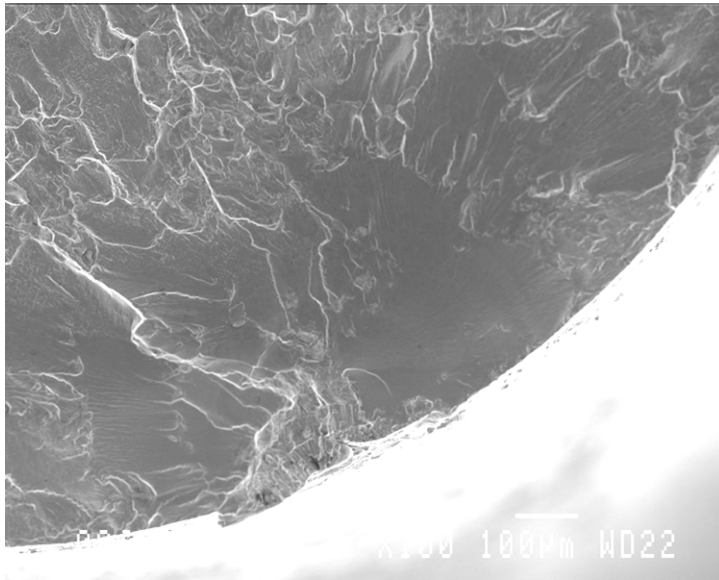
SE mode
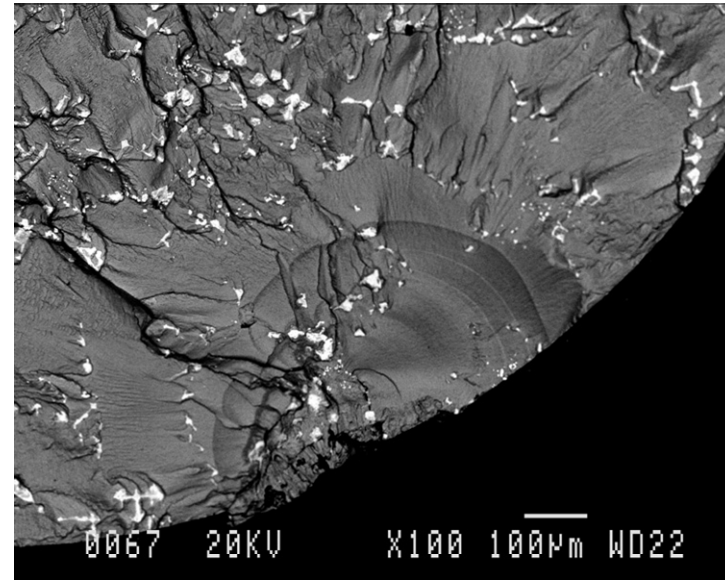
BE mode

CA8L, R = 0, $\Delta\varepsilon$ = 0.50%, 500x

SE mode

BE mode

CA9L, R = -1, Δε = 0.58%, 25x
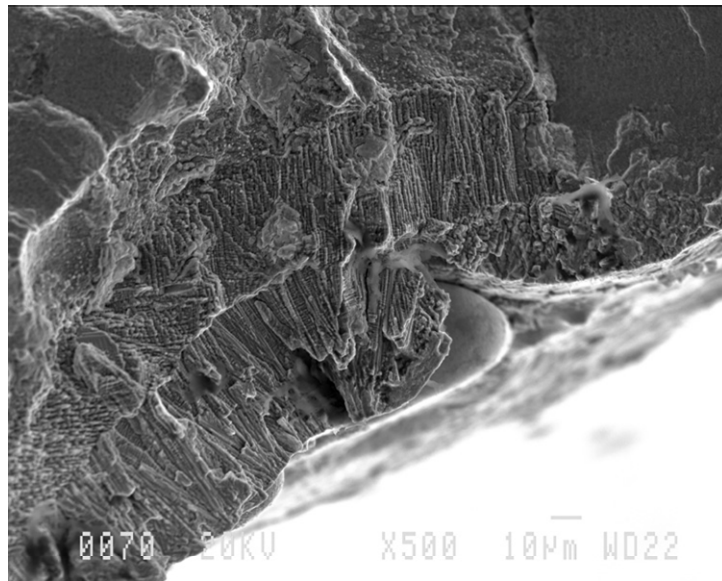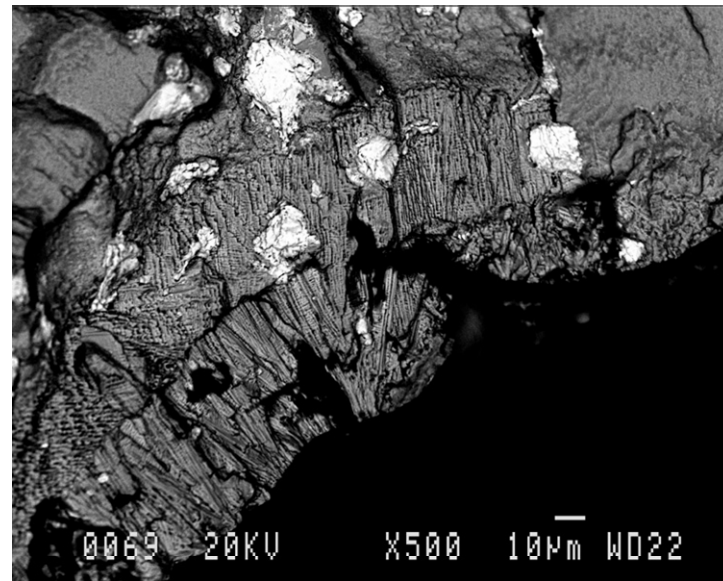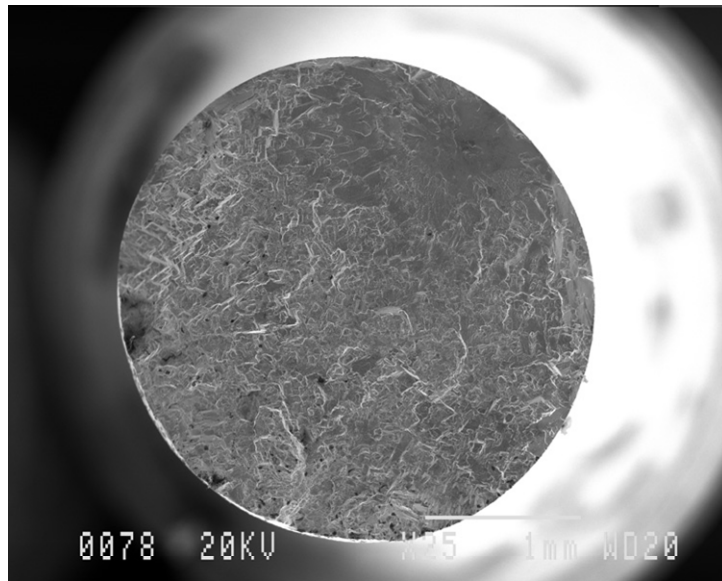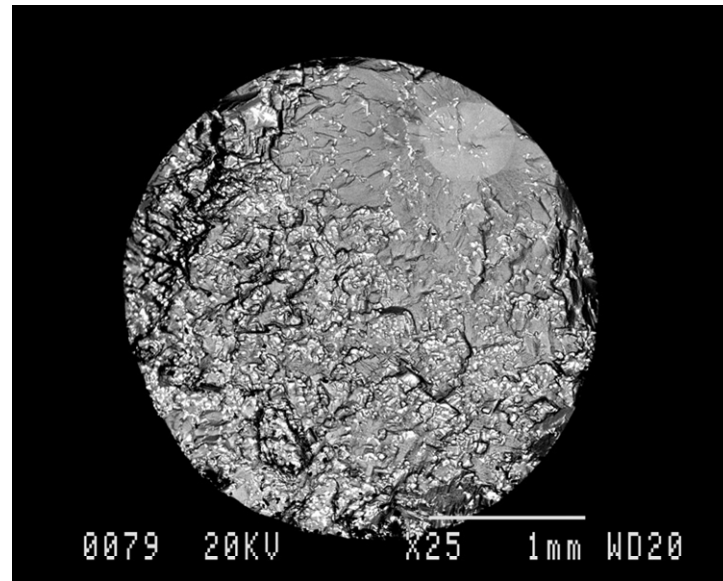
SE mode

BE mode

# CA9L, R = -1, $\Delta\varepsilon$ = 0.58%, 100x
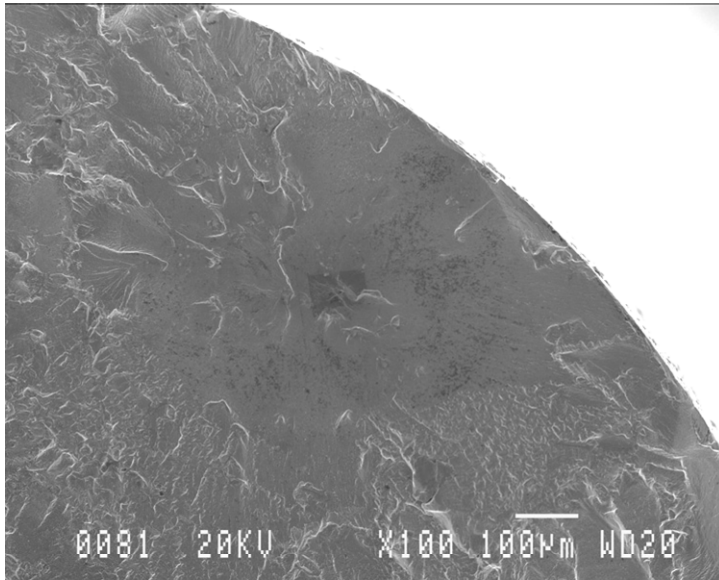
SE mode
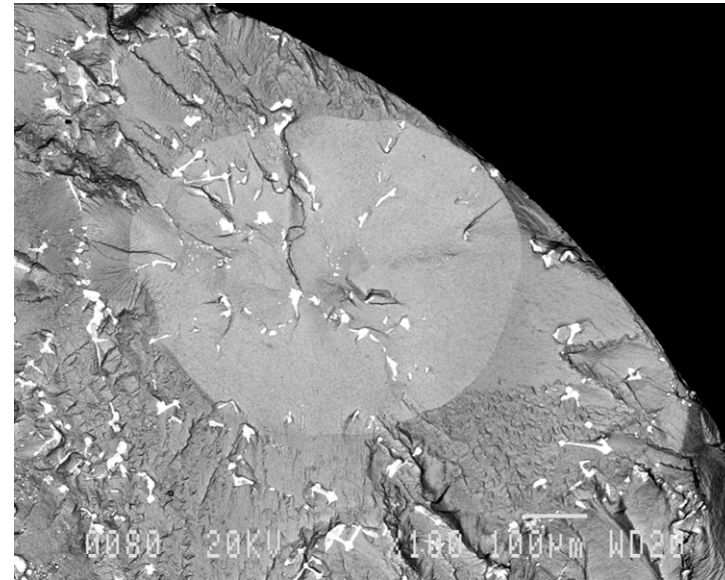
BE mode

CA9L, R = -1, $\Delta\varepsilon$ = 0.58%, 500x

SE mode

BE mode

CB1L, R = -1, Δε = 0.50%, 25x
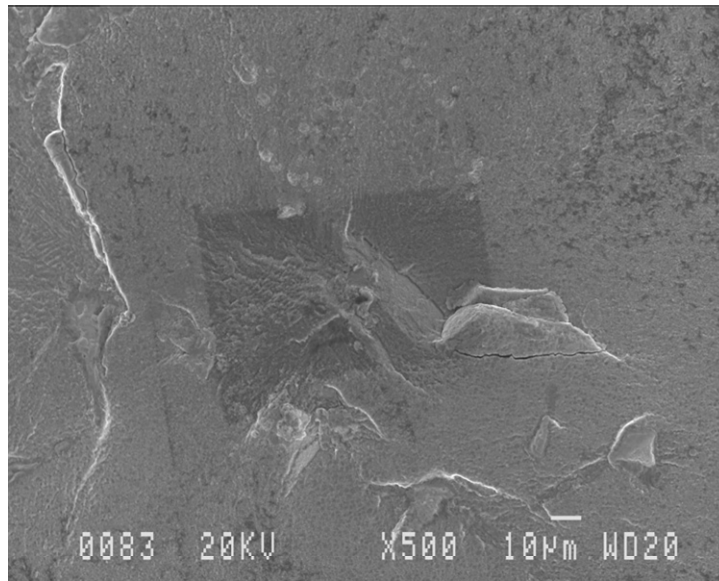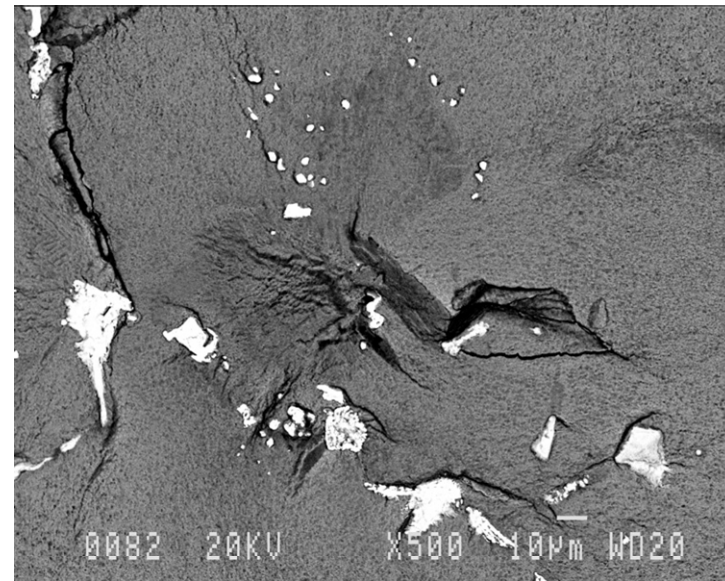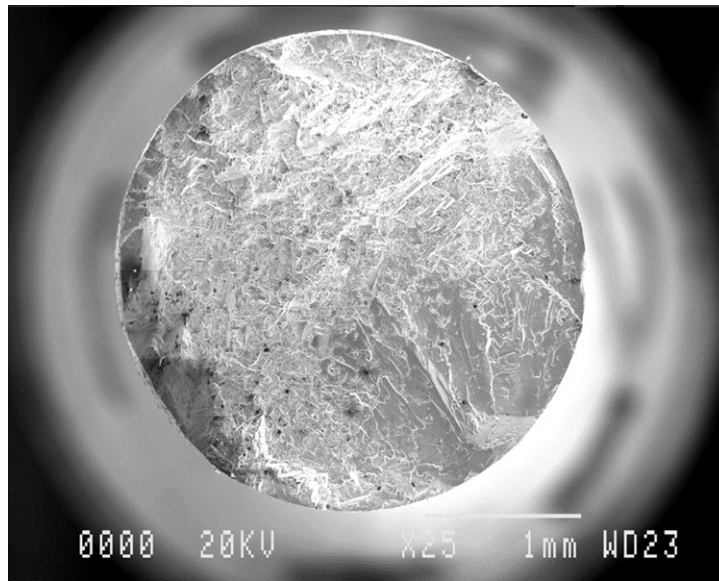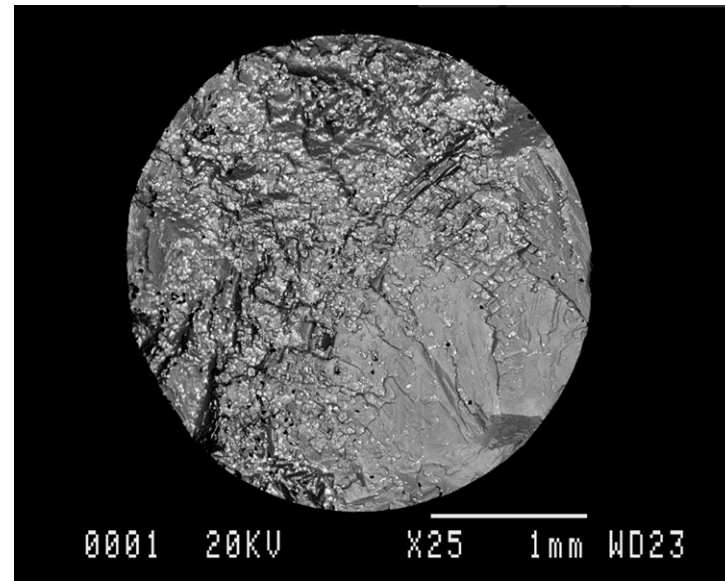


SE mode　　　　　　　　BE mode

CB1L, R = -1, $\Delta\varepsilon$ = 0.50%, 100x
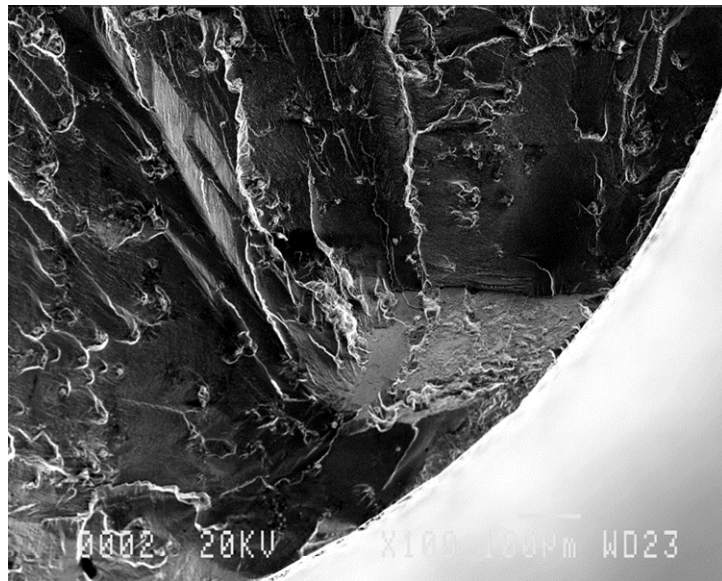
SE mode
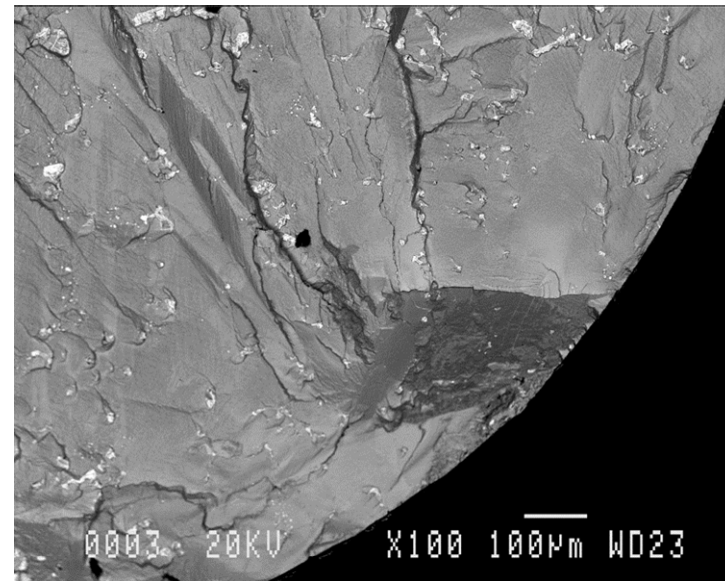
BE mode

CB1L, R = -1, $\Delta\varepsilon$ = 0.50%, 500x

SE mode

BE mode

CB2L, R = 0, Δε = 0.58%, 25x
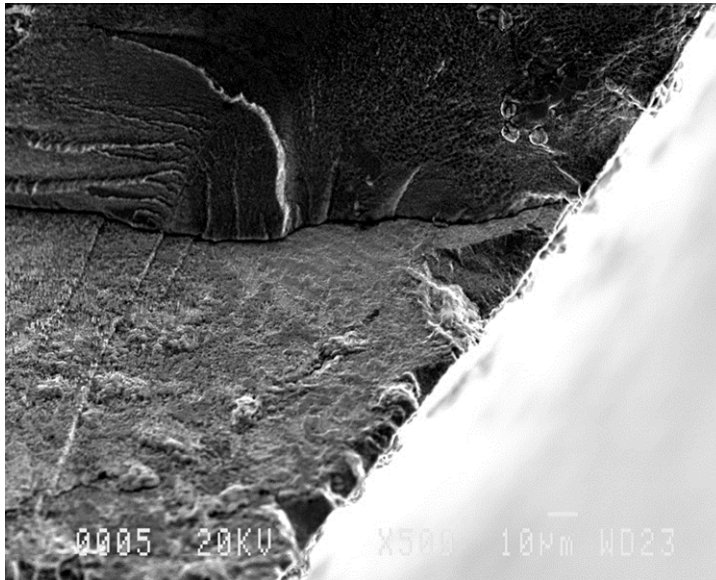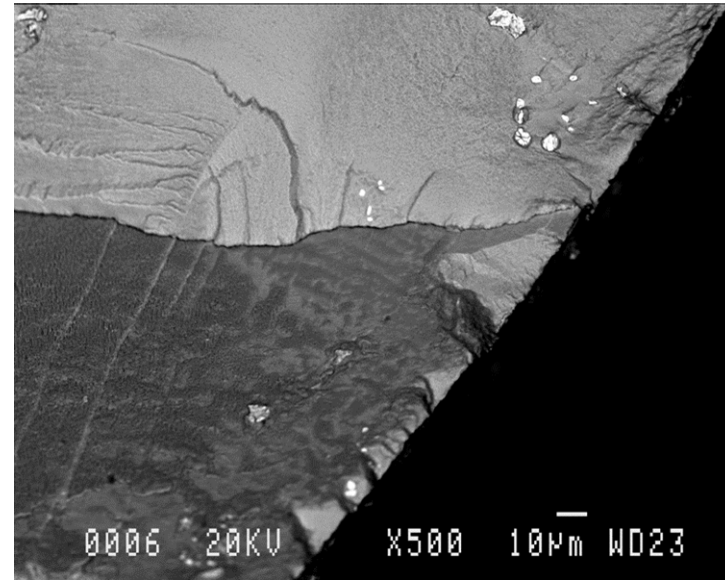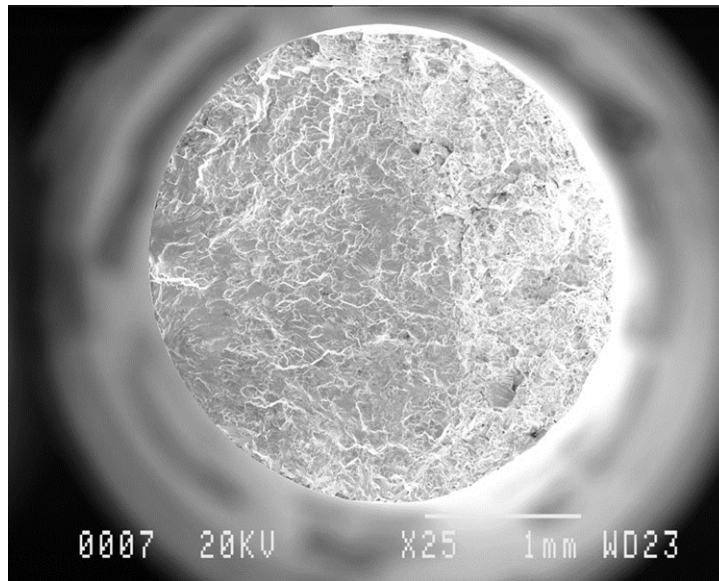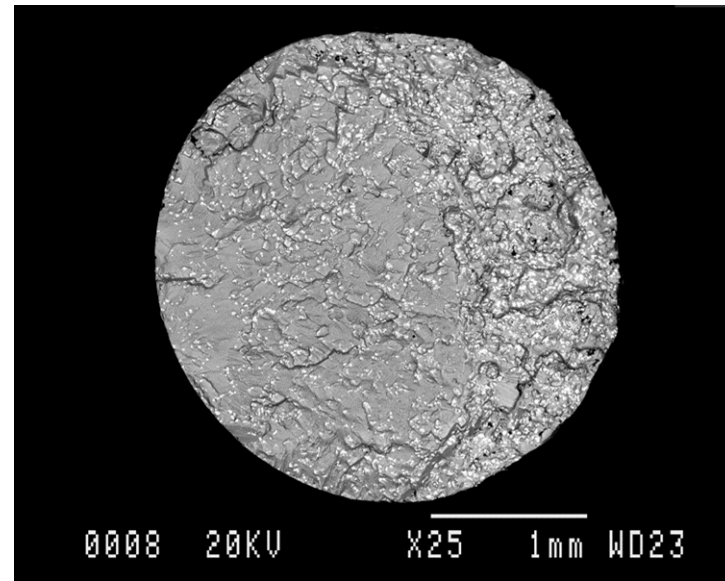
SE mode   BE mode

CB2L, R = 0, $\Delta\varepsilon$ = 0.58%, 100x

SE mode

BE mode

CB2L, R = 0, Δε = 0.58%, 500x

SE mode   BE mode

CB3L, R = -1, Δε = 0.90%, 25x
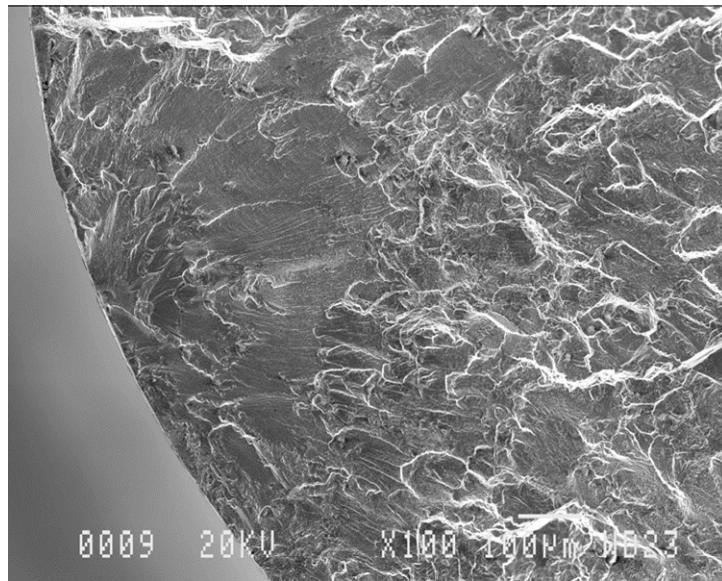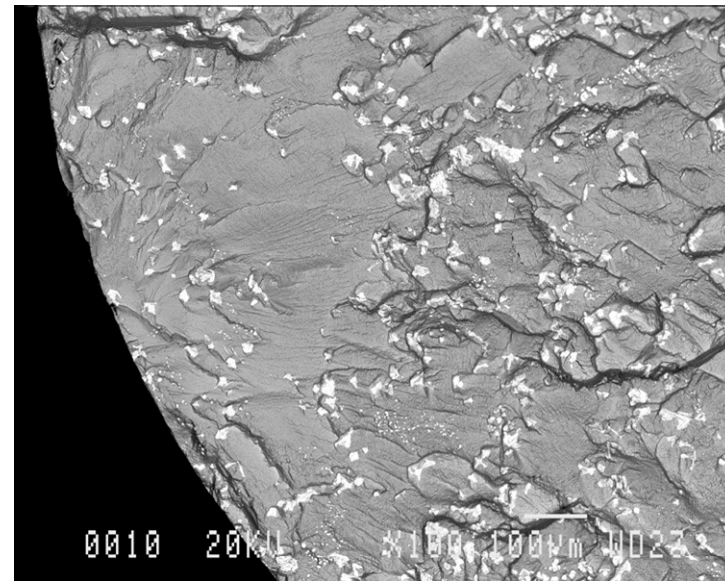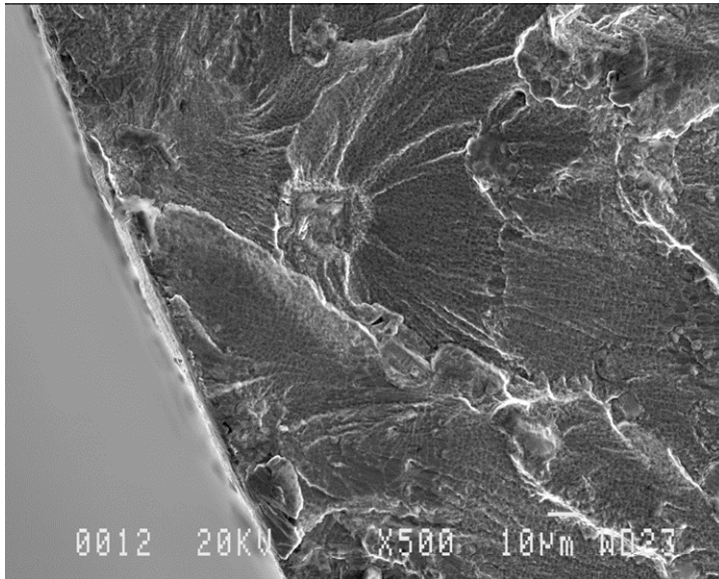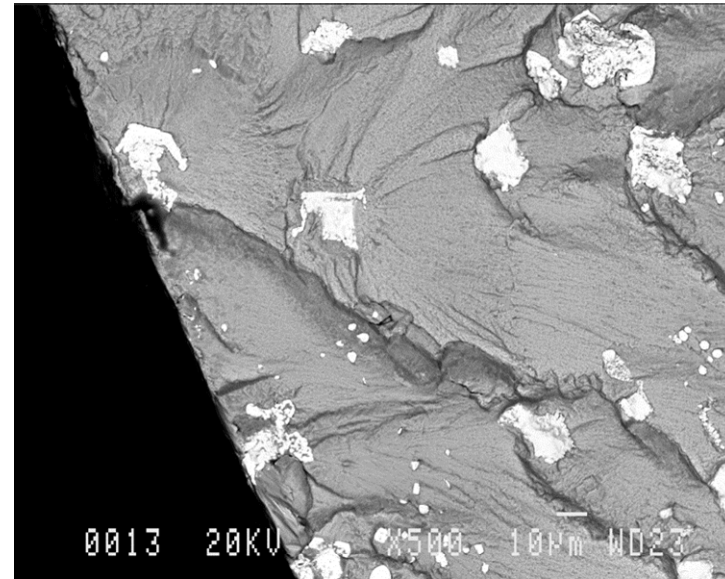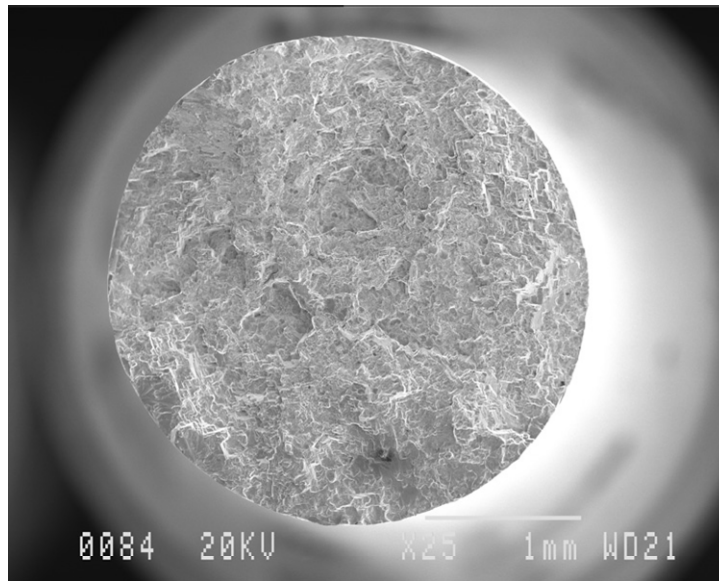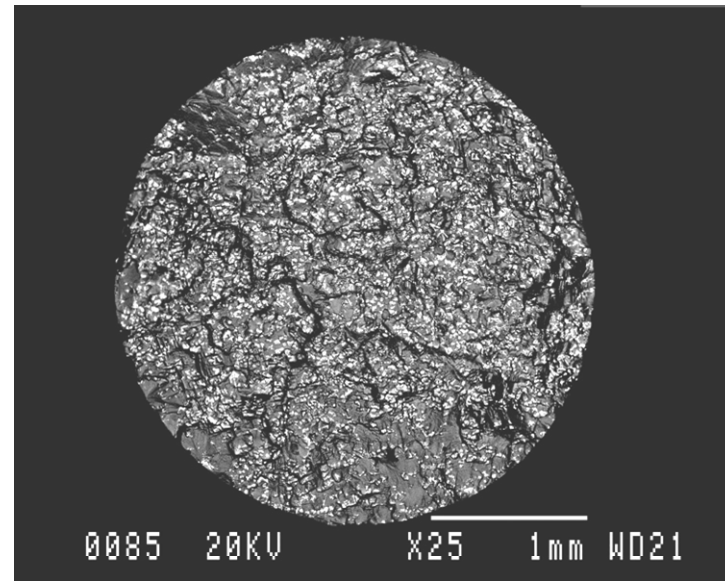
SE mode

BE mode

CB3L, R = -1, $\Delta\varepsilon$ = 0.90%, 100x
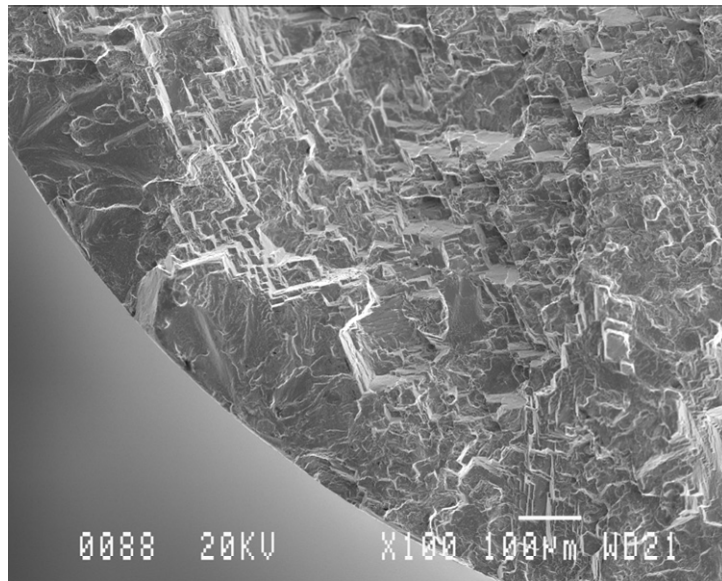
SE mode
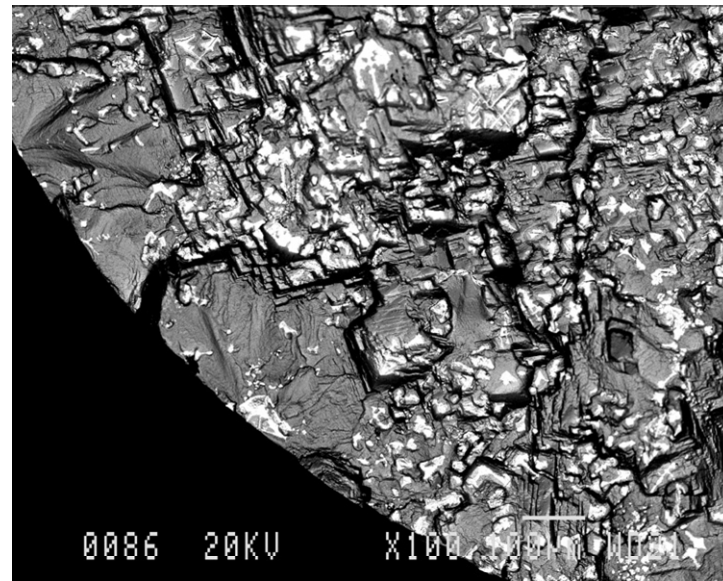
BE mode

CB3L, R = -1, $\Delta\varepsilon$ = 0.90%, 500x
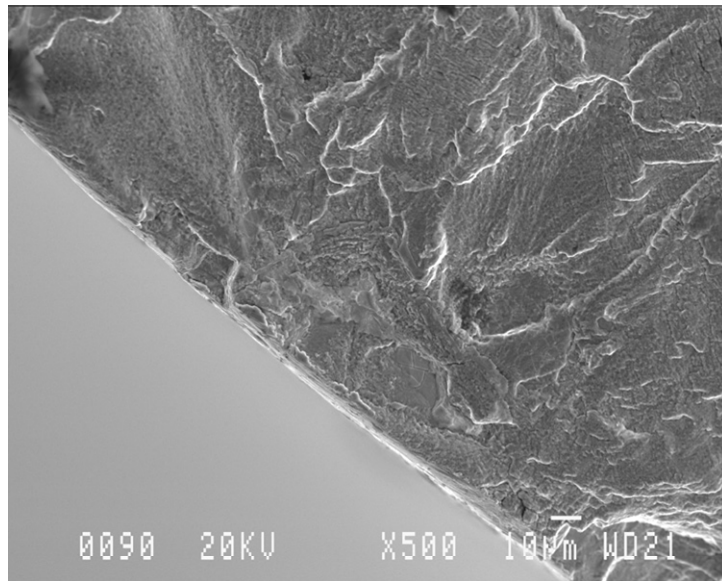
SE mode
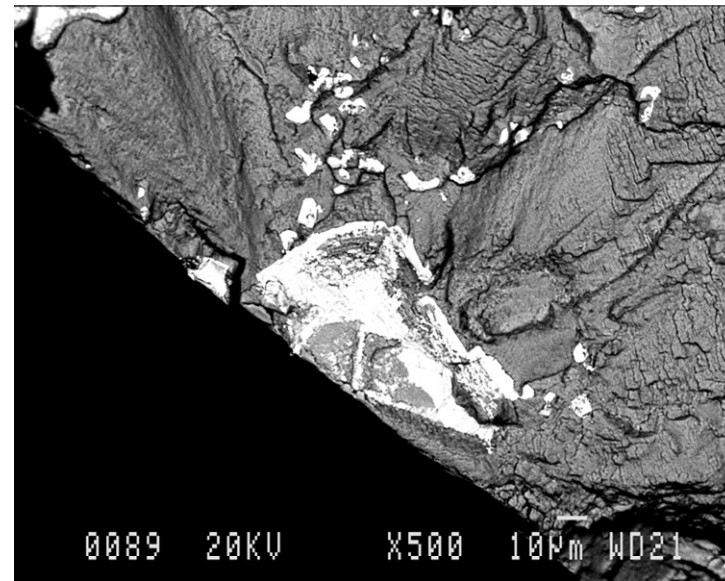
BE mode

CB5L, R = 0, $\Delta\varepsilon$ = 0.67%, 25x
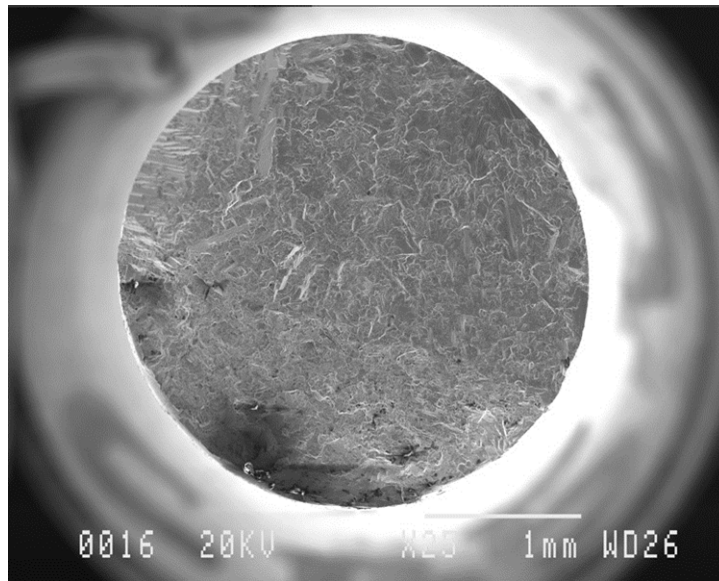
SE mode
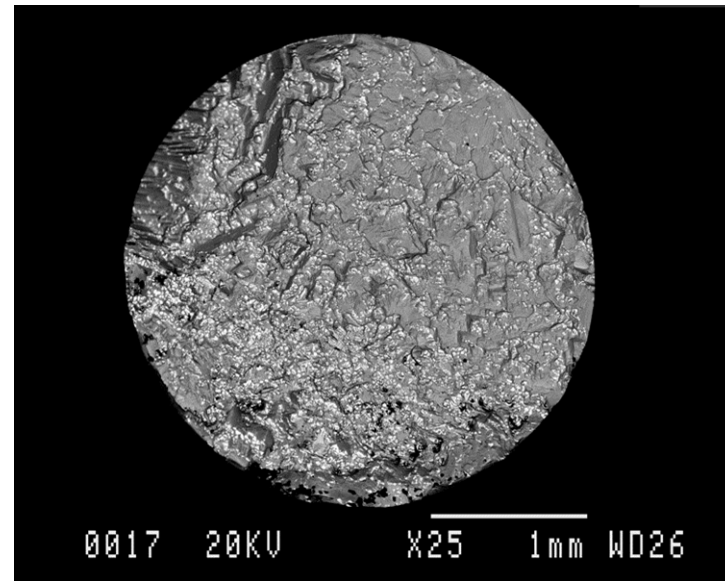
BE mode

CB5L, R = 0, $\Delta\varepsilon$ = 0.67%, 100x
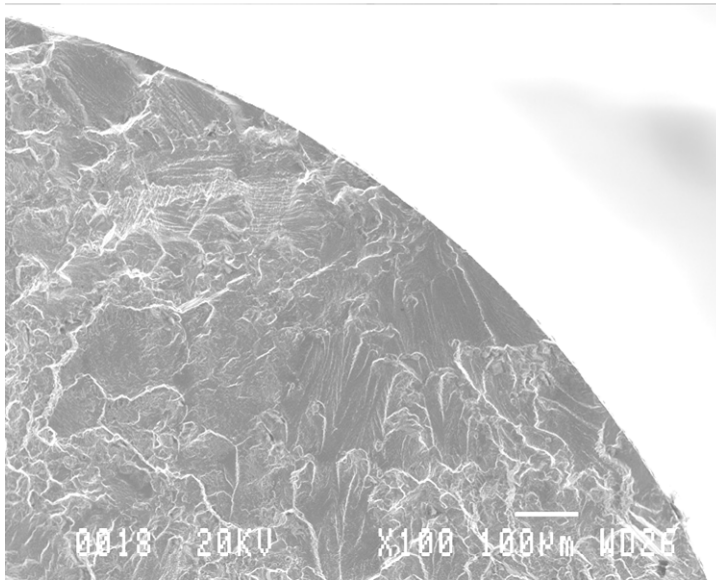
SE mode
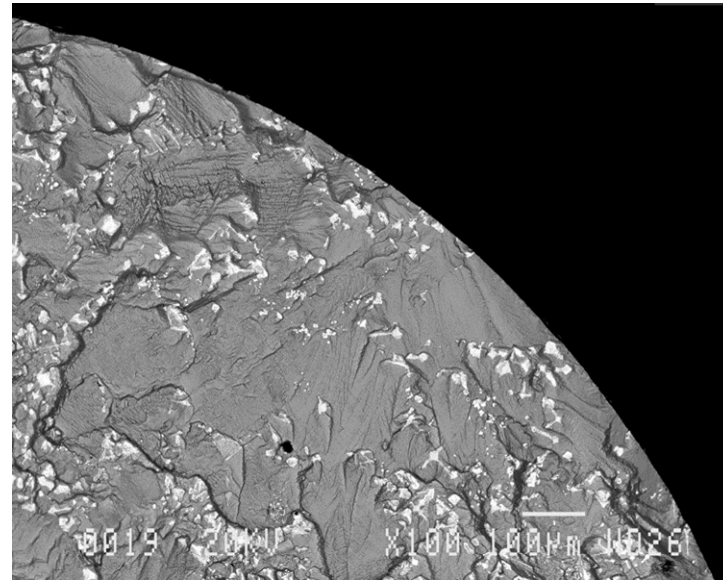
BE mode

# CB5L, R = 0, $\Delta\varepsilon$ = 0.67%, 500x
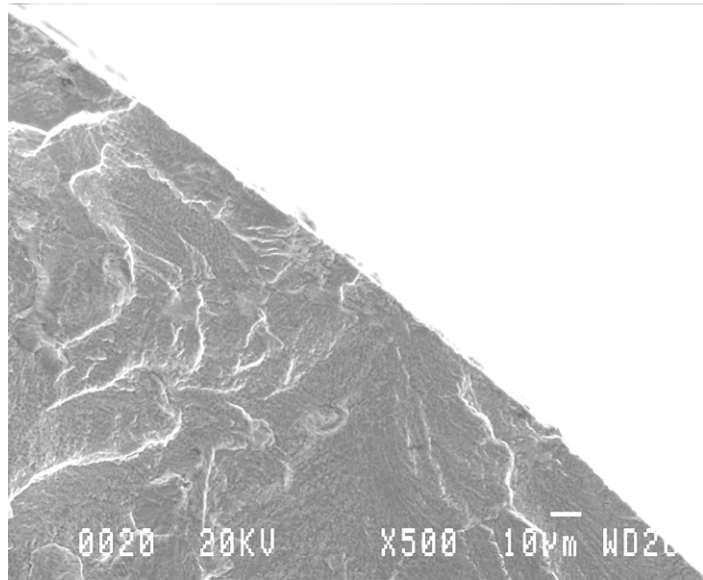
SE mode
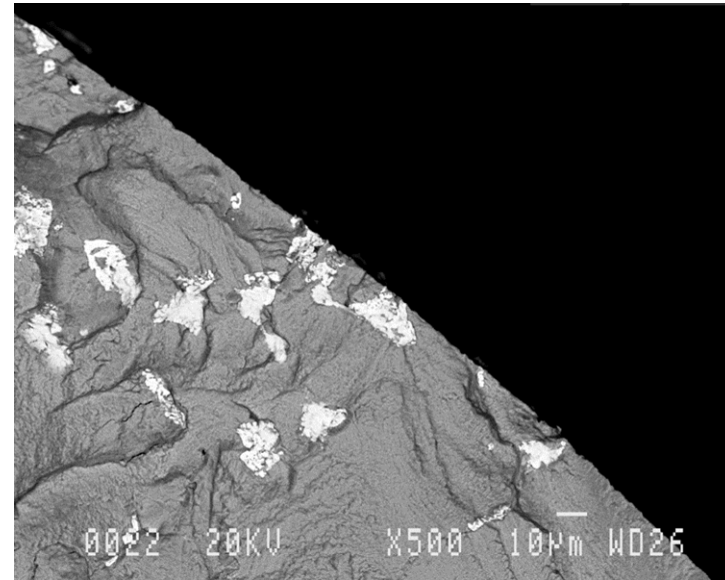
BE mode

CB6L, R = -1, $\Delta\varepsilon$ = 0.78%, 25x
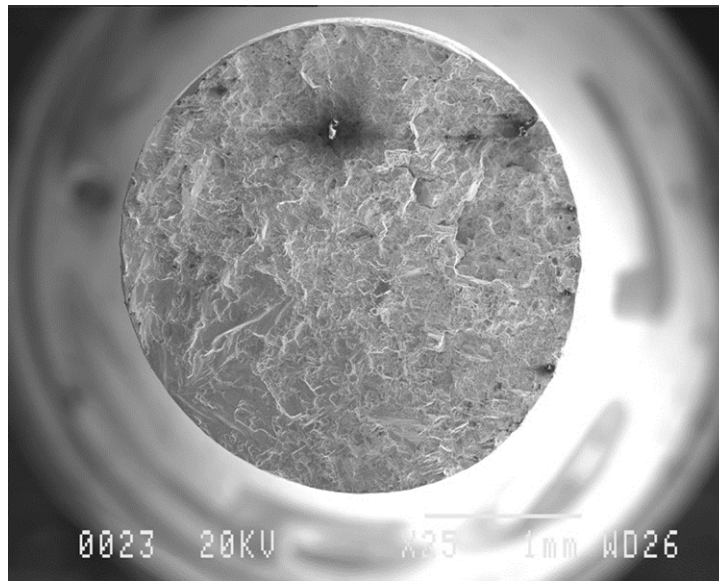
SE mode
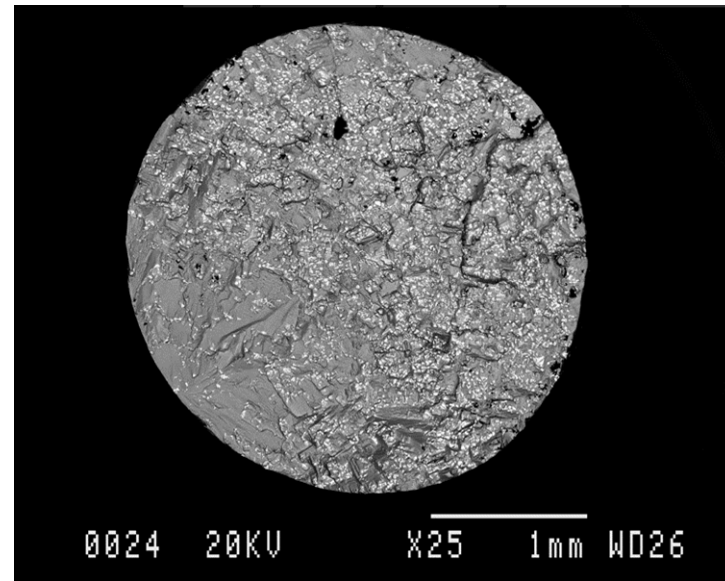
BE mode

CB6L, R = -1, $\Delta\varepsilon$ = 0.78%, 100x
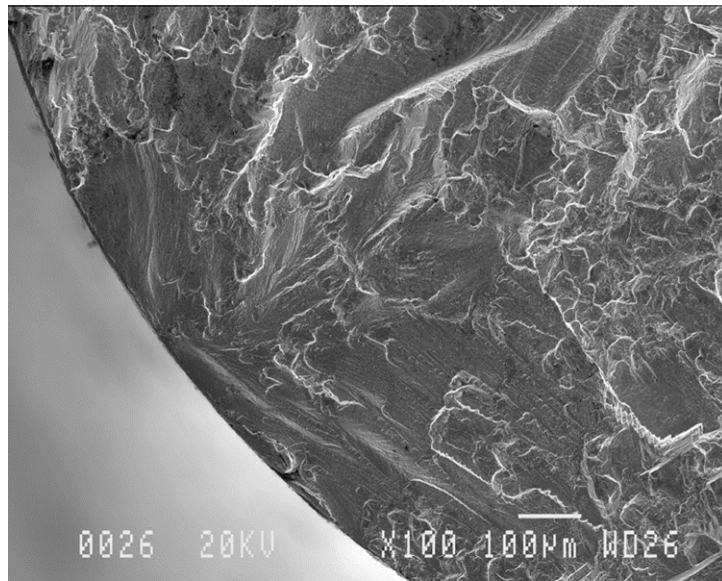
SE mode
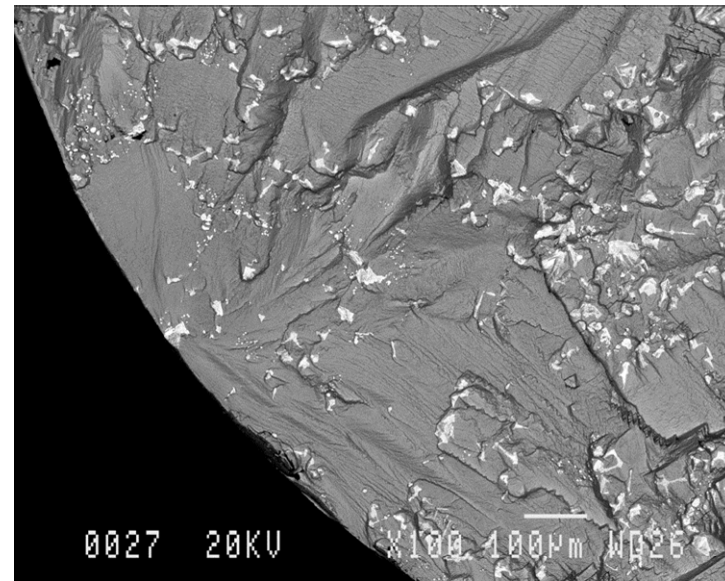
BE mode

CB6L, R = -1, $\Delta\varepsilon$ = 0.78%, 500x

SE mode

BE mode

CB7L, R = 0, Δε = 0.78%, 25x
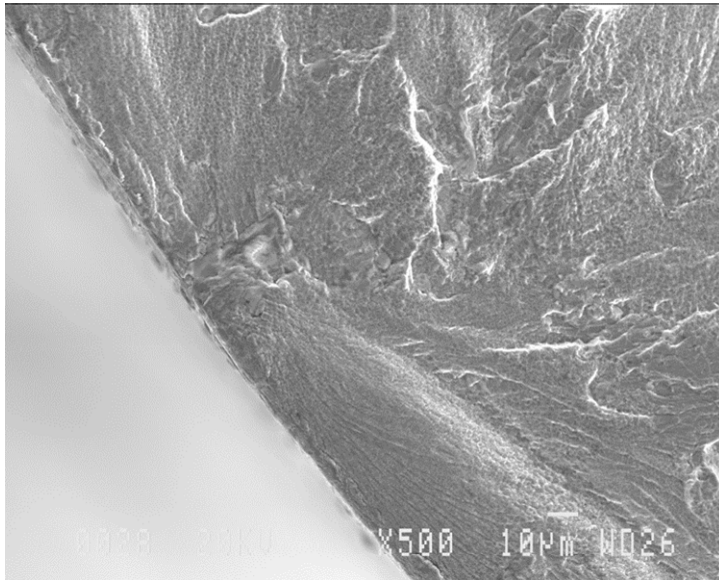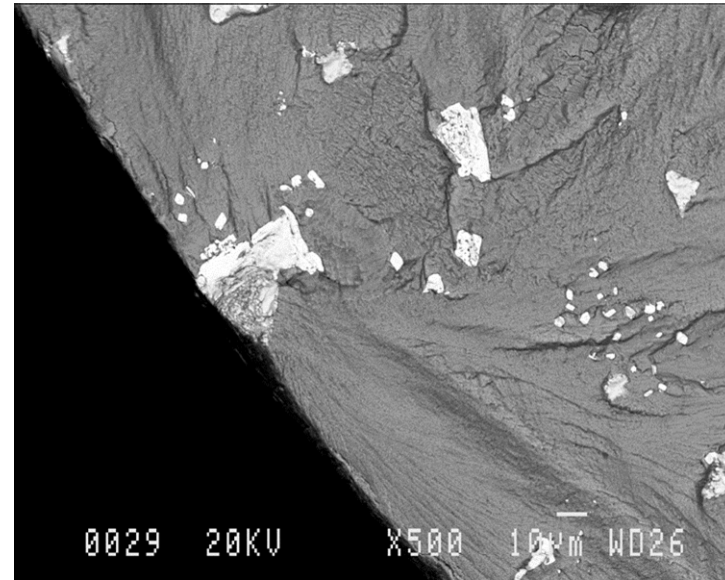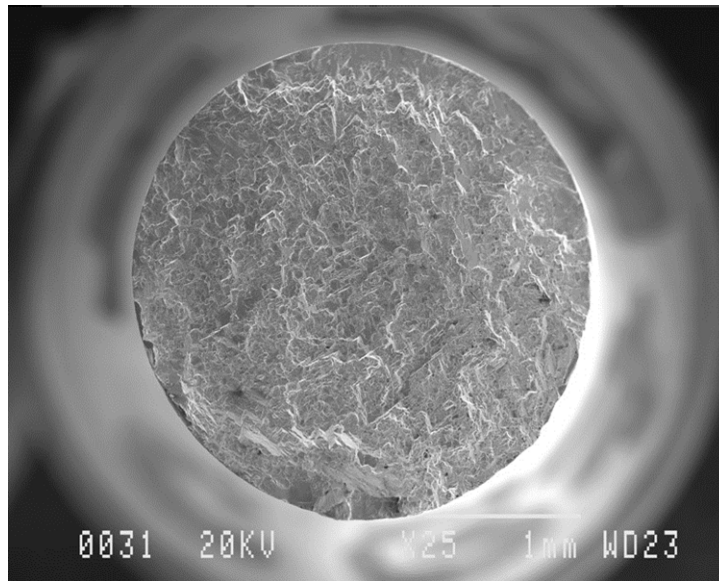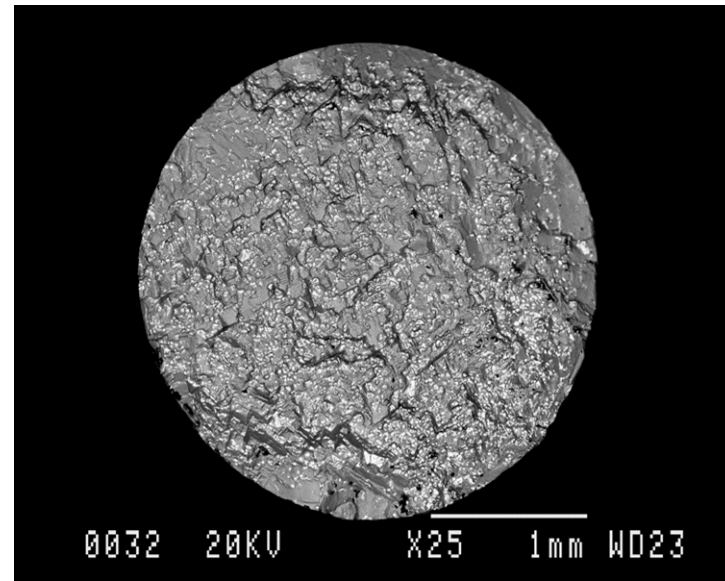
SE mode

BE mode

CB7L, R = 0, $\Delta\varepsilon$ = 0.78%, 100x
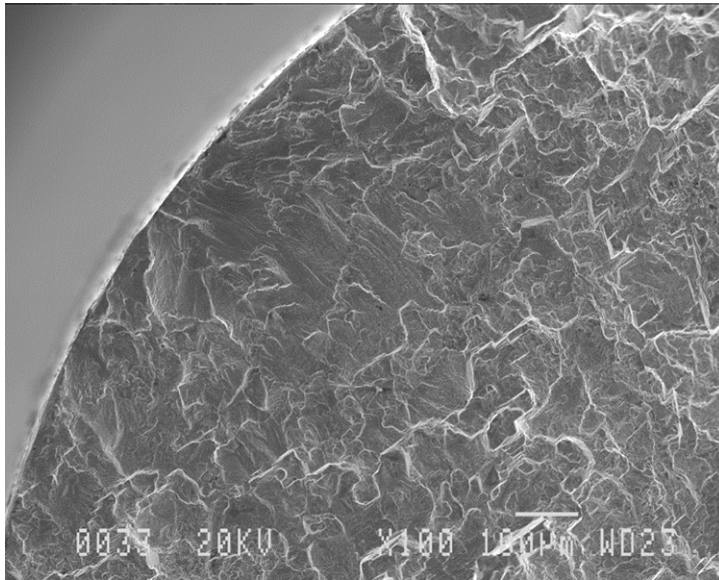
SE mode
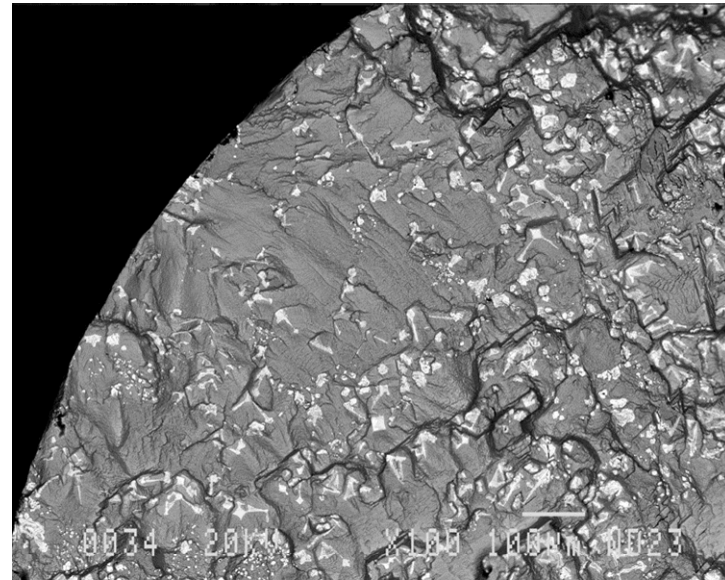
BE mode

CB7L, R = 0, $\Delta\varepsilon$ = 0.78%, 500x

Crack 1
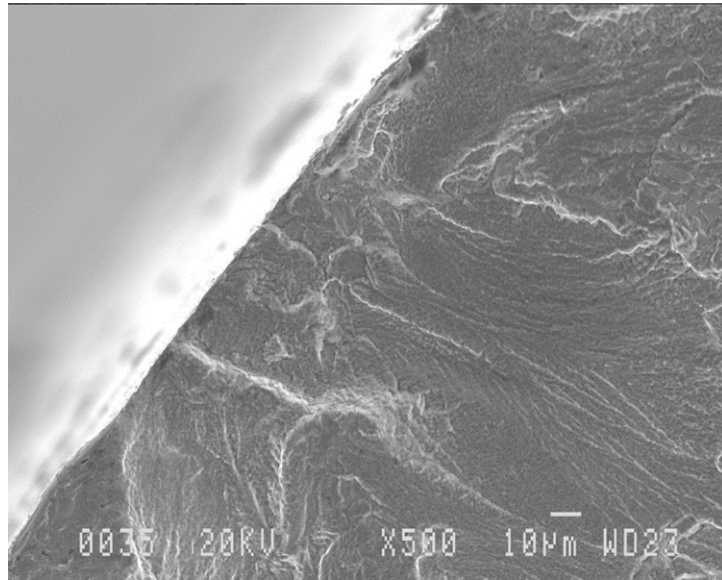
SE mode   BE mode
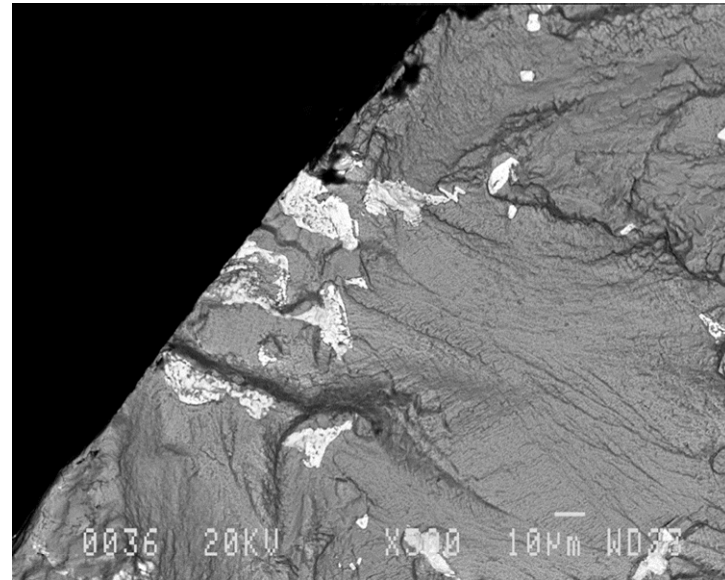
CB7L, R = 0, $\Delta\varepsilon$ = 0.78%, 500x

Crack 2
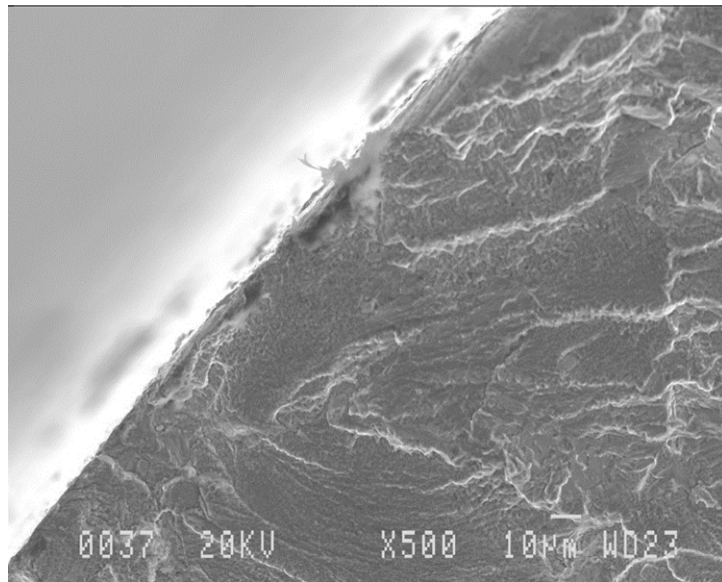
SE mode
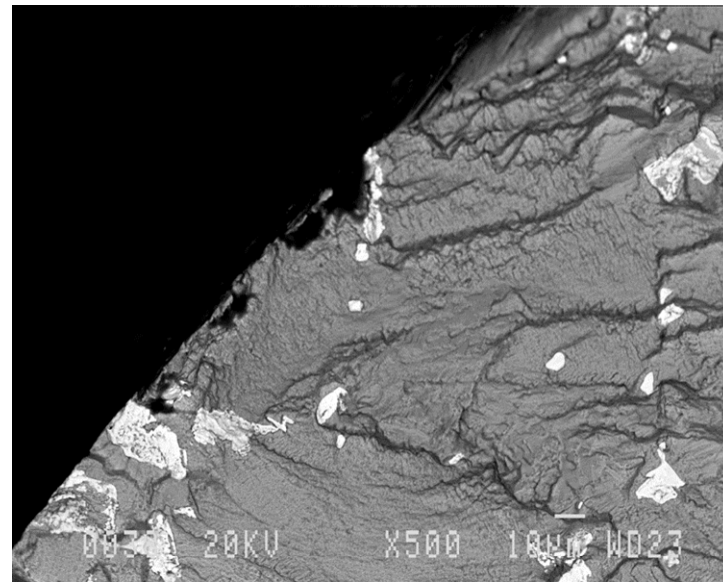
BE mode

CB8L, R = -1, $\Delta\varepsilon$ = 0.67%, 25x
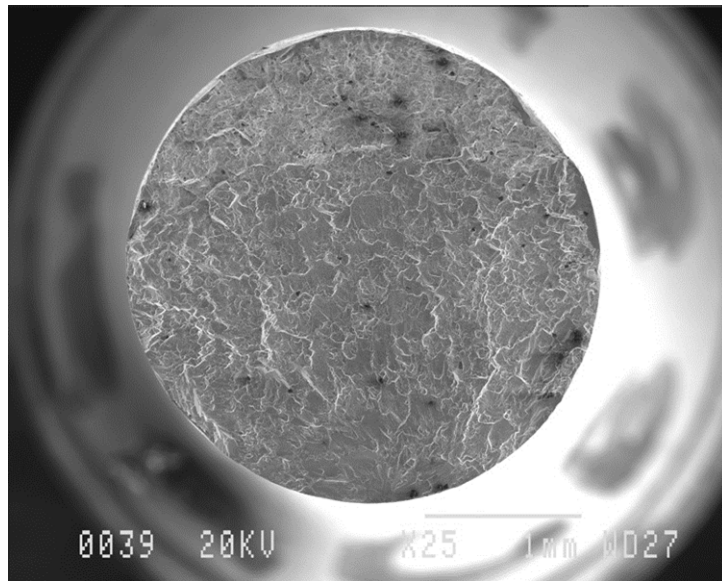
SE mode
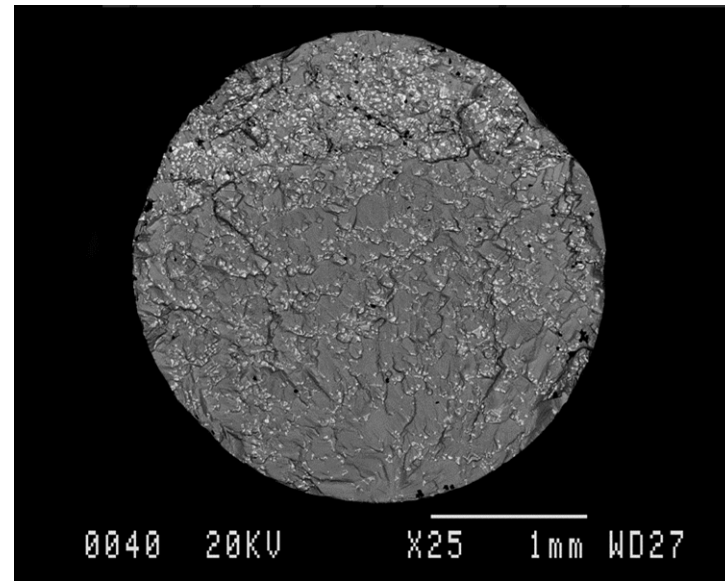
BE mode

CB8L, R = -1, $\Delta\varepsilon$ = 0.67%, 100x
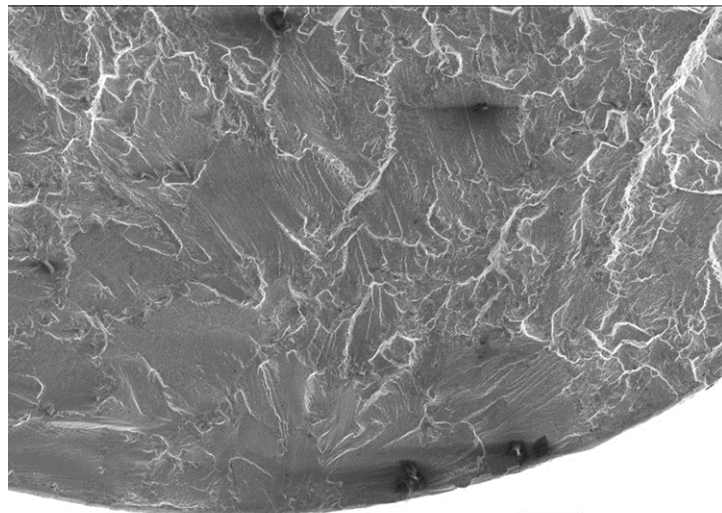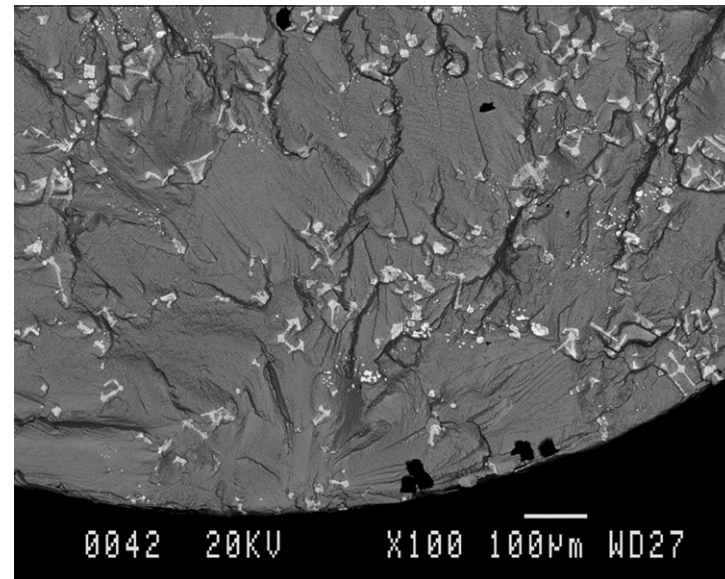
SE mode

BE mode

CB8L, R = -1, $\Delta\varepsilon$ = 0.67%, 500x
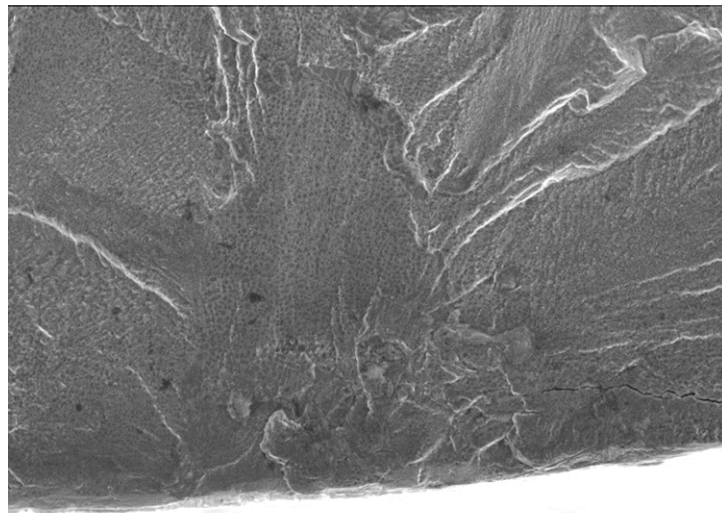
SE mode
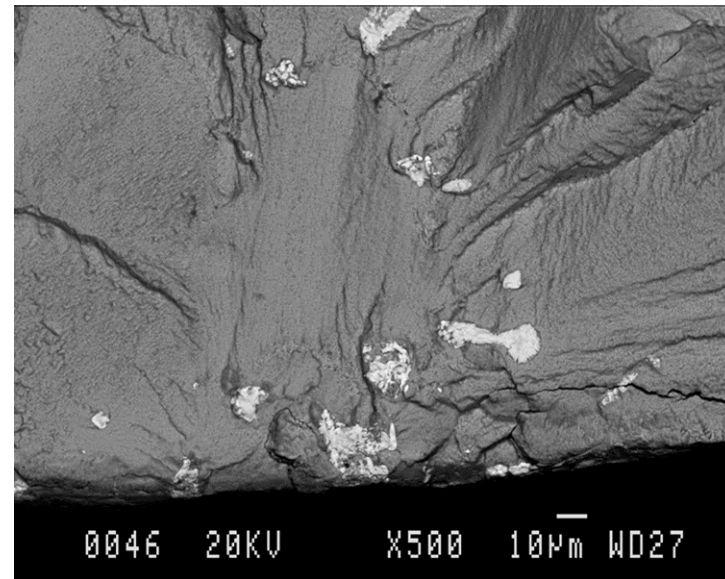
BE mode

CB9L, R = 0, $\Delta\varepsilon$ = 0.90%, 25x
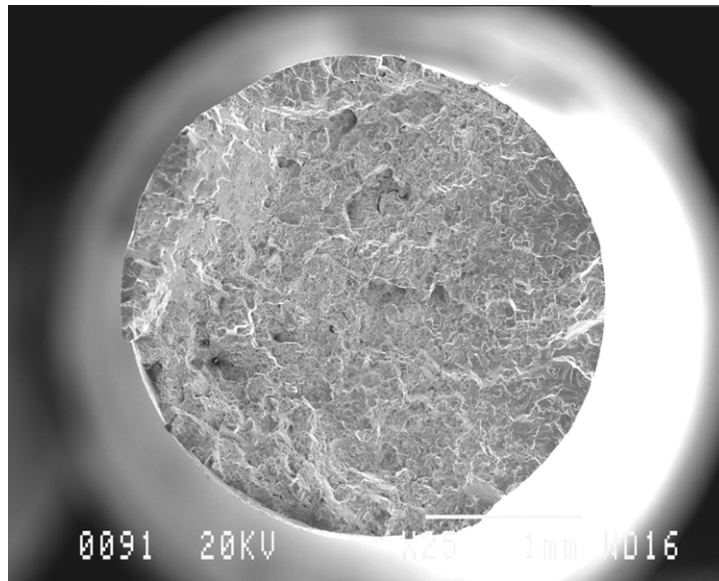
SE mode
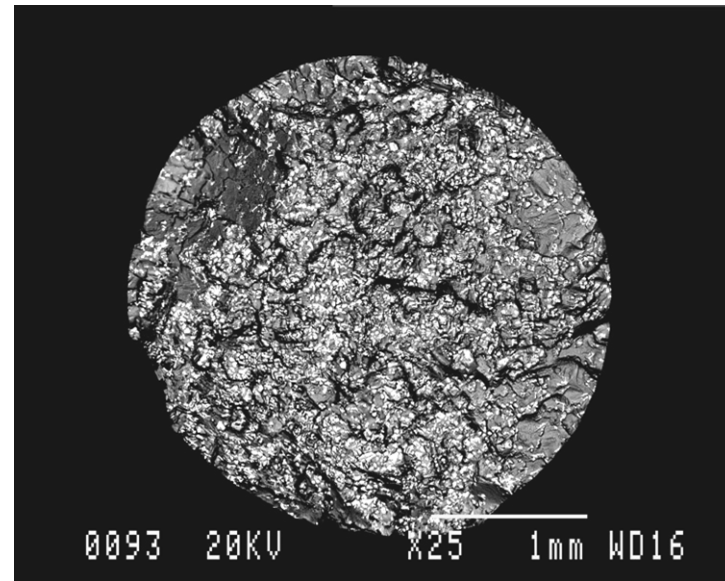
BE mode

CB9L, R = 0, $\Delta\varepsilon$ = 0.90%, 100x
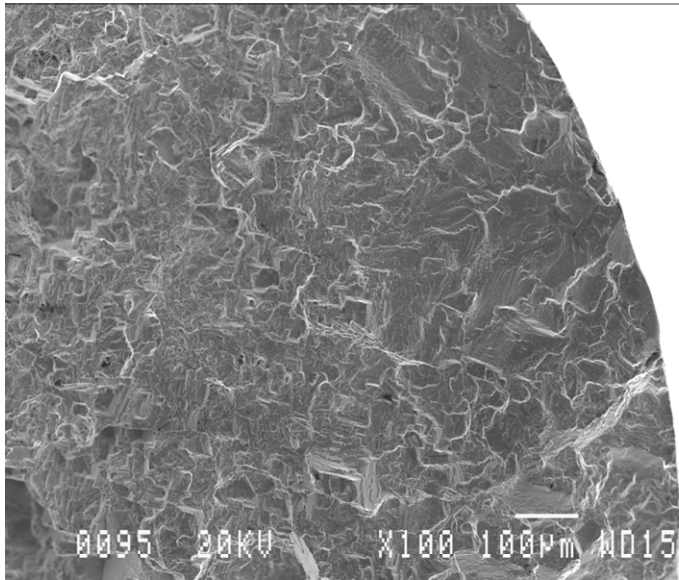
SE mode
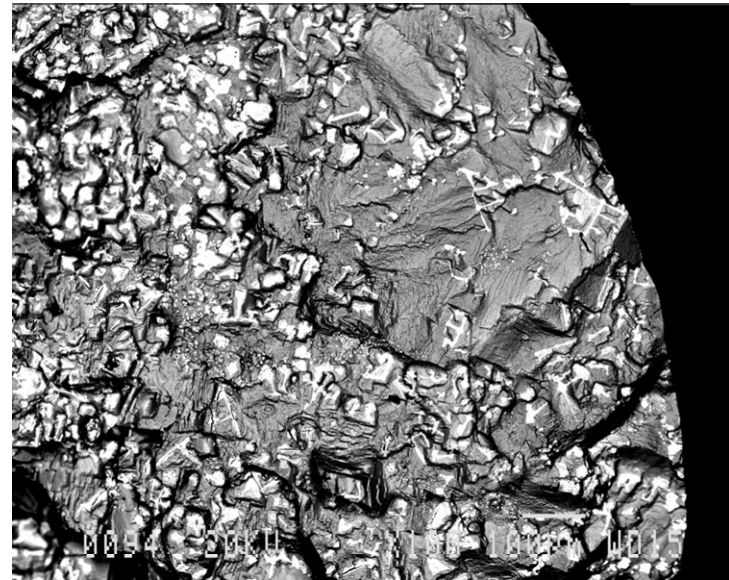
BE mode

CB9L, R = 0, $\Delta\varepsilon$ = 0.90%, 500x
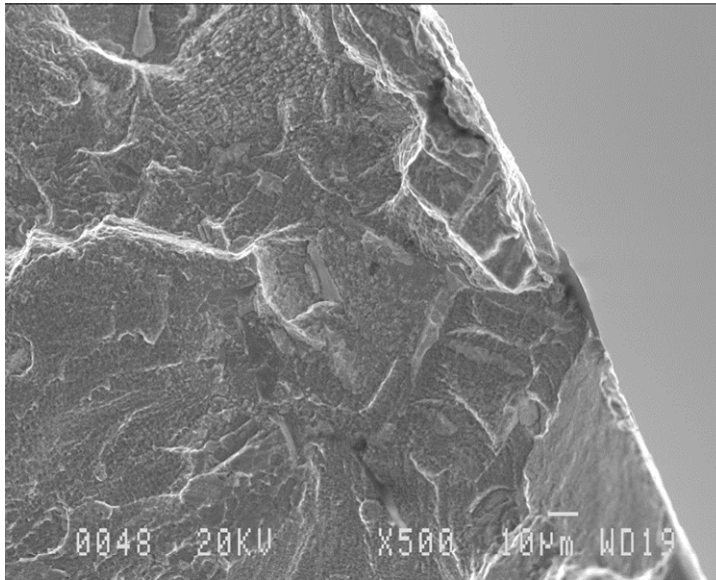
SE mode
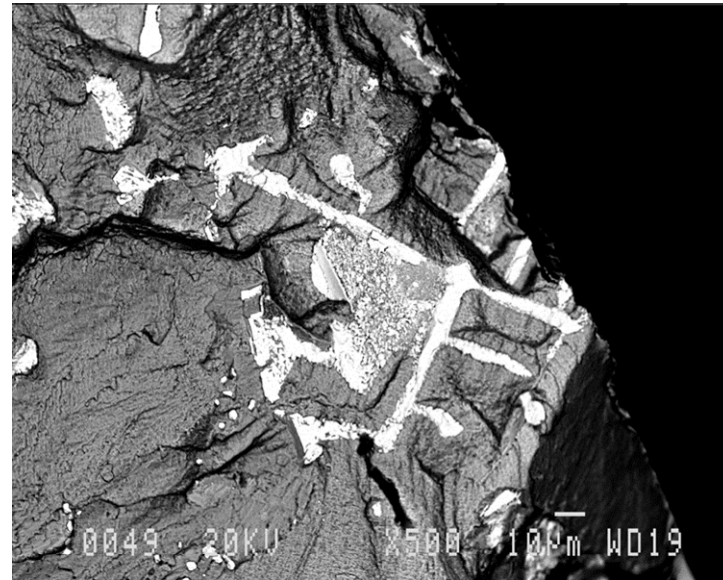
BE mode

12. Appendix D.—Grainex Mar-M 247 Fatigue Crack Growth Specimen SEM Images

Specimen ID	Comments	Page
13K	SE, BE, overall	226
13K	SE, BE, low ΔK region	227
13K	SE, BE, high ΔK region	228
13K	SE, BE, carbide cluster	229
32K	SE, BE, overall	230
32K	SE, BE, low ΔK region	231
32K	SE, BE, high ΔK region	232

Specimen 13K

Tensile Overload

High ΔK

Low DK

EDM notch #2
EDM notch #1

RT Pre-crack
1200F Crack growth
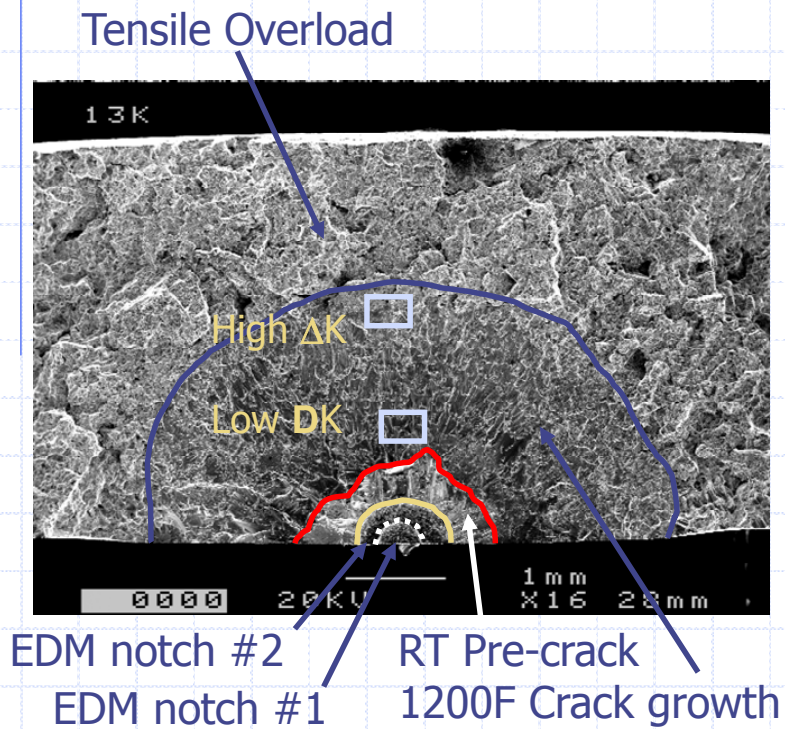
Secondary Electron Image
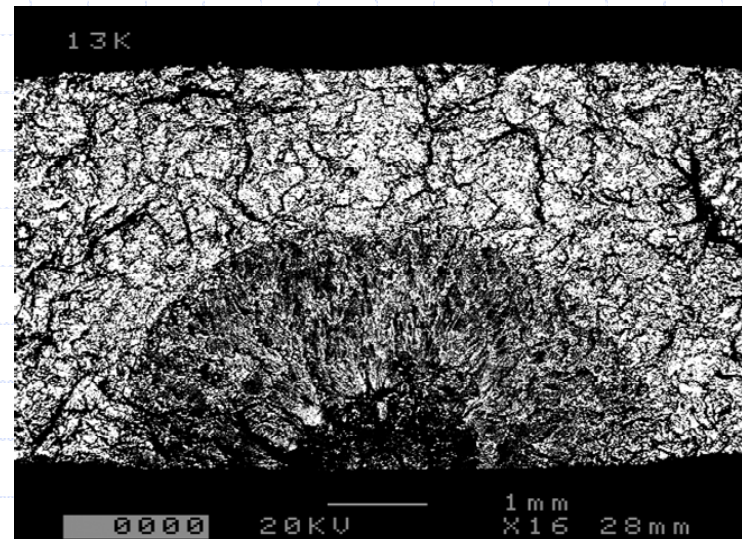
Backscatter Electron Image

Specimen 13K: Low ΔK Region

Secondary Electron Image

Backscatter Electron Image

da/dN
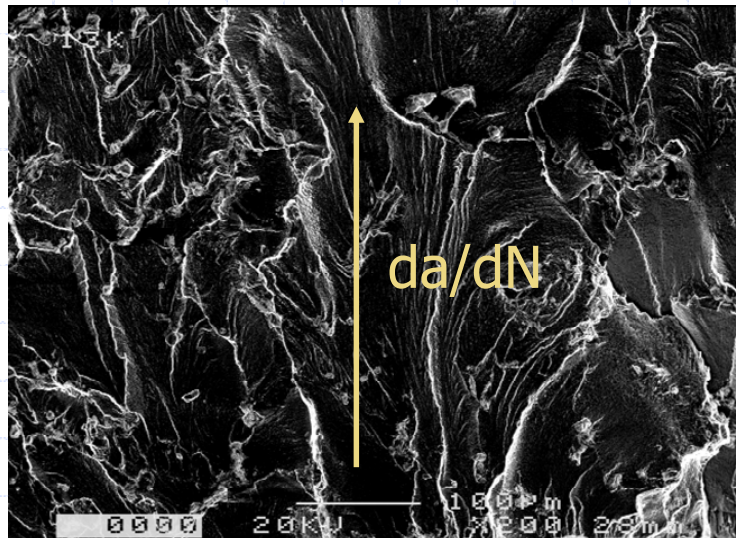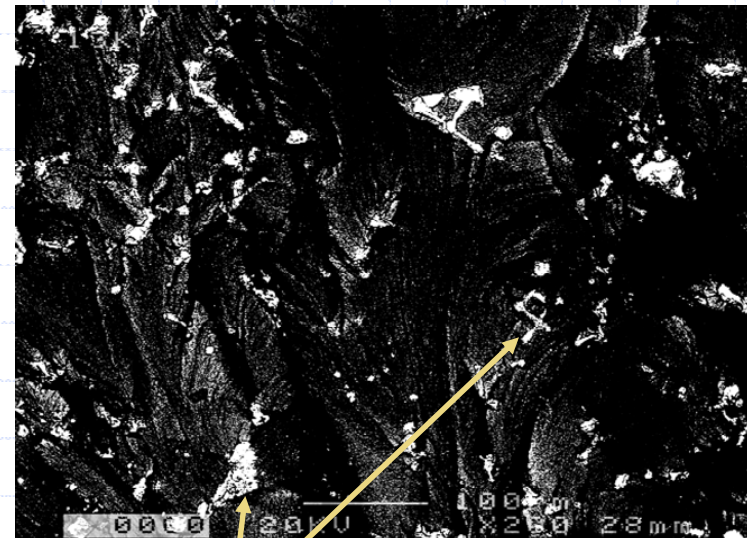
Carbide
Clusters

Crack growth occurred transgranularly

Specimen 13K: High ΔK Region

da/dN
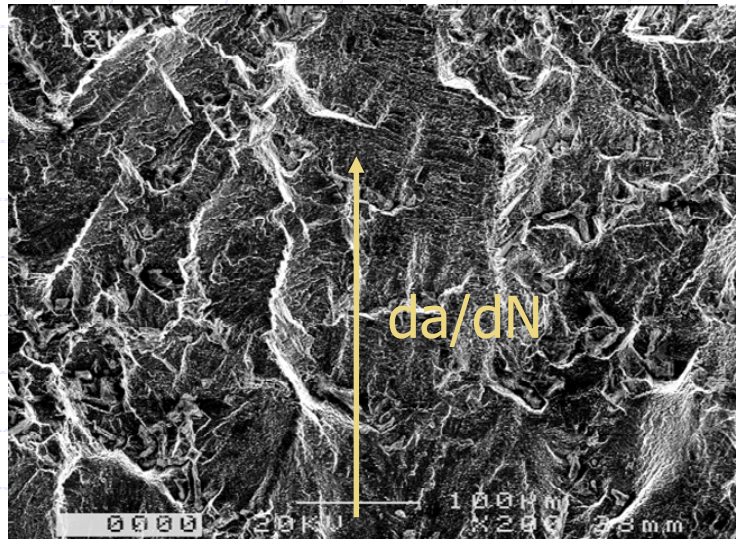
Carbide
Clusters
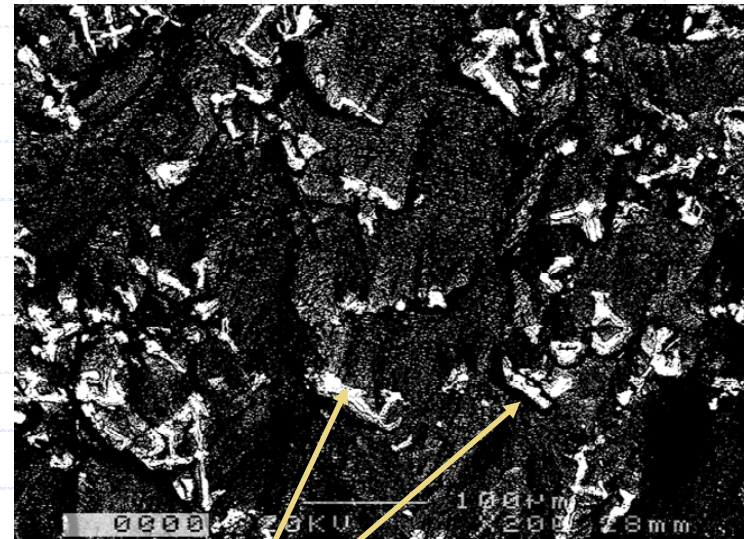
Secondary Electron Image   Backscatter Electron Image

# Specimen 13K: Carbide Cluster
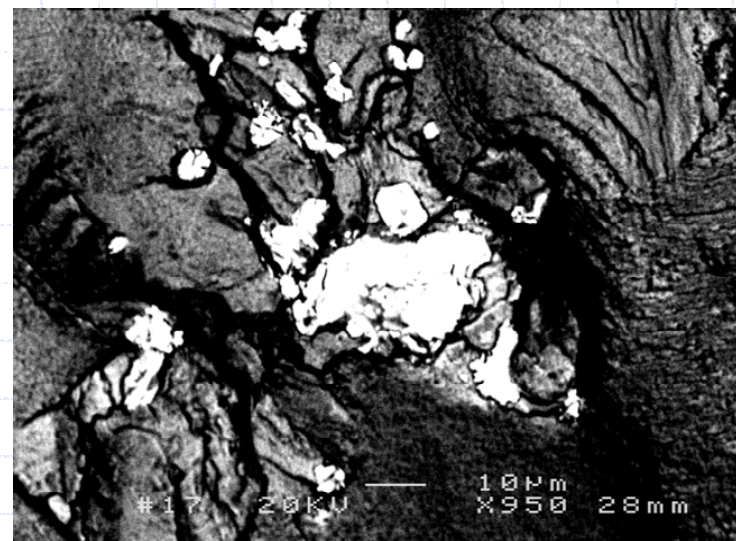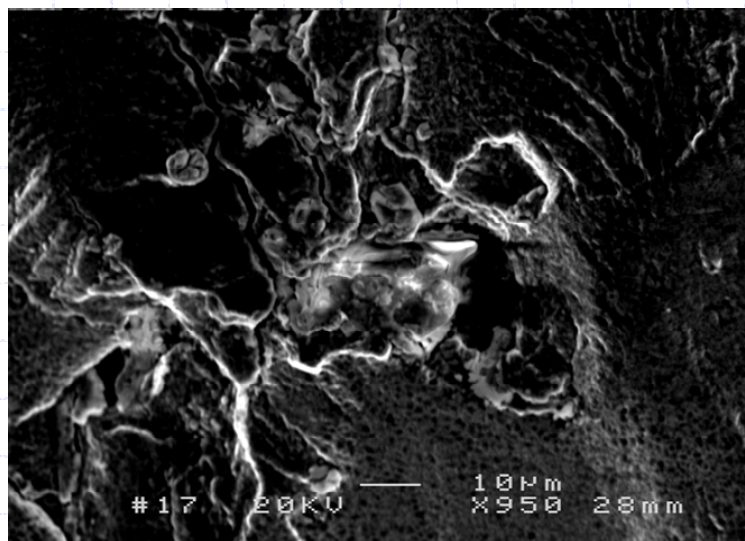
Secondary Electron Image   Backscatter Electron Image

Specimen 32K

Tensile Overload

High ΔK

Low DK

EDM notch #2   RT Pre-crack

1200F Crack growth
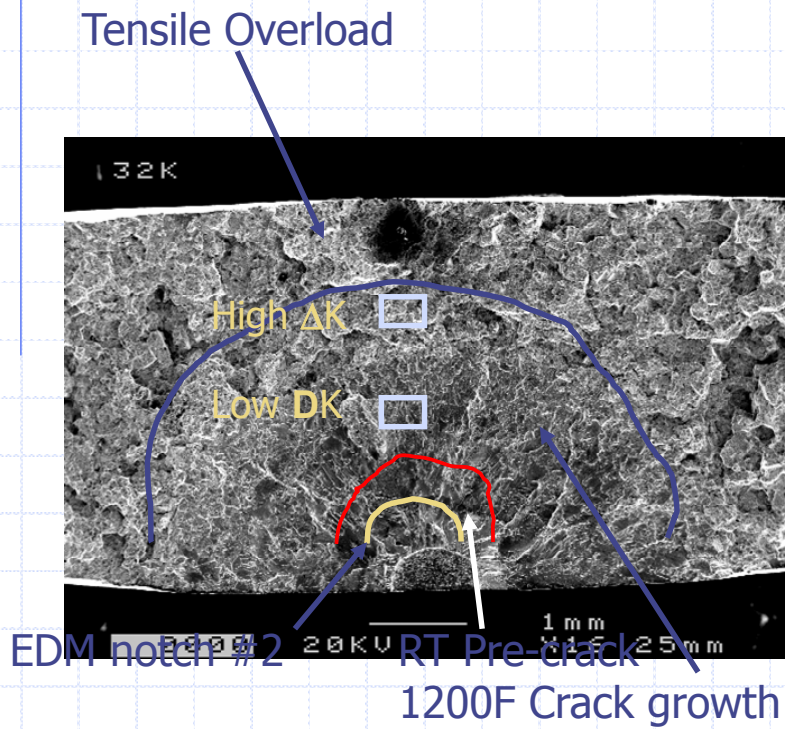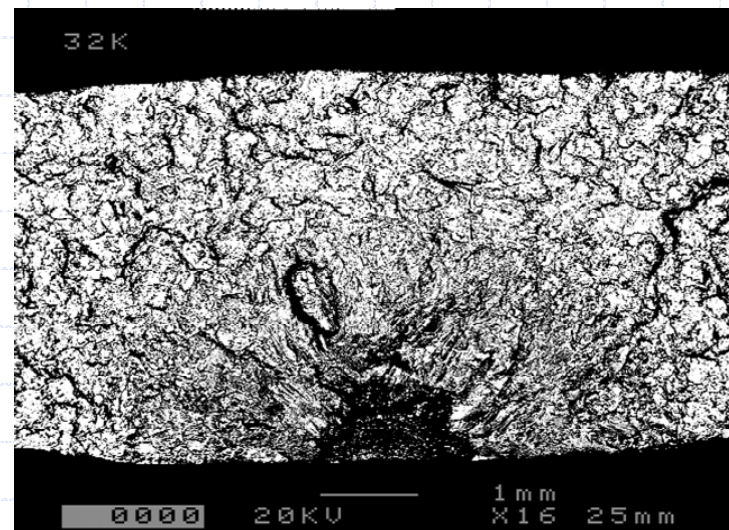
Secondary Electron Image   Backscatter Electron Image

# Specimen 32K: Low ∆K Region

Secondary Electron Image   Backscatter Electron Image

# Specimen 32K: High ΔK Region

Secondary Electron Image   Backscatter Electron Image